UNIVERSITÉ DE LORRAINE

École doctorale IAEM Lorraine

In-vivo Human Head Conductivity Estimation by SEEG and EEG Recorded in Simultaneous with Intracerebral Electrical Stimulation

THÈSE

pour l'obtention du

Doctorat de l'Université de Lorraine

Mention Automatique, Traitement du Signal et des Images, Génie Informatique

Soutenue le 05 Décembre 2017

par

Hamza Fawzi Altakroury

Composition du jury

Rapporteurs: Pr Francois Cabestaing
CRIStAL UMR 9189 Université Lille 1
Dr Christian Bénar
DR INSERM UMR 1106 Aix-Marseille Université

Examinateurs: Dr Estelle Rikir
CHU Liége, Université de Liége
Pr Louis Maillard
CRAN UMR 7039 Université de Lorraine
Dr Laurent Koessler
CRAN UMR 7039 Université de Lorraine
Pr Valérie Louis-Dorr
CRAN UMR 7039 Université de Lorraine

Centre de Recherche en Automatique de Nancy
UMR 7039 CNRS – Université de Lorraine
2 avenue de la forêt de Haye 54516 Vandœuvre-lès-Nancy
Tél +33 3 83 59 59 59 — Fax +33 (0)3 83 59 56 44

First and foremost, I offer my utmost gratitude to the EPIC project-Cardiff Metropolitan University who provided the financial support to this work in the first three years, and to my father-in-law Mr. Wael J. Abu Adas who provided the financial support to this thesis during its fourth year.

I am grateful to all of those whom I have had the pleasure to work with in CRAN laboratory especially to my supervisor Prof. Valérie Louis-Dorr and the co-supervisor of the thesis Dr. Laurent Koessler.

Last but not least I would like to thank my parents, whose advice and love are with me in whatever I do. Most importantly, I am grateful to my loving and supportive wife, Samira, and my wonderful daughter Dua for being with me during these years giving me inspirations and making me forget the pressure of the work.

Abstract: EEG source localization is becoming an important tool for treating epileptic patients by localizing the epileptogenic zones before performing a resection surgery. Given a forward head model, EEG source localization is performed by solving the inverse problem. The forward head model is a biophysical model which describes the electrical distribution in the human head. When considering the propagation as the only way for the current distribution to move in the head, the focus is directed primarily on two parameters for having an accurate forward head model. These parameters are: the geometry of the head model and the conductivity value of each compartment of the head model. Due to the recent advances in computers and imaging techniques (like MRI and CT), it is possible to generate human head models that represent with a high accuracy the geometry of the real head. However, there is still an argument about the conductivity values and the method by which it should be estimated. In literature, the common values for conductivities come mostly from in-vitro experiments. In this work we are performing in-vivo conductivity estimation by considering the data of three epileptic patients. This data consists of MR images and CT scans for building a five-compartment FEM head model for each patient along with SEEG and EEG recordings that were acquired in simultaneous with intracerebral electrical stimulation (IES). The originality of this work lies in evaluating the performance of in-vivo conductivity estimation by EEG and/or SEEG measurements in function of different spatial parameters and locations of the IES. The following work consists of three major parts: the first part aims to determine the most robust optimization algorithm among common algorithms for optimizing the forward head model. The objective of the second part is to analyze the sensitivity of the conductivity values given different conditions on stimulation position, measurement positions and number of compartments. While in the final part, the conductivities of an isotropic and homogeneous five-compartment FEM head model were estimated with previously selected parameters for three drug-resistant epileptic patients. Finally the effect of changing the stimulation frequency on the estimated conductivities was determined.

Key words: Conductivity estimation, Forward problem, Intracerebral electrical stimulation, Propagation model, SEEG/EEG.

Table of Contents

List of Figures

List of Tables

Estimation de conductivités cérébrales in-vivo chez l'homme à partir de la stimulation électrique et de mesures EEG intracérébrales et de scalp: Résumé

La localisation de sources cérébrales est un problème inverse souvent mal posé [1]. Elle s'effectue à partir de mesures EEG/SEEG et un modèle de tête plus ou moins complexe qui dépend de la géométrie et des valeurs de conductivités de différents compartiments cérébraux. Des études récentes ont montré que des erreurs dans les valeurs de conductivités dans le modèle de tête conduisent à des erreurs non négligeables de localisation de sources [2, 3]. Les études actuelles de localisation de sources considèrent des valeurs de conductivités mesurées in-vitro chez l'homme ou chez l'animal [4, 3]. Or les conductivités différent in-vivo et in-vitro, mais également entre individus. Une méthode d'estimation des conductivités in-vivo est réalisée en optimisant les valeurs des conductivités en minimisant l'erreur entre les potentiels électriques mesurés lors d'un protocole de stimulation électrique cérébrale et les potentiels générés par le modèle pour cette même source exogène et parfaitement déterministe. Par conséquent, la géométrie du modèle de tête doit être le plus réaliste possible. La géométrie des différentes structures cérébrales peut être segmentée de l'IRM et du CT-scan de chaque patient. En effet les images IRM permettent de détecter les frontières entre les différents types de tissus mous. Les contours de la boite crânienne plus hautement résistive peuvent être segmentés plus précisément par les images générées par le scanner CT.

Les potentiels dans le modèle de tête réaliste peuvent être déterminés par des méthodes numériques de types BEM ou FEM [5]. La supériorité d'une méthode par rapport à l'autre est discutable selon le type d'application. Cependant, la méthode FEM peut être appliquée aux éléments volumétriques et les conductivités peuvent être soient homogènes soient inhomogènes et isotropes ou anisotropes. En plus de la géométrie, la source dans la tête réelle doit être déterminée afin d'être représentée par une source modélisée dans le modèle de tête. Or les sources physiologiques réelles sont d'une grande complexité selon les échelles spatiale et temporelle auxquelles on souhaite travailler. Du point de vue modélisation elles sont très souvent assimilées à des dipôles ponctuels spatialement. La source spécifiée dans le modèlede tête doit décrire les sources biophysiologiques du cerveau qui sont situées dans le cortex (ou la matière grise).

Une application clinique de la localisation de la source EEG est la localisation de la zone épileptogène chez les patients épileptiques. La crise d'épilepsie se caractérise par une activité paroxystique spontanée ou provoquée d'une population de neurones. Si l'origine de la crise appelée zone épileptogène est focale, le processus peut très vite se généraliser à d'autres structures cérébrales. Les électrodes de scalp telles que l'EEG mesurent l'activité cérébrale qui par son passage par la boite crânienne est atténuée. De plus l'EEG de surface peut être soumise à de nombreux artefacts tels que les artefacts musculaires, oculaires .... Lorsqu'il est nécessaire de localiser parfaitement la zone épileptogène dans des structures relativement profondes en vue d'une exérèse chirurgicale de l'origine de la crise, il est parfois nécessaire d'implanter des électrodes en intracérébrale : c'est la SEEG [6]. En plus d'estimer la zone épileptogène, les électrodes intracérébrales peuvent être utilisées comme générateur de courants entre deux plots successifs afin de stimuler certaines structures pour en déterminer leur fonctionnalité par excitation ou par inhibition de processus cérébraux. Les données acquises chez les patients épileptiques qui contiennent: images RM, images CT (pour déterminer les positions des électrodes intracérébrales), stimulation électrique intracérébrale (IES), en plus des enregistrements EEG et SEEG simultanés, fournissent pour cette étude de nouvelles possibilités qui n'ont pas été considérés dans des études précédentes pour l'estimation de la conductivité in-vivo en optimisant les conductivités du modèle direct.

Dans cette étude, l'estimation de la conductivité in-vivo en optimisant le modèle direct a été réalisée sur trois patients épileptiques pharmaco-résistants en considérant leurs mesures SEEG et EEG acquises en même temps que la stimulation intracérébrale effectuée à divers localisations spatiales. Les

mesures EEG et SEEG ont ensuite été comparées aux potentiels d'un modèle FEM de tête réaliste à cinq compartiments afin d'estimer la conductivité de ces différents milieux considérés isotrope et homogène: le scalp, le crâne, le liquide céphalorachidien (LCR), la matière grise (MG) et la substance blanche (SB). La procédure globale pour l'estimation de la conductivité in-vivo est montrée à la Figure 1. A notre connaissance, à ce jour, aucune étude n'a été faite sur l'estimation des conductivités in-vivo en considérant un modèle de tête FEM à cinq compartiments en plus des mesures EEG et SEEG acquises simultanément avec l'IES. Cette thèse traite de la précision des estimations des conductivités du modèle direct en fonction de la configuration et du conditionnement des mesures, de la localisation de la stimulation électrique.

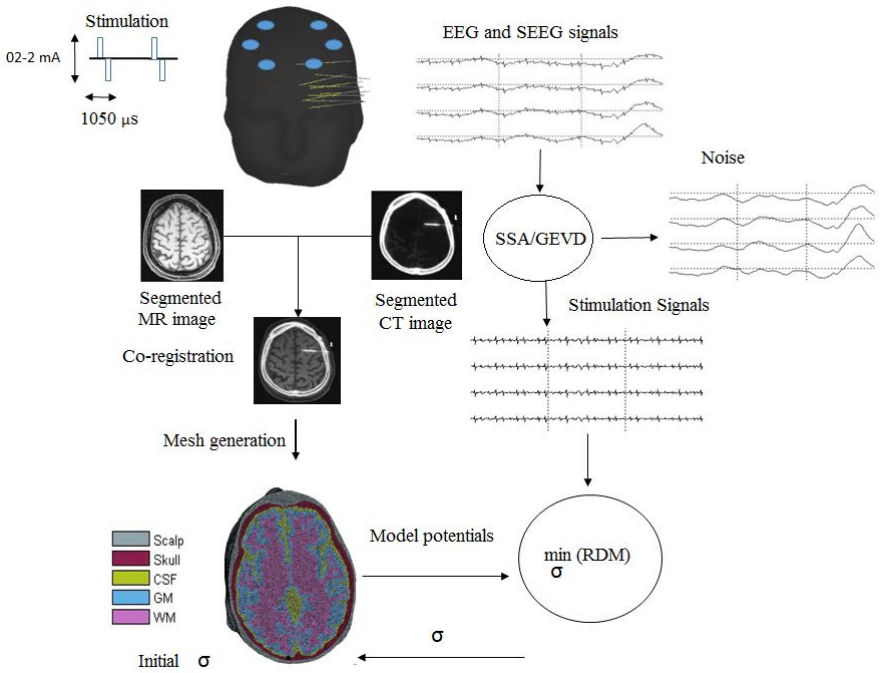

Figure 1: La procédure globale du traitement du signal et de l'image pour l'estimation de la conductivité in-vivo.

Introduction

Le premier chapitre de la thèse donne une brève introduction à l'anatomie du cerveau et à son électrophysiologie. Ensuite, les méthodes de localisation de la source EEG sont détaillées avec un intérêt particulier pour le

traitement des patients épileptiques pharmaco-résistants pour lesquels la réponse thérapeutique est la résection de la zone épileptogène. Après cela, les différents systèmes de mesure électrophysiologies (EEG, MEG, ECoG et SEEG) sont présentés, ainsi que des techniques d'imageries cérébrales (IRM, CT, PET et IRMf) et des techniques de stimulation (EIT, DBS, TMS et tDCS). Enfin, l'importance de l'attribution des valeurs de conductivités précises dans le modèle direct est décrite pour motiver l'objectif de la thèse.

Le cerveau humain peut être étudié à différentes échelles spatiales et temporelles comme le montre la Figure 2. La nature de l'étude détermine les résolutions temporelles et spatiales des mesures à prendre en compte, puis le cerveau et la tête sont modélisés en conséquence à ces résolutions spécifiques. Lors de la construction d'un modèle de tête, il existe un compromis entre la complexité de calcul et la précision, c'est-à-dire que le modèle doit être simple pour éviter les charges de calcul et aussi précis que possible. La Figure 3 montre les modèles les plus communs décrits dans la littérature. Dans le domaine de la localisation de source EEG et de l'estimation des conductivités, l'échelle temporelle considérée est l'échelle temporelle des signaux EEG d'environ une milliseconde et l'échelle spatiale est égale à la résolution des images IRM de 1-2 mm.

Modèles de tête

Le chapitre 2 montre le processus de modélisation de la tête en fonction de ces résolutions spatiale et temporelle ; l'hypothèse de propagation quasi-statique basée sur les équations de Maxwell est considérée parce que les fréquences des signaux sont inférieures à 1 kHz [8]. Compte tenu de l'hypothèse quasi statique, l'équation générale de la méthode des éléments finis a été dérivée compte tenu des définitions de la source (modèle dipolaire), de la géométrie et des valeurs de conductivités (isotropes et homogènes pour chaque compartiment). Ensuite, la génération de la géométrie du modèle de tête à cinq compartiments a été présentée. La robustesse de notre méthode de génération de la géométrie se base sur la similarité du nombre d'éléments et de sommets des modèles de tête générés des différents patients, comme indiqué dans le Tableau 1.

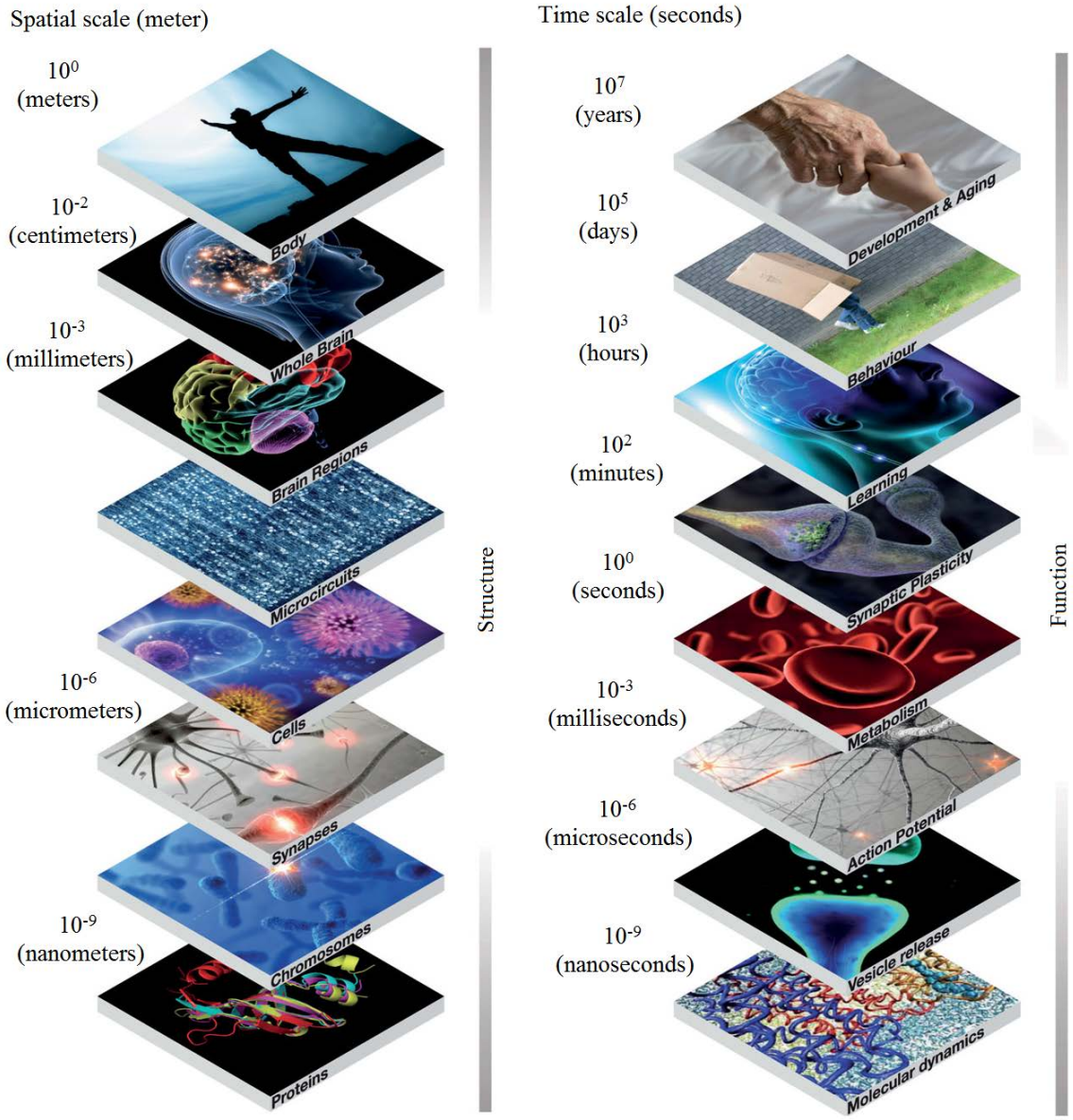

Figure 2: Les différentes échelles spatiales et temporelles considérées pour modéliser le cerveau humain [7].

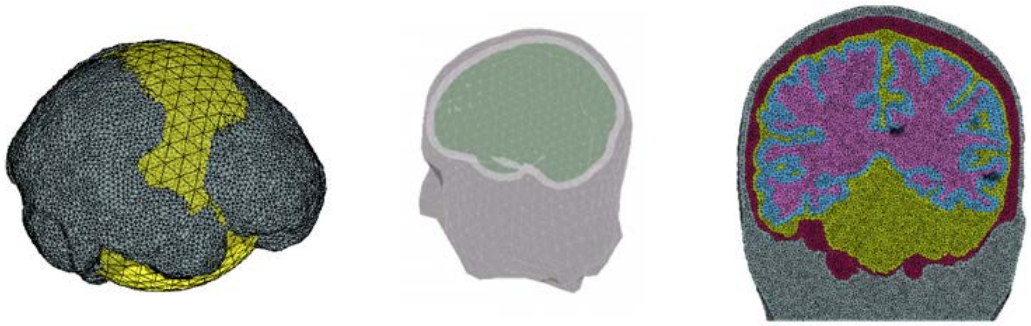

Figure 3: De gauche, un modèle de tête sphérique résolu analytiquement mais pas exactement, un modèle de tête réaliste représenté par des surfaces et résolu par BEM où les conductivités peuvent seulement être isotrope et homogènes et un modèle de tête réaliste représenté par des éléments volumétriques et résolu par FEM où les conductivités peut être soit homogène soit inhomogène, isotrope ou anisotrope.

Table 1: Le nombre d'éléments et de sommets obtenus dans un modèle FEM pour chaque patient épileptique.

Tissu	Nombre de	Patient(1)	Patient(2)	Patient(3)
Scalp	Eléments	1763818	1766024	1793602
	Sommets	304777	305203	310251
Crâne	Eléments	669167	679459	716531
	Sommets	129580	131348	137640
LCR	Eléments	719507	727154	726315
	Sommets	149420	151160	150933
MG	Eléments	676420	678839	661217
	Sommets	154534	155142	152073
SB	Eléments	713401	697771	707475
	Sommets	137163	134560	136130

Comparaison de méthode d'optimisation pour estimation des conductivités in-vivo

L'estimation de la conductivité in-vivo dépend de l'estimation des valeurs de conductivités dans le modèle de la tête en fonction des potentiels réels. Ce processus s'appuie sur des algorithmes d'optimisation qui minimisent l'erreur d'estimation entre les valeurs de conductivité dans le modèle de tête afin de réduire l'erreur entre les potentiels réels et les potentiels du modèle. Par conséquent, le choix d'un algorithme d'optimisation robuste pour l'estimation de la conductivité in-vivo est essentiel. Dans la littérature, de nombreux algorithmes d'optimisation ont été considérés pour l'estimation des conductivités [9, 10, 11, 12, 13, 14, 15]. Dans cette étude, la méthode numérique FEM a été considérée pour déterminer les potentiels de sortie dans le modèle de tête réaliste. Etant donné que la méthode FEM ne peut être résolue analytiquement, l'accent a été mis sur les algorithmes d'optimisation à dérivation libre. Le Chapitre 3 présente une méthode pour comparer trois algorithmes différents d'optimisation de dérivés libres: le simplex de Nelder-Mead, l'algorithme génétique et le simulating annealing. Ces algorithmes ont été considérés car ils sont faciles à mettre en œuvre et relativement communs. De plus, ces algorithmes d'optimisation ont été testés ou recommandés dans des études antérieures sur l'estimation de la conductivité in-vivo. En général, les algorithmes d'optimisation sont testés à partir de différents points initiaux (procédure multistart) pour s'assurer que la performance de l'algorithme d'optimisation est indépendante du choix des conditions initiales. En plus de la procédure multi-start, cette étude a testé les algorithmes d'optimisation avec différentes mesures, différentes positions de stimulation et en considérant du bruit gaussien blanc additif ou du bruit à structure physiologique. Dans tous ces scénarios, les performances des algorithmes Nelder-Mead simplex ont surpassé les performances des deux autres algorithmes en termes de convergence et de temps. De plus, le simplex de Nelder-Mead a donné des résultats robustes lorsque du bruit à structure électro physiologique réel a été ajouté aux potentiels. Cette performance de Nelder-Mead simplex a conduit à être considéré en analyse réelle pour estimer les conductivités in-vivo.

L'estimation de la conductivité in-vivo dépend de la minimisation de l'erreur entre les potentiels du modèle direct et les potentiels réels en itérant les valeurs des conductivités dans le modèle direct. Afin d'avoir une estimation robuste des conductivités in-vivo, la fonction d'erreur doit être sensible aux variations des valeurs de conductivité assignées dans le modèle de tête

direct. Par conséquent, il est essentiel d'effectuer une analyse pour mesurer la sensibilité de la fonction d'erreur en fonction des valeurs de conductivité avant d'effectuer une estimation réelle de la conductivité in-vivo.

Analyse de Sensibilité

Dans le Chapitre 4, une analyse de sensibilité a été réalisée en considérant deux fonctions d'erreur différentes: l'erreur relative et le RDM [16] comme le montre l'Equation 1. En comparant les fonctions d'erreur, il a été montré à partir des résultats que la fonction d'erreur commune dans le domaine du modèle de tête humaine, qui est le RDM, donnait un modèle de sensibilité plus adapté que le modèle de sensibilité de l'erreur relative. De plus, l'analyse de sensibilité a été effectuée compte tenu des différentes positions de stimulation et des différentes positions de mesure et du nombre de mesures en profondeur et en surface. Les positions de stimulation ont été classées en fonction de leur distance de scalp en tant que stimulations profondes, intermédiaires et latérales. Il était évident à partir des résultats que le changement de la distance de la stimulation du scalp change les résultats de sensibilité. De plus, différentes positions de stimulations ayant une profondeur similaire conduisent à une analyse de sensibilité différente comme cela a été noté à partir des résultats de lateral1 et latéral2. La différence entre les résultats de lateral1 et latéral2 peut être expliquée par la différence de l'orientation des dipôles de stimulation qui attache une importance à l'anisotropie du modèle de la tête, ou elle peut s'expliquer par la différence des tissus dans ces positions qui présente une importance à l'inhomogénéité du modèle de tête. En changeant les positions de mesure, on a trouvé que la fonction d'erreur, en général, est plus sensible à la conductivité du scalp et à la boite crânienne lorsqu'on considère les potentiels EEG du scalp. Cela confirme l'importance des mesures EEG du scalp pour estimer les conductivités du scalp et les conductivités de la boite crânienne comme le montre la Figure 4. Il a été montré dans ce chapitre que les résultats sont similaires pour deux patients différents, et que négliger les électrodes les plus éloignées de la stimulation notamment va pas modifier considérablement les résultats. De plus, la différence entre le modèle de tête à trois compartiments et le modèle de tête à cinq compartiments montre qu'il existe une dépendance entre les valeurs de conductivité. En général, il ressort de cette analyse que l'estimation des conductivités invivo dépend de la position de la stimulation, du nombre de compartiments et du nombre d'électrodes de mesure, donc pour que l'étude ait des résultats non biaisés, plus d'une position dipolaire devrait être pris en compte pour l'estimation de la conductivité, et les conductivités obtenues devraient être

assignées dans le modèle de tête avec le même nombre de compartiments.

$$RDM = \sqrt{\sum \left(\frac{V_1}{||V_1||_2} - \frac{V_2}{||V_2||_2} \right)^2}, \quad V : Potentiels \tag{1}$$

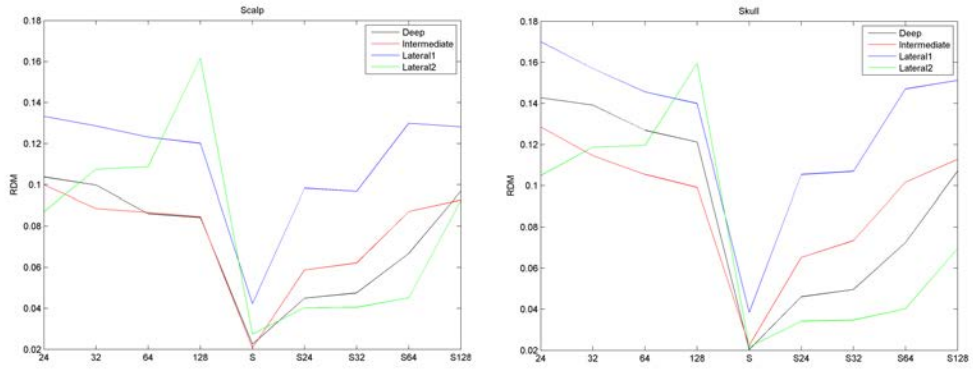

Figure 4: Effet l'attribution d'une valeur de conductivité du scalp erronée (à gauche) et d'une valeur de conductivité du crâne erronée (à droite) sur le RDM de sortie en fonction de différentes mesures.

Estimation des conductivités in-vivo

Au chapitre 5, l'estimation des conductivités in-vivo en optimisant le modèle de tête direct a été réalisée en comparant les potentiels réels (SEEG / EEG) avec les potentiels du modèle, puis en estimant les conductivités assignées dans le modèle de tête jusqu'à ce que l'erreur entre les potentiels du modèle et les potentiels réels atteignent leur valeur minimale. Dans cette étude, le modèle de tête a été supposé isotrope et homogène et contient cinq compartiments (scalp, crâne, LCR, MG et SB). L'estimation des conductivités in-vivo a été réalisée pour trois patients épileptiques pharmaco-résistants différents où les IES ont été classés en trois classes en fonction de leur profondeur: profonde, intermédiaire et latérale. En général, les conductivités estimées dans cette étude se situaient dans la gamme des conductivités que l'on trouve dans la littérature. Sans validation possible car les conductivités des 5 compartiments pour les deux patients ne sont pas connues. La grande difficulté ici est de trouver un critère qui valide les estimations car nous travaillons sans 'golden standard' si ce n'est les valeurs publiées dans la littérature. Nous avons choisi les écarts types des estimations des conductivités obtenus respectivement pour les différentes

localisations des stimulations. En effet, les écarts-types permettent d'évaluer la stabilité des estimations pour plusieurs fichiers de mesures. En fonction des conditionnements et de la localisation de la stimulation les écarts-types varient beaucoup. Les résultats montrent que les estimations sont moins dispersées pour les conductivités des compartiments les plus proches de la stimulation. Ce qui était plus ou moins attendu. En effet par exemple les estimations des conductivités de la boite crânienne et du scalp sont beaucoup moins dispersées et beaucoup plus proche des valeurs de la littérature lorsque la stimulation est latérale. Ceci est d'autant plus vrai lorsque on utilise les données SEEG/ EEG synchrones. En dehors de la variance élevée et de la différence basée sur les mesures et les patients, des conclusions générales peuvent être tirées de cette étude: 1) La conductivité du crâne est plus faible et plus proche des valeurs de la littérature lorsqu'on considère les mesures EEG du scalp avec la SEEG ou EEG seule que lorsqu'on considère la mesure SEEG uniquement. 2) L'écart-type de la conductivité estimée est plus faible lorsque la stimulation est plus proche des compartiments pour lesquels on estime les conductivités. De manière similaire à l'analyse de sensibilité, le fait de négliger les mesures des électrodes les plus éloignées n'a pas modifié de façon notable le résultat de l'estimation de la conductivité. On peut donc restreindre les mesures à injecter dans l'estimateur à la sphère centrée sur la stimulation et d'un de rayon de 50mm. Ce qui signifie que les mesures les plus éloigner n'apportent pas d'information car elles sont suffisamment faibles énergétiquement.

L'équation de Poisson, sur laquelle repose l'estimation de la conductivité in-vivo, dépend de la condition de propagation quasi-statique, ce qui signifie que la conductivité des tissus n'est pas dépendante de la fréquence. Cependant, il y a quelques études qui ont montré que les conductivités estimées dépendraient de la fréquence [17, 18]. En toute fin du chapitre résultats, nous nous sommes intéressés à la décomposition fréquentielle de la stimulation. En effet si le fondamental de la stimulation périodique est à 55Hz, la stimulation par des pulses génère des harmoniques. Nous avons donc filtré les mesures et donc élimination des activités physiologiques pour ne conserver qu'une composante harmonique et cela pour les deux premières harmoniques des décompositions de la stimulation. Les résultats de cette étude montrent qu'il y a un changement dans les conductivités estimées moyenne en fonction des fréquences des harmoniques, cependant, la variance des estimations est également élevée. Il est donc difficile de conclure avec précision sur l'influence de la fréquence sur l'estimation des conductivités. De plus il est possible que l'effet capacitif entre les électrodes de stimulation et le milieu cérébral joue un rôle non négligeable.

Conclusion

Cette thèse a introduit l'estimation de la conductivité in-vivo en optimisant le modèle de la tête avec une méthodologie relativement innovante. Les matériaux considérés comprenaient les enregistrements SEEG et EEG simultanés de stimulations électriques intracérébrales. En dehors de l'introduction, quatre sujets principaux ont été couverts dans ceux-ci. La première partie présentait la génération d'un modèle de tête FEM homogène et isotrope à cinq compartiments (scalp, crne, LCR, MG et SB) segmentées à partir du CT et de l'IRM d'un patient épileptique. Nous avons choisi d'affiner le modèle en cinq compartiments anatomiques alors que d'autres études en localisation de source ont considéré un modèle sphérique ou un nombre de compartiments inférieur. Evidemment, notre modèle est très complexe mais en plus de l'estimation des conductivités, notre objectif était de calculer la sensibilité du modèle vis à vis de ses paramètres telles que la position de la stimulation. La deuxième partie a effectué une comparaison entre les algorithmes d'optimisation communs afin d'optimiser le modèle de tête. La troisième partie a analysé la sensibilité des potentiels par les conductivités avec les différentes conditions de la position de stimulation, les positions de mesure et le nombre de compartiments dans le modèle de tête. Alors que la quatrième partie a fourni des résultats des conductivités in-vivo basés sur les conditions qui ont été appliquées dans l'analyse de sensibilité.

Pour résumer, les points majeurs que nous avons abordés sont donc:

- Le simplex de Nelder-Mead est le plus robuste parmi les algorithmes choisis pour estimer les conductivités dans un modèle de tête FEM.
- Les mesures EEG de surfaces sont importantes pour estimer le scalp et le crâne, tandis que les mesures SEEG sont importantes pour estimer les conductivités des structures profondes.
- L'estimation des conductivités d'un compartiment en optimisant le modèle de la tête dépend fortement de la position de stimulation et des positions des mesures. Mais en, général, les écarts types des valeurs des conductivités sont beaucoup plus réduits quand la stimulation est proche du compartiment considéré.

Bibliographie

[1] Gildas Marin, Christophe Guerin, Sylvain Baillet, Line Garnero and Gérard Meunier. *Influence of skull anisotropy for the forward and in-*

verse problem in EEG: simulation studies using FEM on realistic head models. Human brain mapping, 6(4):250–269, 1998.

[2] B Neil Cuffin. *Eccentric spheres models of the head*. IEEE transactions on biomedical engineering, 38(9):871–878, 1991.

[3] Zeynep Akalin Acar and Scott Makeig. *Effects of forward model errors on EEG source localization*. Brain topography, 26(3):378–396, 2013.

[4] Chris Plummer, A Simon Harvey and Mark Cook. *EEG source localization in focal epilepsy: where are we now?*. Epilepsia, 49(2):201–218, 2008.

[5] Hans Hallez, Bart Vanrumste, Roberta Grech, Joseph Muscat, Wim De Clercq, Anneleen Vergult, Yves D'Asseler, Kenneth P Camilleri, Simon G Fabri, Sabine Van Huffel and others. *Review on solving the forward problem in EEG source analysis*. Journal of neuroengineering and rehabilitation, 4(1):1, 2007.

[6] I. Merlet, and J. Gotman. *The future of human cerebral cartography: a novel approach*. Clinical neurophysiology, 112(3):414–430, 2001.

[7] Richard Frackowiak and Henry Markram. *Dipole modeling of scalp electroencephalogram epileptic discharges: correlation with intracerebral fields*. Philosophical Transactions of the Royal Society B, 370(1668), 2015.

[8] Paul L Nunez and Ramesh Srinivasan. *Electric fields of the brain: the neurophysics of EEG*. Oxford University Press, USA, 2006.

[9] Zeynep Akalin Acar, Can E Acar and Scott Makeig. *Simultaneous head tissue conductivity and EEG source location estimation*. NeuroImage, 124:168–180, 2016.

[10] Seok Lew, Carsten H Wolters, Alfred Anwander, Scott Makeig and Rob S MacLeod. *Improved EEG source analysis using low-resolution conductivity estimation in a four-compartment finite element head model*. Human brain mapping, 30(9):2862–2878, 2009.

[11] Saburo Homma, Toshimitsu Musha, Yoshio Nakajima, Yoshiwo Okamoto, Sigge Blom, Roland Flink and Karl-Erik Hagbarth. *Conductivity ratios of the scalp-skull-brain head model in estimating equivalent dipole sources in human brain*. Neuroscience research, 22(1):51–55, 1995.

[12] Sónia I Gonçalves, Jan C de Munck, Jeroen PA Verbunt, Fetsje Bijma, Rob M Heethaar and F Lopes da Silva. *In vivo measurement of the brain*

and skull resistivities using an EIT-based method and realistic models for the head. IEEE Transactions on Biomedical Engineering, 50(6):754–767, 2003.

[13] Yingchun Zhang, Wim Van Drongelen, Bin He. *Estimation of in vivo brain-to-skull conductivity ratio in humans*. Applied physics letters, 89(22), 2006.

[14] Y Lai and W Van Drongelen, L Ding, KE Hecox, VL Towle, DM Frim, B He. *Estimation of in vivo human brain-to-skull conductivity ratio from simultaneous extra-and intra-cranial electrical potential recordings*. Clinical neurophysiology, 116(2):456–465, 2005.

[15] Thomas C Ferree, K Jeffrey Eriksen and Don M Tucker. *Regional head tissue conductivity estimation for improved EEG analysis*. IEEE Transactions on Biomedical Engineering, 47(12):1584–1592, 2000.

[16] Jan WH Meijs, Onno W Weier, Maria J Peters, Ardiaan Van Oosterom. *On the numerical accuracy of the boundary element method (EEG application)*. IEEE Transactions on Biomedical Engineering, 36(10):1038–1049, 1989.

[17] Juhani Dabek, Konstantina Kalogianni, Edwin Rotgans, Frans CT van der Helm, Gert Kwakkel, Erwin EH van Wegen, Andreas Daffertshofer and Jan C de Munck. *Determination of head conductivity frequency response in vivo with optimized EIT-EEG*. NeuroImage, 2015.

[18] LA Geddes and LE Baker. *The specific resistance of biological material - A compendium of data for the biomedical engineer and physiologist*. Medical and biological engineering, 5(3):271–293, 1967.

Glossaries

BEM: Boundary element method.
CSF: Cerebrospinal fluid.
CT: Computed tomography.
DBS: Deep brain stimulation.
ECG: Electrocardiography.
ECoG: Electrocorticography.
EEG: Electroencephalography.
EIT: Electrical impedance tomography.
FDM: Finite difference method.
FEM: Finite element method.
fMRI: Functional magnetic resonance imaging.
GA: Genetic algorithm.
GM: Gray matter.
IES: Intracerebral electrical stimulation.
MEG: Magnetoencephalography.
MRF: Markov random field.
MRI: Magnetic resonance imaging.
NMS: Nelder-Mead simplex.
PET: Positron-emission tomography.
RDM: Relative difference measurement.
SA: Simulating annealing.
SEEG: Stereoelectroencephalography.
SQUID: Superconducting quantum interference devices.
tACS: Transcranial alternating current stimulation.
tCS: Transcranial current stimulation.
tDCS: Transcranial direct current stimulation.
TMS: Transcranial magnetic stimulation.
tRNS: Transcranial random noise stimulation.
WM: White matter.
WHO: World health organization.

Chapter 1

Introduction

The human brain is believed to be the most complex structure in the universe. It contains billions of neurons in a small volume, where each neuron has thousands of connections. The research in human brain has faced a fast progress in the last 20 years thanks to the evolution of the brain imaging techniques (like the MRI, PET, ... etc.), in addition to the development of algorithms for processing the recorded brain signals (like EEG, MEG, ... etc.). The development of these technologies and methods had opened the door wide for researchers to start new studies related to the brain. One example of brain studies is the brain-computer interface (BCI) in which the acquired brain signals are interpreted by computer algorithms in order to translate the human thoughts into actions. Even though the main purpose for BCI is producing systems that can facilitate the life of the disabled patients, it is still hard to move the BCI systems out of the laboratory in most cases because such systems are not consistent to work with all the subjects, and because the performance of the BCI systems fluctuate over time [1]. Another research that has been evolved is the localization of brain sources. In this research the regions of the brain that are responsible of specific tasks are localized. There are different measurements that are considered for source localization, however, one major problem is the lack of a non-invasive measurement which provides both high temporal and spatial resolution of the brain [2]. The above mentioned studies are just two examples of the huge number of researches that are related to the brain which have been evolved since the invention of the non-invasive measurement techniques.

The brain can be described briefly as the central part of the nervous system from where it controls most of the actions overall the body. The largest part of the brain in which most of actions, thoughts and senses are processed is called the *cerebrum*. The cerebrum is divided into two

hemispheres and each hemisphere consists of four different sections (or lobes) as shown in Fig.1.1. These lobes are: The frontal, the parietal, the occipital and the temporal lobe. Each of these lobes has its own functions. The other two parts of the brain are the *cerebellum* which coordinates the movements and preserved the balance of the body, and the *brainstem* which connects the spinal cord with the other parts of the brain.

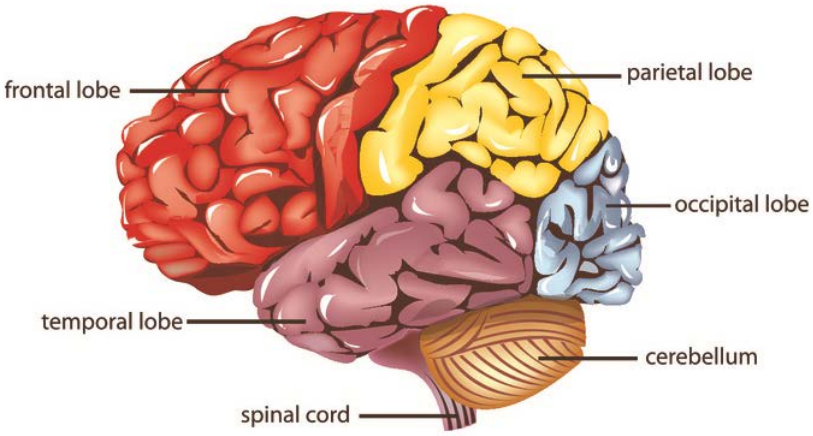

Figure 1.1: The human brain consists of: The cerebrum (which is divided into four lobes), the cerebellum and the spinal cord [3].

In human brain there are around 100 billion neuron cells. Each cell, as shown in Fig.1.2, consists of a cell body (or a *soma*), *dendrites* and an *axon*. The dendrites act as receivers of information while the axon acts as a transmitter. The movement of information occurs due to the movement of the K^+ and Na^+ ions in one neuron and from one neuron to another, and this movement of ions generates potentials. There are two kinds of potentials that are generated in the neurons of the brain: The *post-synaptic potentials* and the *action potentials*. The post-synaptic potentials are the potentials that are received by the dendrites of one neuron from the axon terminals of another neuron. The name of the post-synaptic potential comes from the *synapse* which forms the junction between the axon terminals of one cell and the dendrites of another cell. While the action potentials are the potentials that are spiked by a neuron cell through its axon as a result of the accumulating post-synaptic potentials which exceed a threshold known by the soma of the neuron.

The movement of ions synchronously in a relatively large area (around

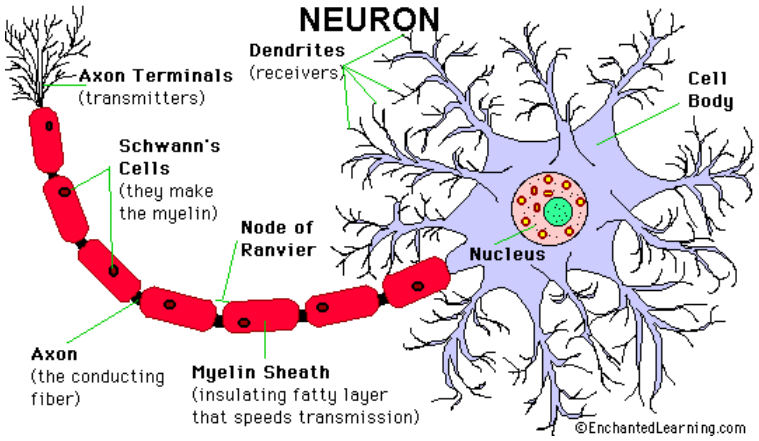

Figure 1.2: The neuron in the human brain [4].

$6^2 cm$ [5]) of the brain generates *primary currents*. These primary currents are mostly due to the post-synaptic potentials that move in well oriented dendritics axes of *pyramidal cells*, and not due to the action potentials that move in varied oriented neocortical axons [5]. The reflection of these primary currents, as *return currents*, at the scalp surface generates a potential difference which can be measured by scalp electrodes as shown in Fig.1.3. In addition, a magnetic flux is generated from both the primary currents and the return currents. This magnetic flux can be measured by special coils placed around the head known as *SQUID* (Superconducting QUantum Interface Device). The measurement of the scalp potentials by electrodes is known as the electroencephalography (EEG), while the measurement of the magnetic flux by the SQUID is known as the magnetoencephalography (MEG) [6].

Since the discovery of EEG signal recordings (which appeared before MEG) the interest in determining the location of the acquired signals have appeared as a special field of research known as electroencephalography (EEG) source localization [8]. Source localization is mainly considered in clinical applications for localizing the origin of the brain disease [9], but it is also applied in other applications like the brain-computer interface in order to reduce the recording sites for such systems [10]. However, one of the main challenges that EEG source localization faces is the lack of precise knowledge of the regions' conductivities through which the electric field propagates to reach the recording electrodes. In the literature, it was found that assigning erroneous conductivity values lead to localization errors of more than 30 mm [11, 12]. Given that one cubic millimeter of human necortex contains around

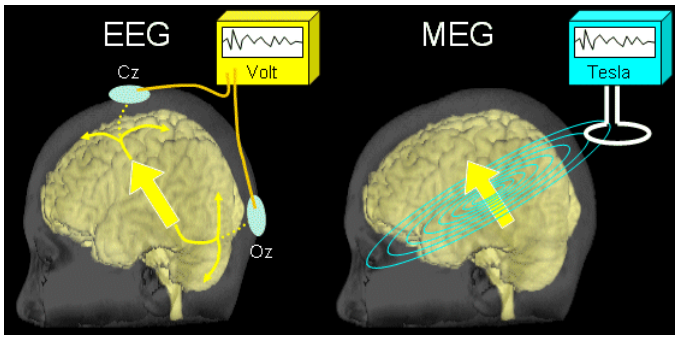

Figure 1.3: The wide arrow represents the primary current while the narrow arrows (to the left) represent the secondary currents. The secondary currents are measured by EEG (to the left) and the magnetic field of the primary currents are measured by MEG (to the right) [7].

10^5 neurons and 10^9 synapse [9], this 30 mm error cannot be neglected. In this chapter, we introduces source localization, then we describe the epilepsy as a common clinical application for source localization, after that we introduce some of the common techniques that are considered in the literature for source localization and conductivity estimation. Finally, we discuss the importance of having accurate conductivity values in source localization.

1.1 EEG Source Localization

EEG source localization is a research field that aims to determine the location of electric current sources from their resulted potentials. For performing EEG source localization, two fundamental problems should be solved: The forward problem and the inverse problem. The forward problem is solved by defining a number of specifications (the shape, the number of compartments and the conductivity values) in the volume conduction model or the head model. The solution of the forward problem determines the potentials at the recording electrodes which are resulted from the propagation of the electric field from a given source through the different compartments. In the inverse problem the recorded potentials are given, and it is required to know the location of the generating source. The inverse problem is an ill-posed problem since an infinite number of source permutations can give the same potential distribution, and because the solution has a high sensitivity to the noisy data [13]. However, the inverse problem can be solved by adding some constrains to the problem related to the sources which are represented by current dipoles. These constrains could be fixed by limiting the number of

sources or assuming that one or more of the dipoles' parameters (position, moment and orientation) is/are known or fixed [14].

The forward model is a biophysical model linking the sources with the generated potentials. It forms an essential factor for solving the inverse problem, however, acquiring the information about the parameters of the forward head model is very complicated since the head compartments are anatomically complex, inhomogeneous and non-isotropic. Also the neuroscience techniques, which provides such information, differ in their temporal and spatial resolution. Moreover, each research has a different view of the brain, for example, in connectivity studies the propagation occurs through the axons while in conductivity estimation studies, the propagation of the electrical and magnetic field takes place in every direction from the sources to the electrodes. In addition, brain sources are complex to model due to their temporal dynamics and organizations. Yet, by considering the quasi-static assumption (when the frequency of the acquired signals is less than 1 kHz) [5], the problem of modeling the human head is reduced to depend only on two important parameters: The geometry of the head model, and the conductivity of each compartment of the head model.

Due to the availability of the MRI, nowadays most of the research depends on accurate realistic head models instead of considering simple spherical models. Unlike the spherical head model in which the potentials can be solved analytically, the numerical Boundary Element Method (BEM), Finite Element Method (FEM) and Finite Difference Method (FDM) are considered to determine the potentials in the realistic head models. With the development of realistic geometries, the forward model is believed to reach a mature stage in terms of geometry. Unlike the geometry of the forward model which has reached a well-developed stage, the considered conductivity values in recent work [9, 12] come from studies that were performed around 50 years ago, like the common study of Geddes and Baker [15]. Most of the common conductivity values that are considered in recent researches are coming from in-vitro conductivity estimation studies. However, the fact that the properties of the tissues change after being removed from their environment [16] urges the researchers to perform new studies for estimating the human conductivities in-vivo.

1.2 Epilepsy

According to the World Health Organization (WHO), epilepsy is defined as: "A chronic disorder characterized by recurrent seizures, which may vary from a brief lapse of attention or muscle jerks to severe and prolonged convulsions" [17]. Epileptic seizures are divided into two categories: The first is the partial or focal seizures which originate in circumscribed part of the brain. The second category is the generalized seizures where the discharge involves bilaterally and synchronously the two hemispheres or the entire gray matter. Partial seizures are divided into two parts: Simple, in which the memory and the awareness are not affected, and complex in which the memory and the awareness are affected before, during or immediately after the seizure.

In order to perform an efficient treatment of epilepsy, an accurate diagnosis of epilepsy should be done. Diagnosis gives information about weather the patient has really an epileptic seizures and what kind of epilepsy he/she has. The diagnosis of epilepsy takes many forms; like questions to the patient about the seizures and the effect of seizures on him/her, physical exams, measuring EEG and MEG, producing MRI and PET for the brain of the candidate, in addition to genetic testing [18]. WHO found that 70% of the epilepsy patients can be treated by inexpensive daily drugs. These drugs are not taken forever, after 2 to 5 years of being seizure-free, the patient can reduce his/her consumption of drugs. However there are still a percentage of patients who respond poorly to drug treatments, for such patients the only option is the surgical treatment where the epileptic tissue is removed [17]. In order to remove the epileptogenic zone, it is important to locate it precisely before the surgery in order to avoid affecting other neurons.

Seizures distinguishes epilepsy from the other brain diseases since seizures can be detected by electric or magnetic sensors. Even though non-invasive scalp EEG electrodes are being considered to give a general information about the position of the epileptogenic zone (like its position in the right or the left hemisphere), it is still necessary to implement intracerebral electrodes for performing a precise localization of the origin of the epileptic seizure activity [19]. Moreover, the electrical stimulation which is generated by the implanted intracerebral electrodes in a specific region helps to detect the function of that region before performing a resection surgery [18]. However, the intracerebral electrodes are expensive and implanting them requires a surgery. In addition, the acquired signals from intracerebral electrodes are limited in spatial sampling [20]. In order to avoid the surgery that is re-

quired for implanting the intracerebral electrodes, it is important to enhance the EEG source localization which depends on building a head model with accurate conductivity values.

1.3 Electrophysiological Measurements

The electrical properties of the biological cells are studied in a domain called *electrophysiology*. In the human body it is common to study the electrophysiology of the heart and the brain. The current study is related to the electrophysiology of the human brain which can be measured in-vivo in various ways. In this study, in-vivo conductivity estimation was based on the acquired EEG and SEEG signals which are common electrophysiological measurements. This section introduces EEG and SEEG measurements that are considered in this research for in-vivo conductivity estimation. In addition, for the purpose of comparison, it introduces MEG and ECoG measurements which are considered in literature for in-vivo conductivity estimation and source localization.

1.3.1 Electroencephalography

The electroencephalogram (EEG) is the measurement of electric potential differences on the scalp resulted from the return currents at the scalp surface, as shown in Fig.1.3. EEG measurements have started since the discovery of Hans Berger (1929) about the ability to measure brain potentials by surface electrodes connected to the scalp [21]. Currently, EEG measurements become very popular in both research and clinics. In addition to be a way for detecting the deepness of sleep by the alpha rhythms [5], EEG signals are considered as one of the most important measurements for diagnosis neurological diseases such as brain tumor [22], Alzheimer [23] and epilepsy [24]. Moreover, it is considered in other applications like the Brain-Computer Interface [25]. EEG is famous due to its simplicity, low cost and high temporal resolution (around 1 millisecond [26]). However, the spatial resolution of EEG is low (around 100 mm [26]). This low spatial resolution is due to the fact that EEG are acquired from the surface of the head. However, the spatial resolution can be enhanced by increasing the number of electrodes that covers the head or by applying other techniques like the surface Laplacian method [27]. In addition to its low spatial resolution, EEG measurements have another disadvantage of being prone to noise and artifacts. These artifacts have many sources like the power supply frequency, the movement of the subject or the patient, the eye blinks

and even the heart pulses (ECG). Many of the artifacts can be detected by observation so the trails which have such artifacts like the epilpetic seizures are eliminated because they cannot be processed. However, other artifacts like the eye movements can be removed from the data segments by methods like the auto-regression, the principal component analysis and the independent component analysis [28, 29].

In order to be able to compare the EEG measurements that are acquired at different times or from different subjects, an international standard has been defined for placing the EEG electrodes on the scalp, this standard is known as the 10-20 system [30]. In the 10-20 system the nasion (the front of the skull), the inion (the back of the skull), the left preauricular and the right preauricular act as landmarks of the skull. The distance between the nasion and the inion, and the distance between the right and the left preauricular (passing through the top of the skull) are divided into 10% and 20% of the total distance representing the interelectrode distances as shown in Fig.1.4. For this reason the system is called the 10-20 system. In the 10-20 system, the letters C,F, Fp, O, P and T stand for Central, Frontal, Fronto-polar, Occipital, Parietal, and Temporal respectively. The electrodes with even numbers are placed in the right hemisphere, whereas, those with odd numbers are placed on the left hemisphere, and the electrodes with the letter z are placed on the mid-line of the skull. Moreover, there are two auricular electrodes that are placed on the earlobes. An extension to the 10-20 system was found by placing the electrodes AF in the middle between the electrodes F and Fp, FC between F and C, FT between F and T, CP between C and P, TP between T and P and PO between P and O. This extension which is shown in Fig.1.5, is known as the 10-10 system. Other extensions are also found in the literature [31].

Recording the EEG potentials can be performed by a bipolar montage in which a differential potential between two electrodes is recorded. Another well-known montage is the referential montage where one cephalic electrode acts as a common reference for all the other electrodes. Cephalic electrodes are usually chosen to be the nasion, the inion, the occipital area or the pre-auricular points. Moreover, the common reference can be non-cephalic like the average reference montage which is based on the assumption that the sum of the potentials in the brain is equal to zero. [32, 33]. The conventional clinical bandwidth of the EEG potentials ranges from under 1 Hz to 50 Hz [34]. In this bandwidth some EEG signals are labelled according to the frequency as shown in Table 1.1. Even though these waves are common in the EEG field, there are other waves that could be found in these ranges of

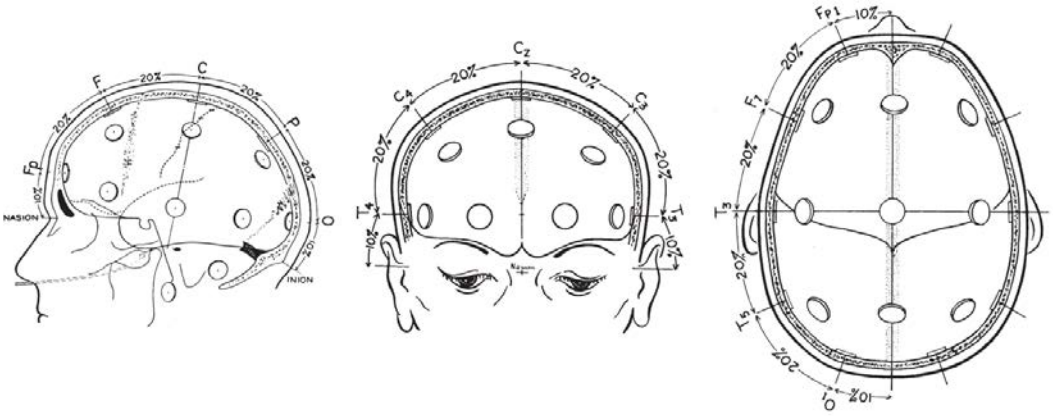

Figure 1.4: From the left: Lateral, frontal, and superior view of the head showing the way of determining the electrodes placement [30].

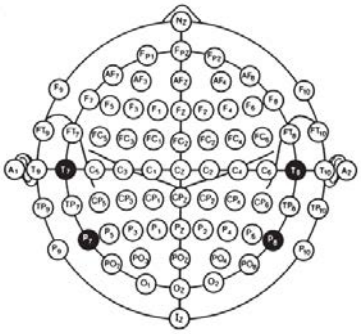

Figure 1.5: A single plane projection of the head showing the electrodes' positions in the 10-10 system. The dark electrodes T7, T8, P7 and P8 have the names T3, T4, T5 and T6 respectively in the 10-20 system [30]

Table 1.1: Some examples of the EEG waves that are classified according to their frequencies and their corresponding states in adults [5, 34]

Wave name	Frequency	State
Delta	1-4 Hz	Deep sleep.
Theta	4-8 Hz	Sleep.
Alpha	8-13 Hz	Relaxing state with closed eyes.
Beta	13-30 Hz	Consciousness state.
Gamma	$\geq$ 30 Hz	Hyper-brain activity.

frequency like the epilepsy seizures which occupy the frequency bands below the 40 Hz [35]. In addition other evoked potentials could be found in these frequency ranges depending on the application like the steady state visually evoked potentials. Because the EEG signals have a low bandwidth, it is possible to record these signals with devices which have a low sampling rate like 256 or 512 sample/second. However, some studies have recorded EEG activity above the 50 Hz [36]. Sampling rate of the recorded EEG signals can goes up to 1024 sample/second which makes it have a high temporal resolution, however, it spatial resolution is limited by the number of the electrodes.

1.3.2 Magnetoencephalography

The Magnetoencephalography (MEG) is the measurement of the magnetic flux which is generated according to the right hand rule from the net effect of the ionic currents (represented by primary currents) and their returns from the surface of the scalp (represented by return currents) as shown in Fig.1.3 [6]. Unlike the low-cost EEG recordings, MEG requires costly sensitive devices known as superconducting quantum interference devices or SQUID for short. Moreover, the MEG measuring system should be installed in a magnetically shielded room. MEG signals are insensitive to radial sources [37] and to the change in conductivity between the different compartments of the head. However, they are sensitive to the tangential and superficial sources [38, 37]. As EEG, MEG is applied in Brain-Computer Interface [39], detection of Alzheimer [40] and epilepsy [41].

Because MEG is less sensitive than EEG to the conductivities of the head and especially the skull and the scalp [42] it cannot be considered alone for in-vivo conductivity estimation but as an additional measurement to the EEG [43]. However, MEG is common in source localization because it is

not affected by the high resistive skull compartment, so it can give more accurate results. Nevertheless, because MEG cannot detect the deep and radial sources, it was recently considered as an additional measurement to EEG for enhancing source localization [37, 44].

1.3.3 Stereo-electroencephalography

The Stereo-electroencephalograhy (SEEG) measurements are recorded from electrodes that are implanted inside the brain. Implanting SEEG electrodes requires a special surgery. Due to this, SEEG recording is not performed for healthy subjects but for patients [45]. As EEG, SEEG has a high temporal resolution (around 1 millisecond [46]) and measures the potential difference due to the return current at the different compartments. However, the SEEG signals has a higher signal to noise ratio and higher spatial resolution in the region of interest (around 1 mm [47]) compared to EEG signals. SEEG was first presented by a group in the St. Anne Hospital - Paris [48]. In addition of being a robust method for localizing the epileptogenic zones, the intracerebral electrodes that are considered to acquire SEEG are considered to generate Intracerebral Electrical Stimulations (IES) in order to give information about the function of the tissues that are situated around the harmful tissue before performing the resection surgery [49, 50]. SEEG signals are acquired by contacts that are placed in multi-contact electrodes as shown in Fig.1.6.

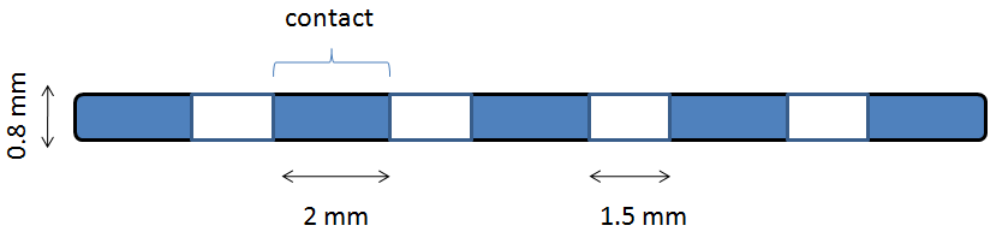

Figure 1.6: The shape intracerebral electrode considered in the CHU Hospital of Nancy [47].

1.3.4 Electrocorticogram

The electrocorticogram (ECoG) measurement is performed by placing the electrodes directly on the surface of the brain under the dura matter. ECoG electrodes are less invasive than the SEEG electrodes, because ECoG electrodes are attached to a grid that is placed on the surface of one compartment

of the brain, while the SEEG electrodes can have contacts in several compartments. ECoG signals were first recorded by the British physician Richard Caton (1875) on exposed brains of animals [51]. ECoG has a similar temporal resolution to EEG (around 1 millisecond), but it has a higher spatial resolution (around 1 mm). Due to the proximity of the ECoG electrodes to the cortical sources, the signal-to-noise ratio of the ECoG is higher than that of the scalp EEG. Thus, ECoG recordings improves the applications in which EEG recordings are applied like the Brain-Computer Interface [52] and source localization [53, 54].

1.4 Brain Imaging

Brain imaging techniques made it possible for clinicians and researches to study the structural information and/or the functional information of the living brain non-invasively. The availability of these information gave the scientists the ability to understand the relationships between the different areas in the brain, and locate the dysfunctional structures. In this study, two brain imaging techniques (MRI and CT-scan) which were acquired from the drug-resistant epileptic patients were considered for generating a head model for each patient. In the following subsections some of the common brain imaging methods are summarized.

1.4.1 Computed Tomography

The computed tomography scan or the CT scan is an imaging technique which depends on X-rays and the computer technology to produce a much more detailed image of the organ than the traditional X-ray imaging. Unlike the X-ray which applies a beam that crosses the body and reaches a plate that captures its energy; in CT scan, the beam turns around the body then it is entered to a computer in order to have different views of the same organs. CT scans have a high spatial resolution (0.5-0.625 mm), however, they have a low temporal resolution (83-135 milliseconds) [55]. They are considered to detect tumor [56], lesions [57] and blood clots [58]. In this study, the CT scans of each head was considered to give a good description of the hard-tissue skull compartment in the head model. In addition, because CT scans can be acquired while the invasive electrodes are implanted in the brain of the patient, they were considered to determine the positions of these electrodes in order to assign them in the head model [59]. Fig.1.7 shows one horizontal CT slice of one of our epileptic patients. As shown in the figure, the limits of the skull compartment in addition to the positions of the invasive electrodes

can be determined easily from the CT.

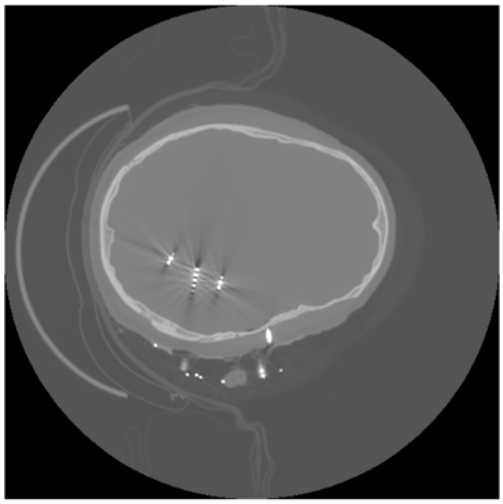

Figure 1.7: A horizontal CT slice of one of our patients showing the SEEG electrodes and the skull of the head. From CT scans, the border of the skull compartment and the positions of the SEEG electrodes can be determined.

1.4.2 Magnetic Resonance Imaging

The Magnetic Resonance Imaging (MRI) is an imaging technique which is based on a combination of powerful magnets and radio waves for generating images that describe the soft tissues of the head. It bases on the Nuclear Magnetic Resonance (NMR) in which the protons of a specific nuclei (the protons of the hydrogen of water molecules in the MRI case) are aligned uniformly, under the effect of a strong external magnetic field to create a magnetic vector along the axis of that external magnetic field. When the external magnetic field is switched off, the vector returns to its resting state, as shown in Fig.1.8, releasing energy in the form of signal. This emitted signal is detected by coils which are placed around the body, then the signal's intensity, which depends on the concentration of the hydrogen ions, is plotted on a gray scale as a volume element called voxel. At the end of this process a 3-dimensional image is produced describing the distribution of hydrogen in the scanned object [60].

After its invention in 1972 [61], MRI devices spread very fast. In 2011, one person out of 10 was scanned with the MRI in USA [62]. Nowadays,

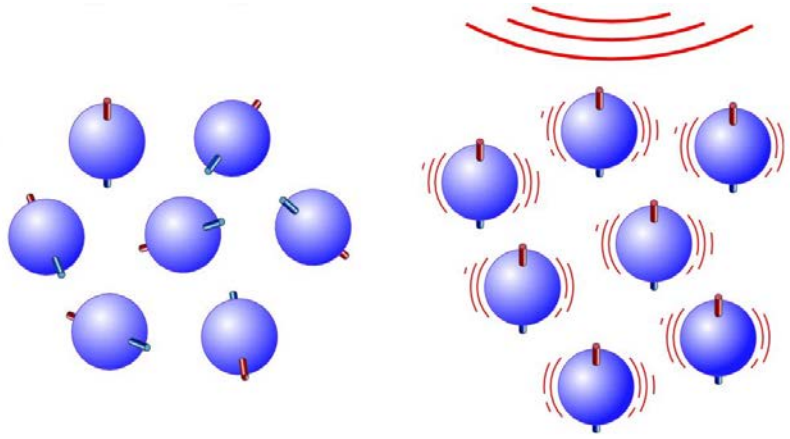

Figure 1.8: The alignment of the hydrogen's protons in the resting state (left) and under the effect of the external magnetic field (right). [60]

the MRI is applied in many applications, like detecting cancers in the brain [63] and the breast [64], investigating soft tissue damages [65] and for segmentation and classification the different tissues [66]. Although the MRI has a high spatial resolution (1-2 mm), it has a low temporal resolution (20-50 millisecond) [55]. In this study, T1-weighted 3D Bravo MRI images of the head of three drug-resistant epileptic patients were considered to build a realistic head model for each patient. From the MR images, the head model gets two important information: The size of the head and the limits between the different compartments in the head model. Fig.1.9 shows an example of MRI of one of our patients.

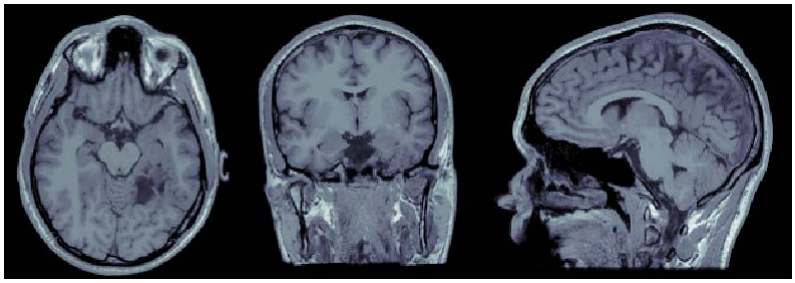

Figure 1.9: From the left: The horizontal, the coronal, and the sagittal planes of the MRI of one of our epileptic patients.

1.4.3 Positron Emission Tomography

The Positron Emission Tomography (PET) is one type of nuclear imaging which is based on injecting the body by positron-emitting radionuclide substances, then detecting the gamma waves resulted from this radioactive substances. Although the temporal resolution for PET is poor (around 30 sec), it has a good spatial resolution (around 10 mm) [67]. PET is considered in many applications like the brain cognition [68], breast cancer [69] and detecting epilepsy, Alzheimer and Parkinson as shown in Fig.1.10

Figure 1.10: Two PET images showing the difference between the brain of a healthy subject and the brain of a patient with Parkinson disease [70]

1.4.4 Functional Magnetic Resonance Imaging

The Functional Magnetic Resonance Images (fMRI) give a description of the brain activity by measuring the oxygen percentage in the blood. It is based on the fact that an active area in the brain requires more energy and hence more oxygen. This method is helpful to know which part of the brain is involved in a particular event [71]. Fig.1.11 shows an example of fMR images. The fMRI, similar to the MRI, has a high spatial resolution (around 1 mm) while it has a low temporal resolution (1-4 seconds) [67].

1.5 Brain Stimulation

Brain stimulation was first introduced as a method of treatment for different diseases. However, nowadays it is being considered as way to have an information about the parameters of the head and how it is possible to model them. In this study, the diagnostic stimulations which were generated by the

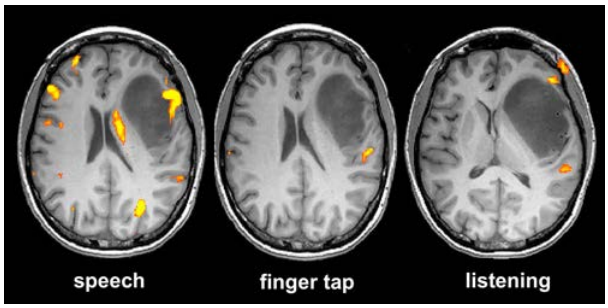

Figure 1.11: The yellow color in the fMRI images show the areas related to different tasks: Speech (left), finger tap (middle) and listening (right) [72].

intracerebral electrodes (or the intracerabral electrical stimulation IES) in drug-resistant epileptic patients were considered. However, there are other stimulation methods that are found in the literature. In the following subsections, some of the common brain stimulation methods are presented.

1.5.1 Electrical Impedance Tomography

Electrical Impedance Tomography or EIT is a technique for stimulating the brain from over the scalp by injecting a current through two electrodes while measuring the resulted potentials via an array of scalp electrodes. EIT has the advantage of being safe, inexpensive, fast and portable and it has been considered for many purposes like detection of the breast cancer [73], monitoring the brain functions [74] and conductivity estimation [75]. Even though the EIT does not require a surgery as the IES, stimulating the brain from the scalp does not give accurate information about the deep structures when these stimulations are acquired again by EEG electrodes because the current has to pass by the high-resistive skull compartment twice.

1.5.2 Deep Brain Stimulation

The Deep Brain Stimulation (DBS) is a method that is applied for stimulating the brain by implanting stimulating electrodes. This method was first introduced by Alim-Louis Benabid in 1980's as a treatment method for Parkinson's disease [76]. Short after its invension, DBS became a tool for treating chronic pain, tremor, and dystonia [77]. Unlike the diagnostic IES which is considered to stimulate the different parts of the gray matter whether they are deep or lateral, the DBS is considered to stimulate the thalamus in the human brain.

1.5.3 Transcranial Magnetic Stimulation

When talking about electrophysiological measurements, there is the EEG which measures the electric potentials on the scalp, and there is also the MEG which measures the magnetic field generated from the brain. And when talking about brain stimulation, there is the electrical stimulation which is achieved by placing stimulating electrodes on the scalp (EIT), and there is the magnetic stimulation, known as the Transcranial Magnetic Stimulation (TMS), which is performed by placing a coil around the head. As shown in Fig.1.12, TMS stimulate the region of the brain under the coil by an electromagnetic induction. As EIT, TMS is considered in many applications like the treatment of auditory hallucinations [78], the treatment of depression [79] and the diagnosis of epilepsy [80]. However, the TMS cannot represent a real source as the IES which stimulates inside the human brain.

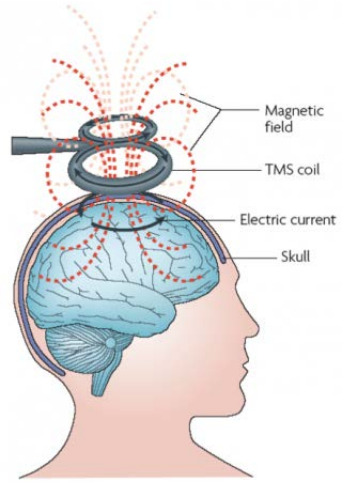

Figure 1.12: The Transcranial Magnetic Stimulation (TMS) [81].

1.5.4 Transcranial Direct Current Stimulation

Transcranial Direct Current Stimulation (tDCS) is a common technique in clinics and neuro-scientific research for stimulating the brain non-invasively and is considered for the treatment of depression [82] and stroke [83]. tDCS is based on applying weak electrical currents to the head via scalp, to generate an electric field which influences the activity of neurons. The idea of tDCS come from the treatment of the headache by the physician Claudius Galen who was applying torpedo fish to the forehead of the patient. When the treatment was failed, he noticed that he was using a dead fish and the key

element of treating was the electrical current that is generated by the torpedo fish [84]. Other form of Transcranial Current Stimulation (tCS) has appeared based on the idea of tDCS such as transcranial Alternate Current Stimulation (tACS) and transcranial Random Noise Stimulation (tRNS) which provide varied set of tools for clinicians and researchers. As EIT, tDCS is considered to stimulate the brain from the scalp, however, the tDCS is performed by large electrodes which make it difficult to consider it in simultaneous with EEG measurements.

1.6 The Conductivity of the Head Model

As mentioned previously, the head model depends on two important factors: The geometry of the head model and the conductivity values. In this section, we describe the effect of the conductivity values on source localization. Then we mention some of the works that have been performed for estimating the head conductivities. And finally, we describe our work that has been performed for estimating in-vivo conductivity while highlighting the difference between our method and the methods which were considered in the literature.

1.6.1 The Effect of Conductivity on Source Localization

The effect of conductivity on source localization was found in different studies with different techniques. In an analytic study, Cuffin et al. found that adding a bubble of a different conductivity in the brain sphere in a spherical head model caused a maximum error of 0.36 cm in EEG source localization, while its effect on MEG source localization was much smaller [11]. In a real analysis of localizing the determined subdural stimulating electrodes in three-compartment BEM head models of two patients, Homma et al. found that changing the skull's relative conductivity to the brain's from 1/1 to 1/120 caused a maximum localization error of 0.306 cm, while the best relative conductivity (given that the brain conductivity equals to scalp conductivity) was found to be 1/80 or 1/100 [85]. In a simulation study of localizing a dipole in a four-compartment template BEM head model, Acar et al. found that changing the brain-to-skull reference conductivity from 25:1 to 80:1 caused localization errors up to 0.31 cm with a median of 12 mm [12]. When a four-compartment FEM head model was considered in a simulation study, Pohlmeier et al. stated that an error of more than 20% of the skull conductivity causes unacceptable localization error [86]. All the above mentioned

studies show that assigning an erroneous conductivity values leads to errors in localization whether the geometry of the head model is simple or realistic.

1.6.2 State of the Art

The first attempts to measure the conductivities of human head were performed in-vitro by taking samples of the head's tissue and allow an electrical current to pass through in order to measure the voltage drop across these samples. In such studies, the conductivities of the scalp, the skull, the cerebrospinal fluid (CSF), the gray matter (GM), and the white matter (WM) were found to be in the ranges of $0.33-1.0$ S/m, $0.0042-0.05$ S/m, $0.33-3.0$ S/m, $0.33-1.0$ S/m and $0.14-0.48$ S/m respectively [15, 42, 87, 88, 89, 90]. Yet, most of in-vitro studies have found that the conductivity of the tissue does not depend on the current frequency [15, 88, 89, 90], or change slightly with the frequency [91]. Even though the conductivity values which were found in in-vitro studies are still common in recent researches [9, 12], these values are believed to be inaccurate since it was found that the conductivity of the tissue changes after its death [16]. Therefore it was important to carry out a research for estimating the conductivities of the different tissues in-vivo.

One way of performing in-vivo conductivity estimation is achieved by optimizing the forward head model when the other parameters are known and when the electrophysiological measurements of the real head are given. In-vivo conductivity estimation by optimizing the conductivity parameters of the forward head model has been performed by modeling the physiological brain sources. In one study of estimating the brain-to-skull conductivity ratio by modeling the physiological brain sources, Acar et al. considered isotropic and homogeneous four-compartment FEM head models of two subjects with their scalp projection maps of near dipolar sources identified by independent component analysis. The resulted brain-to-skull conductivity ratio was 34 for one subject and 54 for the second [92]. In a similar study, Lew et al. estimated the brain conductivity as 0.43 S/m and the skull conductivity as 0.004 S/m for one subject considering his somatosensory evoked response and an isotropic and homogeneous four-compartment FEM head model [93]. Even though such studies do not require any technology for stimulating the brain, they are not as precise as the studies in which the positions of the sources are well-determined.

Another form of in-vivo conductivity estimation by optimizing the forward model has been performed by the Electrical Impedance Tomography (EIT) technique in which the brain is stimulated by scalp electrodes. In one

study, Goncalves et al. have found that the mean brain resistivity (which was assumed to be equal to the scalp resistivity in their study) equal to 301 $\Omega.cm$ (which is equal to a conductivity of 0.33 S/m) with a relative standard deviation of 13% over 6 subjects in three-compartment BEM head models. While the skull resistivity was estimated as 12230 $\Omega.cm$ (0.008 S/m) with a relative standard deviation of 18% [94]. In another EIT-based study, Dabek et al. estimated the skull conductivity over nine subjects in a three-compartment BEM head model as 0.0066 S/m with a confidence interval [0.0034,0.0126] S/m, and the brain conductivity (which was equal to the scalp conductivity) was estimated as 0.34 S/m with a confidence interval [0.25,0.47] S/m [95]. Dabek et al. found that the conductivity value has a significant dependent on the subject, in addition, they found that the estimated conductivity depends on the stimulation frequency of the current, especially the skull conductivity [95]. Although in-vivo conductivity estimation by EIT does not require a surgery or a complex technology, it could not lead to accurate results since stimulating the brain from the scalp and measuring the resulted potentials on the scalp means that this current have to cross the high-resistive skull twice which may affect the accuracy of the results.

To avoid making the current pass through the skull tissue twice as in the EIT, some works have been performed by stimulating the brain with invasive electrodes. Zhang et al., considered the subdural electrodes for stimulation and found an average brain-to skull conductivity ratio of 18.7 $\pm$ 2.1 in inhomogeneous three-compartment FEM head model of two patients [96]. Whereas, Lai et al. found the average of the estimated brain-to-skull conductivity ratio in 5 patients as 25 $\pm$ 7 by considering a three-shell head model and a subdural stimulation. Even though the stimulation by the subdural electrodes are better than the scalp electrodes, still the subdural electrodes does not go deep enough inside the different tissues of the brain.

In order to avoid making the current pass through the high-resistive skull twice as in the EIT application, and in order to avoid the consideration of undetermined physiological brain sources for in-vivo conductivity estimation, the Intracerebral Electrical Stimulation (IES) was considered in this study for in-vivo conductivity estimation. The IES is a diagnostic stimulation that is generated by intracerebral electrodes which are placed in the gray matter of the drug-resistant epileptic patients. IES are considered for epileptic patients in order to verify, before the resection surgery, whether the epileptogenic zone is surrounded by tissues that have important functions like memory, visual functions, auditory function, ... etc. Even though IES has been considered

for in-vivo conductivity estimation in the study of Koessler et al. [97], in that study the conductivity estimation was performed by a Radio Frequency device of 50 kHz and only for the gray matter and the white matter compartments. However, in the current study, and for the first time to the best of our knowledge, the IES in addition to the simultaneous EEG and SEEG recordings were considered for estimating in-vivo conductivities of the scalp, the skull, the CSF, the GM and the WM in the homogeneous and isotropic five-compartment FEM head model. Estimating in-vivo conductivity considering the SEEG and EEG acquired in simultaneous with IES makes it possible to study the different parameters that should be considered in in-vivo conductivity estimation and gives an explanation for the large variance of conductivity values which are found in the literature.

1.7 Summary

EEG source localization is based on having an accurate forward model which depends on both the geometry and the conductivity values of the head model. Errors in the conductivity values in the head model leads to non-negligible source localization errors. Recent source localization studies consider conductivity values that were measured in vitro either in humans or in animals. Since the conductivity of the tissue changes after being removed from its environment, the need for estimating the conductivities of the head in-vivo becomes necessary. One way of in-vivo conductivity estimation is carried out by optimizing the forward model until its potentials become comparable to the potentials of the real head.

When performing in-vivo conductivity estimation by optimizing the forward model, the other parameters of the head model should represent accurately the real head in order to assume that the error between the potentials of the real head and the potentials of the model is only due to the error in the conductivity values of the head model. Hence, the geometry of the head model should be realistic. Realistic head models are generated based on the MR images of the head. MR images provide the size and the limits of the soft tissues, but it cannot give a description of the hard tissues. The hard tissue in the head is represented by the skull which is one of the most important tissues since it has a high resistivity compared to the other compartments. The skull can be represented accurately by the CT-scan of the head, however, this CT-scan cannot be applied on healthy subjects.

The potentials in the realistic head model can be determined by the

BEM method or the FEM method. The superiority of one method over the other is arguable. However, the FEM method can be applied to volumetric elements the conductivities can be either homogenous or inhomogenoeous and isotropic or anisotropic, so the FEM is more feasible for in-vivo conductivity estimation. In addition to the geometry, the source in the real head should be determined in order to represent by a similar source in the head model. The determined source in the real head should represent the real biophysiological sources of the brain which are situated in the cortex (or the gray matter). Even though EIT-EEG can be applied on healthy subjects, it is not feasible since the source is situated on the scalp and the current has to cross the high resistive skull twice before reaching the EEG electrodes.

One clinical application of EEG source localization is localizing the epilptogenic zone in epileptic patients. Epilespy is distigingused from other brain deseases by having siezures which can be detected by EEG electrodes. Since EEG source localization does not provide accurate localization results, currently epileptogenic zones are localized by applying intracerebral SEEG electrodes. In addition to detecting the seizures, intracerebral electrodes perform diagnosis by stimulating the region around the harmful tissue in order to generate sezures and to know the function of the region near the harmful tissue. The data that are acquired from the epileptic patients which contains: The MR-images, the CT-images (for determining the positions of the intracerebral electrodes), the intracerebral electrical stimulation (IES), in addition to the simultaneous EEG and SEEG recordings provides new information which has not been considered before, for in-vivo conductivity estimation by optimizing the forward model.

In this study, in-vivo conductivity estimation by optimizing the forward model was performed on three-drug resistant epileptic patients by considering their SEEG and EEG measurements that were acquired in simultaneous with IES. The EEG and SEEG measurements were then compared to the potentials of the realistic five compartment FEM head model in order to estimate the isotropic and homogeneous conductivity of each compartment (Scalp, skull, CSF, GM, WM). To the best of our knowledge, no study have been done on estimating in-vivo conductivity in a five-compartment FEM head model with EEG and SEEG measurements acquired in simultaneous with IES. This thesis treats many topics that are related to in-vivo conductivity estimation by optimizing the forward model. These topics are divided into the following chapters as follows:

- **Chapter 2**: Provides the background on the forward head model and

the mathematical formulation for determining the potentials from a dipolar source in a realistic FEM head model.

- **Chapter 3**: Introduces three common optimization algorithms in the field of in-vivo conductivity estimation and compares their performance by simulation given different parameters. Comparing different optimization algorithms for in-vivo conductivity estimation has not been performed before to the best of our knowledge.

- **Chapter 4**: Introduces a method for estimating the sensitivity of the potentials to the change in the conductivity values. This sensitivity analysis was performed in simulation given different parameters in the head model. The chapter shows that the change in a conductivity value has different effects on the potentials depending on the measurement setup and the stimulation position.

- **Chapter 5**: Provides the results of in-vivo conductivity estimation on three drug-resistant epileptic patients and discusses these results. In addition, it shows some results on the effect of estimating conductivities with different frequency components of the stimulation.

Chapter 2

Head Models

2.1 Background

The human brain can be studied at different spatial and temporal scales as shown in Fig.2.1. The nature of the study decides the temporal and the spatial resolutions of the measurements that should be considered, then the brain and the head are modeled accordingly in these specific resolutions. When building a head model, there is a trade-off between the computation complexity and the accuracy, i.e., the model should be as simple as possible to avoid computational loads and as accurate as possible to represent the real head. In the field of EEG source localization and conductivity estimation, the considered temporal scale is the temporal scale of the EEG signals which is around 1 millisecond.

The spatial resolution of the head model, in the field of EEG source localization and conductivity estimation should be in the scale of 1 mm so that the different brain regions and tissues can be studied. In order to get an accurate and a realistic head model, MR images, which has a spatial resolution of 1-2 mm, are considered. In these realistic head models, conductivity tensors are assigned for each region, so that, in general, one compartment of the head model has more than one conductivity value (inhomogeneous model) and these conductivities depend on the direction of the current (anisotropic model). The direction of the conductivities are obtained from the diffusion tensor magnetic resonance imaging (DTI) which measures the self-diffusion tensor of water in the tissue [98]. However, in order to reduce the complexity of the model, the local variations and/or the direction-dependency of the conductivity can be neglected so that the generated model becomes homogeneous and/or isotropic. In addition, a

Table 2.1: Maxwell's equations: $\boldsymbol{E}$ is the electric field (V/m), ρ is the free charge density (C/m^2), ε_o the permitivity of the empty space $(8.84 \times 10^{-12} S \cdot s/m)$, $\boldsymbol{D}$ is the electric displacement vector (C/m^2), $\boldsymbol{B}$ is the magnetic induction (T) ,$\boldsymbol{J}$ is the free current density (A/m^2), c is the velocity of the light (m/s), and $\boldsymbol{H}$ is the magnetic field (A/m) [5]

Microscopic fields	Macroscopic fields
$\nabla \cdot \boldsymbol{E} = \rho_t/\varepsilon_o$	$\nabla \cdot \boldsymbol{D} = \rho$
$\nabla \times \boldsymbol{E} = -\frac{\partial \boldsymbol{B}}{\partial t}$	$\nabla \times \boldsymbol{E} = -\frac{\partial \boldsymbol{B}}{\partial t}$
$\nabla \cdot \boldsymbol{B} = 0$	$\nabla \cdot \boldsymbol{B} = 0$
$\nabla \times \boldsymbol{B} = \frac{\boldsymbol{J}_t}{\varepsilon_o c^2} + \frac{1}{c^2}\frac{\partial \boldsymbol{E}}{\partial t}$	$\nabla \times \boldsymbol{H} = \boldsymbol{J} + \frac{\partial \boldsymbol{D}}{\partial t}$

more simpler head model can be generated without the requirement of the MR images by assigning a sphere corresponding to each compartment. This model is known as the spherical head model which can be only isotropic and homogeneous.

In EEG source localization, the head model which is a volume conduction model is defined as a biophysiological model that links an assigned source (representing a real source) with the generated potentials. In contrary to the field of connectivity, the generated potentials are resulted due the current distribution of the source and not due to the movement of the potentials through the axons. The theory of volume conduction models, on which all head models are based, originates from Maxwell's equations which are shown in Table 2.1. If the fields in Maxwell's equations are constant with time, the time derivatives vanishes. In this case the electric fields can be calculated without considering the magnetic fields (as if the magnetic fields do not exist), which is known as *electrostatics*. Moreover, the magnetic fields can be calculated as if the electric fields do not exist, which is known as *magnetostatic*. A less restricting condition is found in Maxwell's equations when the fields are changing with time but at low frequency ($f \leq 2000Hz$ [6]), in this case, which is known as a *quasi-static* approximation, the electric fields and the magnetic fields can be assumed as uncoupled, in addition, the time derivatives vanishes and the capacitive component of the tissue impedance and the inductive effect can be neglected [5].

The quasi-static approximation can be applied to the Maxwell's equations in our study because the frequencies of the brain electrophysiological signals

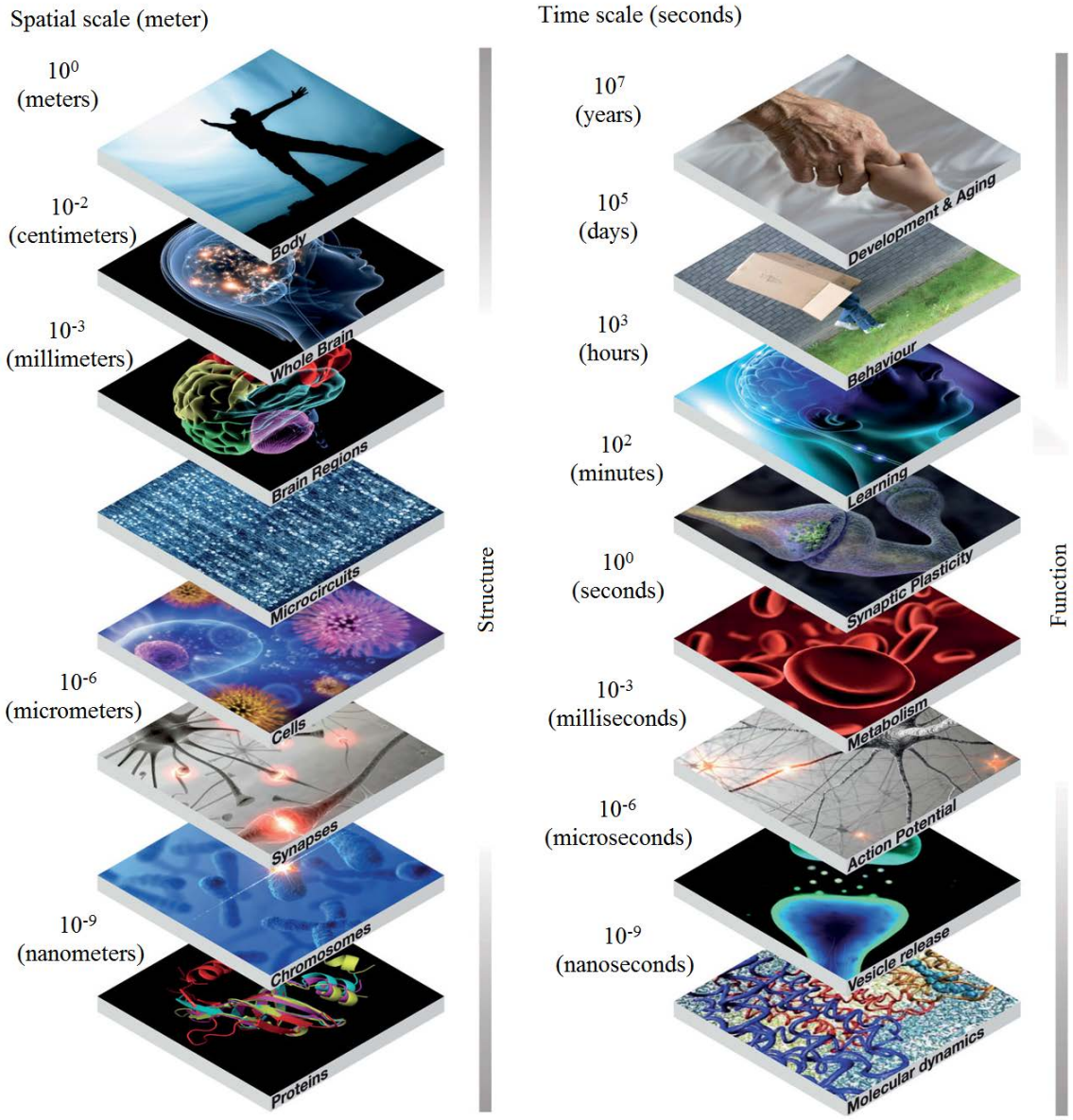

Figure 2.1: The different spatial and time scales which can be considered for modeling the human brain [99].

are less than $2000Hz$ [34], and the fundamental frequency of the intracerebral electrical stimulation, which were generated in the brains of the epileptic patients, was equal to $55Hz$. By considering the quasi-static approximation, the infinitesimal rotation of the electric field, or mathematically, the curl of the electric field ($\nabla \times \boldsymbol{E}$) would be zero. However, the curl of gradient of any scaler f ($\nabla \times \nabla f$) is equal to zero. Hence, the electric field $\boldsymbol{E}$ can be defined as a gradient of a scalar. This scalar is defined to be the potential V as shown in Eq.2.1

$$\boldsymbol{E} = -\nabla V \tag{2.1}$$

The negative sign in Eq.2.1 is due to the decrease in the potential as the electric field moves from the positive charge toward the negative charge. The total current density inside the brain ($\boldsymbol{J}$) can be expressed as the sum of the primary current density ($\boldsymbol{J}^p$) representing the activity of the brain and the conduction current $\sigma\boldsymbol{E}$, as shown in Eq.2.2

$$\boldsymbol{J} = \boldsymbol{J}^p + \sigma\boldsymbol{E} = \boldsymbol{J}^p - \sigma\nabla V \tag{2.2}$$

Due to the quasi-static condition, the total current density should be solenoidal, i.e., its divergence should be equal to zero. By taking the divergence of Eq.2.2, the resulted equation would be:

$$\nabla \cdot \boldsymbol{J}^p = \nabla \cdot (\sigma\nabla V) \tag{2.3}$$

Eq.2.3 is known as the Poisson equation which forms the basis for estimating the electrical potentials in the volume conduction model. In the case of head models, the Poisson's equation should be solved inside a boundary describing the shape of the head. Therefore, in order to solve the potentials (V) in Eq.2.3 when the current source ($\boldsymbol{J}^p$) is defined, the geometry and the conductivity (σ) of the head model should be defined. The geometry of the head model can be simple (like a single sphere), or complex describing the real shape of the head. Moreover, the conductivity of the head model can be defined to be equal for different compartments or different for different compartments in the homogeneous head model. However, in the inhomogeneous head model one compartment can have several conductivity values. In addition, the conductivity can be fixed for all the directions of the current in the isotropic head model, or it can have different values for different directions of the current in the anisotropic head model. In this chapter, the different geometries that were considered in the literature for estimating in-vivo conductivities are discussed. Then the geometry and the mathematical method which were considered in this study are described.

2.2 The Source Model

In order to determine the output potentials resulted from an electrical source in the volume conduction model, a mathematical model of the electrical source should be obtained to represent the primary current density $\boldsymbol{J}^p$ in Eq.2.3. As was mentioned in Chapter 1, the primary currents in the brain are mostly due to the post-synaptic potentials that move in a well oriented dendritic axes of pyramidal cells, and not due to the action potentials that have a short period of time and move in varied oriented neocortical axons. Post-synaptic potentials could be excitory or inhibitory. Excitory post-synaptic potentials increases the probability of the neuron to fire an action potential while inhibitory post-synaptic potentials decreases the probability of the neuron to fire an action potential as shown in Fig.2.2.

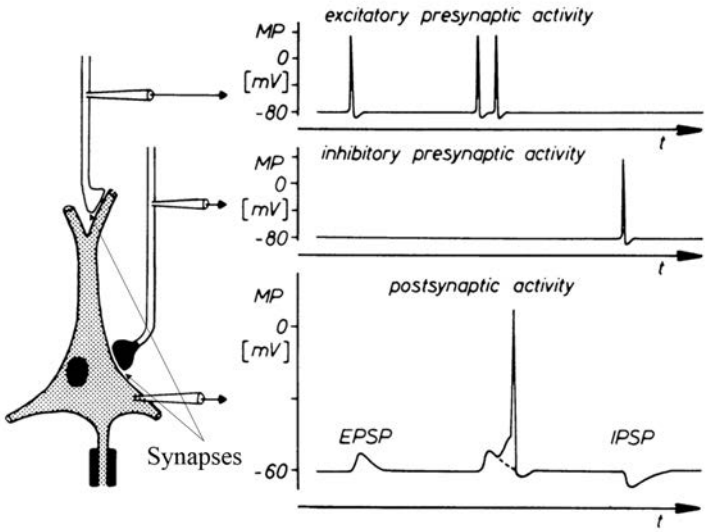

Figure 2.2: The effect of the action potentials coming to the neuron through the different synapses could be exitory or inhibitory [100].

The excitory and the inhibitory post-synaptic potentials are generated due to the movement of ions through the cellular membranes. The excitory post-synaptic potentials are carried by the positive sodium ions Na^+ inwards from the dendrite, while the inhibitory post-synaptic potentials are carried by the positive potassium K^+ ions outwards. Since there is no accumulation of charge anywhere in the medium, the currents that flow in or out of the neuron are compensated by currents which follow in the opposite direction elsewhere. Therefore, in the case of excitory post-synaptic

potentials, besides the sinks that are generated in the level of the synapse, distributed sources are generated along the soma-dendritic membrane, while the opposite happens in the case of inhibitory post-synaptic potentials as shown in Fig.2.3 [101].

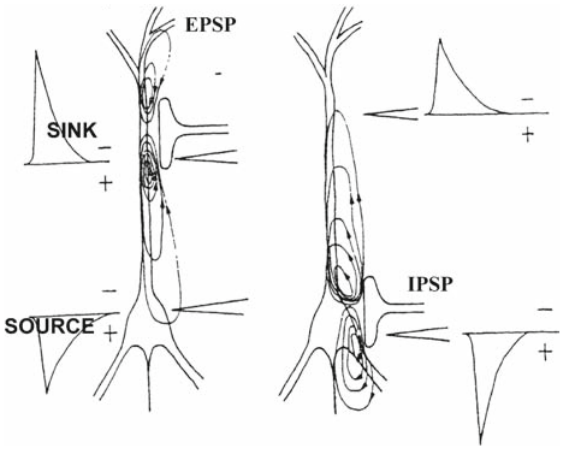

Figure 2.3: The generation of sources and sinks in the case of exitory postsynaptic potentials (left) and inhibitory postsynaptic potentials (right) [101].

The synchronous movement of the ions in a relatively large area of the brain (around $6^2 cm$ [5]) generates primary currents. The generators of the primary currents could be modeled as a source-sink or as a current dipole.

The Source-Sink Model The primary current $\boldsymbol{J}^p$ at a point r which is resulted from a source and a sink due to the post-synaptic potentials can be determined by:

$$\boldsymbol{J}^p = (\delta(\boldsymbol{r} - \boldsymbol{r}_+) - \delta(\boldsymbol{r} - \boldsymbol{r}_-))\boldsymbol{q} \tag{2.4}$$

Where δ is the Dirac delta function, $\boldsymbol{r}_+$ is the position of the source, $\boldsymbol{r}_-$ is the position of the sink, and $\boldsymbol{q}$ is the moment of the source-sink (defined as the magnitude of the source current times the distance between the source and the sink). However, if the distance between the source and the sink is very small compared to the distance from the source-sink to the point r, then the source and the sink can be modeled as a current dipole.

The Current Dipole The current dipole is defined to have an infinite current exiting one pole and entering the other [102]. The resulted current

density at a position r away from dipole is determined by the following equation:

$$\boldsymbol{J}^p = \delta(\boldsymbol{r} - \boldsymbol{r_o})\boldsymbol{q} \tag{2.5}$$

Where δ is the Dirac delta function, r_o is the midpoint between the source and the sink and $\boldsymbol{q}$ is the moment of the dipole (defined as the magnitude of the current times the distance between the source and the sink). In order to consider the dipole representation, the distance between $\boldsymbol{r}$ and $\boldsymbol{r_o}$ should be much larger than the distance between the source and the sink, hence the source and the sink can be viewed as a point relative to the point $\boldsymbol{r}$.

In this study, the real source was represented by the IES which is generated by two adjacent contacts in one intracerebral electrode shown in Fig.1.6. In order to model the IES source, the dipole model was considered because the measurements of the contacts on the same electrode that produced the IES were neglected. Hence the distance from the two contacts generating the IES to all other measuring contacts were much larger than the separation between the two contacts that generate the IES.

2.3 The Geometry of the Head Model

The geometry of the head model can be classified into spherical and realistic geometries. The spherical geometry, whether it is a single sphere or multiple spheres, cannot give an accurate representation of the head model. Moreover, the gray matter and the white matter cannot be modeled by spheres. However, the forward problem of the spherical head model can be solved analytically. On the other hand, the realistic head models give a lifelike representation of the head by considering the segmented MR images. Yet, the segmentation of these MR images into different homogeneous compartments is based on another field of study known as image segmentation. The segmentation of MR images used to be performed manually by an expert. Nevertheless, the difference between the experts' vision of the image and the long time periods which were consumed for performing manual segmentation urged the scientists to generate an algorithms of MR image segmentation. Nowadays, MR image segmentation is performed on computers based on different algorithms. Nevertheless, these segmenting algorithms are prone to errors and it is recommended to check the performance of the computer segmentation by an expert [103].

Unlike spherical head models which can be solved analytically, realistic head models are solved numerically by different numerical methods. If the realistic head model is represented by surfaces, then the Boundary Element Method (BEM) is usually considered to find the potentials on these surfaces. But if the head model is represented by volumetric 3D elements (voxels), then the Finite Element Method (FEM) or the Finite Difference Method (FDM) are considered to determine the potentials at each element. The FEM and FDM have a higher computational complexity than the BEM. However, when applying the FEM or the FDM, the conductivity can be either homogeneous or inhomogeneous, isotropic or anisotropic, whereas in the BEM, the conductivity can be only homogeneous and isotropic. Even though the BEM, FEM and FDM are mathematical methods that are utilized to solve realistic geometries, people in the research field may say "BEM head model" or "FEM head model" meaning that the realistic head model that is solved by the BEM or the FEM. A good review of the different methods for solving the head models is found in the work of Hallez et al. [104].

2.3.1 State of the Art

In the literature, most of the recent work that has been performed on in-vivo conductivity estimation has considered realistic head models solved by the BEM method [94, 95] and the FEM method [93, 92, 96]. In addition, spherical head models have been considered for estimating in-vivo conductivities [105, 106, 107]. However those who have considered the spherical head model in their in-vivo conductivity studies have proposed the estimation of in-vivo conductivities in realistic head models [107, 106]. The most common realistic head models are solved by the FEM method and the BEM method. The BEM has been considered in the literature because it has a simpler geometry and a lower computational cost [95], while the FEM offers the most flexibility for assigning detailed conductivity attributes and an accurate geometry to the model [93].

Some previous studies have worked on the comparison between the BEM and the FEM, however, their results cannot be generalized to all the different cases. In one study, M. Clerc et al. [108] concluded that for equivalent triangulation, the FEM was significantly faster than BEM and provided a better or similar accuracy. However, in another work from the same group, G. Adde et al. [109] found that the symmetric BEM outperformed the FEM model for deep dipole positions. In our laboratory, J. Hofmanis in his PhD thesis [47] found that the performance of a three-compartment low resolution FEM outperformed a three-compartment symmetric BEM when

considering a tangential dipole but not a radial dipole as shown in Fig.2.4. In the same study a single compartment FEM head model outperformed a single compartment BEM head model for both tangential and radial dipole. From these studies, it is hard to decide on a numerical method for solving the realistic head model. However, since the goal of this study is to estimate in-vivo conductivities, we considered the FEM method for solving the head model, because the FEM realistic model can be extended to have anisotropic and inhomogeneous conductivities. Nevertheless, for simplifying the computations, we assumed that the conductivities in the FEM head model are isotropic and homogeneous. as was assumed in previous studies for estimating conductivities [93, 92].

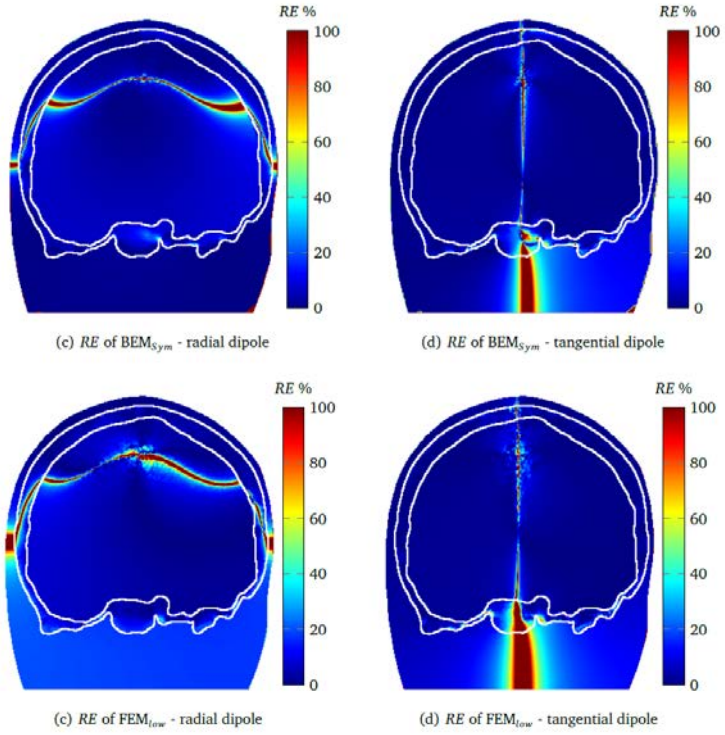

Figure 2.4: The resulted RE% ($RDM \cdot 100\%$) when comparing a symmetric BEM model (upper row) and a low resolution FEM model (lower row) with a three-compartment FEM reference head model [47].

The previous studies on in-vivo conductivity estimation have built three-compartment (Scalp, skull, brain) [94, 95, 105, 106] or four-compartment (Scalp, skull, cerebrospinal fluid, brain) head models [93, 92, 96, 107]. However, Ramon et al. found that separating the cerebrospinal fluid from the

brain compartment had a significant effect on the head model [110]. In addition, Vorwerk et al. found that considering the gray matter and the white matter as two separate compartments was as important as considering the CSF as separate compartment [111]. Thus, in this study, and for the first time to the best of our knowledge, a homogeneous and isotropic five-compartment (Scalp, skull, cerebrospinal fluid (CSF), gray matter (GM), white matter (WM)) FEM head model was considered for in-vivo conductivity estimation.

2.3.2 The Finite Element Head Model

In this work a homogeneous and isotropic five-compartment realistic FEM head model was considered for performing in-vivo conductivity estimation. Building this realistic head model was based on the work that has been done by J. Hofmanis in his PhD thesis [47]. The following subsection shows the derivation of the general equation according to which the potentials are determined in the realistic head model due to a dipolar source by the FEM method.

Mathematical Background

Eq.2.3 shows the basic equation for estimating the potentials due to a determined source in any volume conduction model. However, solving this equation in a surface or a volume representing the head requires boundary conditions to be defined for this equation. The first boundary condition states that if there is a surface S separating two regions i and j, where the first region has a conductivity σ_i and the second region has a conductivity σ_j, then the current density that leaves the region i towards the region j will be equal to the current density that enters the region j from the region i. This condition which is shown in Eq.2.6, is known as the Neumann's boundary condition.

$$\boldsymbol{J}_i \cdot \boldsymbol{n}(\boldsymbol{r}) = \boldsymbol{J}_j \cdot \boldsymbol{n}(\boldsymbol{r}) \tag{2.6}$$

From Eq.2.3, Eq.2.6 can be written as:

$$(\boldsymbol{\sigma}_i \nabla V) \cdot \boldsymbol{n}(\boldsymbol{r}) = (\boldsymbol{\sigma}_j \nabla V)\boldsymbol{n}(\boldsymbol{r}) \tag{2.7}$$

However, as shown in Fig.2.5, after crossing the outermost surface of the head, the current faces the air region which has a zero conductivity ($\sigma_{air} = 0$). From this, Eq.2.7 can be reduced for the outermost region to Eq.2.8:

$$(\boldsymbol{\sigma}_N \nabla V) \cdot \boldsymbol{n}(\boldsymbol{r}) = 0 \tag{2.8}$$

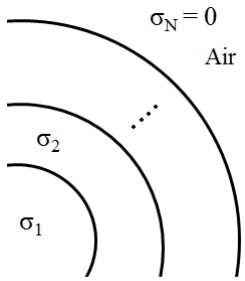

Figure 2.5: Each region (or compartment) in the head model has a specific conductivity and the conductivity of the air which bounds the head is zero.

Where N represent the air region which bounds the head.

When solving the potentials in a realistic head model by the FEM method, the volume representing the head model is tessellated into a number of volumetric elements Δ_j where $j = 1, ..., n_{tet}$. The volumetric elements that are considered in this work has a tetrahedron form where each tetrahedron is represented by four nodes. Due to this tessellation, the potential V in Eq.2.3 will be approximated by the sum of the potentials over all the nodes which forms one mesh in the head model as shown in Eq.2.9

$$V(\boldsymbol{r}) \approx \hat{V}(\boldsymbol{r}) = \sum_{i=1}^{n_{node}} V_i \phi_i \tag{2.9}$$

Where $V(\boldsymbol{r})$ is the potential of the $\boldsymbol{r}$ mesh, V_i is the potential at each node p_i, and ϕ is the 3D piece-wise linear shape function defined for each element. When the approximated potential ($\hat{V}(\boldsymbol{r})$) is substituted in Eq.2.3, the result would have an error term η due to this approximation as shown in Eq.2.10

$$\nabla \cdot \boldsymbol{J}^p - \nabla \cdot (\sigma \nabla \hat{V}) = \eta \tag{2.10}$$

One method to minimize this error η is known as weighted residual method [112] in which the integral of the error factor η multiplied by a weighting function (W) over all the domain Ω is set to zero as shown in Eq.2.11. In this study, the Galerkin's method is considered. In Galerkin's method, the weighting function (W) is defined to be equal to the linear shape function ϕ that is defined for each node.

$$\int_{\Omega} W_j \eta \ d\Omega = 0, \quad j = 1, 2, \cdots, n_{node} \tag{2.11}$$

By substituting Eq.2.10 in Eq.2.11 we get:

$$\int_{\Omega} W_j(\nabla \cdot \boldsymbol{J}^p - \nabla \cdot (\sigma \nabla \hat{V}))\ d\Omega = 0, \quad j = 1, 2, \cdots, n_{node} \tag{2.12}$$

By substituting $W = \phi$ in Eq.2.12 then solving it by the product rule and the divergence theorem, we get:

$$-\int_{\Omega} \nabla\phi_j \cdot (\sigma \nabla \hat{V})\ d\Omega + \int_{d\Omega} \phi_j (\sigma \nabla \hat{V}) \cdot \boldsymbol{n}\ dS = \int_{\Omega} \phi_j (\nabla \cdot \boldsymbol{J}^p)\ d\Omega, \quad j = 1, 2, \cdots, n_{node} \tag{2.13}$$

Because we deal only with the interface Ω, the second term in Eq.2.13 vanishes. Then, the final equation, after substituting the $\hat{V}$ from Eq.2.9, would have the following form:

$$\sum_{i=1}^{n_{node}} V_i \int_{\Omega} \nabla\phi_j \cdot (\sigma \nabla \phi_i)\ d\Omega = -\int_{\Omega} \phi_j (\nabla \cdot \boldsymbol{J}^p)\ d\Omega, \quad j = 1, 2, \cdots n_{node} \tag{2.14}$$

Finally, Eq.2.14 can be written in the following matrix form:

$$AV = B \tag{2.15}$$

Where A is the called the "stiffness matrix" and has the form:

$$a_{ji} = \int_{\Omega} \nabla\phi_j \cdot (\boldsymbol{\sigma} \nabla \phi_i)\ d\Omega \tag{2.16}$$

And B is the "force vector" and has the form

$$b_j = -\int_{\Omega} \phi_j (\nabla \cdot \boldsymbol{J}^p)\ d\Omega \tag{2.17}$$

The system in Eq.2.15 is solved in this study by the preconditioned conjugate gradients algorithm (with successive over-relaxation). As shown in Eq.2.16, the stiffness matrix depends only the shape function and the conductivity of the region. While the force vector B, as can be noted in Eq.2.17, depends on the source $\boldsymbol{J}^p$. The stiffness matrix A is symmetric such that $a_{ij} = a_{ji}$ for all i and j.

The stiffness matrix

Solving the stiffness matrix in Eq.2.16, requires the determination of the shape function ϕ and the conductivity $\boldsymbol{\sigma}$. When choosing the weighted residual method, the definition of the linear shape function, which is defined locally for each element Δ_k, should be:

- Continuous on the transition from one element to another.
- At least one time differentiable within each element.

If the tetrahedron element Δ_k, which is shown in Fig.2.6, with its four nodes (vertices) $p_j^k, j = 1, 2, 3, 4$ are given, then the local linear shape function is defined as:

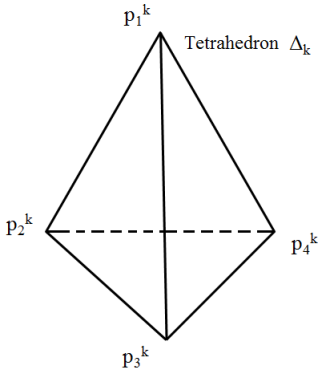

Figure 2.6: The tetrahedron element with its four nodes

$$\phi_t^k(r) = c_t^k \cdot \hat{r}, \quad t = 1, 2, 3, 4 \tag{2.18}$$

where $\hat{r} = (1, x, y, z)$ is the augmented position vector and c_t^k is the 4D coefficient vector which is found by making ϕ_t^k equal to 1 at the t^{th} vertex and decreases to zero at all other vertices of Δ_k:

$$\phi_t^k(p_j^k) = \begin{cases} 1 & \text{if } t = j \\ 0 & \text{if } t \neq j \end{cases} \tag{2.19}$$

From the above, the system can be summarized as:

$$\hat{P} c_t^k = \hat{d}_t \tag{2.20}$$

where

$$\hat{P} = \begin{bmatrix} 1 & p_1^k \\ 1 & p_2^k \\ 1 & p_3^k \\ 1 & p_4^k \end{bmatrix} = \begin{bmatrix} 1 & x_1 & y_1 & z_1 \\ 1 & x_2 & y_2 & z_2 \\ 1 & x_3 & y_3 & z_3 \\ 1 & x_4 & y_4 & z_4 \end{bmatrix} \tag{2.21}$$

is the augmented matrix with the positions of all the nodes forming the element Δ_k, and $\hat{d}_t$ is a vector of four entries, three of them is equal to zero and the t^{th} element is equal to one. By solving Eq.2.20, c_t^k is found, then it can be considered to solve Eq.2.18.

The calculation of the stiffness matrix coefficients a_{ij} is performed for each node-pair that has the same tetrahedron element Δ_k. While for the other node-pairs the coefficients $a_{lm} \forall l \neq i, m \neq j$ are set to zero because the local shape function ϕ_t^k is zero outside the element Δ_k for all t. Since the shape functions ϕ_i^k and ϕ_j^k are linear, their gradient would be constant, then the integration in Eq.2.16 for the node-pair (i, j) would be:

$$a_{ji} = \sum_{\forall k, \{p_j, pk\} \in \Delta_k} \Gamma_k \nabla \phi_j^k \cdot (\boldsymbol{\sigma}_k \nabla \phi_i^k) \tag{2.22}$$

where Γ_k is the volume of the tetrahedron element Δ_k and determined by:

$$\Gamma_k = \frac{1}{6} |\hat{P}| \tag{2.23}$$

and $\hat{P}$ is found by Eq.2.21.

In general, the conductivity $\boldsymbol{\sigma_k}$ is a tensor function, and it is defined locally for each element Δ_k. In this general case, the model is an anisotropic (the conductivity is defined as a tensor) and inhomogeneous (the conductivity is defined locally for each element Δ_k). However, if the model is an isotropic where the conductivity is defined as a scaler σ_k, then Eq.2.22 can be simplified as:

$$a_{ji} = \sum_{\forall k, \{p_j, pk\} \in \Delta_k} \sigma_k \Gamma_k (\nabla \phi_j^k \cdot \nabla \phi_i^k) \tag{2.24}$$

Moreover, if the conductivity is defined to be constant for all the element Δ_k in one region Ω_h, where h is the number of the regions, then in this

homogeneous model, Eq.2.15 can be rewritten as:

$$\boldsymbol{\sigma} \cdot AV = B \tag{2.25}$$

where

$$a_{ji}^{h} = \sum_{\forall k, \{p_j, pk\} \in \Delta_k} \Gamma_k (\nabla \phi_j^k \cdot \nabla \phi_i^k) \quad if \quad \Delta_k \in \Omega_h \tag{2.26}$$

In this study, for determining the potentials in the homogeneous and isotropic head model, the open source library SciRUN [113] was considered to solve the stiffness matrix A. It can be seen from Eq.2.25 that in the homogeneous case the potentials can be determined for new conductivity values in a faster manner than the inhomogeneous case because there is no need to re-estimate the stiffness matrix for new conductivity values. Since our goal in this study is to estimate in-vivo conductivities by optimizing the forward model which depends on iterating the conductivity values, considering the homogeneous head model made our computations simpler and faster.

The force vector

The force vector, as shown in Eq.2.17, depends on the shape function which was described when talking about the stiffness matrix, and the current source $\nabla \cdot \boldsymbol{J}^p$ which depends on the representation of the sources in the brain. In this study the current dipole model was considered for representing the primary currents. When simplifying Eq.2.17 by the product rule and the divergence rule, the force vector becomes:

$$b_j = -\int_{\partial\Omega} \phi_j \boldsymbol{J}^p \cdot \boldsymbol{n} dS + \int_{\Omega} \nabla \phi_j \cdot \boldsymbol{J}^p d\Omega \tag{2.27}$$

By substituting the dipole representation (Eq.2.5) in Eq.2.27 while noting that the integration over $\partial\Omega$ is zero, the final form of the force vector becomes:

$$b_j = \boldsymbol{q} \cdot \nabla \phi_j(\boldsymbol{r}_o) \tag{2.28}$$

From Eq.2.28, it can be noted that if $\boldsymbol{r}_o$ is located within a tetrahedron element Δ_k that is shown in Fig.2.6; the same shape function ϕ_j^k will be considered whatever the location of $\boldsymbol{r}_o$ within this tetrahedron element. However, if the dipole position $\boldsymbol{r}_o$ is located on the edge of the tetrahedron or a node, then all the local shape functions of all the elements that share the same edge or node should be considered.

2.3.3 Realistic Head Model for Three Patients

In this study, for building a realistic head model for each drug-resistant epileptic patient the T1-weighted 3D Bravo MR images in addition to the 3D CT scans were considered. The realistic head model was chosen to be isotropic and homogeneous consisting of five different compartments: The scalp, the skull, the cerebrospinal fluid (CSF), the gray matter (GM) and the white matter (WM). Considering the isotropic and homogeneous head model is a key factor for reducing the computational time when estimating in-vivo conductivities by optimizing the forward model. In addition, M. Dannhauer et al. found that considering anisotropic FEM head model does not yield a significant improvement for source localization [114]. For generating the realistic head model in this study, the MR images were first segmented into scalp, skull, CSF, gray matter (GM) and white matter (WM) by the freesurfer software. Freesurfer performs an automated labelling of each voxel of the MRI by anisotropic Markov random field (MRF) after aligning the subject surface to a probabilistic atlas [115]. This probabilistic atlas was generated by a training set of 41 manually labelled brains.

Many of the previous studies on conductivities have considered only the MRI to build the realistic head model [116, 92]. However in order to determine the position of the SEEG electrodes inside the brain the CT images were considered because it is not possible to acquire MRI images while the SEEG electrodes are inside the head of the patients [59]. In addition, the CT images give a better description of the hard tissues like the skull than the MRI. In a study of the effect of segmentation on dipole localization, Montes-Restrepo et al. have showed that a CT-based segmented skull give a better localization results than the MRI-based segmented skull [117]. In another study, Huiskamp et al. found that incorrect skull modeling due to not considering the CT scan of the head leads to errors comparable to those generated when considering wrong skull conductivity [118]. In this work, segmenting the CT-scan was based on intensity-based segmentation as shown in Fig.2.7, while the localization of intracerebral electrodes was done by an algorithm that have been designed in the CRAN laboratory [59].

As shown in Fig.2.8, after the segmentation, the CT and the MRI are co-registered by maximizing the mutual information [119], then the tetrahedrons which forms the elements of the realistic head model are generated as shown in Fig.2.9. These tetrahedrons are generated by the TetGen program which is based on the Delaunay triangulation technique [120]. Table 2.2 shows the number of elements (tetrahedrons) and the number of nodes (vertices)

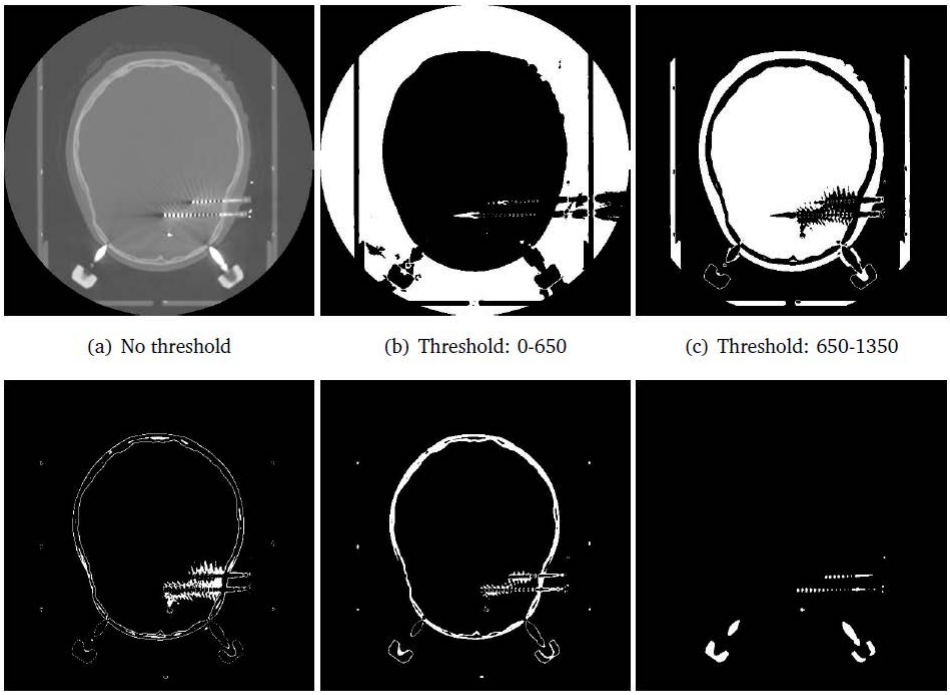

Figure 2.7: Increasing the threshold of intensity extracts the hard tissue of the skull and the intracerebral electrodes [47].

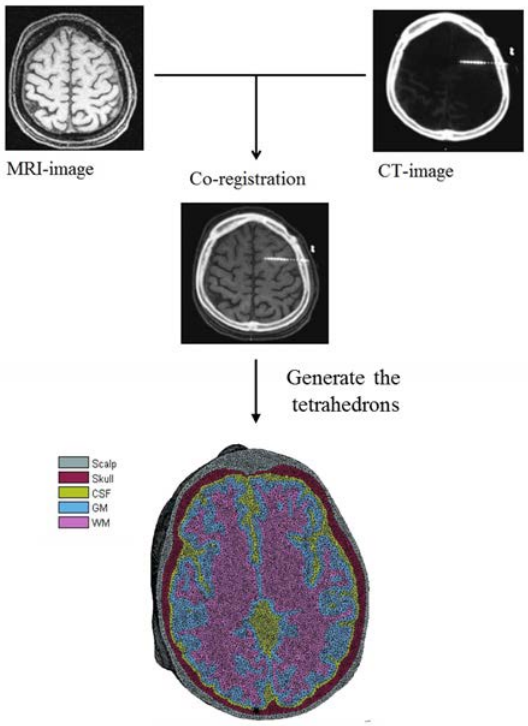

Figure 2.8: The segmented MRI is registered with the segmented CT images, then the tetrahedrons are generated in each different compartment.

that we got for each epileptic patient. It can be noted from Table 2.2 that the number of elements and the number of nodes are similar for the three patients. These number are determined by the Tetgen after fixing the radius-edge ratio (Q) to 1.414 and the maximum volume of tetrahedrons to 1 mm^3 [47]. The radius-edge ratio is defined as the ratio between the bounding sphere radius and the smallest edge length of the tetrahedron [120].

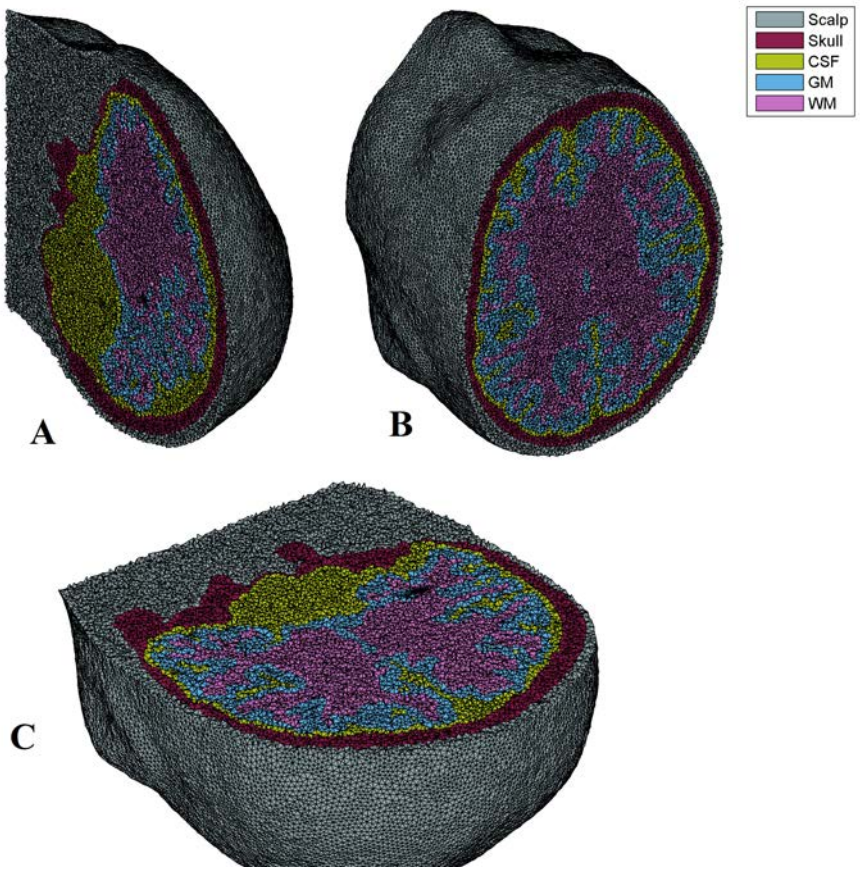

Figure 2.9: (A) Sagittal (B) Horizental and (C) Coronal views of the generated head model.

2.4 Summary

Modeling the head depends on the spatial and the temporal information which are considered for the modeling. In EEG source localization head modeling is based on the volume conduction model in which the current moves in all directions from the source to the measuring electrodes. The

Table 2.2: The number of elements (tetrahedrons) and the number of nodes (vertices) for each epileptic patient

Tissue	Number of	Patient(1)	Patient(2)	Patient(3)
Scalp	Elements	1763818	1766024	1793602
	Nodes	304777	305203	310251
Skull	Elements	669167	679459	716531
	Nodes	129580	131348	137640
CSF	Elements	719507	727154	726315
	Nodes	149420	151160	150933
GM	Elements	676420	678839	661217
	Nodes	154534	155142	152073
WM	Elements	713401	697771	707475
	Nodes	137163	134560	136130

movement of the current in a volume conduction model is derived from the well-known Maxwell's equations. Since the brain signals have frequencies less than 2000 Hz, it is possible to consider the quasi-static assumption in which the capacitive component of the tissue impedance and the inductive effects can be neglected. In general, the head model has different conductivities for one compartment (inhomogeneous), and different conductivities for different current directions (anisotropic). However, this general model cannot be applied to simple spherical geometries but to volumetric geometries. Since this research is dealing with in-vivo conductivity estimation, the volumetric FEM head model is considered because it can be extended to have anisotropic and inhomogeneous conductivities.

This chapter showed the derivation of the equations for estimating the potentials in a homogenous and isotropic FEM head model resulting from a dipolar source. Considering the homogenous and isotropic FEM head model has an advantage of simplifying the computational load since there is no need to re-estimate the stiffness matrix and the force vector when iterating the conductivities for optimizing the forward model for estimating in-vivo conductivities. For generating the FEM head model, the following softwares and packages were considered in this study:

- SciRUN open library source [113]: Calculation of the stiffness matrix.
- CGAL 3.6 (Computational Geometry Algorithms Library) [121]: Extraction the surfaces from labeled images.

- Tetgen 1.4 [120]: Tetrahedron generation and refinement.
- Iso2mesh toolbox [122]: Mesh visualization.

Chapter 3

A Comparison of Optimization Methods for in-vivo Conductivity Estimation

From the previous chapter, it was shown that for determining the potentials resulted from a current source in a volume conduction model the Poisson equation (shown in Eq.3.1) is considered.

$$\nabla \cdot \boldsymbol{J}^p = \nabla \cdot (\boldsymbol{\sigma} \nabla V_{model}) \tag{3.1}$$

For performing in-vivo conductivity estimation, the model potentials V_{model} are compared to real potentials V_{real} which are acquired from the subject for whom the model is built. If V_{real} does not equal V_{model}, then the unequality is allocated to the error in the conductivity values $bm\sigma$. Therefore, new conductivity values are assigned in Eq.3.1, then the new V_{model} is determined for repeating the comparison between V_{model} and V_{real}. Ideally, this process is repeated until V_{model} becomes equal to V_{real} as shown in Fig.3.1. This iterative method for estimating conductivities is performed by optimization.

In Latin, the word optimum means "the ultimate ideal", and the word optimus means "the best". From these terms, the optimization can be defined as "trying to bring what we deal with toward its ultimate state" [123]. In engineering and economics, optimization is applied to solve decision making problems by finding the "best" alternative between various alternatives. The goodness of the alternatives is measured by the *objective function* or the performance index [124], while the domain of various alternatives is known as the *decision variable*. An objective function could be

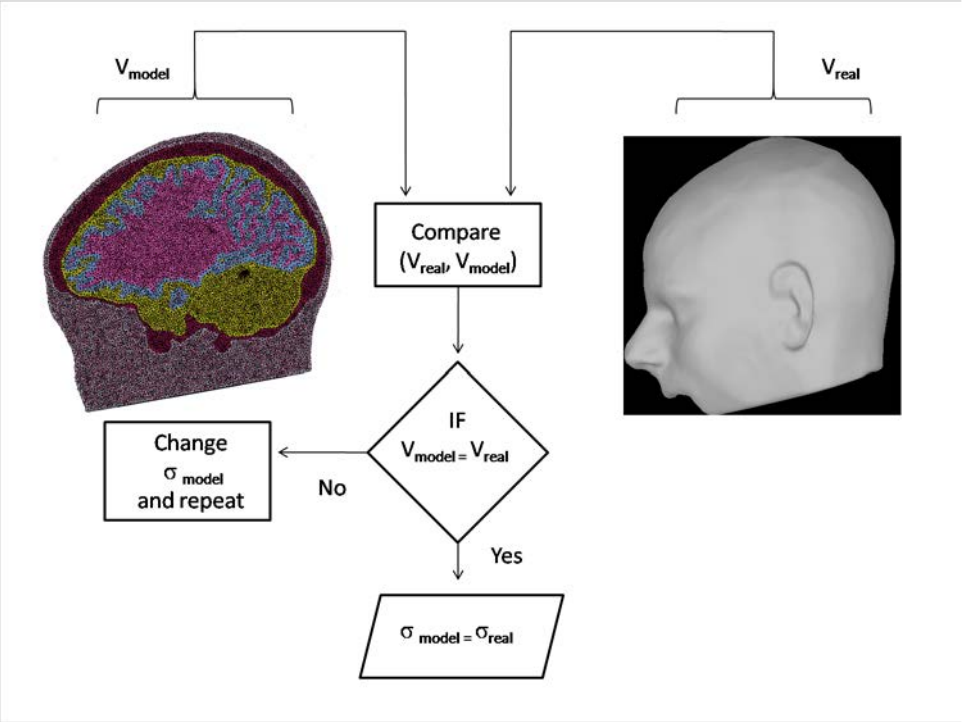

Figure 3.1: A flowchart showing the iterative method for estimating in-vivo conductivities. In this problem, all the parameters of the head model are chosen to resemble the parameters of the real head. The method starts by assigning initial conductivities in the head model.

multi-variable linear or non-linear, differentiable or non-differentiable. Due to this variety, there are many optimization algorithms which are found in the field of optimization. One way of classifying the optimization algorithms depends on the definition of the problem and its decision variable. If there are constrains on the decision variable that should be considered; then the problem needs a constrained optimization method, otherwise unconstrained optimization methods are considered. In addition, the optimization methods are classified according to the optimal solution that they calculate. If the solution is optimal among all the points on which the problem is defined; then the method is known as a global optimization method. However, if the solution is optimal among a local range; then the method is known as a local optimization method. Another class of optimization method is known as the direct or the free-derivative. The methods that are defined as free-derivative are distinguished by the ability to solve the optimization problem without the need to determine the derivatives of the objective function. Such methods are useful when it is hard to determine the derivatives of the objective function.

The field of optimization is full of different methods that are applied to different types of problems. Therefore, it is impossible to confirm the superiority of a chosen optimization algorithm on a specific application without performing a comparison among the feasible algorithms for that application. In this study, the FEM method was considered to determine the resulted potentials in the human head model. Since the FEM method is solved numerically and not analytically, the chosen optimization algorithms were all free-derivative algorithms. From local optimization algorithm the Nelder-Mead simplex (NMS) was chosen since it is robust, easy to be programmed and fast. In addition, NMS was considered in many studies which performed in-vivo conductivity estimation [85, 94, 96, 105, 107], so the motivation is to validate or refute their choice. On the other hand, from the global optimization algorithms, the genetic algorithm (GA) and the simulating annealing (SA) were chosen. The GA was chosen because of its ease of implementation, intuitiveness and ability to solve highly nonlinear optimization problems [125]. While the SA was chosen because it is effective in localizing multiple parameters and because it prevents the search to be trapped in a local minimum [126], in addition, it was considered for in-vivo conductivity estimation in the work of S. Lew et al. [93]. This chapter introduces first the chosen optimization algorithms, then it shows the procedure that was considered for comparing the optimization algorithms and finally, it presents and discusses the results which were obtained in this study.

3.1 Theoretical Background: The Optimization Algorithms

In this study, three derivative-free optimization algorithms were considered: The genetic algorithm (GA), the Nelder-Mead Simplex (NMS) and the Simulating Annealing (SA). These optimization algorithms are described in the following subsections.

3.1.1 The Genetic Algorithm

The Genetic algorithm (GA) is a well-known optimization algorithm classified as one of the derivative-free methods. Even though there is no general theory to prove that the GA converges always to the global optima (or even to a local optima), GA is often described as a global search method [127]. The idea of GA, which first appeared in 1975 in an article by Holland and his student [128], originated from the evolution theory, where good individuals are selected to be parents for the next generations while bad individuals die out.

The GA consists of three main steps: Selection, crossover and mutation. The algorithm starts by generating an initial random population from the range of the solution where each individual of the population represents a chromosome consisting of many genes in a form of vector. The genes of the chromosome could be either binaries or real numbers (in this study, the genes are real numbers representing the conductivities of the five-compartment FEM). Each chromosome of the initial population is assigned with a value called fitness value. This fitness value represents how good is the corresponding chromosome when it is substitute in the objective function of the problem. Therefore, the chromosome with a high fitness value has a high probability for being a parent in the next generation.

The GA algorithm that was considered in this study [129] starts by generating an initial population of 20 random 5-element vectors of conductivities in the range of the solution. One of these vectors is set by the user while the others 19 are generated according to a uniform distribution. Each of these vectors represents the five conductivity values of the scalp, the skull, the CSF, the GM and the WM. The number of the population in each iteration was chosen to be 20 in order to have a search that covers a wide range with low computational cost. From the 20 vectors, the two vectors that have highest fitness values are selected to pass to the new generation

(the generation of the second iteration) without any modification. These two selected vectors are known as the elite. While the other 18 vectors in the new generation are generated by crossover and mutation.

In crossover, each parent vector is separated into two off-spring vectors in order to be connected with other two off-spring vectors from another parent vector. In this study, 80% of the remaining number of vectors (after selection) perform the crossover, while the rest perform the mutation. The crossover depends on a stochastic uniform operation, in which each parent is given a section in a line in proportion to $1/\sqrt{(r)}$, where (r) represents the rank of the vector according to the fitness value. Then, the GA moves along a line in a uniform steps (each has a size of $1/N$) and at each step it allocates a parent. If the vector has a high rank, it will have a high probability of being chosen as a parent for more than one time. While in mutation, the GA randomly generates directions (vectors of 1, 0 and -1) and added them to the parents in order to generate the new vectors for the new generation.

3.1.2 The Nelder-Mead Simplex Algorithm

The Nelder-Mead simplex (NMS) algorithm is one of the most common algorithms in the optimization field. According to Google Scholar, the article of J. A. Nelder and R. Mead was cited around 1200 times since 2015. Even though the NMS is different than the simplex method which is found in linear programming, the NMS had taken its basics from there. In mathematics, a simplex is defined in the R^n space as the $(n + 1)$ points in that space. For example in the 2D dimension, the simplex is a triangle; while in the 3D, the simplex is a tetrahedron. The NMS algorithm depends on an adaptive simplex that walks and shrinks smoothly to find the minimum of any non-linear function. In this study the simplex is defined by 6 points where each point is a five element vector representing the five conductivity values. In the first iteration of the NMS, the simplex is defined from 6 vectors where one vector is given by the user while the other 5 vectors are generated to be near the user defined vector. Each of the 5 other initial vectors is generated by changing one element of the user-defined vector while keeping the other elements equal to the values of the user-defined elements as shown in Fig.3.2. The vector of conductivities which has the largest objective output (the worst vertex) is then determined and reflected in the centroid of the other n vertices, according to Eq.3.2 [130].

$$x_{reflected} = 2 * \overline{x} - x_l \tag{3.2}$$

Where, x_l is the worst vector and $\overline{x}$ is the centroid, which is defined as the average overall the points n that define the simplex as shown in Eq.3.3. By the reflection, a new simplex is formed. Then, the objective function is determined at this new vertex and the process continued.

$$\overline{x} = \frac{1}{n}\sum_{i=1}^{n} x_i \tag{3.3}$$

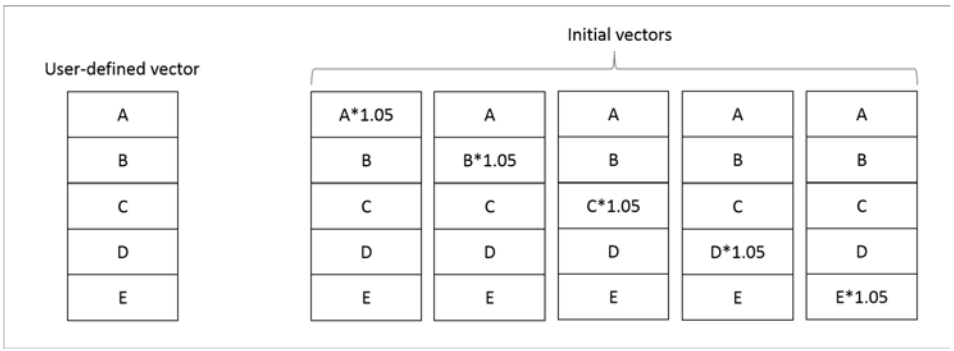

Figure 3.2: The process of generating the five initial vectors from the user-defined vector in the NMS algorithm, where each letter represents a real-value. If one of the elements in the user-defined vector is zero then instead of multiplying by 1.05, 0.00025 is added to the zero value.

However if the new vertex of the simplex has also the largest objective value in the new simplex, then the reflection would cause that algorithm to return to the previous point that had the largest value in the previous simplex, this will end up in an infinite oscillation. To avoid this oscillation, the simplex shrinks by replacing all the vectors, except the vector with smallest objective value, by new ones half the way along the distance to the smallest vector [131]. That is, if the smallest vertex is x_s, then in the shrinkage process all the vertices x_i will be replaced by new ones x_i^* according to Eq.3.4 [130].

$$x_i^* \leftarrow \frac{x_i + x_s}{2} \quad \forall\{i \in n, i \neq s\} \tag{3.4}$$

3.1.3 The Simulating Annealing

Simulating annealing (SA) is a heuristic that depends on an iterative improvement strategy. In the iterative improvement strategy, the optimization algorithm makes its steps according to the value of the cost function related

to these steps: The new chosen point will be accepted only if it gives a smaller cost. However, as shown in Fig.3.3, if this strategy finds a local minimum point, then it will stuck with it. In order to avoid this problem, the SA accepts points that give larger cost with a given probability. The SA, which was introduced in the work of Kirkpatrick et al., 1983 [132], took its idea from annealing the solids. In general, to put a material at its low-energy state, it should be heated first then cooled gradually in order to make it reach the thermal equilibrium state at each temperature. Heating the material to put it to its low-energy state is similar to accepting high cost values in order to find the global minimum point.

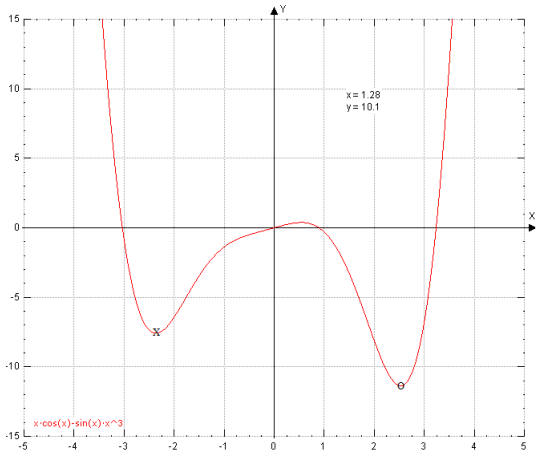

Figure 3.3: This graph shows the problem of being trapped in a local minimum point. "x" shows a local minimum point while "o" shows a global minimum.

In this study, the SA algorithm was set to search for the optimal conductivity values, so each point was represented by a five-element vector. The algorithm starts from an initial vector that the user provides (x_i), then in the first iteration $(k = 1)$ a new point (x_r) is generated according to Eq.3.5.

$$x_r = \frac{y}{||y||} \times T + x_c \tag{3.5}$$

Where the elements of the y vector are drawn from a standard normal distribution, x_c is the current vector which is the initial vector (x_i) in the first iteration. And T is called the temperature coefficient. The SA then compares the resulted objective output $(f(\cdot))$ from the current vector and

the new vector as shown in Eq.3.6.

$$\Delta f = f(x_r) - f(x_c) \tag{3.6}$$

If the conductivities x_r gives a lower cost than the current conductivities x_c ($\Delta f < 0$), x_r is accepted and the iteration continues. If not, the boltzmann distribution (Eq.3.7) is compared to a random number R that is generated uniformly between 0 and 1. If $h > R$, the point x_r will be accepted, if not, it will be rejected.

$$h = \frac{1}{1 + \exp^{\frac{\Delta f}{T}}} \tag{3.7}$$

Since the algorithm was set to search in the domain of positive real numbers, if the new vector of conductivities contains negative elements, these negative elements are replaced by zeros then the vector is modified as shown in Eq.3.8. The defined temperature factor T, was chosen to start as 100, so that the probability of accepting the new vector is equal to the probability of rejecting it. Then in each iteration k, the temperature factor T is reduced according to Eq.3.9, so that the probability of accepting bad points becomes smaller as the algorithm continue [126].

$$x_r = R \times x_r + (1 - R) \times x_c \tag{3.8}$$

$$T_{new} = T_{old} \times 0.95^k \tag{3.9}$$

3.2 Materials and Methods

In this work a simulation analysis for comparing the optimization algorithms was performed on an isotropic and homogeneous five-compartment FEM head model of a 23 years old male drug-resistant epileptic patient: Patient(1). For generating the head model, the MRI and the CT of Patient(1) were segmented (into five compartments), co-registered, and then discretized into tetrahedron elements so that the potential can be determined at each node of the generated elements. Two head models of the Patient(1) were built: a reference head model and a test head model as shown in Fig.3.4. In the reference head model the conductivity values that are common in the literature were assigned. These common conductivities are 0.33 S/m for scalp, 0.008 for skull, 1.79 S/m for CSF, 0.33 S/m for GM and 0.14 S/m for WM [15, 87, 88].

While in the test head model, initial conductivity values were assigned and were set to variate by the optimization algorithm in order to estimate the reference conductivities. In order to have an unbiased comparison, each optimization algorithm was set to start from three different initial conductivities: multi-start approach. The multi-start approach is important to ensure that the performance of the algorithm is independent of the chosen initial point. Moreover, in order to ensure that the performance of the algorithm is independent of the stimulation position and the measurements' positions, each algorithm was set to estimate the reference conductivities given three different stimulation positions: Deep, intermediate and lateral, and given two different measurement setups: SEEG and SEEG-EEG. In addition, to make sure that the performance of the optimization algorithms would not change when applying them to real data, each optimization algorithm was set to optimize in-vivo conductivities without additional noise and with additional white Gaussian noise. The combination of these different conditions (three initial points × three stimulation positions × two measurement setups × two noise configurations) generated 36 cases for each optimization algorithms as described below:

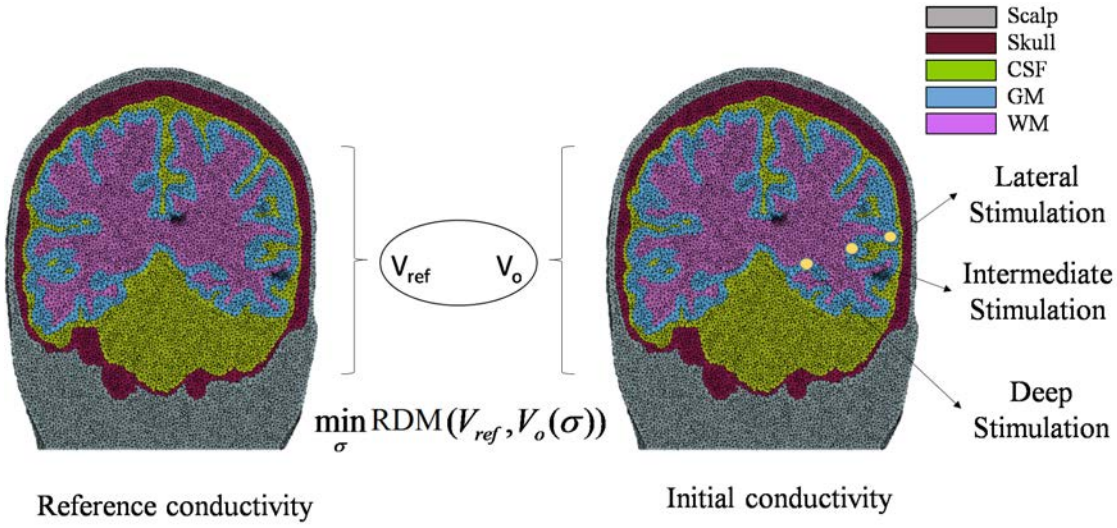

Figure 3.4: A scheme shows the procedure along with the three stimulation positions that were considered to compare the optimization algorithms. The error function that was considered in this study is the RDM which is shown in Eq.3.10

.

- The position of measurements: The SEEG (107 measurements) and

SEEG-EEG (107+19 measurements). Considering first the SEEG measurements then adding the EEG shows if the performance of algorithm is enhanced or not by adding the EEG measurement positions.

- The initial conductivities : In order to verify whether the performance of the optimization algorithm is independent of the choice of the initial conductivities, three different initial points were considered. The first and the second initial points ([0.38, 0.0158, 3.50, 0.49, 0.25], [0.42, 0.1190, 2.66, 0.49, 0.21] S/m) were generated by $initial = ref * rand + ref$, while the third initial point ([0.11, 0.0077, 0.27, 0.02, 0.05] S/m) was generated by $initial = ref - ref * rand$, where ref represents the conductivities that are assigned in the reference model and $rand$ is a random number generated uniformly between 0 and 1.

- The position of the stimulation: The robustness of each optimization algorithm was tested considering three different stimulation positions: Deep, intermediate and lateral. In order to estimate the deepness of the stimulation, the contacts of the intracerebral electrodes were divided into three classes as shown in Fig.3.5. Since the objective of the optimization algorithm is to search for the conductivity values, the performance of the algorithm was tested for different stimulation positions, to ensure that this performance is independent of the stimulation position.

- Additional noise: Even though the comparison of the optimization algorithms is performed by simulation, the main purpose was to apply the most robust optimization algorithm to real signals which are affected by different kind of noise. Therefore, the optimization algorithms were tested without additional noise, and with additional white Gaussian noise which makes the SNR of the generated potentials 80 dB. The reason behind choosing the SNR as 80 dB is to represent the noise that rests with the stimulation signal after filtering it with SSA-GEVD **??**. This resting noise is assumed to be small compared to the signal power.

The Error Function The objective function or the error function between the two models was chosen to be the Relative Error Measurement (RDM) (Eq.3.10) [133] which estimates the topographic error by comparing the distribution of the generated potentials. It has a minimum value of zero and a maximum value of 2. The RDM which is common in the field of head models [92, 111, 116, 114] was considered here because it is not sensitive to amplitude difference as the MAG function [111, 114], and the amplitude

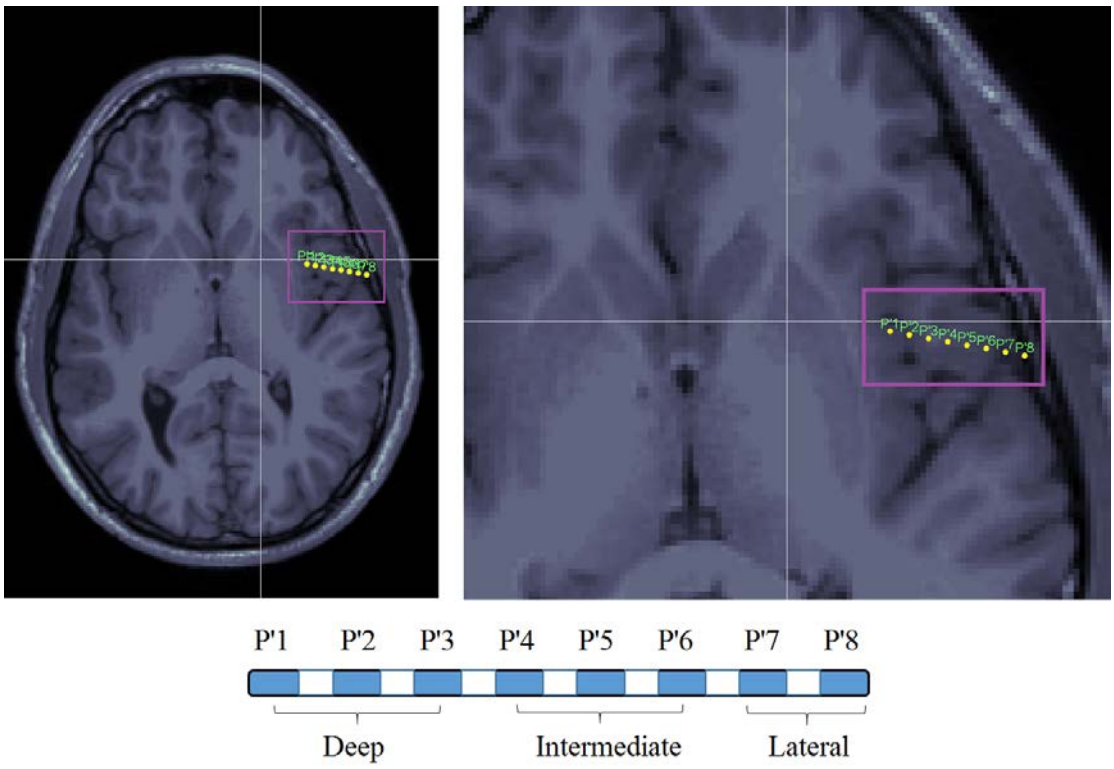

Figure 3.5: An image shows how the contacts are divided into deep, intermediate and lateral. The contacts of the intracerebral electrodes are given number starting from the deepest contact, i.e., the deepest contact is given number 1, the next is 2,... etc.

does not hold any useful information for EEG source localization [116, 114].

$$RDM = \sqrt{\sum \left(\frac{V_o(\boldsymbol{\sigma})}{||V_o(\boldsymbol{\sigma})||_2} - \frac{V_{ref}}{||V_{ref}||_2} \right)^2} \tag{3.10}$$

Where V_o is the output potentials of the test model, V_{ref} is the output potentials of the reference model, $||\cdot||$ is the l^2 norm, and $\boldsymbol{\sigma}$ is a vector of the five-compartment conductivities. In order to have an unbiased comparison, all the optimization algorithms were set to search in the positive range and they were set to stop if the number of iteration reached 1000 or if the tolerance of the output function became 10^{-4}.

After the comparison, the robustness of the successful optimization algorithm was tested in the presence of real noise which was added to the potentials of the head model. The real noise represents the filtered signals from the acquired stimulation that are acquired from Patient(1). As in the case of adding the white Gaussian noise, the SNR was chosen to be 80 dB. Again, the optimization in the presence of real noise has been performed by the successful optimization algorithm for 18 different times given the combinations of the following conditions:

- The position of measurements: SEEG (107 measurements) and SEEG-EEG (107+19 measurements).
- The initial conductivities : Three different initial points.
- The position of the stimulation: Deep, intermediate and lateral.

3.3 Results

The chosen optimization algorithms were set to search for the reference conductivity values in the test head model given the potentials of the reference head model. In order to have an unbiased comparison among the chosen optimization algorithms, the stopping criteria and the boundary of the search were set to be equal for the optimization algorithms. It should be noted that if x is a vector of the five-compartment conductivity values, then x and $(constant \cdot x)$ will give the same voltage distribution as shown in Fig.3.6. Since the RDM which measures the topological error is chosen as an error function, to compare the resulted conductivities, the following operation

Table 3.1: The estimated conductivities, the initial RDM, the final RDM and the time required for optimization by NMS given the SEEG potentials of the reference model without additional noise

Source	Initial conductivity	Resulted conductivity (S/m)	Initial RDM	Resulted RDM	Time (Hours)
Deep	First	[0.33,0.0080,1.79,0.33,0.14]	$1.95 * 10^{-2}$	$2.89 * 10^{-6}$	2.07
	Second	[0.33,0.0080,1.79,0.33,0.14]	$4.66 * 10^{-2}$	$2.65 * 10^{-6}$	2.46
	Third	[0.33,0.0080,1.79,0.33,0.14]	$5.23 * 10^{-2}$	$1.53 * 10^{-5}$	2.05
Intermediate	First	[0.33,0.0080,1.79,0.33,0.14]	$4.13 * 10^{-2}$	$5.85 * 10^{-6}$	2.33
	Second	[0.33,0.0080,1.79,0.33,0.14]	$5.84 * 10^{-2}$	$5.37 * 10^{-6}$	2.92
	Third	[0.33,0.0080,1.79,0.33,0.14]	$5.08 * 10^{-1}$	$1.12 * 10^{-5}$	3.23
Lateral	First	[0.33,0.0080,1.79,0.33,0.14]	$1.15 * 10^{-1}$	$7.04 * 10^{-6}$	2.35
	Second	[0.33,0.0080,1.79,0.33,0.14]	$1.07 * 10^{-1}$	$5.52 * 10^{-6}$	2.46
	Third	[0.33,0.0080,1.79,0.33,0.14]	$6.36 * 10^{-1}$	$1.40 * 10^{-5}$	2.47

Table 3.2: The estimated conductivities, the initial RDM, the final RDM and the time required for optimization by GA given the SEEG potentials of the reference model without additional noise

Source	Initial conductivity	Resulted conductivity (S/m)	Initial RDM	Resulted RDM	Time (Hours)
Deep	First	[0.33,0.0080,1.76,0.33,0.14]	$1.95 * 10^{-2}$	$2.12 * 10^{-4}$	10.90
	Second	[0.33,0.0088,1.23,0.22,0.11]	$4.66 * 10^{-2}$	$6.29 * 10^{-3}$	10.74
	Third	[0.33,0.0094,1.49,0.26,0.12]	$5.23 * 10^{-2}$	$5.85 * 10^{-3}$	10.83
Intermediate	First	[0.33,0.0087,1.52,0.29,0.13]	$4.13 * 10^{-2}$	$4.58 * 10^{-3}$	12.23
	Second	[0.33,0.0079,1.74,0.32,0.14]	$5.84 * 10^{-2}$	$5.57 * 10^{-4}$	12.33
	Third	[0.33,0.0072,1.32,0.25,0.11]	$5.08 * 10^{-1}$	$6.58 * 10^{-3}$	12.07
Lateral	First	[0.33,0.0080,1.72,0.32,0.13]	$1.15 * 10^{-1}$	$8.59 * 10^{-4}$	10.82
	Second	[0.33,0.0110,1.29,0.25,0.10]	$1.07 * 10^{-1}$	$1.29 * 10^{-2}$	10.34
	Third	[0.33,0.0171,0.63,0.18,0.06]	$6.36 * 10^{-1}$	$6.02 * 10^{-2}$	10.33

Table 3.3: The estimated conductivities, the initial RDM, the final RDM and the time required for optimization by SA given the SEEG potentials of the reference model without additional noise

Source	Initial conductivity	Resulted conductivity (S/m)	Initial RDM	Resulted RDM	Time (Hours)
Deep	First	[0.33,0.0136,3.03,0.42,0.22]	$1.95 * 10^{-2}$	$1.95 * 10^{-2}$	9.45
	Second	[0.33,0.0935,2.09,0.39,0.16]	$4.66 * 10^{-2}$	$4.66 * 10^{-2}$	7.81
	Third	[0.33,0.0086,0.72,0.27,0.09]	$5.23 * 10^{-2}$	$3.95 * 10^{-2}$	10.00
Intermediate	First	[0.33,0.0136,3.03,0.42,0.22]	$4.13 * 10^{-2}$	$4.13 * 10^{-2}$	10.29
	Second	[0.33,0.0935,2.09,0.39,0.16]	$5.84 * 10^{-2}$	$5.84 * 10^{-2}$	8.42
	Third	[0.33,0.0120,1.07,0.37,0.29]	$5.08 * 10^{-1}$	$5.50 * 10^{-2}$	10.48
Lateral	First	[0.33,0.0838,0.50,0.23,0.08]	$1.15 * 10^{-1}$	$1.07 * 10^{-1}$	9.16
	Second	[0.33,0.01,1.41,0.31,0.10]	$1.07 * 10^{-1}$	$7.24 * 10^{-2}$	7.63
	Third	[0.33,0.0730,12.48,2.08,0.86]	$6.36 * 10^{-1}$	$7.56 * 10^{-2}$	9.23

was applied to the resulted conductivity vector c before comparing it to the reference conductivity:

$$c_{new} = (0.33 \cdot c)/c(1) \tag{3.11}$$

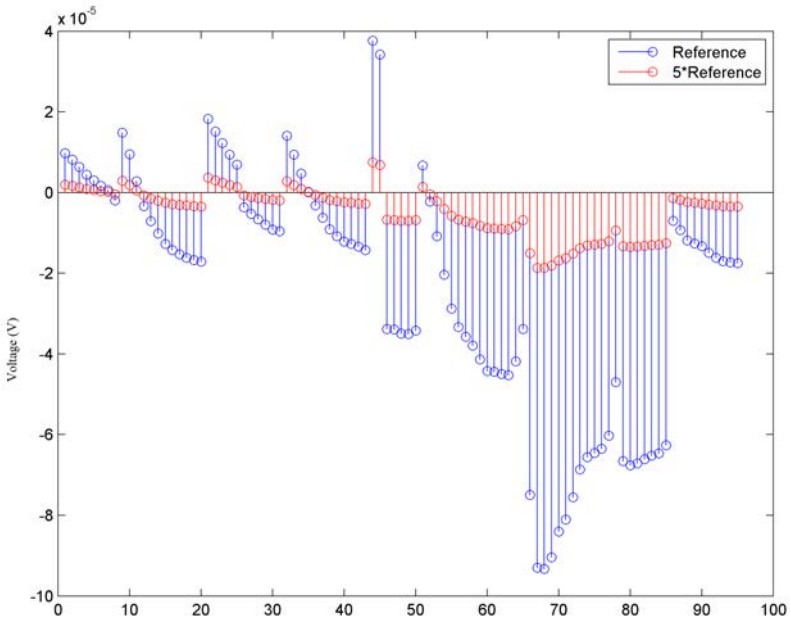

Figure 3.6: Two voltage distributions generated by the reference conductivities and the reference conductivity times 5. The RDM between the two distributions is zero.

Table 3.1, Table 3.2 and Table 3.3 show the results of optimization considering only the SEEG potentials by the NMS, the GA and the SA respectively. It can be noted from the tables that the NMS converges always to the reference conductivity values. In addition, in terms of the time required to find the optimal conductivities, it can be noted from the tables that the NMS is the fastest algorithm compared to the GA and the SA. Both the GA and the SA failed to find the reference conductivity although they required much more time than the NMS. However, the GA, in terms of RDM, did better optimization than the SA. It can be noted also that the SA in some cases returned the same initial value after finishing the search, this indicates that it could not find better conductivities than the initial conductivities. In addition, it can be noted from the tables that the initial RDM are different for different stimulation position (Deep, intermediate

and lateral). This indicates that in-vivo conductivity estimation depends on the stimulation position. The dependency between in-vivo conductivity estimation and the position of the stimulation is described in the next chapter.

The results of the comparison given the SEEG plus EEG measurements and given an additional white Gaussian noise does not differ form the results shown in Table 3.1, Table 3.2 and Table 3.3. In all the different conditions, the NMS outperformed both the GA and the SA in convergence to the solution and speed. Therefore the NMS was chosen to perform the optimization for in-vivo conductivity estimation. However, before performing real in-vivo conductivity estimation, the performance of the NMS was tested in simulation for estimating the reference conductivity when the reference potentials are perturbed by additional real biophysiological noise.

The biophyiological noise which was acquired from Patient(1) was added to the reference potentials so that the SNR of the resulted potential became equal 80 dB. This 80 dB was chosen to represent the noise that rests in the acquired IES signal after the filter in real in-vivo conductivity estimation. The results of estimating the reference conductivities by the NMS considering the SEEG potentials and the SEEG-EEG potentials of the reference model when real noise was added to the reference potentials are shown in Table 3.4 and Table 3.5 respectively. It can be noted from the tables that the NMS converged always to the reference conductivity values given the different initial points and the different stimulation positions. This indicates that the NMS is robust for performing in-vivo conductivity estimation in the five-compartment FEM head model.

3.4 Discussion

Estimating the conductivity parameters in the forward head model according to real potentials depends on the optimization algorithms. Many studies have performed in-vivo conductivity estimation using different optimization algorithms [92, 93, 85, 94, 96, 105, 107], and many has considered the Nelder-Mead simplex algorithm [85, 94, 96, 105, 107], but no study has checked the superiority of the chosen optimization algorithm over the other feasible algorithms. The lack of information about the superiority of the considered optimization algorithm has opened the way for the researchers to propose testing other optimization algorithms in future studies like Ferree et al. who considered the Nelder-Mead simplex for

Table 3.4: The resulted RDM by the Nelder-Mead simplex given the SEEG of the reference model in addition to real noise

Source	Initial conductivity	Resulted conductivity (S/m)	Initial RDM	Resulted RDM	Time (Hours)
Deep	First	[0.33,0.0080,1.79,0.33,0.14]	$1.95 * 10^{-2}$	$2.41 * 10^{-5}$	2.22
	Second	[0.33,0.0080,1.79,0.33,0.14]	$4.66 * 10^{-2}$	$2.41 * 10^{-5}$	1.91
	Third	[0.33,0.0080,1.79,0.33,0.14]	$9.48 * 10^{-2}$	$3.03 * 10^{-5}$	2.56
Intermediate	First	[0.33,0.0080,1.79,0.33,0.14]	$4.13 * 10^{-2}$	$3.20 * 10^{-5}$	2.21
	Second	[0.33,0.0080,1.79,0.33,0.14]	$5.83 * 10^{-2}$	$3.15 * 10^{-5}$	2.42
	Third	[0.33,0.0080,1.79,0.33,0.14]	$5.10 * 10^{-1}$	$3.57 * 10^{-5}$	2.32
Lateral	First	[0.33,0.0080,1.79,0.33,0.14]	$7.15 * 10^{-2}$	$3.53 * 10^{-5}$	2.30
	Second	[0.33,0.0080,1.79,0.33,0.14]	$1.07 * 10^{-1}$	$4.02 * 10^{-5}$	2.29
	Third	[0.33,0.0080,1.79,0.33,0.14]	$4.28 * 10^{-1}$	$3.70 * 10^{-5}$	3.11

Table 3.5: The resulted RDM by the Nelder-Mead simplex given both the SEEG potentials and the EEG potentials of the reference model in addition to real noise

Source	Initial conductivity	Resulted conductivity (S/m)	Initial RDM	Resulted RDM	Time (Hours)
Deep	First	[0.33,0.0080,1.79,0.33,0.14]	$4.72 * 10^{-2}$	$2.86 * 10^{-5}$	2.30
	Second	[0.33,0.0080,1.79,0.33,0.14]	$1.36 * 10^{-1}$	$2.87 * 10^{-5}$	3.25
	Third	[0.33,0.0080,1.79,0.33,0.14]	$9.48 * 10^{-2}$	$3.03 * 10^{-5}$	2.56
Intermediate	First	[0.33,0.0080,1.79,0.33,0.14]	$4.74 * 10^{-2}$	$3.33 * 10^{-5}$	2.58
	Second	[0.33,0.0080,1.79,0.33,0.14]	$9.09 * 10^{-2}$	$4.38 * 10^{-6}$	2.25
	Third	[0.33,0.0080,1.79,0.33,0.14]	$5.1 * 10^{-1}$	$3.57 * 10^{-5}$	2.32
Lateral	First	[0.33,0.0080,1.79,0.33,0.14]	$7.15 * 10^{-2}$	$3.55 * 10^{-5}$	2.67
	Second	[0.33,0.0080,1.79,0.33,0.14]	$1.07 * 10^{-1}$	$4.07 * 10^{-5}$	2.50
	Third	[0.33,0.0080,1.79,0.33,0.14]	$4.28 * 10^{-1}$	$3.70 * 10^{-5}$	3.11

optimizing the forward model then recommended the investigation of other global methods like the simulating annealing and the genetic algorithm [107].

In this study, and for the first time to the best of our knowledge, three common optimization algorithms were compared for optimizing the forward head model in the purpose of estimating in-vivo conductivities. These optimization algorithms are: the Nelder-Mead simplex, the genetic algorithm and the simulating annealing. These optimization algorithms were chosen because of their robustness and easiness to implement. In addition, as they were considered or recommended in previous studies on in-vivo conductivity estimation, the purpose was to validate or refute their consideration. In general, to test a robustness of an optimization algorithm, it is set to start the search from more than one initial point to ensure that the performance of the optimization algorithm is independent of the choice of the initial point. In this research three different initial points were considered, and from these initial points the NMS converged always to the reference conductivity values while the GA and the SA gave different results for different initial points.

The nature of the current study urges to consider other parameters, in addition to the starting point, for checking the performance of the optimization algorithms. These parameters are: the number of measurements and the stimulation position. In real analysis, IES occurs at different anatomical position in the head of the epileptic patient, so in simulation these stimulation position are chosen accordingly. In addition, there are two different measurement that are acquired while performing the IES: the scalp EEG measurements and the intracerebral SEEG measurements. Therefore, the optimization algorithms were tested considering three different stimulation positions classified according to their deepness (their distance from the scalp), and considering the two different measurement setups: SEEG and SEEG-EEG. In these different setups, the NMS converged always to the reference conductivity in smaller period of time than the GA and the SA, while the GA and the SA did not converge to the reference conductivity values although they required more time compared to NMS.

Simulation analysis acts as an ideal case for real analysis, because real analysis includes uncontrolled factors like the noise. In simulation analysis, these uncontrolled factors do not appear unless they are added by the user. So it is not guaranteed that the performance of an optimization algorithm in the real analysis is as good as its performance on simulation analysis. However, in order to ensure that the performance of an optimization algorithm in real analysis is as close as possible to its performance in the

simulation analysis an extra noise (mostly white Gaussian noise) is added to the simulated data [134, 107]. For the purpose of comparing the optimization algorithms in this study, a white Gaussian noise was added to the output potentials of the forward model in a way to make the SNR of the output potential 80 dB. The performance of the NMS in converging to the reference conductivity was as good as its performance when no noise was added. As expected, the NMS outperformed the GA and SA in both the solution and the speed in searching for the reference conductivity when additional noise was added as it outperformed them when no noise was considered. Moreover, the performance of the NMS was inspected in simulation analysis when real noise was added. The real noise is filtered from the acquired stimulations by the EEG and the SEEG electrodes. In the presence of real noise, the NMS was found to converge always to the reference conductivity.

Due to the superiority of the NMS over the GA and SA, it was considered to perform real in-vivo conductivity estimation. This study considered the NMS for optimizing the forward head model as many studies in the field did [85, 94, 96, 105, 107]. However, no study before did perform a comparison of the different optimization algorithm on the forward head model, this lack of comparison could be due to the computation complexity that the forward head models require especially because most of the studies considered either the BEM or the FEM. Yet, it is important to note that the superiority of the NMS over the GA and the SA was found on fixing the stopping criteria to be the same for the three algorithms. However, there are more parameters that are special for each optimization algorithm which should be fixed according to the problem of the study. In this work, these specific parameters (like the temperature factor for SA and the number of elite vectors in GA) were chosen to have a search that does not trapped in a local minimum and cover a wide range, but in order to obtain the best parameters for this problem, an additional study should be performed. Likely, because no additional parameters should be fixed in the NMS compared to GA and SA, most of previous studies chose the NMS for performing the estimation in their forward head model studies.

3.5 Summary

In-vivo conductivity estimation depends on correcting the conductivity values in the forward head model based on the real potentials. This process is leaned on optimization algorithms which modify the conductivity values in the head model in order to reduce the error between the real potentials

and the model potentials. Hence, the choice of a robust optimization algorithm for in-vivo conductivity estimation is essential. In the literature, many optimization algorithms were considered for estimating conductivities, however, no study gave strong arguments on their consideration. This lack of information on the superiority of an optimization algorithm over the others has left the door open for other researchers to try or recommend different optimization algorithms.

In this study, the numerical FEM method was considered to determine the output potentials in the realistic head model. Since the FEM method cannot be solved analytically, the talk was focused on free-derivative optimization algorithms: The Nelder-Mead simplex, the genetic algorithm and the simulating annealing. These algorithms were considered because they are easy to implement and common. In addition, these optimization algorithms were tested or recommended in previous studies on in-vivo conductivity estimation, so the aim was to validate or refute the consideration of previous studies. In general, optimization algorithms are tested from different initial points (multi-start procedure) to ensure that the performance of the optimization algorithm is independent of the choice of the starting point. In addition to the multi-start procedure, this study has tested the optimization algorithms given different measurements, different stimulation positions and when considering white Gaussian noise. In all these scenarios, Nelder-Mead simplex outperformed the other two algorithms in terms of convergence and time. Moreover, Nelder-Mead simplex gave a robust results when real noise was added to the model's potentials. This performance of Nelder-Mead simplex leaded it to be considered in the real analysis for estimating in-vivo conductivities.

Chapter 4

Sensitivity Analysis

The accuracy of the EEG forward head model depends on the geometry and the conductivity values which are assigned to the different compartments in the head model. Since the FEM head model is solved numerically, the influence of the conductivities on the model's output is still not well understood. In this study, a sensitivity analysis is performed to determine the effect of changing or perturbing the conductivity values on the generated potentials and how much the generated potentials are sensitive to the input conductivities. Estimating in-vivo conductivities by optimizing the forward model requires the output potentials to be sensitive to the conductivity values. This explains why EEG potentials are considered for estimating the in-vivo conductivity of the skull and not MEG, because EEG is more sensitive to the skull conductivity than MEG. In this study, due to the new materials (SEEG/EEG in simultaneous with IES) that we considered, the sensitivity of the generated potentials to the conductivities are determined given different intracerebral stimulation positions and given different measurement setups. Performing the sensitivity analysis given different stimulation positions and given different measurement setups is important for examining the dependency of the sensitivity to the stimulation position and the measurement setup.

The purpose of this work is to show under which conditions in-vivo conductivity estimation of the different head compartments is possible and to evaluate the confidence of the estimated values according to conditioning the measurements and the location of the intracerebral electrical stimulation. This chapter presents the sensitivity analysis of the SEEG/EEG forward problem with respect to the conductivities. The analysis is performed on the intracerebral SEEG and the scalp EEG topographies, by considering two error functions: The RDM which is common in the field of head models and

measures the topographic error, and the relative error which is common in many fields of science. The results presented in this chapter are generated by simulation where the spatial conditioning of the electrodes is only imposed by structuring the brain's digitization. The objective from this analysis is to show the spatial limits and also to heuristically discuss the best condition depending on the real localisation of the SEEG electrodes.

4.1 Materials and Method

In this study, a one-at-a-time sensitivity analysis was performed in which the sensitivity of the output to each input conductivity value is determined independently of the other conductivity values. For implementing the sensitivity analysis, two head models of the same patient were generated. The first head model acted as a reference head model and its output potentials V_{ref} (as shown in Eq.4.1) are determined based on fixed conductivity values $\boldsymbol{\sigma} = [\sigma_1, \sigma_2, \cdots, \sigma_N]$ where N is the number of the compartments in the head model (in this sensitivity analysis we consider N as five in one case and three in another case).

$$\nabla \cdot \boldsymbol{J}^p = \nabla \cdot (\boldsymbol{\sigma} \nabla V_{ref}) \tag{4.1}$$

The conductivity values in the second head model (test head model) are set equal to the reference conductivity values except one conductivity value which is set to change linearly in order to determine the effect of that change in the output error between the reference model and the test model as shown in Eq.4.2.

$$error = f(V_{ref}, V_{test}) \tag{4.2}$$

Where

$$\nabla \cdot \boldsymbol{J}^p = \nabla \cdot (bm\sigma^* \nabla V_{test}) \tag{4.3}$$

And

$$\boldsymbol{\sigma^*} = [\sigma_1, \cdots, \sigma_r^*, \cdots, \sigma_N] \tag{4.4}$$

Where

$$\sigma_r^* = \sigma_r(0.5 + 0.1 * n) \quad \forall r \in [1, N], n \in [1, 10] \tag{4.5}$$

Since the purpose of the analysis is to determine the sensitivity of the output error only to conductivity values, the other parameters of

the test head model were set to be equal to those of the reference head model. Therefore, the resulted error in Eq.4.2 is only due to the change in one conductivity value. The sensitivity analysis was performed given different conditions (Different number of head compartments, different stimulation positions and different measurement positions) different error functions (Relative difference measurement and relative error) and for two different drug-resistant epileptic patients (Patient(1): male, 23 years old and Patient(2): female, 34 years old). Carrying out the sensitivity given different conditions and different patients enabled us to determine the effect of these parameters on in-vivo conductivity estimation.

For performing the sensitivity analysis in a FEM head model, the data which generates the stiffness matrix A and the force vector B was considered. This data includes the the T1-weighted MR images in addition to the CT scans of each patient for generating homogeneous and isotropic FEM head models. From the CT scans the positions of the SEEG contacts were detected. Two of the SEEG contacts were chosen to represent the IES. While the positions of the scalp EEG electrodes were chosen according to the 10-20 and 10-10 standards.

4.2 Standard Measurement Positions

For estimating in-vivo conductivities, the scalp EEG and the intracerebral SEEG measurements which were acquired in simultaneous with IES in drug-resistant epileptic patients were considered. However, for obtaining a robust estimation of the conductivity values by optimizing the forward model, the output of the forward model should be sensitive to these conductivity values. Hence, it is important to perform a sensitivity analysis based on these real measurement positions of the scalp EEG and the intracerebral SEEG. In our study, the positions of the SEEG electrodes were obtained from the CT-scans [59], so they were fixed equal to their real positions for each patient, while the scalp EEG measurements were acquired by an average of 21 scalp electrodes (over three patients). Yet, it is important to examine the sensitivity of the output for different numbers of EEG electrodes since other studies have considered a larger number of EEG channels for estimating in-vivo conductivities like Acar et al. who considered 128 EEG channels [92] and Lew et al. who considered 63 EEG channels [93]. Thus, by considering different EEG placements for sensitivity analysis, the effect of increasing the number of EEG channel can be examined in simulation analysis. Moreover, the sensitivity analysis was performed considering the SEEG measurements in

addition to EEG measurements to find out if the sensitivity of the output is affected by adding the EEG measurements to the SEEG measurements. The measurement positions which were considered for performing the sensitivity analysis were as follows:

- 24-channel EEG measurements.
- 32-channel EEG measurements.
- 64-channel EEG measurements.
- 128-channel EEG measurements.
- SEEG measurements.
- SEEG measurements plus 24-channel EEG measurements.
- SEEG measurements plus 32-channel EEG measurements.
- SEEG measurements plus 64-channel EEG measurements.
- SEEG measurements plus 128-channel EEG measurements.

Where the EEG positions were according to th 10-20 and 10-10 standards [135]. Each intracerebral electrode contains many SEEG contacts, some of them are close to the skull and the scalp while the others are deeper and close to the white matter as shown in Fig.3.5. In order to study the sensitivity of the output to the conductivity values given these different stimulation positions, three different stimulations were considered for each sensitivity analysis: Deep, intermediate and lateral stimulation. These three stimulation positions were chosen from the same electrode, so their orientation were the same. However, in order to check the effect of changing the orientation of the stimulation, another lateral stimulation was considered. To differentiate between the two lateral stimulations, the one which has the same orientation as deep and intermediate stimulations was called: lateral1, while the other lateral stimulation was called: lateral2. The positions of the chosen stimulations are shown in Fig.4.1

4.2.1 Sensitivity of the RDM: Five-compartment Head Model of Patient(1)

Since the purpose of the in-vivo conductivity estimation is to enhance source localization. The RDM is considered in this study, because it is not affected

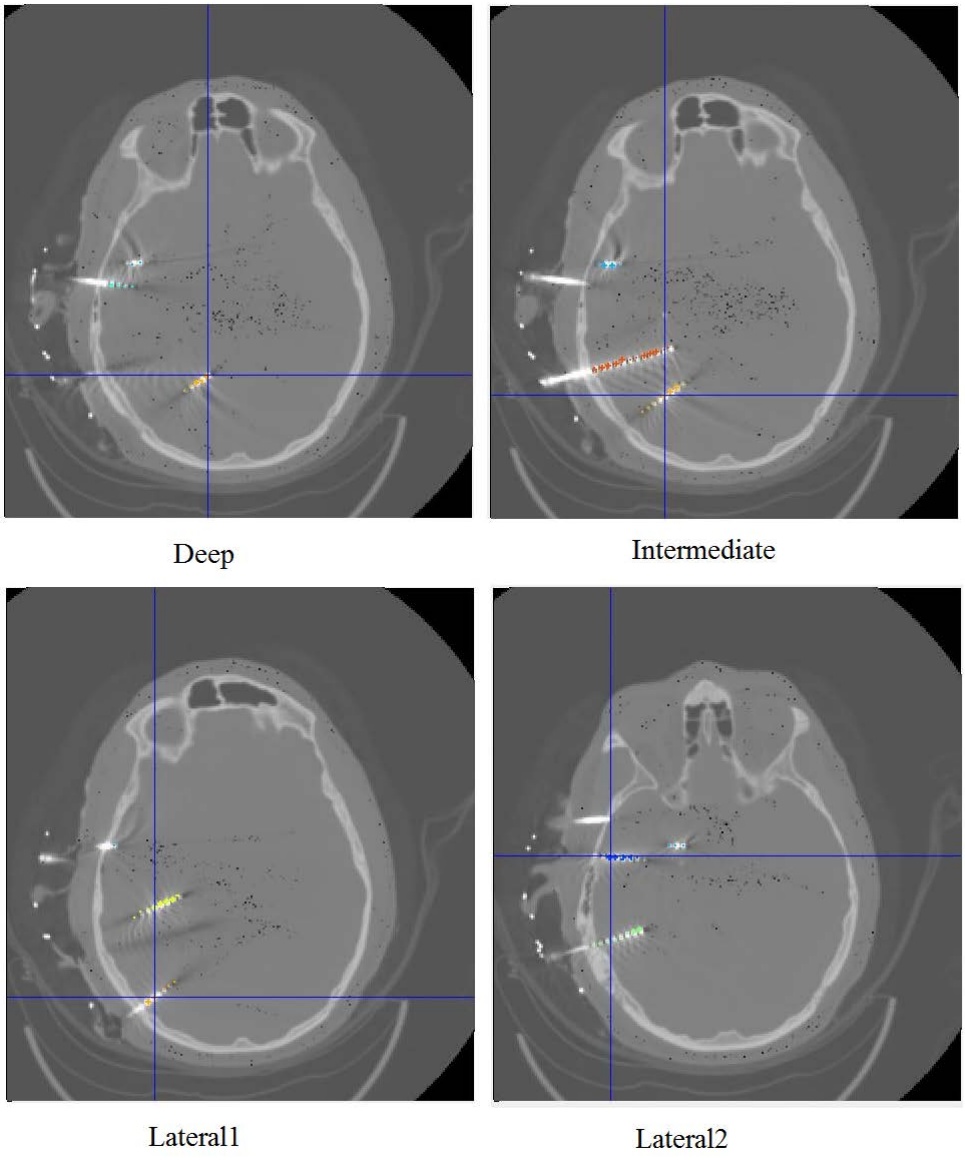

Figure 4.1: The anatomical positions of the deep, intermediate and lateral stimulation which where considered in this study. The blue cross shows the position of the stimulation.

by the amplitude which does not influence source localization. However, in-vivo conductivity estimation depends on the sensitivity of the RDM to these conductivity values. Thus for predicting the performance of real conductivity estimation, sensitivity analysis was implemented on a five-compartment FEM head model of Patient(1). In the reference head model of this one-at-a-time sensitivity analysis, the conductivity values were fixed as: 0.33 S/m for scalp, 0.008 S/m for skull, 1.79 S/m for CSF, 0.33 S/m for GM and 0.14 S/m for WM [15, 87, 88].

Scalp electrodes

Fig.4.2 shows the sensitivity of the RDM to the five conductivities when 24 scalp EEG electrodes were considered. It can be noted from the figure that in the case of deep, intermediate and lateral1 stimulations, the sensitivity of the RDM to the GM and WM conductivities is low compared to the sensitivity to the scalp, the skull and the CSF. This is not surprising since the scalp measurements are acquired far from the WM and the GM compartments. However, the sensitivity to the WM in lateral2 stimulation is comparable to the sensitivity to the skull and the scalp. The difference between the sensitivity pattern in lateral1 and lateral2 indicates that the deepness is not the only factor that leads to differences in the resulted in-vivo conductivities. Fig.4.3 shows the sensitivity of the RDM to the five conductivities when 32 scalp EEG electrodes were considered. As in Fig.4.2, in the case of deep, intermediate and lateral1 stimulations, the sensitivity of the RDM to the GM and WM conductivities is low compared to the sensitivity to the scalp, the skull and the CSF. The increase in the number of EEG electrodes from 24 to 32 cause a slight drop in the sensitivity to the scalp and the skull in the case of deep, intermediate and lateral1 stimulations. While the increase in the number of EEG electrodes caused a slight increase in the sensitivity to the GM and the WM in the case of deep, intermediate and lateral1 stimulations. The decrease in the RDM sensitivity to the scalp and the skull conductivities can be explained by the decrease in the RDM between the test model and the reference model as more EEG data are considered. Therefore, the increase in EEG sensors reduces the error which is resulted from an erroneous conductivity assignment.

Increasing the number of EEG measurements from 32 to 64 did not change the pattern remarkably as can be seen in Fig.4.4. As in Fig.4.3, Fig.4.4 shows that the sensitivity of the RDM to the GM and WM conductivities is low compared to the sensitivity to the scalp, the skull, and the CSF in the case of in the case of deep, intermediate and lateral1 stimulations. The

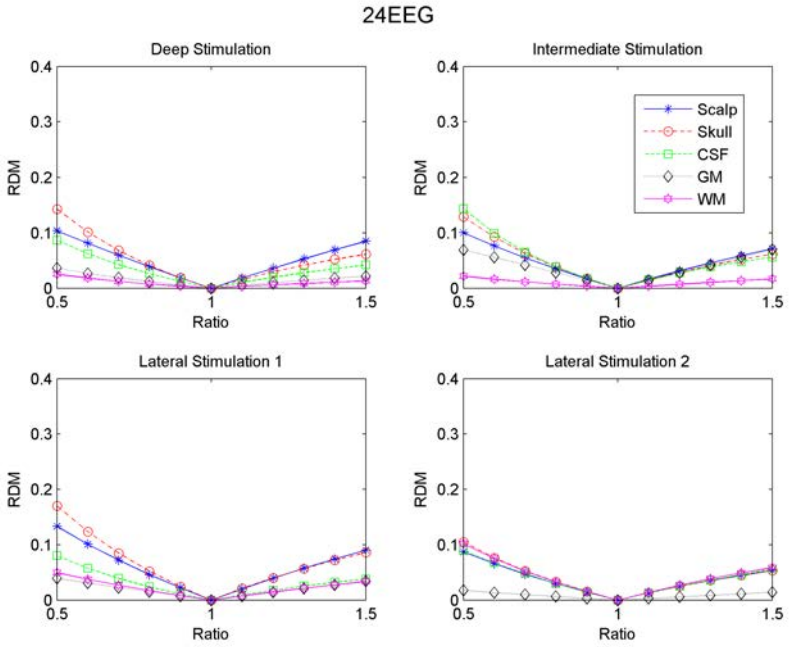

Figure 4.2: The error function RDM resulted from changing one conductivity value in a five-compartment FEM head model compared to the reference model when considering the 24 EEG positions for Patient(1).

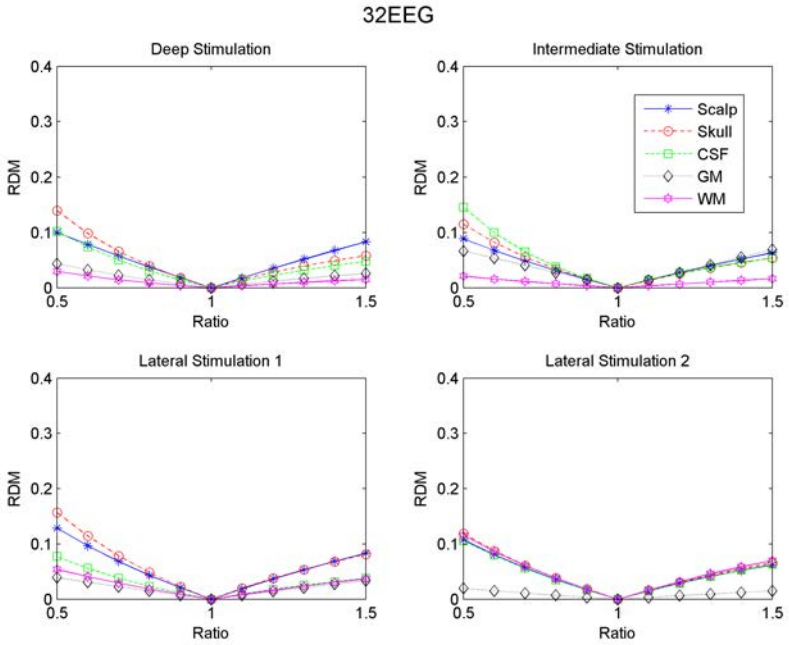

Figure 4.3: The error function RDM resulted from changing one conductivity value in a five-compartment FEM head model compared to the reference model when considering the 32 EEG positions for Patient(1).

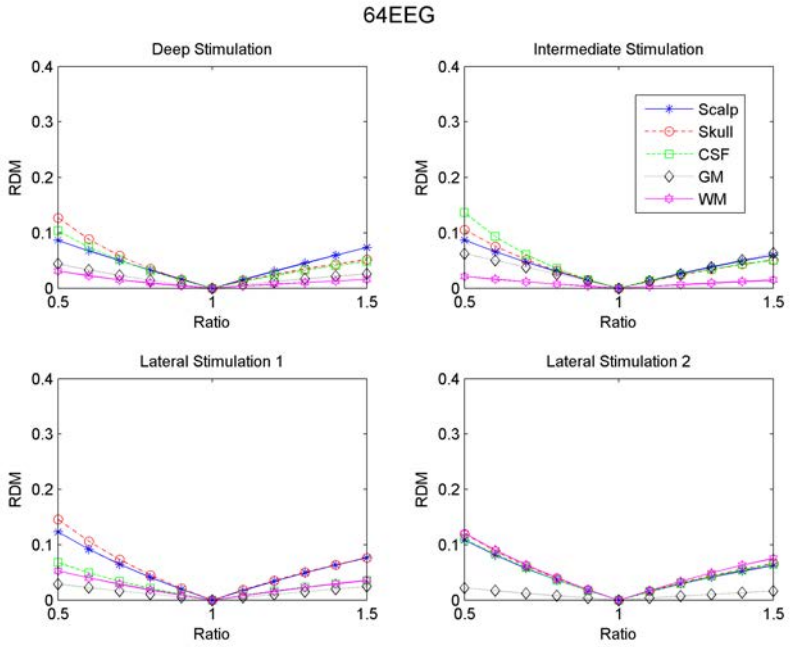

Figure 4.4: The error function RDM resulted from changing one conductivity value in a five-compartment FEM head model compared to the reference model when considering the 64 EEG positions for Patient(1).

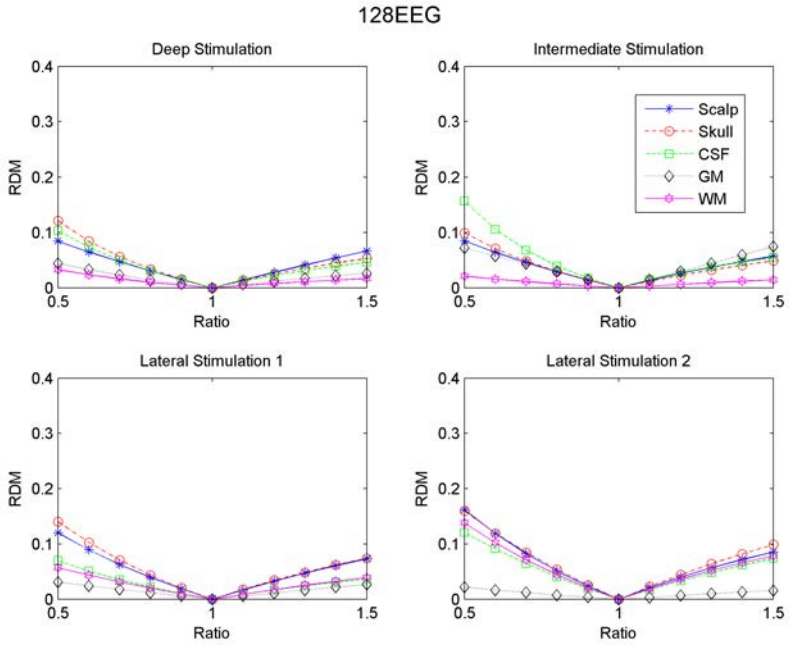

Figure 4.5: The error function RDM resulted from changing one conductivity value in a five-compartment FEM head model compared to the reference model when considering the 128 EEG positions for Patient(1).

sensitivity of the RDM to the skull and the scalp decreases notably (except for lateral2) as more EEG electrodes are added (from 32 to 64). While the sensitivity of the RDM to the GM decreases in the case of intermediate and lateral1 stimulation as the number of electrodes increases from 32 to 64. The decrease in sensitivity is due to the increase in accuracy as more electrodes are considered. When more EEG electrodes are added (from 64 to 128) as shown in Fig.4.5, the sensitivity pattern change similarly to the change from 32 to 64 in the case of deep, intermediate and lateral1 stimulations. However, there is a notable jump in the sensitivity of the RDM to all the conductivities except the WM in the case of lateral2 stimulation. On the contrary to the deep, intermediate and lateral2 stimulations in which the sensitivity has a smooth change to the WM, the change in the sensitivity in the case of lateral1 stimulation was sharp and notable when the number of EEG electrodes increased from 64 to 128.

Intracerebral electrodes

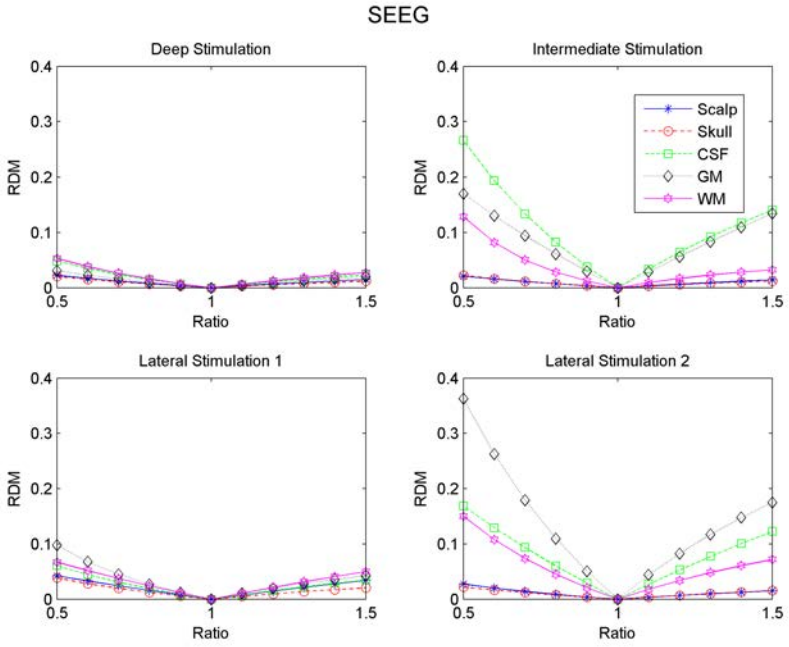

Figure 4.6: The error function RDM resulted from changing one conductivity value in a five-compartment FEM head model compared to the reference model when considering the SEEG positions for Patient(1).

Fig.4.6 shows the sensitivity of the RDM to the five-compartment conduc-

tivities when considering the intracerebral SEEG measurements. In contrast to the sensitivity results when considering the EEG scalp measurements, when considering the SEEG, the RDM is less sensitive to the scalp and the skull than to the CSF, the GM and the WM conductivities. This result makes sense since the current distribution does not pass through the scalp and the skull conductivities before reaching the SEEG electrodes. Even though the sensitivity to the WM in case of deep stimulation is the highest compared to the other conductivities (which is expected since the deep stimulation is the nearest to the WM compartment), this sensitivity is relatively low. The sensitivity to the CSF conductivity is the highest when considering the intermediate stimulation, since the intermediate stimulation is performed close to the CSF compartment. The order of the pattern in lateral1 is similar to the order of the pattern in lateral2, however, the sensitivity to the deep compartments in lateral2 is higher than the sensitivity to the deep compartments in lateral1 which indicates that other factors than the deepness of the stimulation do affect in-vivo conductivity estimation.

Intracerebral and Scalp Electrodes

Adding 24 EEG electrodes to the SEEG electrodes did change the pattern of the sensitivity analysis notably as shown in Fig.4.7. The change in the pattern is only due the increase of the sensitivity of the scalp and the skull compartments. The sensitivity to the scalp and the skull became the highest in lateral1 stimulation since the lateral stimulation is the nearest to these compartments. However, this was not the case in lateral2 stimulation. Adding 24 EEG electrodes did not change the sensitivity to the deep compartment in general except for the intermediate stimulation in which the sensitivity to the CSF, the GM and the WM decreases slightly after adding the measurements of the 24 EEG electrodes. On the other hand, increasing the number of EEG measurements (from 24 EEG to 32 electrodes) as shown in Fig.4.8 did not change the pattern of the sensitivity in general. There is only a slight increase in the sensitivity to the scalp and the skull compartments in all stimulations, in addition to a vague decrease in the sensitivity of the RDM to the CSF, the GM and the WM in the case of intermediate stimulation.

Increasing the number of EEG scalp electrodes from 32 to 64 while considering the SEEG measurements as shown in Fig.4.36, increases the sensitivity of the RDM to the scalp and the skull conductivities. This increase in the sensitivity pattern to the scalp and the skull is very significant in intermediate and lateral1 stimulations because they are nearer to the scalp and the skull

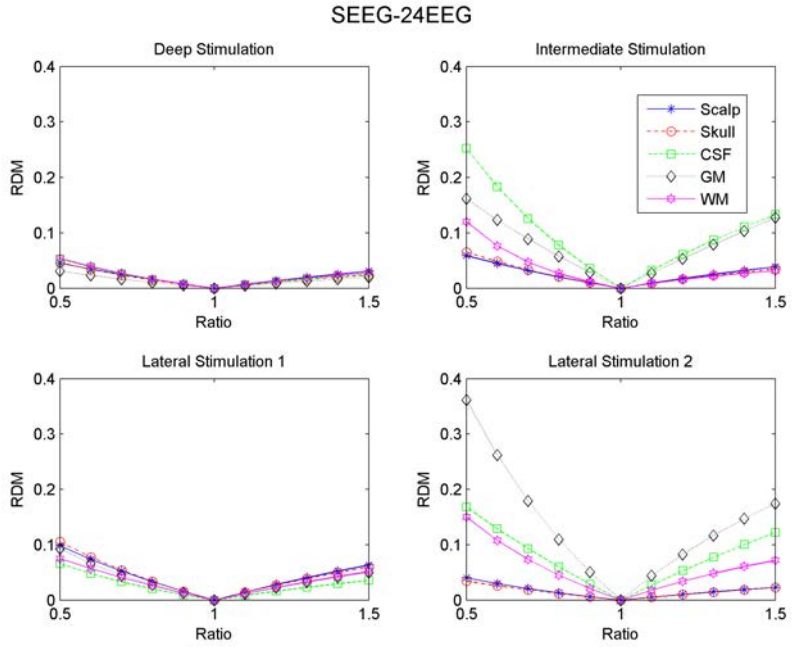

Figure 4.7: The error function RDM resulted from changing one conductivity value in a five-compartment FEM head model compared to the reference model when considering the SEEG-24 EEG positions for Patient(1).

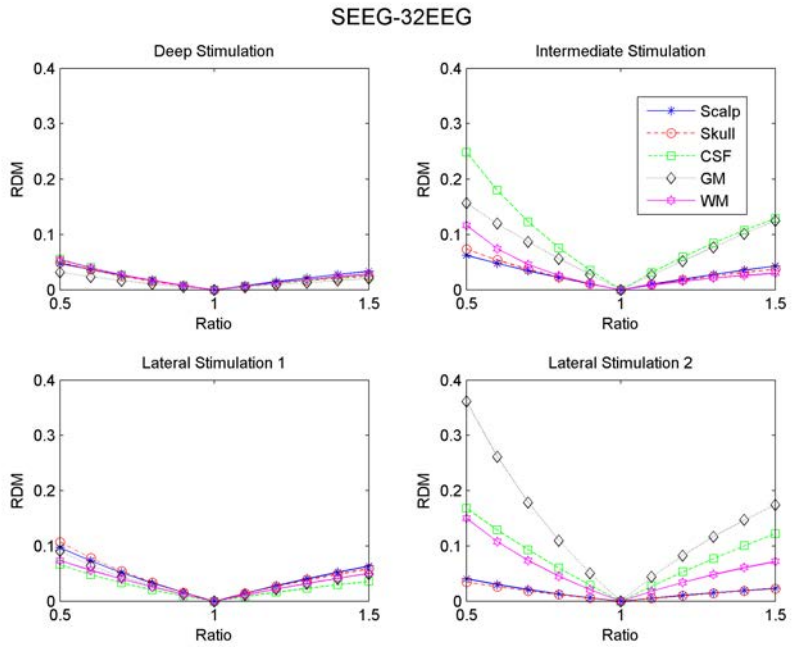

Figure 4.8: The error function RDM resulted from changing one conductivity value in a five-compartment FEM head model compared to the reference model when considering the SEEG-32 EEG positions for Patient(1).

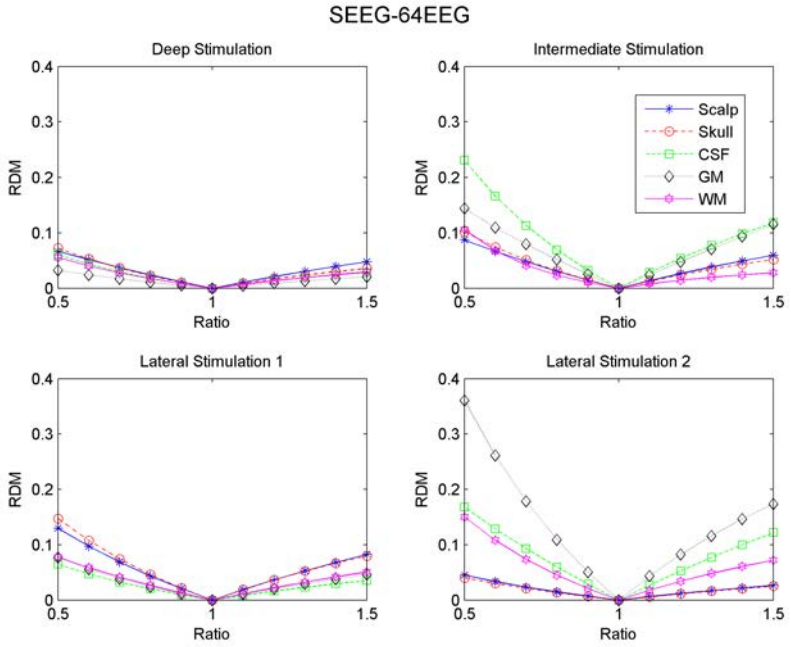

Figure 4.9: The error function RDM resulted from changing one conductivity value in a five-compartment FEM head model compared to the reference model when considering the SEEG 64 EEG positions for Patient(1).

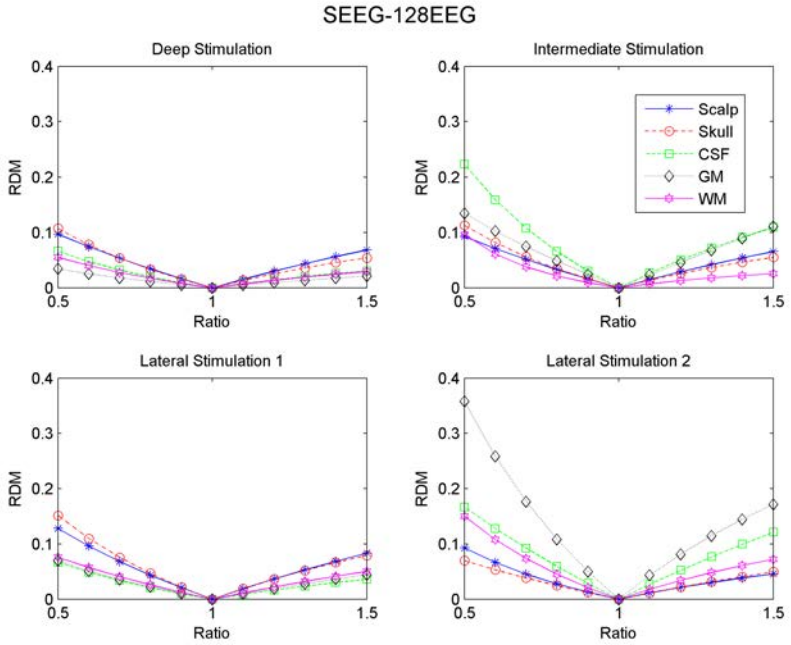

Figure 4.10: The error function RDM resulted from changing one conductivity value in a five-compartment FEM head model compared to the reference model when considering the SEEG-128 EEG positions for Patient(1).

compartments than the deep stimulation. However, the increase of the sensitivity to the scalp and the skull compartment after increasing the number of EEG electrodes from 32 to 64 is slight in the case of lateral2 stimulation. Yet, when the EEG scalp electrodes are increased from 64 to 128, as shown in Fig.4.10, the sensitivity to the scalp and the skull compartments increases notably in both the deep and lateral2 stimulations but slightly in the case of intermediate and lateral1 stimulations. In general, the increase of RDM sensitivity to the scalp and the skull compartment makes sense as more EEG electrodes are considered. However, the difference in the increase pattern in the different stimulations (specially between lateral1 and lateral2) indicates that there are other factors than the deepness which affect the sensitivity.

4.2.2 Sensitivity of the Relative Error: Five-compartment Head Model of Patient(1)

For performing in-vivo conductivity estimation by optimizing the forward head model an error measurement function should be considered. Since the purpose of estimating accurate conductivities is to enhance source localization, the RDM was considered because it is not affected by the magnitude which does not affect source localization [116, 114]. However, in order to check if other error measurements give a better sensitivity profile, the relative error function, which is shown in Eq.4.6, was considered for performing the sensitivity analysis on the five-compartment FEM head model of Patient(1) given the different measurement positions and the different stimulation positions. In the reference head model, the conductivity values were fixed as: 0.33 S/m for scalp, 0.008 S/m for skull, 1.79 S/m for CSF, 0.33 S/m for GM and 0.14 S/m for WM.

$$\frac{\sum(|V_o - V_{ref}|)}{\sum(|V_{ref}|)} \tag{4.6}$$

Scalp Electrodes

Fig.4.11 shows the sensitivity of the relative error to the five-compartments conductivities when considering the 24 EEG scalp electrodes. As expected, since the EEG electrodes are located over the scalp, the sensitivity of the relative error to the scalp and the skull conductivities is higher than the sensitivity to the WM and the GM, this can be noted in the case of deep and lateral2 stimulations. However, in both the intermediate and lateral1 stimulation, the sensitivity to the GM is larger than the sensitivity to the scalp and the skull compartments. In addition, it can be noted that the

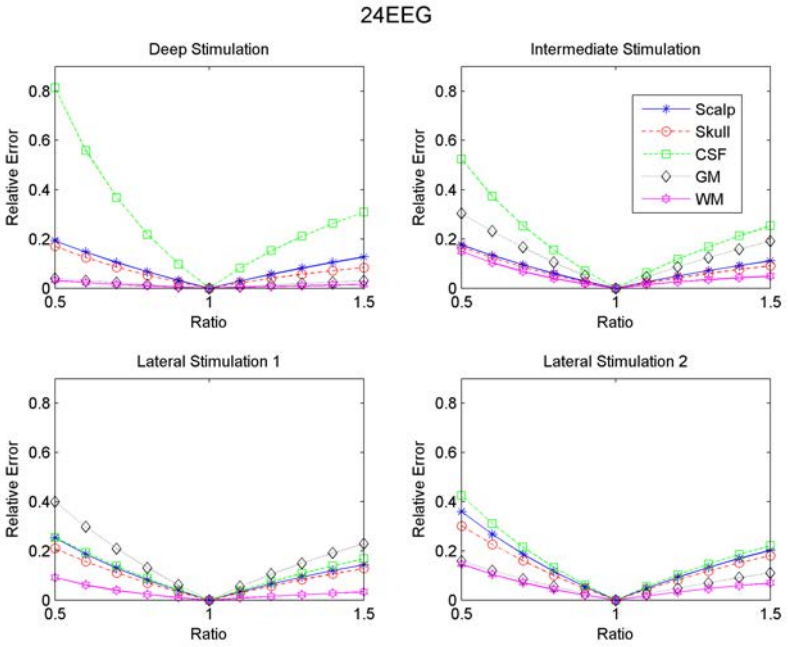

Figure 4.11: The relative error resulted from changing one conductivity value in a five-compartment FEM head model compared to the reference model when considering the 24 EEG positions for Patient(1).

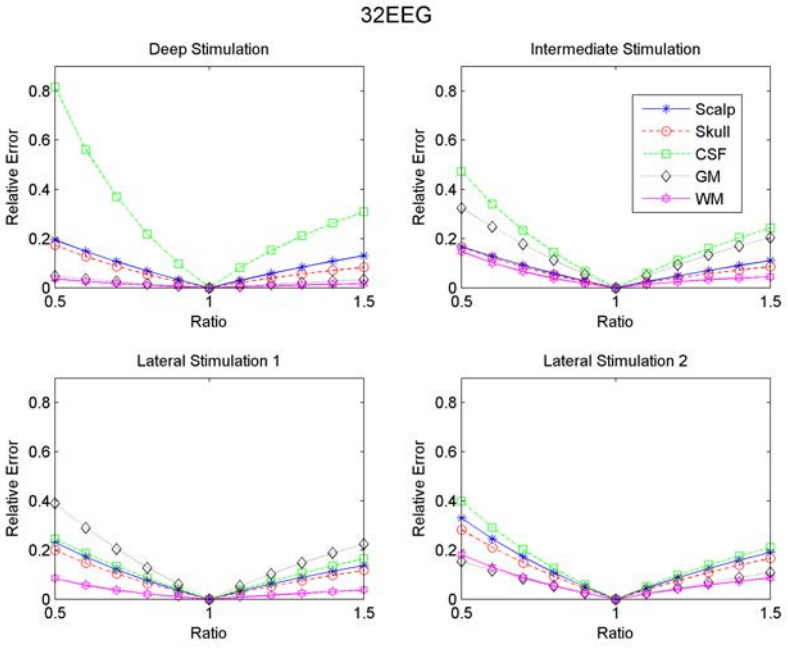

Figure 4.12: The relative error resulted from changing one conductivity value in a five-compartment FEM head model compared to the reference model when considering the 32 EEG positions for Patient(1).

sensitivity of the relative error to the CSF compartment is the highest in all the stimulations except the lateral2 stimulation. Adding more EEG scalp electrodes, change the pattern of the sensitivity slightly as shown in Fig.4.12. In general, the sensitivity of the relative error to the scalp and the skull compartment decreases as more EEG electrodes are added (this can be noted in the case of lateral2 stimulation). Adding more EEG electrodes, reduces the relative error due to an erroneous conductivity assignment in the scalp and the skull. While the sensitivity to the CSF, the GM and the WM conductivities does not have a uniform change as more EEG electrodes are added. The sensitivity to the CSF decreases notably as more EEG electrodes are added in both intermediate and lateral2 stimulations. While the sensitivity to the GM increases as more EEG electrodes are added in both deep and intermediate stimulation but decreases in both lateral1 and lateral2 stimulations. When considering the WM conductivity, the sensitivity of the relative error to it increases as more EEG electrodes are added in lateral2 stimulation while it decreases in lateral1 stimulation.

In contrast to the decrease in the sensitivity to the scalp and the skull conductivities as EEG scalp electrodes increases from 24 to 32, in Fig.4.13 it can be noted that the sensitivity of the relative error to the scalp and the skull conductivities in all the stimulations (except lateral2) increases as the EEG scalp electrodes increases from 32 to 64. The decrease in the sensitivity to the scalp and the skull conductivities from 24 EEG to 32 EEG and then its increase from 32 EEG to 64 EEG makes it hard to make a conclusion about the sensitivity of the relative error as more EEG electrodes are considered. For the deep compartments, as the number of EEG electrodes increases from 32 to 64, the sensitivity of the relative error to the WM increases slightly for all stimulations. The sensitivity of the relative error to the CSF conductivity increases for lateral1 while it decreases for lateral2 as shown in Fig.4.13. Fig.4.14 shows the sensitivity of the relative error to the five-compartment conductivities when 128 EEG electrodes are considered. When comparing the sensitivity pattern in Fig.4.13 to the sensitivity pattern in Fig.4.14 it can be noted that the sensitivity of the relative error to the scalp and the skull conductivities increases notably in the case of deep and lateral2 stimulations as the EEG scalp electrodes increases from 64 to 128.

Intracerebral Electrodes

Fig.4.15 shows the sensitivity of the relative error to the five-compartment conductivities when the intracerebral SEEG measurements are considered. It can be noted that the sensitivity of the relative error to the scalp and the

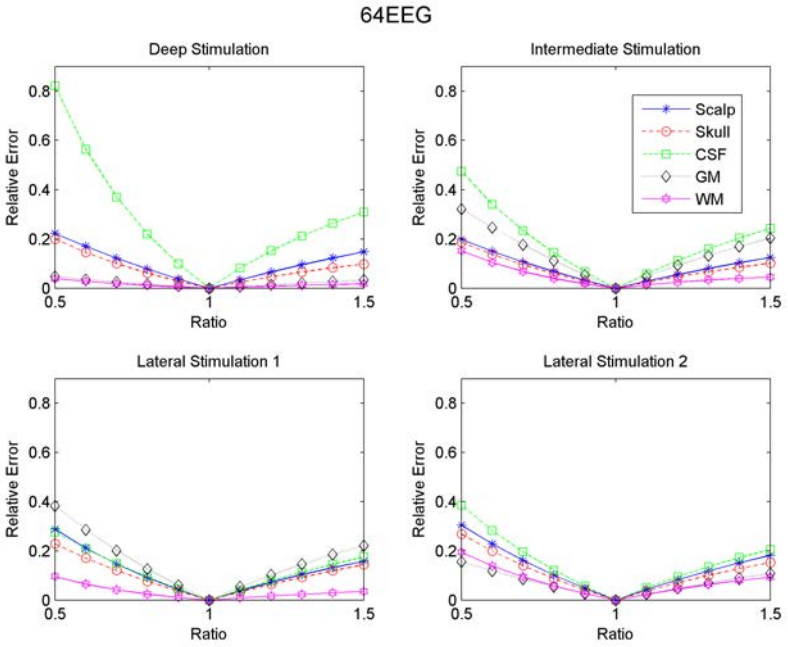

Figure 4.13: The relative error resulted from changing one conductivity value in a five-compartment FEM head model compared to the reference model when considering the 64 EEG positions for Patient(1).

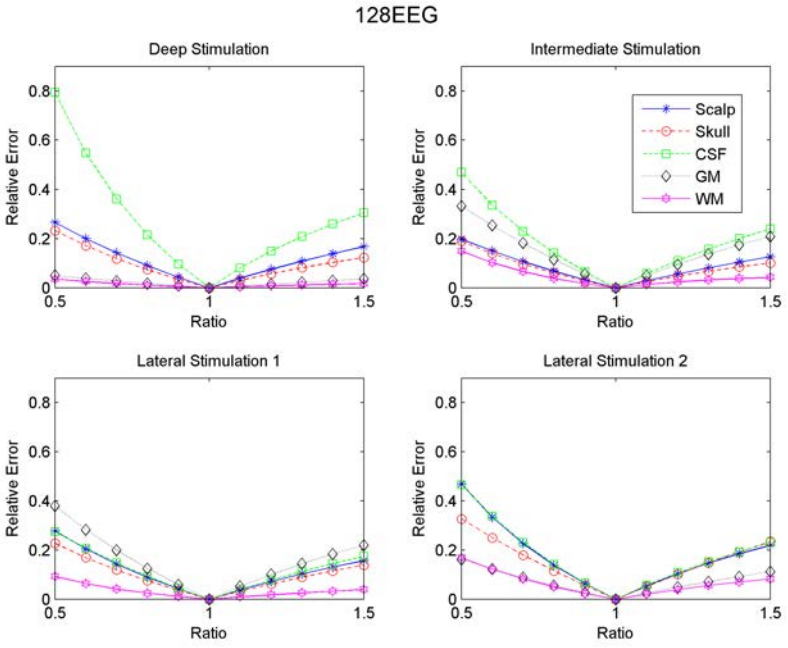

Figure 4.14: The relative error resulted from changing one conductivity value in a five-compartment FEM head model compared to the reference model when considering the 128 EEG positions for Patient(1).

skull conductivities drops remarkably when Fig.4.15 is compared to previous Fig.4.14. The drop in the sensitivity to the scalp and the skull when considering only the SEEG measurements is expected since the current distribution does not pass through the scalp and the skull compartments. However, the sensitivity of the relative error to the CSF compartment did not change (or change slightly for some stimulations) when the Fig.4.15 is compared to Fig.4.14. The constant pattern of the sensitivity to the CSF conductivity despite the total change in the measurements is unexpected.

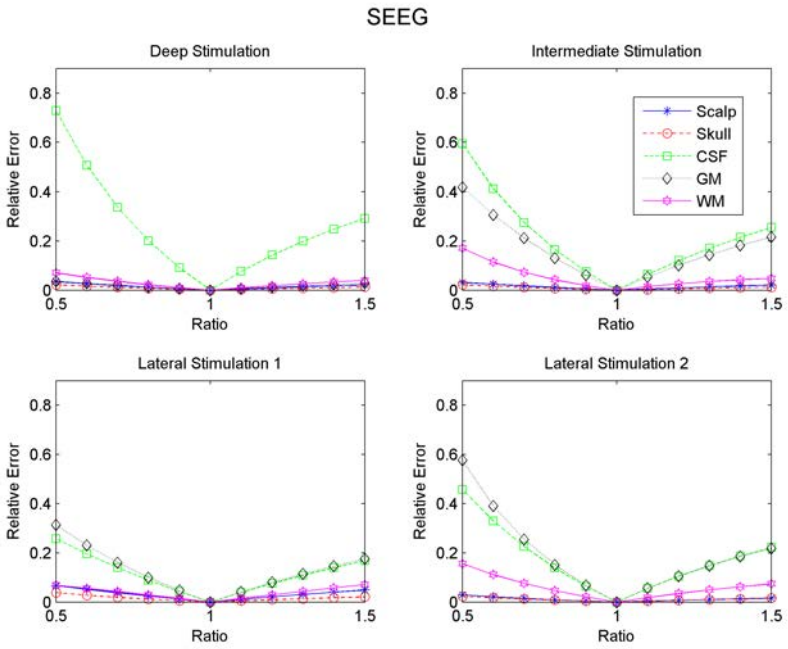

Figure 4.15: The relative error resulted from changing one conductivity value in a five-compartment FEM head model compared to the reference model when considering the SEEG positions for Patient(1).

Intracerebral and Scalp Electrodes

Adding 24 EEG scalp electrodes to the SEEG electrodes change the sensitivity of the relative error to the scalp and the skull conductivities as shown in Fig.4.16. Since the EEG electrodes are placed over the scalp compartment, adding EEG electrodes is expected to change the sensitivity to the scalp and the skull compartments. As expected, when Fig.4.15 is compared to Fig.4.16 the sensitivity of the relative error to the scalp and the skull compartment increases notably (especially for the intermediate

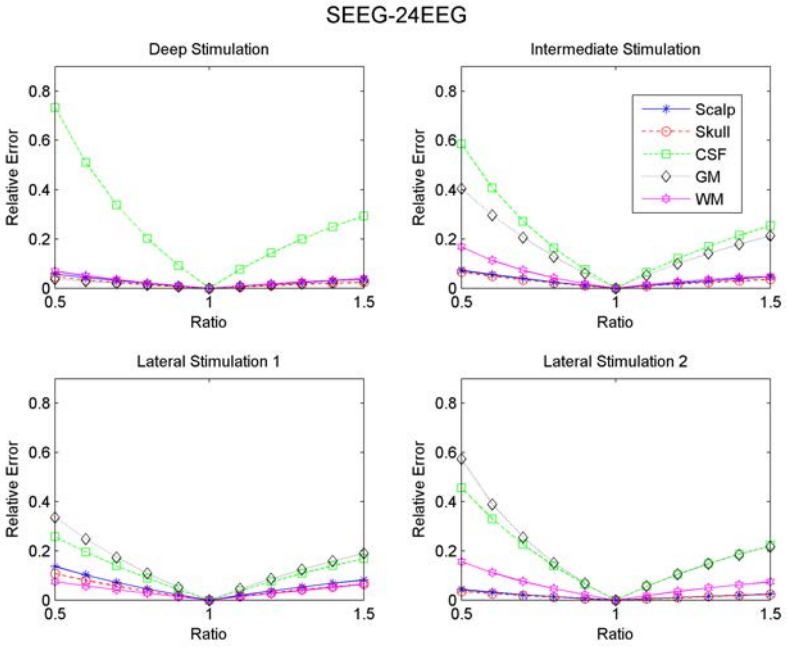

Figure 4.16: The relative error resulted from changing one conductivity value in a five-compartment FEM head model compared to the reference model when considering the SEEG-24 EEG positions for Patient(1).

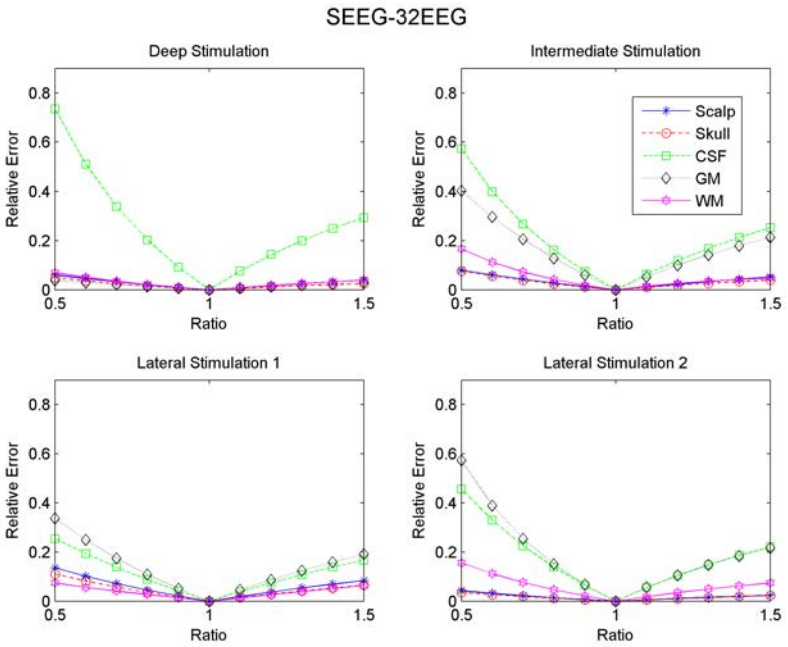

Figure 4.17: The relative error resulted from changing one conductivity value in a five-compartment FEM head model compared to the reference model when considering the SEEG-32 EEG positions for Patient(1).

and lateral1 stimulations). However, adding more EEG electrodes (from 24 to 32) does not change the pattern remarkably. When considering 32 scalp EEG electrodes, the sensitivity to the scalp and the skull conductivities change very vaguely as shown in Fig.4.17.

On the contrary to the slight change in the sensitivity of the relative error to the scalp and the skull compartment as EEG electrodes increase from 24 to 32, the sensitivity to the scalp and the skull compartments increases notably (especially for intermediate and lateral1 stimulations) as EEG electrodes increases from 32 to 64 as shown in Fig.4.18. However, when Fig.4.18 that represents the 64 EEG with SEEG measurements case is compared to Fig.4.13 that represents 64 EEG measurements, it can be noted that the sensitivity to the scalp and the skull conductivities when there is no SEEG measurements is higher. Increasing the number of EEG scalp electrodes from 64 to 128 while considering the SEEG intracerebral electrodes increases the sensitivity of the relative error notabley to the scalp and the skull conductivity as shown in Fig.4.19. However, the sensitivity to the CSF and the GM conductivities is larger when the SEEG are considered with 128 EEG than when only the 128 EEG measurements are considered as is shown in Fig.4.14.

In general, the relative error was found to have a high and fixed sensitivity to the CSF conductivity. In addition, the sensitivity of the relative error did not have a uniform increase or decrease as EEG scalp electrodes were increasing. When EEG scalp electrodes increased from 24 to 32, the sensitivity to the scalp and the skull compartment decreased, however, when the EEG electrodes increased from 32 to 24, the sensitivity to the scalp and the skull conductivities increased. Yet, similar to the sensitivity of the RDM, the sensitivity of the relative error to the five-compartment conductivities were biased toward the small conductivity values, that is the relative error was found to be more sensitive to small conductivity assignment than to larger conductivity assignment.

4.2.3 Sensitivity of the RDM: Three-compartment Head Model of Patient(1)

In the literature, it was found that separating the CSF compartment from the brain, and the GM from the WM is important for performing an accurate source localization [110, 111]. However, there are many work which were based on three-compartment head model since the three-compartment head model can be solved analytically (when a sphere is considered) or numeri-

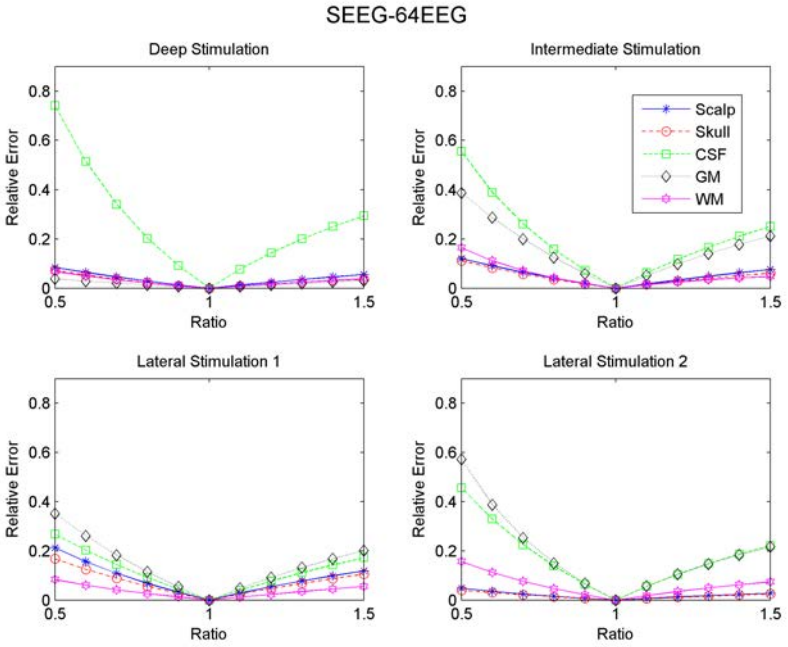

Figure 4.18: The relative error resulted from changing one conductivity value in a five-compartment FEM head model compared to the reference model when considering the SEEG-32 EEG positions for Patient(1).

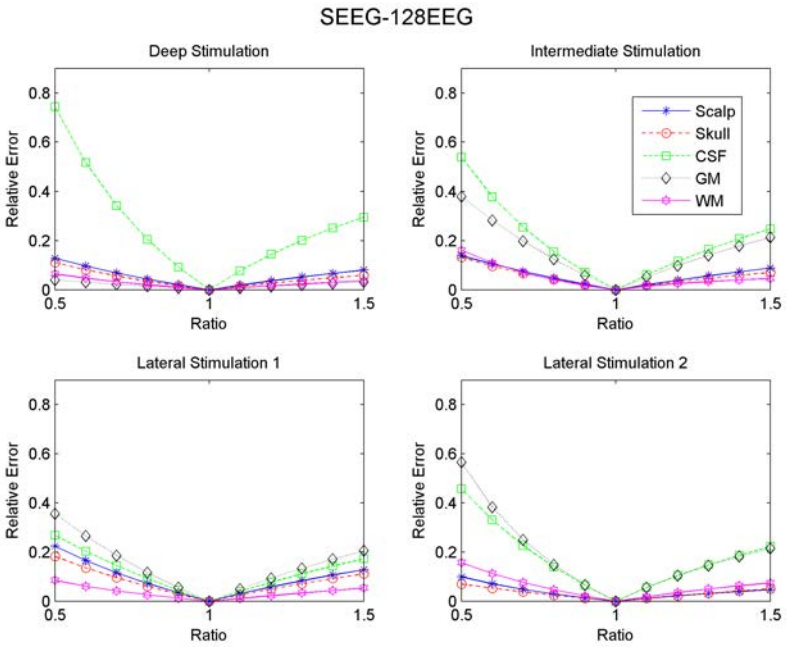

Figure 4.19: The relative error resulted from changing one conductivity value in a five-compartment FEM head model compared to the reference model when considering the SEEG-128 EEG positions for Patient(1).

cally (when a realistic head model is considered). In this study, and for the purpose of examining the difference between the five-compartment and the three-compartment head models, the sensitivity analysis was performed on a three-compartment FEM head model of Patient(1). In this analysis, the conductivities which were assigned in the reference head model were: 0.33 S/m for scalp, 0.008 for skull and 0.33 S/m for brain.

Scalp Electrodes

Fig.4.20 shows the sensitivity of the RDM to the three-compartment conductivities when considering 24 EEG scalp electrodes. It can be noted from the figure that the sensitivity of the RDM to the scalp and the skull conductivities in all stimulations is higher than the sensitivity of the RDM to the brain compartment. The high sensitivity to the scalp and the skull conductivities when considering only scalp EEG electrodes is expected since the current distribution passes by these compartments before reaching the scalp EEG electrodes. As the EEG electrodes increases from 24 to 32, the sensitivity to the scalp and the skull conductivities increases, however, this increase is not remarkable. Yet, increasing the number of EEG electrodes from 24 to 32 for the five-compartment head model decreases the sensitivity of the RDM to the scalp and the skull compartment, which was explained by the decrease in the effect of assigning erroneous conductivity values as the number of EEG electrodes increases.

Fig.4.22 shows the sensitivity of the RDM to the three-compartment conductivities when considering 64 EEG scalp electrodes. When increasing the number of EEG scalp electrodes from 32 to 64, a very slight change appears in the sensitivity of the RDM to the three-compartment head model. However, when the number of EEG scalp electrodes increases from 64 to 128 as shown in Fig.4.23 , the sensitivity of the RDM to the scalp and the skull compartments increases notabley especially for the lateral2 stimulation. It can be noted also from Fig.4.23 that the sensitivity of the RDM to the scalp and the skull conductivities are very similar in the case of lateral1 and lateral2 stimulations, but the difference between lateral1 and lateral2 is more significant when considering the sensitivity of the RDM to the brain conductivity.

Intracerebral Electrodes

Fig.4.24 shows the sensitivity of the RDM to the three-compartment conductivities when considering the intracerebral SEEG electrodes. As expected, the sensitivity of the RDM to the brain compartment is higher than the sen-

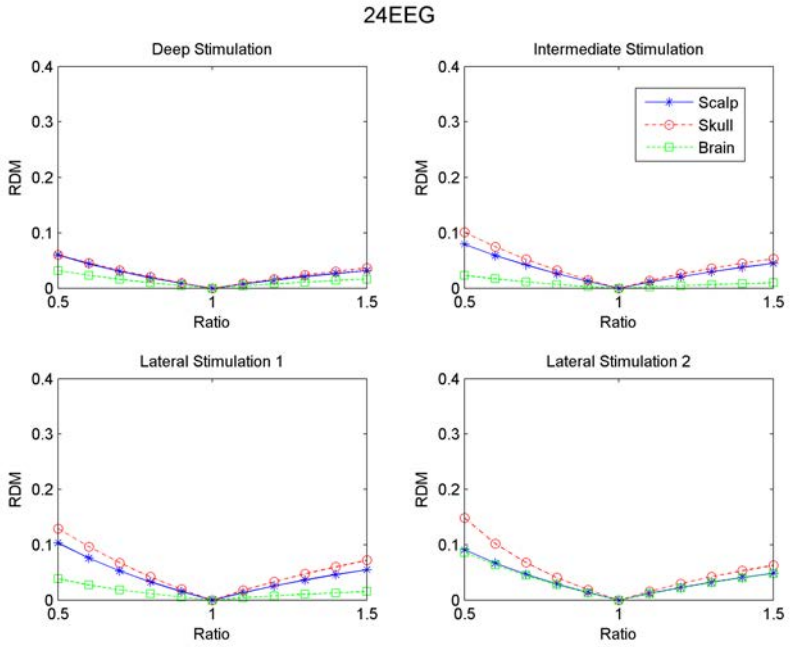

Figure 4.20: The error function RDM resulted from changing one conductivity value in a three-compartment FEM head model compared to the reference model when considering the 24 EEG positions for Patient(1).

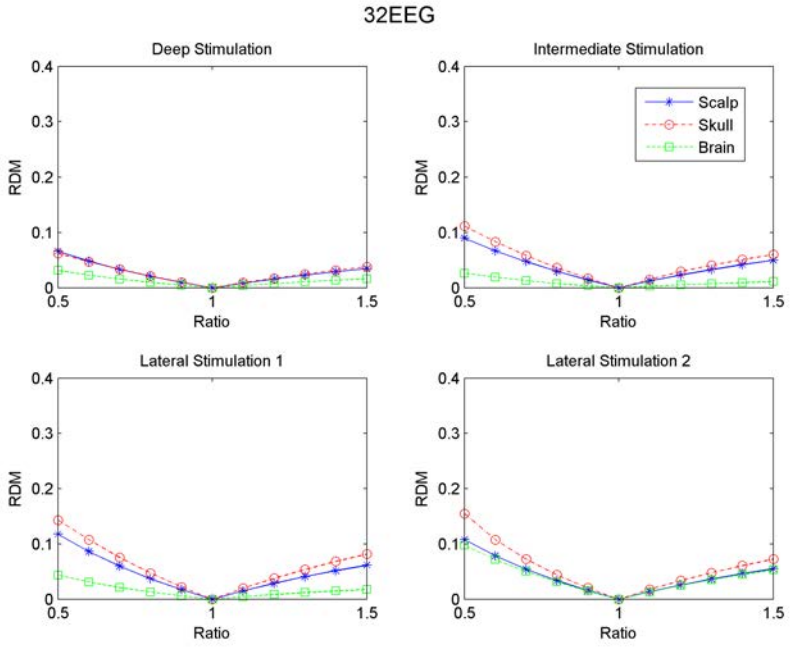

Figure 4.21: The error function RDM resulted from changing one conductivity value in a five-compartment FEM head model compared to the reference model when considering the 32 EEG positions for Patient(1).

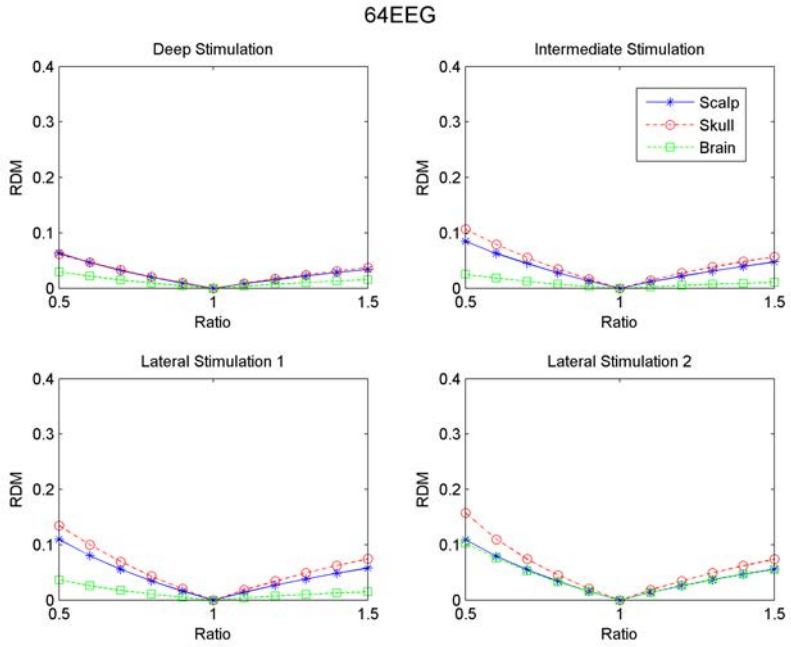

Figure 4.22: The error function RDM resulted from changing one conductivity value in a three-compartment FEM head model compared to the reference model when considering the 64 EEG positions for Patient(1).

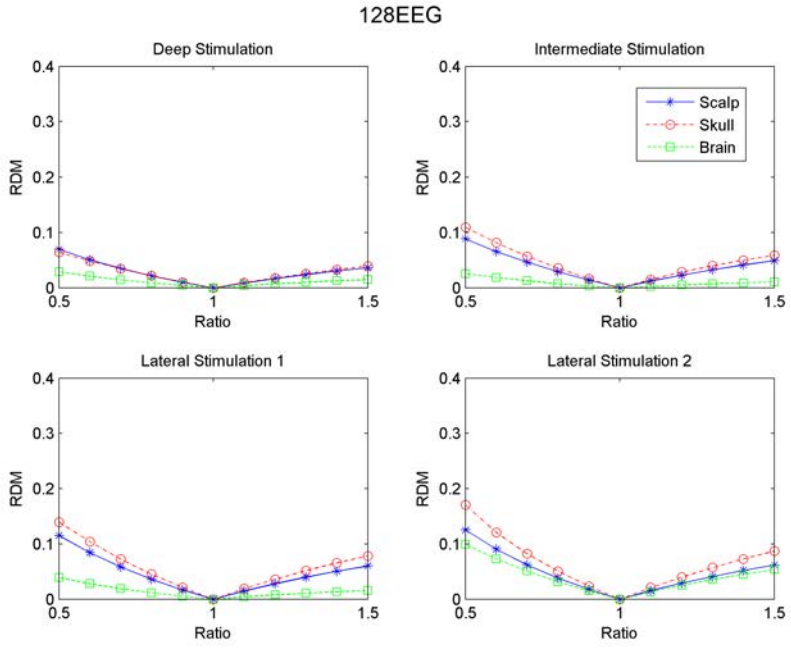

Figure 4.23: The error function RDM resulted from changing one conductivity value in a three-compartment FEM head model compared to the reference model when considering the 128 EEG positions for Patient(1).

sitivity of the RDM to both the scalp and the skull compartment. However, the sensitivity of the RDM to the scalp and the skull compartment is higher in lateral2 stimulation than in other stimulations, which indicates that lateral2 stimulation has a larger effect on the scalp and the skull conductivities than the other stimulations.

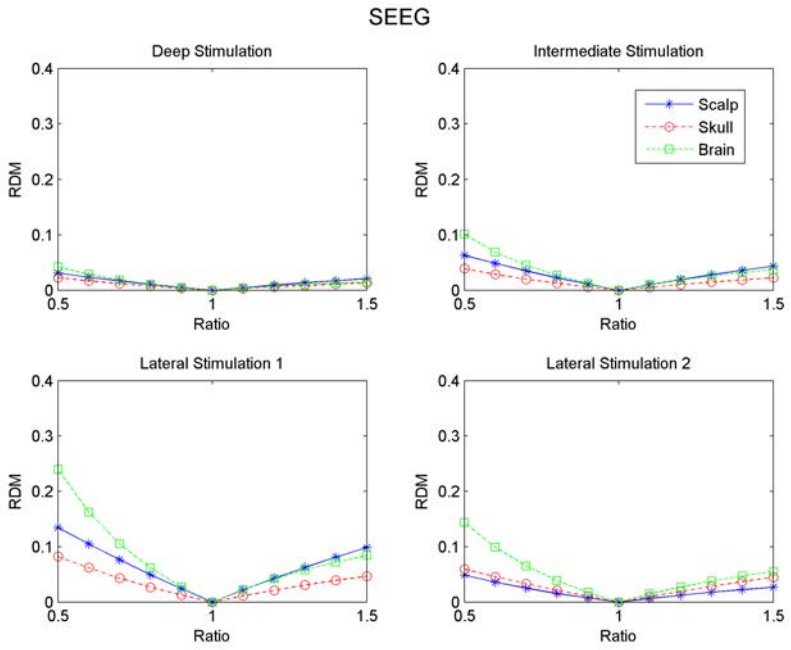

Figure 4.24: The error function RDM resulted from changing one conductivity value in a three-compartment FEM head model compared to the reference model when considering the SEEG positions for Patient(1).

Intracerebral and Scalp Electrodes

Fig.4.25 shows the sensitivity of the RDM to the three-compartment conductivities when considering the 24 scalp EEG electrodes in addition to the intracerebral SEEG electrodes. When it is compared to Fig.4.24 it can be noted that the sensitivity of the RDM to the scalp and the skull conductivities increases remarkably as the 24 EEG electrodes are added to the SEEG measurements. Even though the number of the added EEG electrodes (24) is small compared to the number of the SEEG contacts (107), the sensitivity of to the scalp and the skull compartments become comparable to the sensitivity to the brain compartment in all stimulations except lateral2. Adding 24 EEG electrodes to the EEG did not change

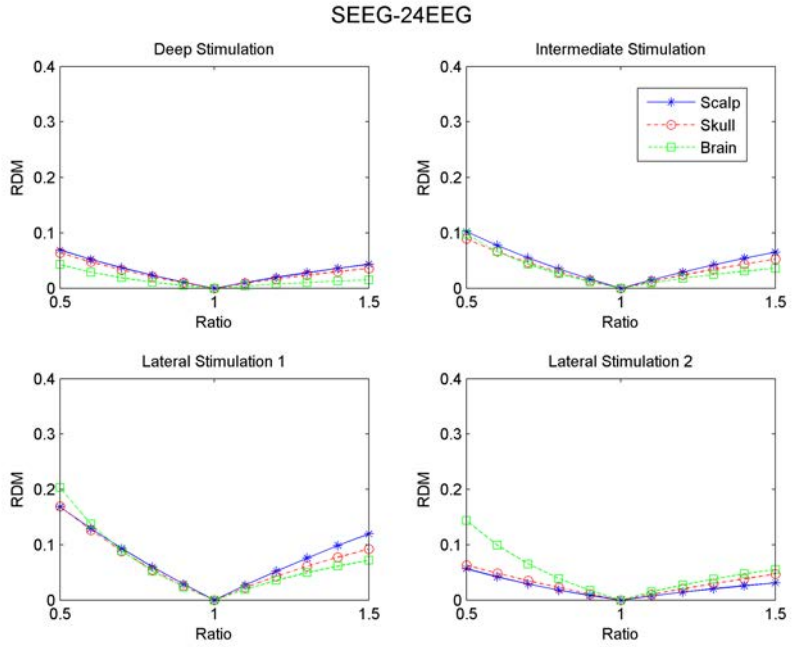

Figure 4.25: The error function RDM resulted from changing one conductivity value in a three-compartment FEM head model compared to the reference model when considering the SEEG-24 EEG positions for Patient(1).

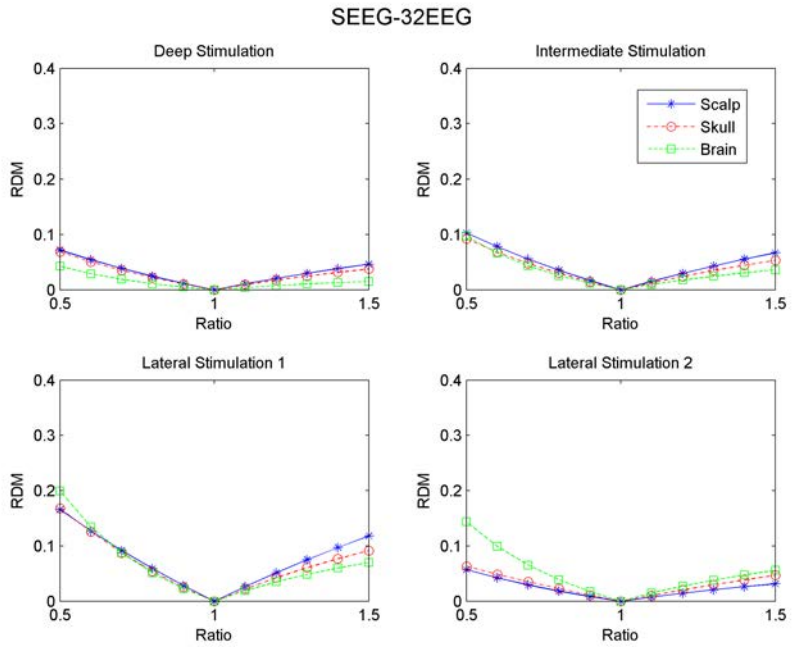

Figure 4.26: The error function RDM resulted from changing one conductivity value in a three-compartment FEM head model compared to the reference model when considering the SEEG-32 EEG positions for Patient(1).

the sensitivity of the RDM to the brain conductivity except for lateral1 stimulation where there is a notable decrease in the sensitivity to the brain conductivity. As shown in Fig.4.26 The change in the sensitivity of the RDM to the three-compartment conductivities when the number of EEG electrodes increases from 24 to 32 is very slight and is hard to notice. However, the increase in the sensitivity of the RDM to the scalp and the skull conductivities when the number of EEG electrode increases from 32 to 64 is remarkable and for all the stimulations as shown in Fig.4.27. This increase in the sensitivity to the scalp and the skull compartments is also notable when the number of EEG electrodes increases from 64 to 128 as shown in Fig.4.28.

When the sensitivity results of the five-compartment head model are compared to the results of the three-compartment head model, it can be noted that the sensitivity to the change in the scalp and the skull are smaller when considering the three-compartment head model. For example, when comparing the sensitivity to the skull conductivity when considering 24 EEG measurement position and deep stimulation as shown in Fig.4.20 for the three-compartment head model and Fig.4.2 for the five-compartment head model, it can be noted that the sensitivity to the skull conductivity is larger when considering the five-compartment head model. This indicates that the conductivity of a compartment depends on the conductivity values of the other compartments.

4.2.4 Sensitivity of the RDM: Five-compartment Head Model of Patient(2)

Even though, the head models of the different patients were similar to each other regarding the number of nodes and elements, as was shown in Table 2.2, the sensitivity analysis was performed on the data of Patient(2) in order to examine if the results obtained on Patient(1) can be generalized to other patients. The sensitivity analysis on Patient(2) was performed considering the five-compartment FEM head model with the RDM as an error function. In the reference head model the conductivity values were fixed as: 0.33 S/m for scalp, 0.008 S/m for skull, 1.79 S/m for CSF, 0.33 S/m for GM and 0.14 S/m for WM.

Scalp Electrodes

Fig.4.29 shows the sensitivity of the RDM to the five-compartment conductivities of Patient(2) when considering 24 EEG scalp electrodes. It can

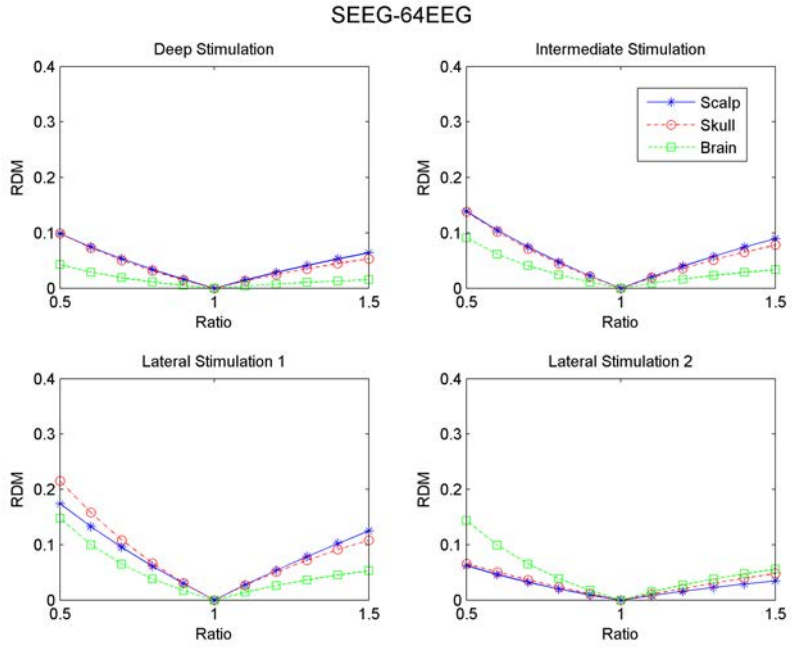

Figure 4.27: The error function RDM resulted from changing one conductivity value in a three-compartment FEM head model compared to the reference model when considering the SEEG-64 EEG positions for Patient(1).

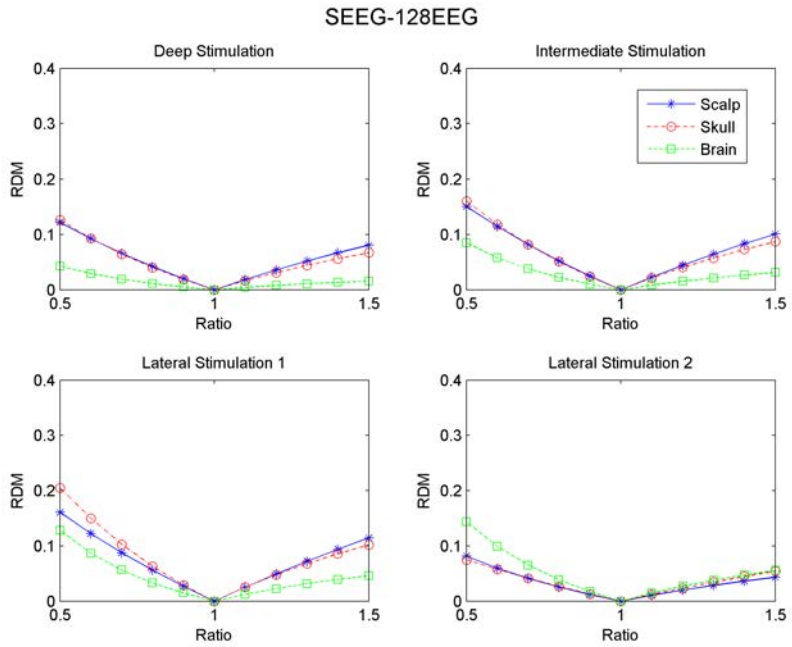

Figure 4.28: The error function RDM resulted from changing one conductivity value in a three-compartment FEM head model compared to the reference model when considering the SEEG-128 EEG positions for Patient(1).

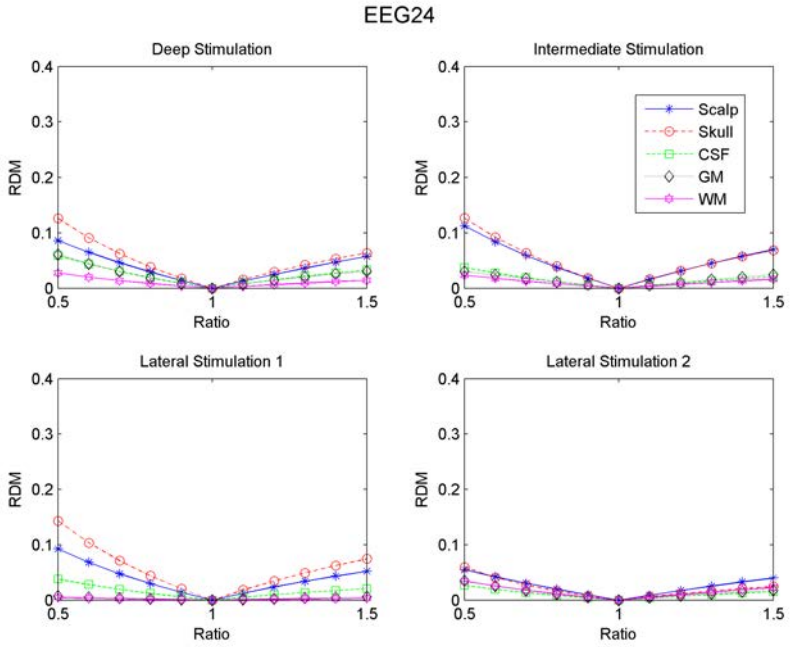

Figure 4.29: The error function RDM resulted from changing one conductivity value in a five-compartment FEM head model compared to the reference model when considering the 24 EEG positions for Patient(2).

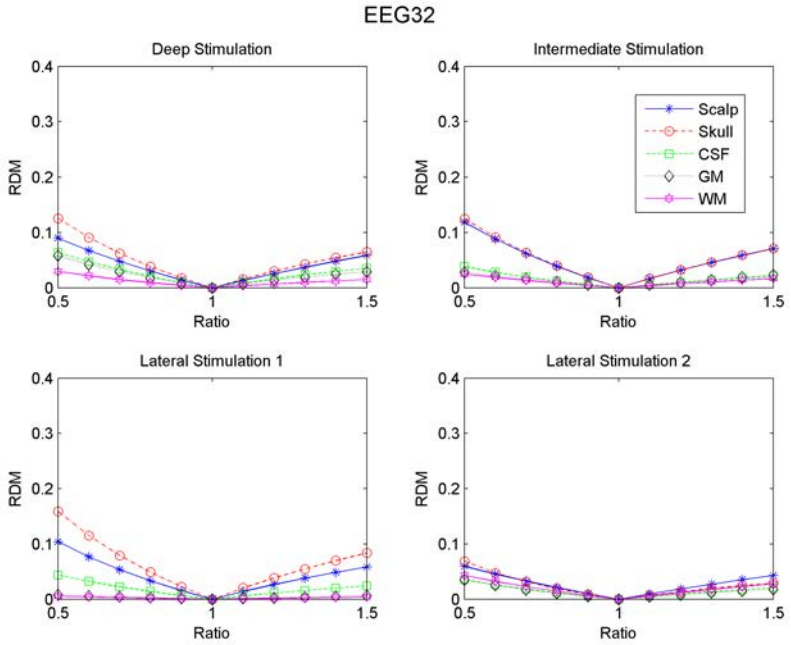

Figure 4.30: The error function RDM resulted from changing one conductivity value in a five-compartment FEM head model compared to the reference model when considering the 32 EEG positions for Patient(2).

be noted from the figure that the sensitivity of the RDM is the highest for the scalp and the skull conductivities in the case of all stimulations. Since the current distribution of the source passes by the scalp and the skull compartments before reaching the measuring electrodes, having a high sensitivity to the scalp and the skull conductivities is expected. When the number of EEG scalp electrodes increases from 24 to 32, as shown in Fig.4.30, there is an insignificant change in the sensitivity of the RDM to the scalp and the skull compartments for all stimulations except for lateral1 where the sensitivity to the skull and the scalp face a slight increase.

Doubling the number of EEG scalp electrodes (from 32 to 64), as shown in Fig.4.31, decreases the sensitivity of the RDM to the scalp and the skull conductivities in all the stimulations except lateral2 where there is a remarkable increase in the sensitivity of the RDM to the scalp and the skull compartments. The difference change in the pattern from stimulation position to another stimulation as the number of measurements changes indicates that the importance of considering the stimulation position when performing invivo conductivity estimation. Increasing the number of EEG scalp electrodes from 64 to 128, as shown in Fig.4.32, change the sensitivity of the RDM to the scalp and the skull slightly for deep and intermediate stimulations. However, for lateral1 and lateral2 stimulations there is a notable increase in the sensitivity of the RDM to the scalp and the skull conductivities.

Intracerebral Electrodes

Fig.4.33 shows the sensitivity of the RDM to the five-compartment conductivities of Patient(2) when considering the SEEG intracerebral electrodes. Strikingly, the sensitivity of the scalp and the skull is still the highest in the case of lateral1 stimulation even though there is no EEG scalp electrodes. The closeness of this lateral stimulation to the scalp and the skull compartment makes its effect on the scalp and the skull compartments more significant than the other compartments. In addition, in the case of deep and intermediate stimulation, there is no remarkable increase in the sensitivity of the RDM to the deep compartments (CSF, GM and WM) even though these stimulations are near to these compartments.

Intracerebral and Scalp Electrodes

The effect of adding 24 EEG scalp electrodes to the SEEG electrodes on the sensitivity of the RDM is shown in Fig.4.34. As expected, the sensitivity of the RDM to the scalp and the skull compartments increases

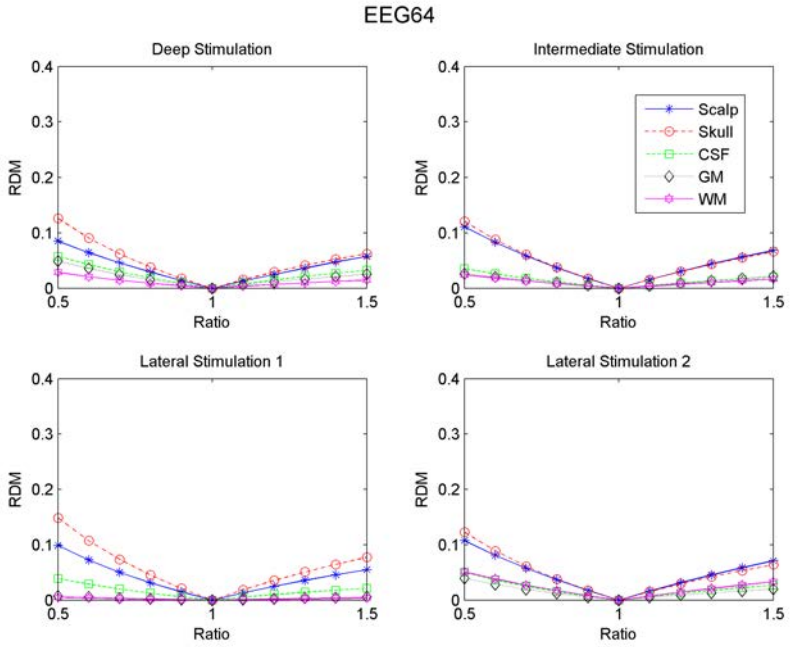

Figure 4.31: The error function RDM resulted from changing one conductivity value in a five-compartment FEM head model compared to the reference model when considering the 64 EEG positions for Patient(2).

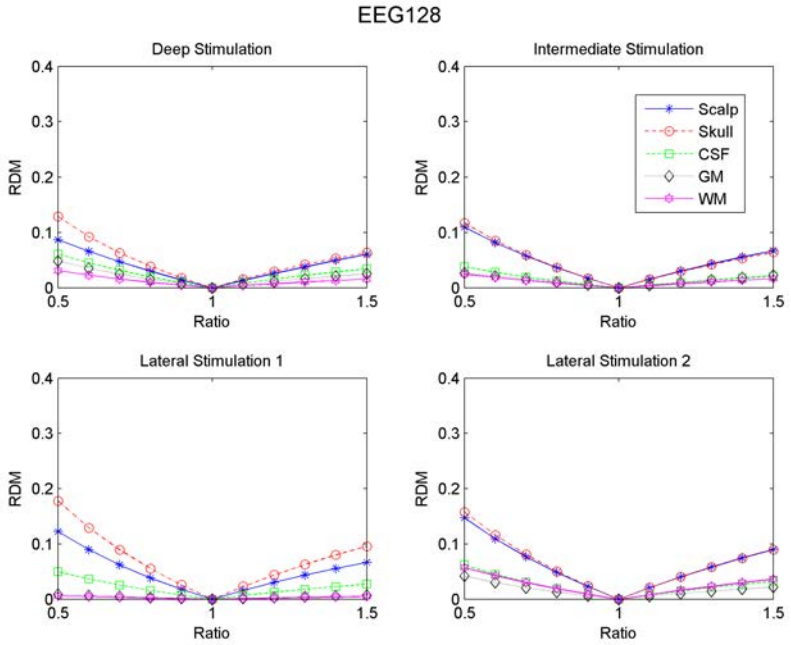

Figure 4.32: The error function RDM resulted from changing one conductivity value in a five-compartment FEM head model compared to the reference model when considering the 128 EEG positions for Patient(2).

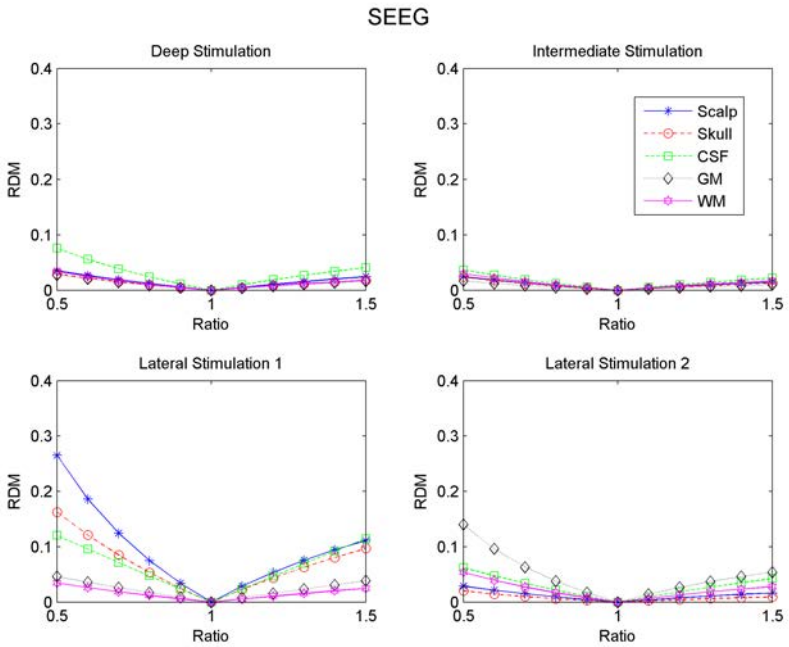

Figure 4.33: The error function RDM resulted from changing one conductivity value in a five-compartment FEM head model compared to the reference model when considering the SEEG positions for Patient(1).

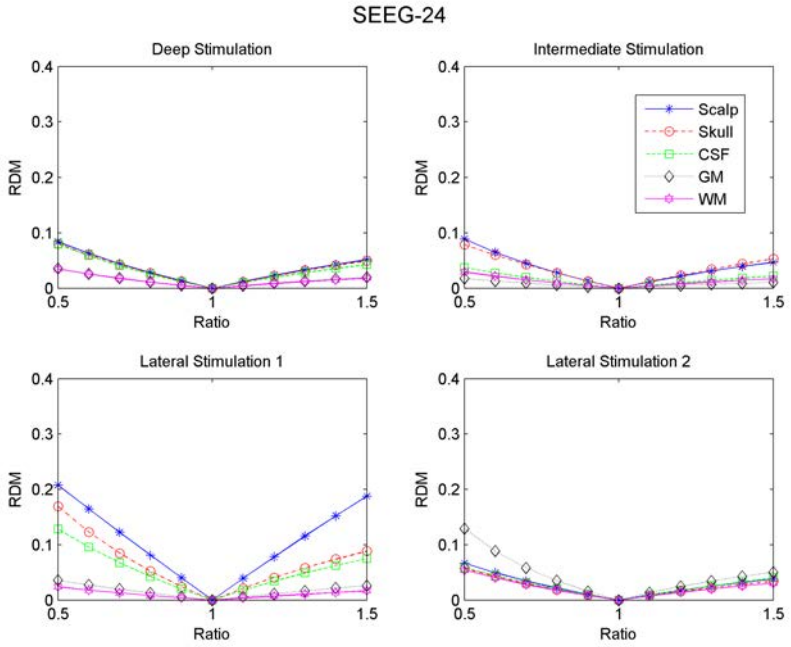

Figure 4.34: The error function RDM resulted from changing one conductivity value in a five-compartment FEM head model compared to the reference model when considering the SEEG-24 EEG positions for Patient(2).

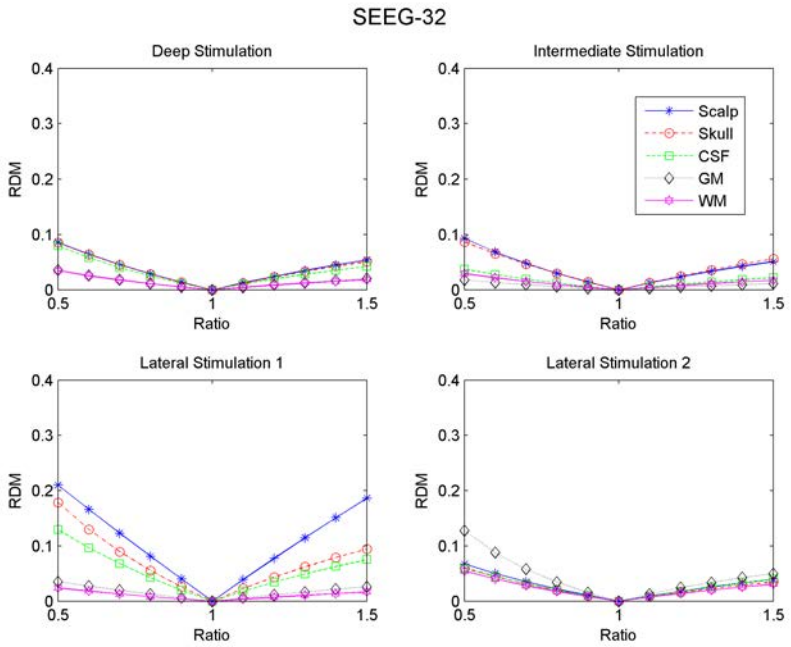

Figure 4.35: The error function RDM resulted from changing one conductivity value in a five-compartment FEM head model compared to the reference model when considering the SEEG-32 EEG positions for Patient(2).

notable as the 24 EEG electrodes are added for deep, intermediate and lateral2 stimulations. However, in the case of lateral1, the effect of adding 24 EEG scalp electrodes can be noted on the sensitivity of the RDM to the scalp conductivity which become unbiased as the scalp electrodes are added. By unbiased sensitivity to a conductivity, we mean that assigning larger conductivity values than the true value will lead to an error equal to assigning smaller conductivity values than the true value. By increasing the number of EEG scalp electrodes from 24 to 32 while considering the SEEG scalp electrodes, the change in the sensitivity to of the RDM to the five-compartment conductivity is very vague as shown in Fig.4.35.

Fig.4.36 shows the sensitivity of the RDM to the five-compartment conductivities of Patient(2) given the SEEG measurements in addition to 64 EEG scalp measurements. As expected, increasing the number of EEG electrodes from 32 to 64 increases the sensitivity of the RDM to the scalp and the skull compartment for all the stimulations except for lateral1 where there is a notable decrease in the sensitivity of the RDM to all the conductivities. However, as the number of EEG electrodes increases from 64 to 128 while considering the SEEG measurements, the sensitivity of the RDM to the scalp and the skull compartments increases in the case of lateral1 stimulation as for all the other stimulations.

Even though there are many differences between Patient(1) and Patient(2) like the number of the SEEG measurement positions, the positions of the stimulations, and the distance between the stimulation and the measurement positions, the similarities between the patterns can be noted when comparing the results of the sensitivity of Patient(1) and Patient(2). As the results of Patient(1), it can be noted from the results which were obtained from Patient(2), as shown in Fig.4.29 to Fig.4.32, that the RDM is most sensitive to the change of the scalp and the skull compartments in the cases. When considering only the SEEG measurement positions, in all cases, except lateral1, the sensitivity to the change in the scalp and the skull conductivities is the lowest, however, this sensitivity increases as more EEG measurement positions are added.

4.3 Brain Nodes As Measurements

Considering only the real measurement positions for determining the sensitivity analysis gave an important insight before performing in-vivo conductivity estimation. However, the differences in the results between

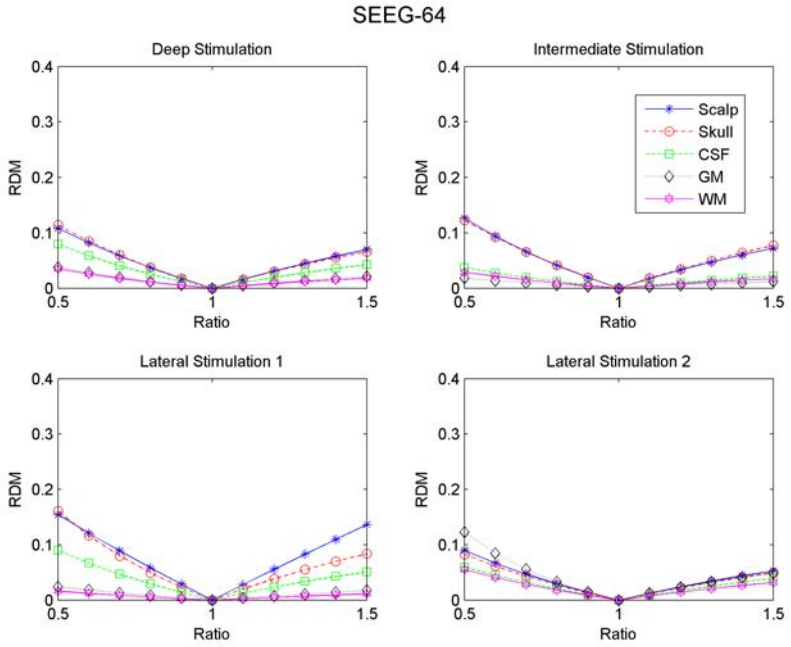

Figure 4.36: The error function RDM resulted from changing one conductivity value in a five-compartment FEM head model compared to the reference model when considering the SEEG-64 EEG positions for Patient(2).

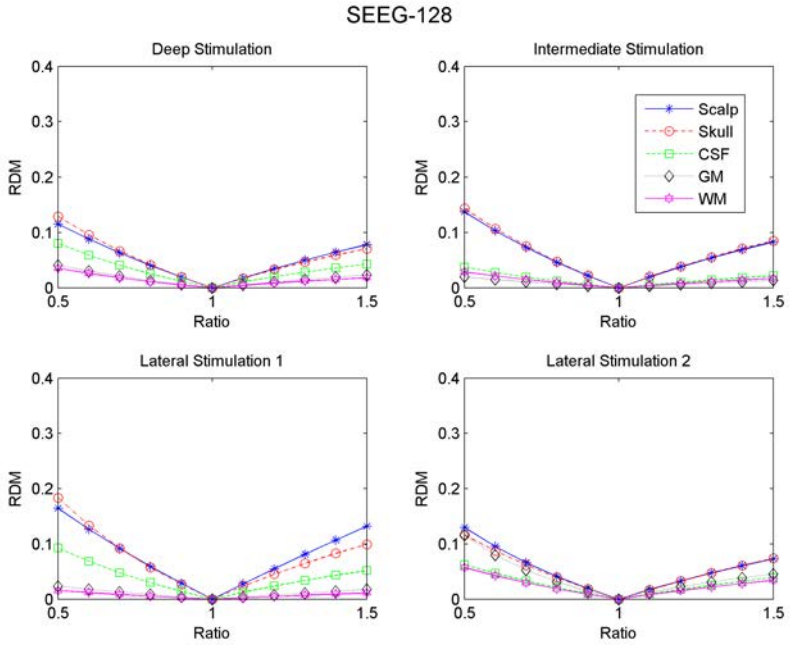

Figure 4.37: The error function RDM resulted from changing one conductivity value in a five-compartment FEM head model compared to the reference model when considering the SEEG-128 EEG positions for Patient(2).

the stimulation positions, especially between lateral1 and lateral2 could be due to the variety of the distances between the measurement positions and the stimulation position. Therefore, in order to neglect the effect of the distance from the stimulation electrode, another sensitivity analysis was performed in which all the nodes of the brain (CSF, GM and WM) were considered. This unrealistic scenario was applied to the five-compartment FEM head model of Patient(1) with the RDM as the error function. As in the real measurement positions case, four different stimulation positions (deep, intermediate, lateral1 and lateral2) were considered in addition to 5 different setups for EEG positions (24-channel EEG, 32 channel EEG, 64-channel EEG and 128-channel EEG). Two five-compartment FEM head models of Patient(1) were generated where the reference model has the conductivity values: 0.33 S/m for scalp, 0.008 S/m for skull, 1.79 S/m for CSF, 0.33 S/m for GM and 0.14 S/m for WM.

Fig.4.38 shows the sensitivity of the RDM to the five-compartment conductivities when the nodes of the CSF, the GM and the WM are considered as measurement positions. Adding EEG scalp electrodes to this configuration does not affect the sensitivity pattern as shown in Fig.4.39 when 128 EEG scalp electrodes are added. Since the number of EEG scalp electrodes are smaller than the number of the brain nodes (300 000), it is expected to have low influence from adding the EEG scalp electrodes. However, when these results are compared to the results when the real SEEG and EEG positions were considered, it can be noted that the sensitivity in general is low for all the conductivities when considering all the nodes of the brain. This may be due to considering the measurements of the neighbour nodes to the stimulation which have large amplitudes compared to the far nodes. Moreover, the current may be not affected by the conductivity when it passes from the stimulation node to the neighbour nodes. In order to examine these assumptions, the previous method was repeated but without considering the measurements of the nearest 1000 nodes.

Fig.4.40 shows the sensitivity of the RDM to the five-compartment conductivities when considering all the potentials at the nodes of the deep compartments (CSF, GM and WM). In contrary to Fig.4.38, the RDM in Fig.4.40 has a high sensitivity to the deep compartments (CSF, GM and WM) especially for intermediate, lateral1 and lateral2 stimulations. Adding the 24 scalp EEG electrodes to the measurements, as shown in Fig.4.41 increases the sensitivity to the scalp and the skull slightly. In addition to the slight change in the scalp and the skull compartments, there is a notable increase in the sensitivity to the GM conductivity in both lateral1

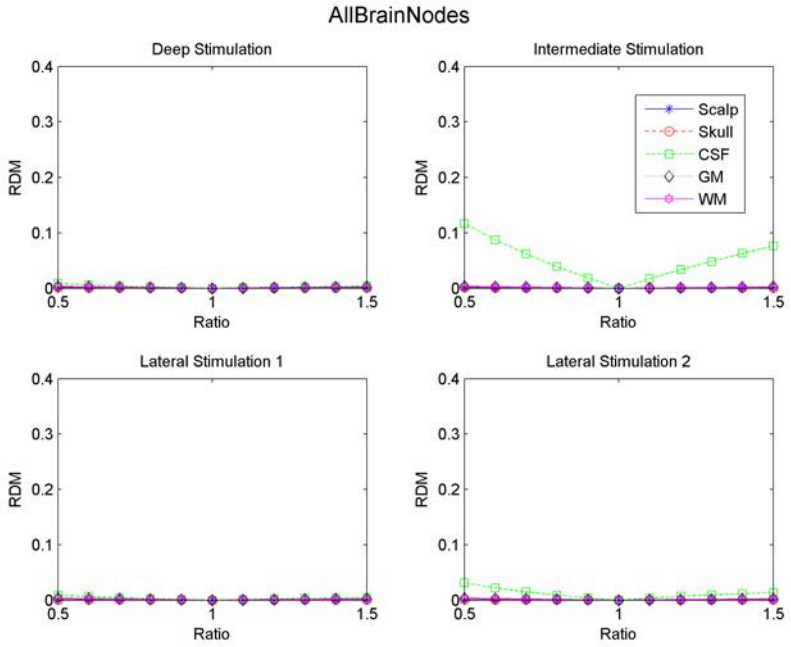

Figure 4.38: The sensitivity to the change in each conductivity value in a five-compartment FEM head model when considering the brain nodes as measurement positions for Patient(1) given the RDM as the error function

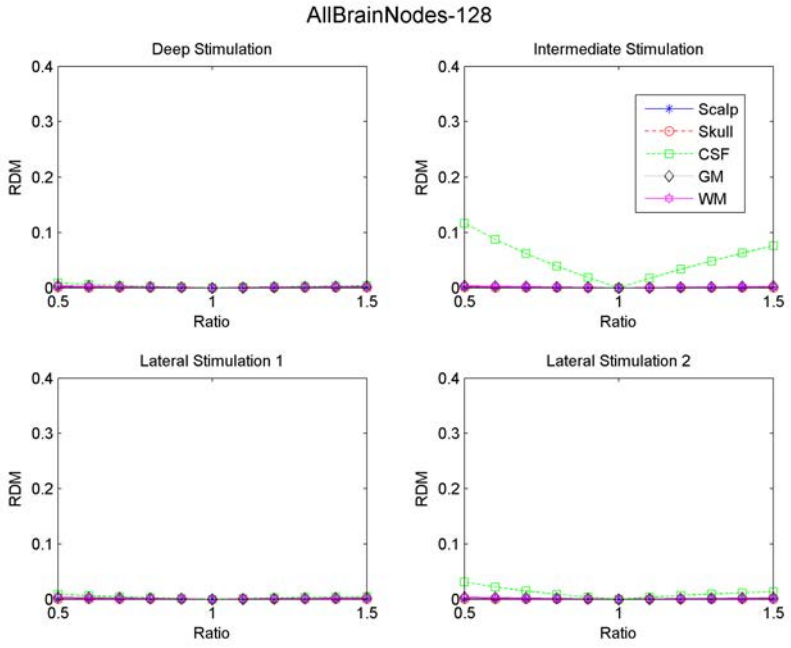

Figure 4.39: The sensitivity to the change in each conductivity value in a five-compartment FEM head model when considering the brain nodes and the 128-channel EEG as measurement positions for Patient(1) given the RDM as the error function

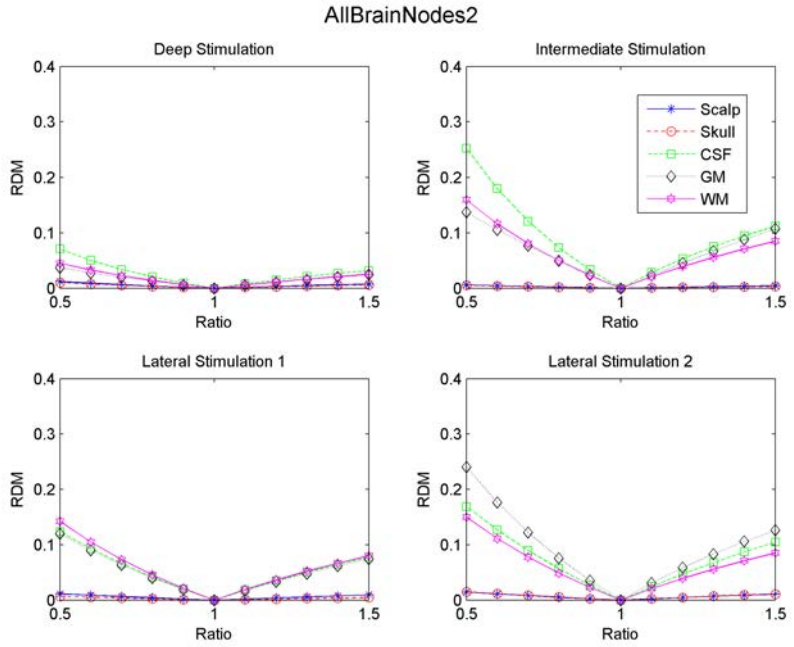

Figure 4.40: The sensitivity to the change in each conductivity value in a five-compartment FEM head model when considering the brain nodes except the nearest 1000 nodes as measurement positions for Patient(1) given the RDM as the error function

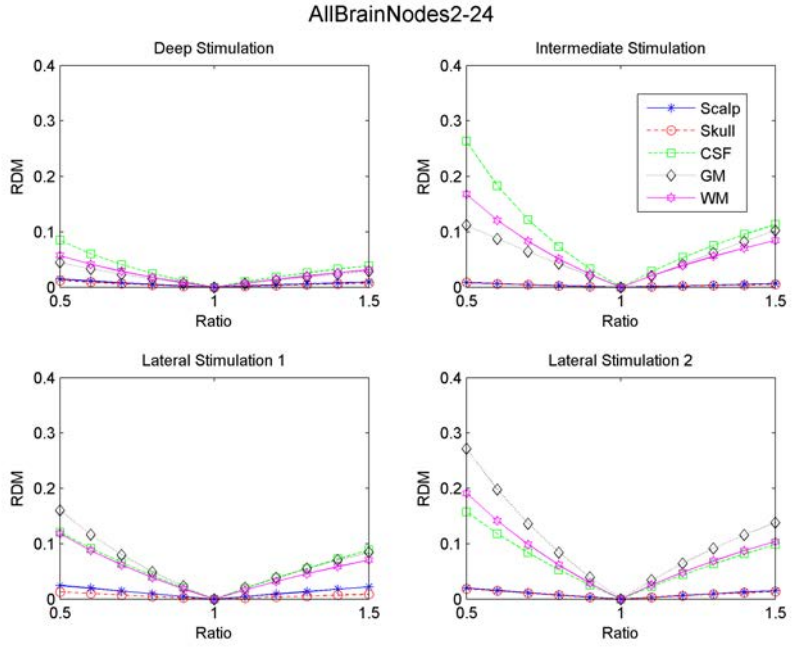

Figure 4.41: The sensitivity to the change in each conductivity value in a five-compartment FEM head model when considering the brain nodes except the nearest 1000 nodes and the 24-channel EEG as measurement positions for Patient(1) given the RDM as the error function

and lateral2 stimulations while it decreases in the intermediate stimulation. Moreover, the sensitivity of the WM increases notably when the 24 scalp EEG electrodes are added in the case of lateral1 stimulation.

When the number of scalp EEG electrodes increases to 32 and then to 64 while considering the measurements of all the nodes of the deep compartments, the sensitivity of the RDM to the scalp and the skull changes very slightly while the sensitivity to the CSF, the GM and the WM change remarkably as shown in Fig.4.42 and Fig.4.43. The sensitivity of the RDM to the brain compartments increases in the case of deep stimulation while it decreases in the case of intermediate and lateral1 stimulations. While the sensitivity to the CSF and to the GM decreases as the number of EEG scalp electrodes increases from 24 to 32 and to 64, the sensitivity to the WM increases remarkably as shown in Fig.4.42 and Fig.4.43. Increasing the number of EEG scalp electrodes to 128 while considering the potentials of all the nodes of the brain compartment has again a slight effect on the sensitivity of the RDM to the scalp and the skull compartment as shown in Fig.4.44. While there is a notable decrease in the sensitivity to the CSF, the GM and the WM in the case of intermediate and lateral1 stimulations. But in the case of lateral2 stimulation, the sensitivity of the RDM to the WM increases notably as shown in Fig.4.44.

In general, Fig.4.40 to Fig.4.44 shows the results of the sensitivity analysis of the RDM to the change of the five conductivities of Patient(1) when considering all the nodes of the brain except the nearest 1000 nodes from the stimulation in addition to the EEG measurement positions. It can be noted when comparing these results with the previous results shown in Fig.4.38 to Fig.4.39 that in order to increase the sensitivity of the RDM to the change of the conductivities, the nearest measurements of the stimulation position should not be considered. However, the change in the sensitivity of the RDM when adding and changing the number of the EEG positions to the scalp and the skull conductivities as shown in Fig.4.40 to Fig.4.44 indicates that the EEG positions does not have an effect on changing the sensitivity because their number is small compared to the number of the brain nodes. Nevertheless, increasing or adding the EEG measurement position did have an effect on the sensitivity of the brain compartments.

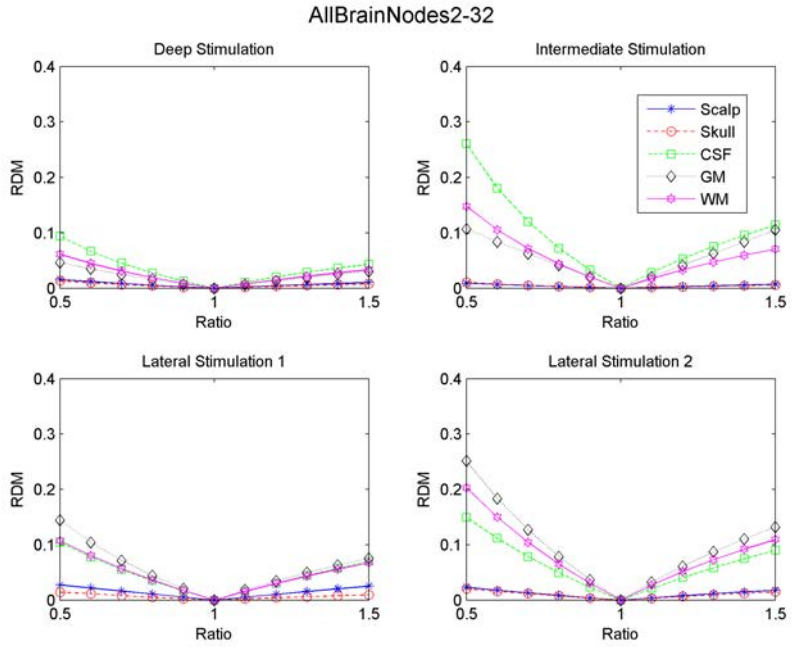

Figure 4.42: The sensitivity to the change in each conductivity value in a five-compartment FEM head model when considering the brain nodes except the nearest 1000 nodes and the 32-channel EEG as measurement positions for Patient(1) given the RDM as the error function

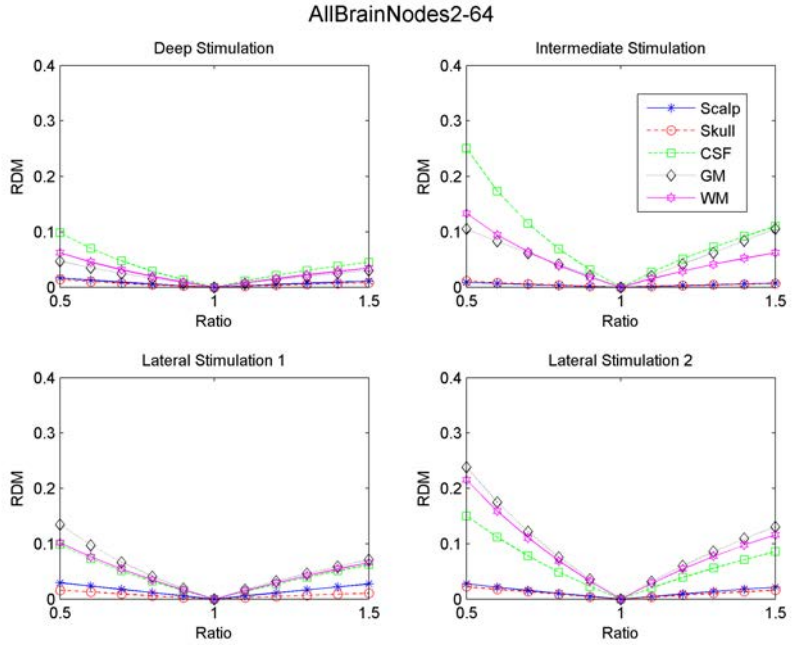

Figure 4.43: The sensitivity to the change in each conductivity value in a five-compartment FEM head model when considering the brain nodes except the nearest 1000 nodes and the 64-channel EEG as measurement positions for Patient(1) given the RDM as the error function

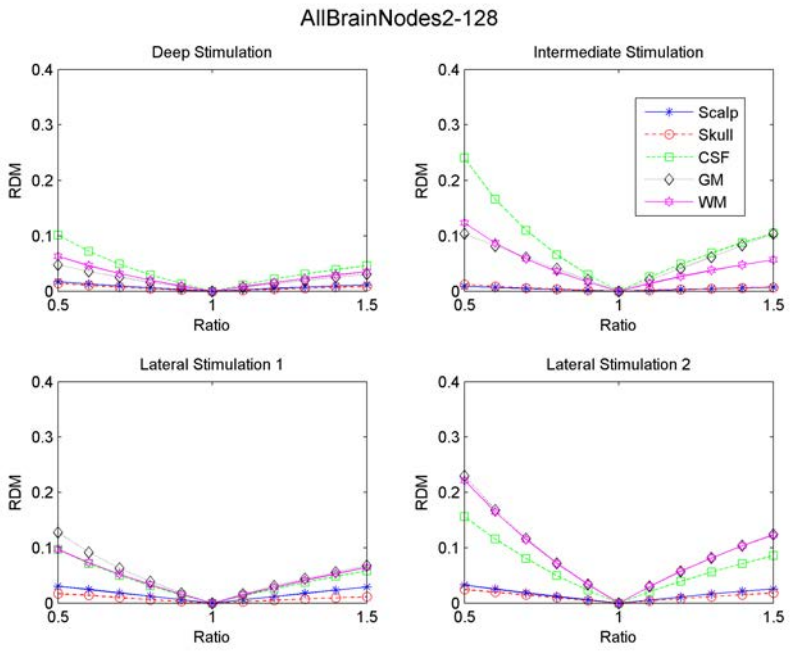

Figure 4.44: The sensitivity to the change in each conductivity value in a five-compartment FEM head model when considering the brain nodes except the nearest 1000 nodes and the 128-channel EEG as measurement positions for Patient(1) given the RDM as the error function

4.4 Local Measurements

The results which were obtained when considering all the nodes of the brain indicated that the neighbour nodes should not be considered. However, considering the local measurements around the stimulation may give better sensitivity results since the far measurements are assumed to be not affected by the stimulation electrodes as the near measurements. In order to examine this assumption, a simulation was performed by considering the the SEEG measurement positions within the 50 mm range from the stimulation in addition to the 128-channel EEG measurement positions which are within 50 mm distance from lateral1 stimulation. From the 107 SEEG measurement positions, 40 were considered for the deep stimulation, 45 for the intermediate, 39 for lateral1 and 74 for lateral2. The EEG measurement positions were fixed for all stimulations as 17 positions.

Fig.4.45 shows the sensitivity results of Patient(1) when considering the SEEG the measurement positions within the 50 mm range from the stimulation in addition to the 128-channel EEG measurement positions which are within 50 mm distance from lateral1 stimulation. It can be noted that there is no big difference between Fig.4.45 and Fig.4.10 when all the SEEG and the 128-channel EEG positions are considered. This similarity between these results gives an indication that there is no effect of considering the local measurement positions for in-vivo conductivity estimation.

4.5 The Effect of Changing the Measurement Positions

The previous results of the sensitivity analysis show that the output depends on the measurement positions in addition to the stimulation positions. This was noted as the sensitivity of the error function to a specific compartment changes when the number of measurement changes. In order to have an overall view of the effect of changing the measurement positions on the RDM when assigning an erroneous conductivity, another simulation was performed by considering two five-compartment FEM head model of Patient(1). The reference head model has the common conductivity values: 0.33 S/m for scalp, 0.008 S/m for skull, 1.79 S/m for CSF, 0.33 S/m for GM and 0.14 S/m for WM. In the test head model, each time one conductivity value was assigned by multiplying it with 0.5 of its reference value while the other conductivities were set equal to the reference conductivities. Then the RDM was determined between the two head models for different measurement

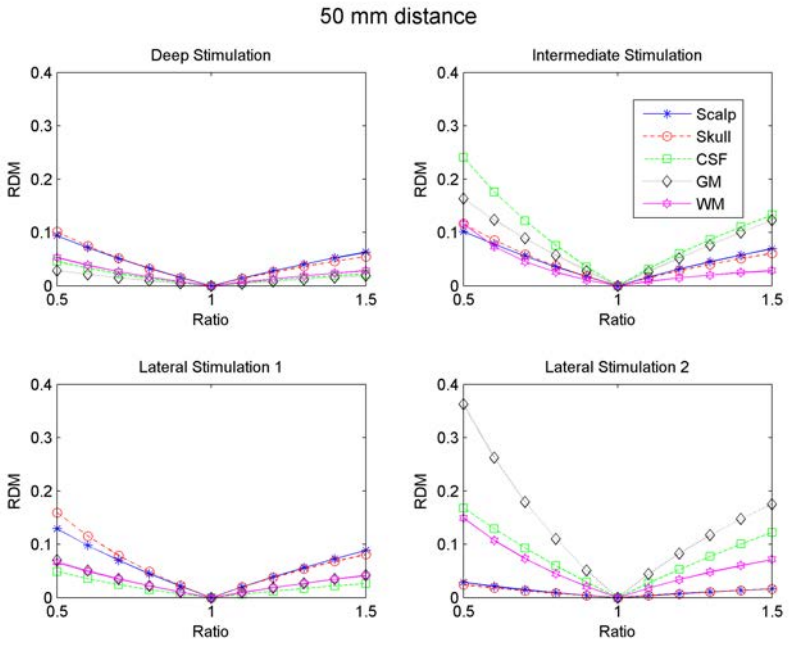

Figure 4.45: The sensitivity to the change in each conductivity values when considering the SEEG measurement positions within 50 mm distance from the stimulation in addition to the EEG measurement position within 50 mm distance from lateral1 stimulation for Patient(1)

positions.

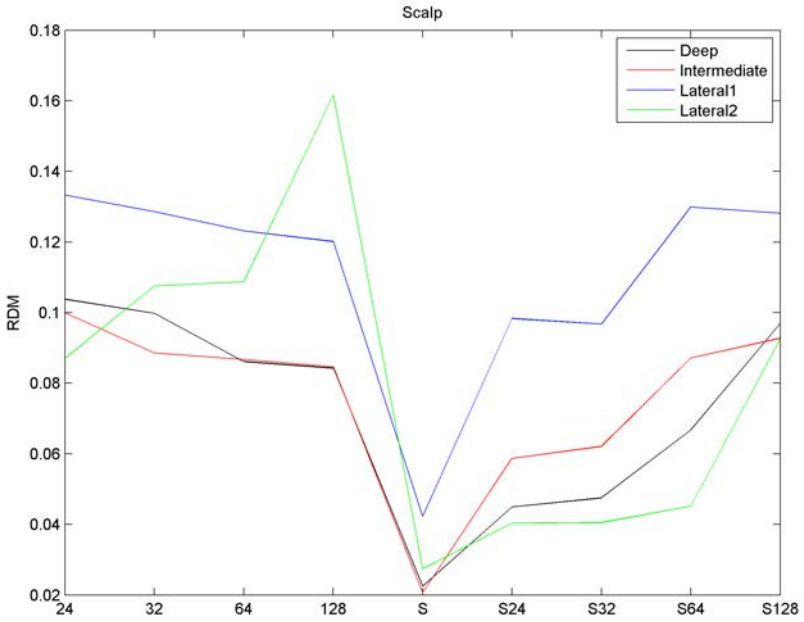

Figure 4.46: The effect of changing the number of the measurement positions on the RDM when the scalp conductivity in the testing head model equals to 0.5 of its value in the reference model of Patient(1). The numbers in the x-axis indicates the number of the EEG measurement positions (24 means 24 EEG scalp electrodes) while the S indicates the SEEG measurement positions (S means SEEG and S24 means SEEG plus 24 EEG scalp electrodes).

Fig.4.46 shows the effect of changing the number of measurements on the RDM when assigning 0.17 S/m as a scalp conductivity value in the test model. Except for lateral2, as the number of EEG scalp electrodes increases, the RDM decreases, when considering only EEG scalp electrodes. The decrease in the RDM as the number of EEG scalp electrodes increases can be explained by the fact that a larger number of scalp EEG electrodes reduces that error that is generated due to assigning an erroneous scalp conductivity. However, for lateral2, increasing the number of scalp EEG electrodes have the inverse effect on the RDM. The RDM has its lowest value in Fig.4.46 for all stimulations when considering only the SEEG intracerebral electrodes. The low effect of assigning an erroneous scalp conductivity on the intracerebral SEEG potentials is expected since the current distribution that

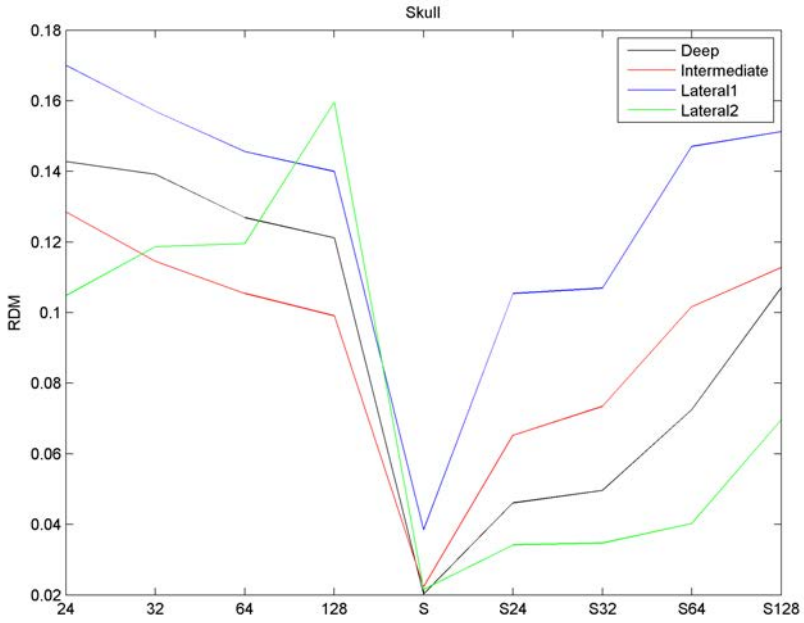

Figure 4.47: The effect of changing the number of the measurement positions on the RDM when the skull conductivity in the testing head model equals to 0.5 of its value in the reference model of Patient(1). The numbers in the x-axis indicates the number of the EEG measurement positions (24 means 24 EEG scalp electrodes) while the S indicates the SEEG measurement positions (S means SEEG and S24 means SEEG plus 24 EEG scalp electrodes).

is generated from IES does not pass through the scalp compartment. When both the SEEG and the EEG are considered (from S24 to S128 in Fig.4.46, the RDM increases with the increase in the number of EEG measurements that are considered in simultaneous with SEEG measurements. The increase in the RDM with the increase in the number of EEG scalp measurements is expected since the SEEG and EEG do not have the same information about the scalp compartment, so increasing the number of EEG scalp electrodes will increase the difference between the two information. It can be noted that the effect of changing the measurement position on the RDM when assigning 0.004 S/m skull conductivity in the test head model, as shown in Fig.4.47 has the same pattern that is shown in Fig.4.46 when assigning an erroneous scalp conductivity. The fact that both the scalp and the skull compartments lie between the stimulation and the scalp EEG measurements makes the their pattern similar.

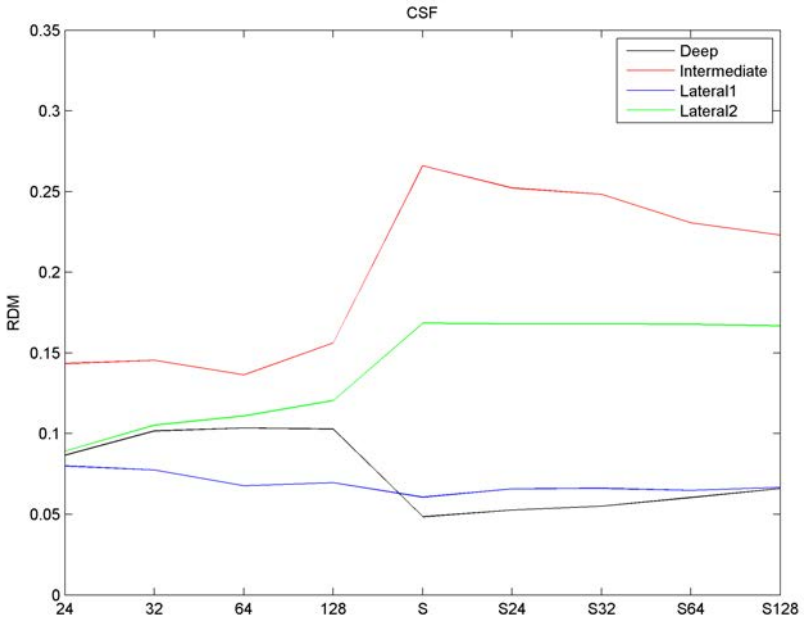

Figure 4.48: The effect of changing the number of the measurement positions on the RDM when the CSF conductivity in the testing head model equals to 0.5 of its value in the reference model of Patient(1). The numbers in the x-axis indicates the number of the EEG measurement positions (24 means 24 EEG scalp electrodes) while the S indicates the SEEG measurement positions (S means SEEG and S24 means SEEG plus 24 EEG scalp electrodes).

Fig.4.48 shows the RDM versus the number of measurements when assigning 0.90 S/m CSF conductivity in the test model while assigning 1.79 S/m in the reference model. It can be noted from the figure that there is a slight change in the RDM when considering only the EEG scalp measurement in all the stimulations. The slight change in the RDM is expected since these scalp EEG measurements are far from the CSF compartment and there is a high resistive skull between the EEG scalp measurements and the CSF. When considering only the SEEG measurements the RDM gets its highest value for both intermediate and lateral2 stimulations. However, since the intermediate stimulation is the nearest to the CSF compartment, then having the highest RDM when considering only the SEEG compartment in the case of intermediate stimulation is not surprising. In contrast to intermediate and lateral2 stimulations, in the case of deep stimulation, the RDM has its minimum value when considering the SEEG measurements. Since the deep stimulation lies beneath the CSF compartment, its effect will be similar to the effect of all stimulations to the scalp and the skull compartments, so it is normal to have the minimum RDM value when considering only the SEEG measurements. When considering both the SEEG and the EEG measurements, the RDM decreases slightly in the case of intermediate stimulation while it increases slightly in the case of deep stimulation. Nevertheless, for lateral1 stimulation, changing the measurement positions did not change the RDM value. The difference between the pattern of lateral1 and lateral2 in Fig.4.48 shows that electrodes of similar deepness may have different patterns.

When assigning 0.17 S/m as a GM conductivity value in the testing model while assigning 0.33 S/m in the reference model, the effect of this erroneous conductivity value does not appear in the RDM before considering the SEEG measurements for all stimulations (except the deep stimulation) as shown in Fig.4.49. Since the EEG measurements are far from the GM compartment their effect does not appear in the RDM before considering the SEEG measurements. It can be noted that as the number of EEG electrodes increases, while considering the SEEG, the pattern of lateral1 does not change, but the pattern of the intermediate and the lateral1 stimulations decreases slightly. Since the EEG measurements and many of the SEEG measurements are located above the GM, the information that are coming from the EEG and the SEEG measurement are the same, due to this, the RDM decreases as the number of the EEG measurements increases while considering the SEEG measurements. In the case of deep stimulation, the RDM has its minimum value when considering the SEEG measurements, as in the CSF case, since the deep stimulation lies in

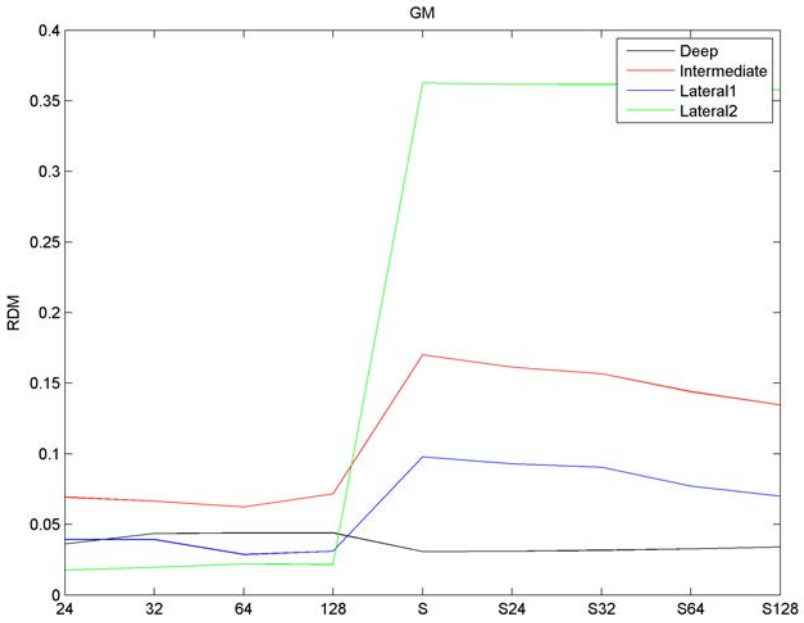

Figure 4.49: The effect of changing the number of the measurement positions on the RDM when the GM conductivity in the testing head model equals to 0.5 of its value in the reference model of Patient(1). The numbers in the x-axis indicates the number of the EEG measurement positions (24 means 24 EEG scalp electrodes) while the S indicates the SEEG measurement positions (S means SEEG and S24 means SEEG plus 24 EEG scalp electrodes).

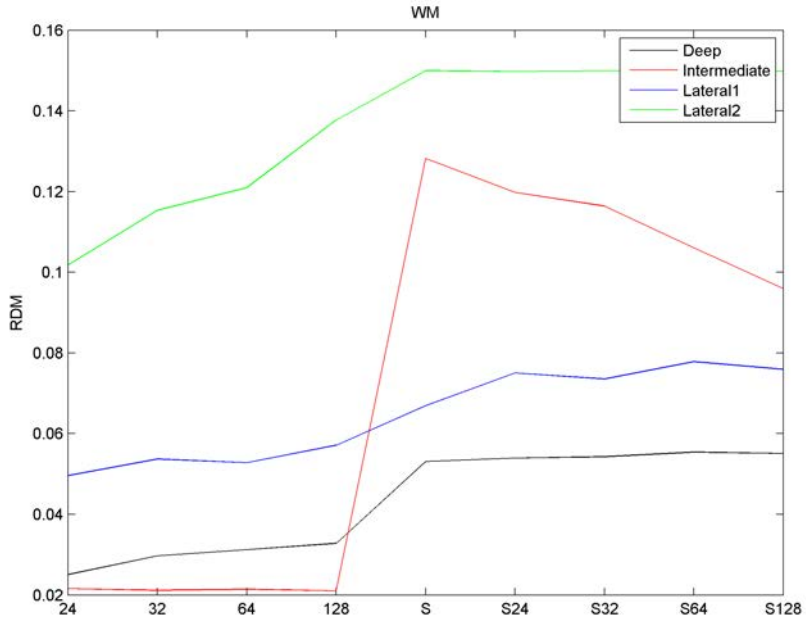

Figure 4.50: The effect of changing the number of the measurement positions on the RDM when the WM conductivity in the testing head model equals to 0.5 of its value in the reference model of Patient(1). The numbers in the x-axis indicates the number of the EEG measurement positions (24 means 24 EEG scalp electrodes) while the S indicates the SEEG measurement positions (S means SEEG and S24 means SEEG plus 24 EEG scalp electrodes).

the bottom of the GM, its effect will be the opposite to the other stimulations.

Fig.4.50 shows the RDM versus the measurement positions when assigning 0.07 S/m conductivity value for the WM compartment. On the contrary to the assigning erroneous GM conductivity, the RDM is affected by assigning erroneous WM conductivity when considering only EEG measurement positions (except for intermediate stimulation). However, the RDM has its highest value for all stimulations except lateral1 when considering only SEEG measurement positions. While considering the SEEG measurements, as the number of EEG scalp electrodes increases, the RDM decreases for intermediate simulation while it increases slightly for both deep and lateral1 stimulations.

4.6 Discussion

In this study, in-vivo conductivity estimation depends on optimizing the parameters of the forward model given the real data. However, for having a robust in-vivo conductivity estimation, the error function which estimates the error between the forward model and the real data should have a high sensitivity to the conductivity values. If the error function is not sensitive to the conductivities, two different conductivity values of one compartment can lead to the same resulted error. In other words, if the error function is not sensitive to the conductivities, the optimization algorithm could find more than one conductivity value as an optimal solution. Therefore, in this chapter, a simulation study was performed to determine the sensitivity of the error function to the conductivities.

The first obvious result that can be observed from this analysis is the importance of the EEG scalp electrodes for in-vivo conductivity estimation of the scalp and the skull compartments. This was noted by the increase in the sensitivity of the error functions to the scalp and the skull conductivities when the EEG potentials are added. A similar results were found by S. Vallaghé [116] and J. Haueisen et al. [136] who concluded that the most effect on the EEG potentials of the forward model is coming from the skull and the scalp compartments which are located between the dipole and the measurement positions. In addition, Vairis Caune have found in his PhD thesis that localization of the sources is more accurate when considering the nearer measurements when he performed source localization by intracerebral electrodes [137]. However, when considering only the EEG measurements, the sensitivity of the output error to the scalp and the skull conductivity

were decreasing as more EEG electrodes were added. This decrease (specially in RDM sensitivity) confirms the importance of a high number of EEG scalp electrodes for performing an accurate source localization [138] because the low sensitivity indicates that an erroneous scalp or skull conductivity assignment does not affect significantly the output error if the number of EEG electrodes is large. On the other hand, while considering the SEEG measurements, adding more EEG measurements increases the sensitivity of the error function to the scalp and the skull compartments, this increase in the sensitivity which was caused by an increase in the error can be explained by the different information that are coming from the deep SEEG measurements and the scalp EEG measurement, so that as more EEG electrodes are added to the SEEG the difference between the two measurements leads to a higher error and a higher sensitivity.

Even though the RDM is very common in source localization and conductivity estimation field [116, 13, 92], other error measurement functions were considered like the relative error function [96]. When comparing the sensitivity results of the relative error function to the sensitivity results of the RDM, similarities do exists like the low sensitivity of the error function to the scalp and the skull compartment when the EEG measurement are not considered. However, the high and fixed sensitivity pattern to the CSF compartment for different measurement positions cannot be explained. Even though a fixed sensitivity pattern is important to get a robust in-vivo conductivity estimation, this high sensitivity to the CSF change compared to other compartments is not expected especially when the EEG measurements are added. In one previous study for estimating the brain-to-skull ratio in a FEM head model, Zhang et al. considered the relative error and found that different stimulation positions, by subdural electrodes in two epileptic patients, leads to different brain-to-skull conductivity ratio [96].

The sensitivity of the RDM to the scalp and the skull conductivities was larger when considering the the five-compartment FEM head model compared to the three-compartment FEM head model for the same measurement positions. This indicates that there is dependency between the conductivities of the different compartments, and the higher sensitivity to the scalp and the skull conductivities which happened when the brain compartment is divided into three different compartments (CSF, GM and WM) is better for in-vivo conductivity estimation. Moreover, it was found that these sensitivity results can be generalized to other subjects as shown when the results of Patient(1) compared to the results obtained from the head model of Patient(2). On the other hand, when performing in-vivo

conductivity estimation, the neighbour nodes of the stimulation should not be considered since these near nodes have large amplitudes compared to the other nodes and because the current is not affected by the conductivity to reach the near nodes. Even though the number of measurement positions affect the sensitivity results, performing the sensitivity analysis for local region around the stimulation did not change the results in a notable way.

In general, it can be said that the the brain compartments affect the RDM when the SEEG measurement positions are considered, while the scalp and the skull affect the RDM when the scalp EEG are considered. Even though other studies have performed sensitivity analysis like the study of G. Marin [13] and the study of S. Vallage [116], the different between the results obtained from lateral1 and lateral2 in Patient(1) indicates that it is not possible to do a comparison between different studies without knowing the anatomical positions of the stimulation and the measurements. However, this study strengthen the conclusion that J. Haueisen had stated in his study that the output potentials is sensitive to the tissues that are close to the measurement electrodes [136].

4.7 Summary

In-vivo conductivity estimation depends on minimizing the error between the potentials of the forward head model and the real potentials by iterating the conductivities in the forward head model. In order to have a robust in-vivo conductivity estimation, the error function should be sensitive to the changes in the conductivity values which are assigned in the forward head model, otherwise more than one conductivity value can be the optimal solution of in-vivo conductivity estimation. Hence, performing a sensitivity analysis to measure the sensitivity of the error function to the conductivity values is essential before performing real in-vivo conductivity estimation. One way of performing the sensitivity analysis is known as “one-at-a-time” sensitivity analysis in which each parameter (conductivity value) is set to change to inspect its effect on the output error independently of the other parameters.

In this work, a one-at-a-time sensitivity analysis was performed considering two different error functions: the relative error and the RDM. When comparing the error functions, it was found that the RDM, gave a sensitivity pattern more reasonable than the sensitivity pattern of the relative error. In addition, the sensitivity analysis was performed given different stimulation

positions and different measurement positions. The stimulation position were classified according to their relative distance from scalp as deep, intermediate and lateral stimulations. It was obvious from the results that changing the distance of the stimulation from the scalp changes the resulted sensitivity pattern. In addition, different positions for stimulations of similar deepness leads to different sensitivity analysis as it was noted from the results of lateral1 and lateral2. The difference between the results of lateral1 and lateral2 can be explained by the difference of their orientation which gives an importance to the anisotropy of the head model, or it can be explained by the difference of the tissues in these positions which gives an importance to the inhomogeneity of the head model. When changing the measurement positions, it was found that the error function, in general, is more sensitive to the scalp and the skull compartments when considering the scalp EEG potentials. This confirms the importance of the scalp EEG measurements for estimating the scalp and the skull conductivities.

It was shown in this chapter that the results are similar for two different patients, and that neglecting the far electrodes from the stimulation does not change the results notably. In addition, the difference between the pattern of three-compartment head model and the five-compartment head model shows that there is dependency between the conductivity values. In general, it is concluded from this analysis that in-vivo conductivity estimation depends on the position of the stimulation, the number of compartments and the number of measuring electrodes, so in order for the study to have unbiased results, more than one dipole position should be considered for conductivity estimation and the estimated conductivities should be assigned in the head model having the same number of compartments as the model considered for estimation.

Chapter 5

In-vivo Conductivity Estimation

It was shown in the first two chapters that EEG source localization depends mostly on the geometry and the conductivity properties of the different head tissues of the head model. Still, the conductivity values which are found in the literature have large variances due to the different methods by which they are obtained and due to the dependence of conductivity values on the subject [92]. However, the materials which are considered for localizing the epeliptogenic zone in epileptic patients provide new data which can be exploited to discover other variables on which in-vivo conductivity estimation depends. In addition, the intracerebral electrical stimulation (IES) which are performed in the head of the epileptic patients provides a determined source in the gray matter since its location, direction and time course are known precisely. The stimulation is considered to move through the different structures of the head only by propagation and not by axons. Still there are limits for this method since the the head remains imperfect with the reduced parameters and presents some geometric inaccuracies and the power of the stimulation does not lead to a high signal-to-noise ratio. However, the greatest difficulty of in-vivo conductivity estimation that there is no possible validation because there is no actual values of these conductivities. Therefore, the only option is to compare the estimated conductivities with the values proposed in the literature and to discuss the variations of the estimates given the different.

This chapter describes the analysis that were performed for in-vivo conductivity estimation given the real measurements. The objective is to estimate the conductivities in the heads of three epileptic patients which are assumed to contain five different structures. This estimation was based on the

analysis of the SEEG/EEG data which were recorded in simultaneous with IES in the head of each epileptic patient. The first section shows the the results of in-vivo conductivity estimation of homogeneous and isotropic five-compartment head models for three drug-resistant epileptic patients. Then the analysis continued with specific conditions to examine if reducing the number of electrodes gives more accurate results. After that, an analysis was performed to find out if the compartments of the head are pure resistors or if they have some capacitive effects. Finally, the a source localization of the stimulation was performed given the estimated conductivity values as a way to examine the robustness of our method.

5.1 Materials

In this study, in-vivo conductivity estimation was performed in a homogeneous and isotropic five-compartment FEM head model by an optimization algorithm given the SEEG and the EEG measurements which were acquired in simultaneous with IES as shown in Fig.5.1. For this purpose, the data of three drug-resistant epileptic patients were considered: Patient(1) (male, 23 years old), Patient(2) (female, 34 years old) and Patient(3) (female, 21 years old). These patients were considered in a previous study by CRAN laboratory for estimating in-vivo conductivity values in the head using the radio frequency (50 kHz) and only for the gray matter and the white matter [97]. From the acquired MRI and CT-scans of each patient, an isotropic and homogeneous five-compartment (scalp, skull, CSF, GM and WM) FEM head model was generated. In addition, EEG and SEEG measurements were recorded in simultaneous with IES at different positions. The positions of the stimulations were classified into three classes: Deep, intermediate and lateral as shown in Fig.3.5. For each patient, a specific number of EEG and SEEG electrodes were placed as shown in Table 5.1. Each IES was set to five-second period. From the recorded five-second data, two seconds from the beginning and one second from the end were neglected in order to decrease the effect of the system baseline [139].

5.2 Preprocessing and Denoising SEEG/EEG Signals

The acquired SEEG and EEG signals contain the stimulation, evoked potentials due to stimulation, and physiological signals. In order to remove the undetermined physiological and evoked signals from acquired signals, the

Table 5.1: The number of SEEG electrodes, SEEG contacts and EEG electrodes along with the position of the epileptogenic zone for each drug-resistant epileptic patient.

Patient	SEEG electrodes	SEEG contacts	EEG electrodes	Epileptogenic zone
Patient(1)	10 Left	107	19	Left basal temporal and parahippocampal regions
Patient(2)	10 Right and 2 Left	106	20	Right mesial temporal lobe
Patient(3)	14 Right	157	24	Right anterior insular cortex

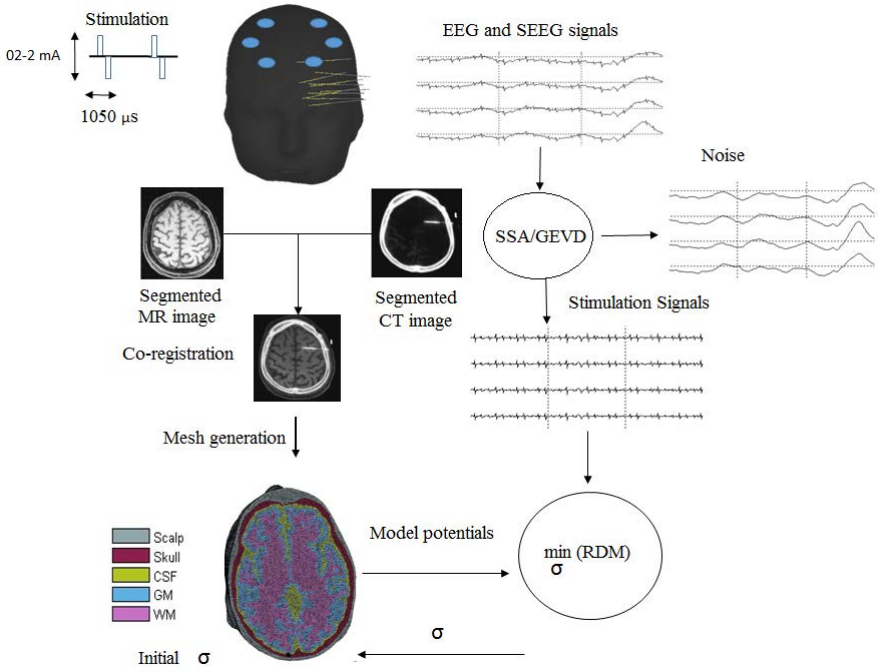

Figure 5.1: The overall procedure of signal and image analyses for in-vivo conductivity estimation.

singular spectrum analysis (SSA) in addition to the generalized eigenvector decomposition (GEVD) were considered. The combination of SSA and GEVD was considered in this study because Hofmanis et al. have found in a similar data that SSA/GEVD gave the best performance than other filtering approaches for separating the stimulation from the brain activity [139]. This signal processing method is briefly presented in the following:

Singular Spectrum Analysis

The SSA is a mono-dimensional non-parametric technique in which a sequence generated by a stochastic process $\{x(1), x(2), \cdots, x(N)\}$ is decomposed into a sum of independent components as shown in Fig.5.2. These components can be classified as a trend, slowly oscillating components and highly oscillating components. The decomposition can be summarized in four main steps:

1. Generating a trajectory matrix T from the input signal.
2. Computing the eigenvalues and the eigenvectors of the covariance matrix of T
3. Selection of the eigenvectors which corresponds to the desired components.
4. Reconstruction of the one-dimensional vector

The acquired SEEG and EEG signals are ordered in a matrix form X of $M \times N$ dimension, where M is the number of channel while N is represents the time elements. Each row vector $\mathbf{x}$, representing a signal from one channel, is entered to the SSA filter. The input sequence or signal is first converted to a trajectory matrix T as shown in Eq.5.1, where the dimension of the trajectory matrix depends on the selected window size L. In this study, the window size was chosen in a way to have each pulse of the stimulation in a separate vector ($L = round(\frac{F}{f})$) where F is the sampling frequency and f is the frequency of the stimulation).

$$T = \begin{bmatrix} x(1) & x(2) & \cdots & x(L) \\ x(2) & x(3) & \cdots & x(L+1) \\ \vdots & \vdots & \ddots & \vdots \\ x(N-L+1) & x(N-L+2) & \cdots & x(N) \end{bmatrix} \tag{5.1}$$

Then, the eigenvalues λ and eigenvectors U are calculated for the trajectory matrix T. The eigenvalues are then ordered from the highest to

the lowest. These eigenvalues indicate if the eigenvector is highly oscillating (small eigenvalue) or slowly oscillating (large eigenvalue). From these eigenvectors the number I of components are considered and the trajectory matrix is again constructed as shown in Eq.5.2.

$$\hat{T} = U_I V_I \tag{5.2}$$

Where $V = TU$. Usually, as in here, the vector corresponding to the highest eigenvector ($I = 1$) is chosen which corresponds to the trend of input sequence. However, this filtered trend is then removed by the GEVD. Finally, the components of the resulted matrix $\hat{T}$ are averaged according to Eq.5.3.

$$\mathbf{y} = \begin{cases} \frac{1}{n}\sum_{m=1}^{n} \hat{T}(m, n-m+1), & 1 \le n \le L \\ \frac{1}{L}\sum_{m=1}^{L} \hat{T}(m, n-m+1), & L+1 \le n \le N-L \\ \frac{1}{N-n+1}\sum_{m=1}^{N-L+1} \hat{T}(m, n-m+1), & L+1 \le n \le N \end{cases} \tag{5.3}$$

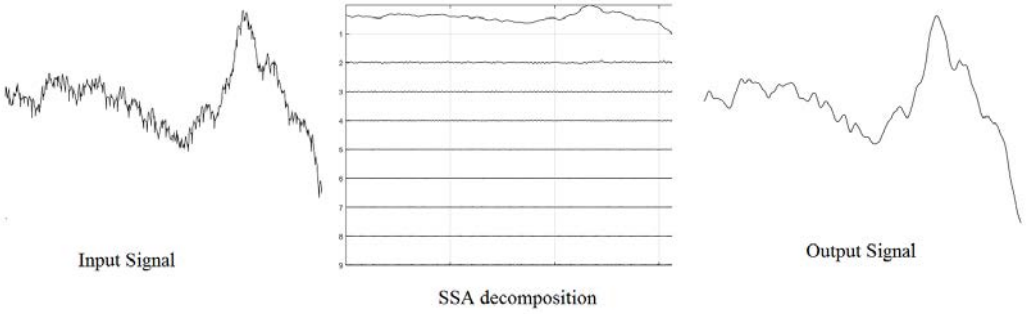

Figure 5.2: The input signal to the SSA (left) is decomposed into signals from slow oscillating to high oscillating (middle), the output (right) is the output of the SSA after choosing the first component (I = 1) in Eq.5.2.

SSA decomposes the input signal into one non-periodic component corresponding to biophysiological sources and the baseline, while the other components are periodic corresponding to the stimulation as shown in Fig.5.2. However, in order to ensure that the eigenvalues of the biophysiological sources are higher than those of stimulation source, a trend line ([-1500,1500] microvolt) was added to the input signal before applying the SSA, then it was subtracted from the output signal after the filter [47].

Generalized Eigenvector Decomposition

The Generalized Eigenvector Decomposition (GEVD) is a filtering approach that spatially filters mixed sources based on given information. This filter-

ing method has been considered for electrocardiogram (ECG) decomposition [140], MRI artifacts removal [141] and for filtering IES from background EEG activity [139]. The GEVD solution depends on two matrices. The first matrix corresponds to the correlation matrix (Eq.5.4) of the input signals Y which has the dimension of $M \times N$. While the second correlation matrix (Eq.5.5) is calculated from the output of a temporal filtering function that is applied to each row of the input matrix of the signals: $S = H(Y)$.

$$R_Y = \frac{1}{N} Y Y^T \tag{5.4}$$

$$R_S = \frac{1}{N} S S^T \tag{5.5}$$

The solution of the GEVD, gives the maximum of the Rayleigh quotient as shown in Eq.5.6. Maximizing the Rayleigh quotient implies maximizing the variance of the filtered SEEG/EEG signals while minimizing the variance of the unfiltered SEEG signals. Maximizing the Rayleigh quotient leads the two formulas that are shown in Eq.5.7

$$Q(E) = \frac{E^T R_S E}{E^T R_Y E} \tag{5.6}$$

$$\begin{cases} E^T R_S E = \Lambda \\ E^T R_Y E = I_M \end{cases} \tag{5.7}$$

Where Λ is a matrix of the eigenvalues ordered in a descending order, E is the $M \times M$ matrix of the generalized eigenvectors and I_M is the $M \times M$ identity matrix. The decomposed sources by the GEVD are given by $V = E^T Y$. However, in order to remove the unwanted components from these decomposed sources, the decomposed sources are multiplied by a diagonal matrix of 0's and 1's where the 0's corresponds to the unwanted components while the 1's corresponds the considered components. Finally the matrix is multiplied by E^{-T} in order to get the matrix of the signals without the unwanted components as shown in Eq.5.8.

$$\begin{cases} Z = E^{-T} G E^T Y \end{cases} \tag{5.8}$$

Where Z is the output of the GEVD filtering. In this study, the eigenvector that corresponds to the largest eigenvalue is considered to reconstruct the filtered signals [47]. The magnitude of reconstructed signal or the propagation coefficients were represented by the first row vector of the matrix E^{-T} as shown in Fig.5.3. The result of applying the SSA/GEVD to some SEEG channels is shown in Fig.5.4.

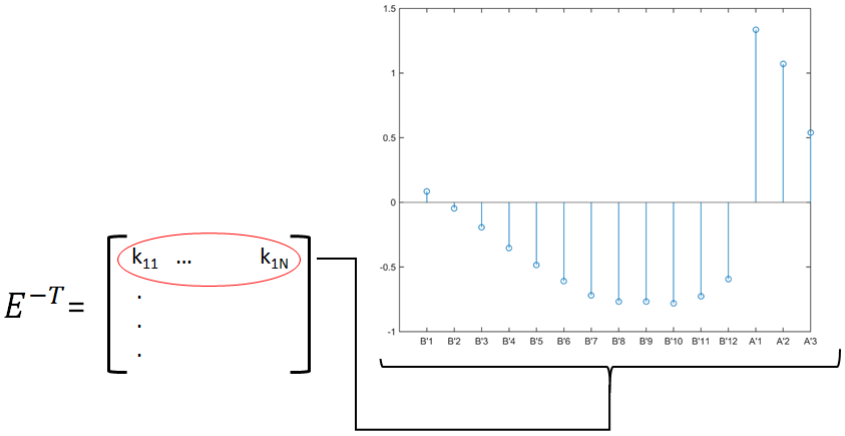

Figure 5.3: The propagation coefficients which are extracted from the measurements. Where N is the number of the measuring electrodes.

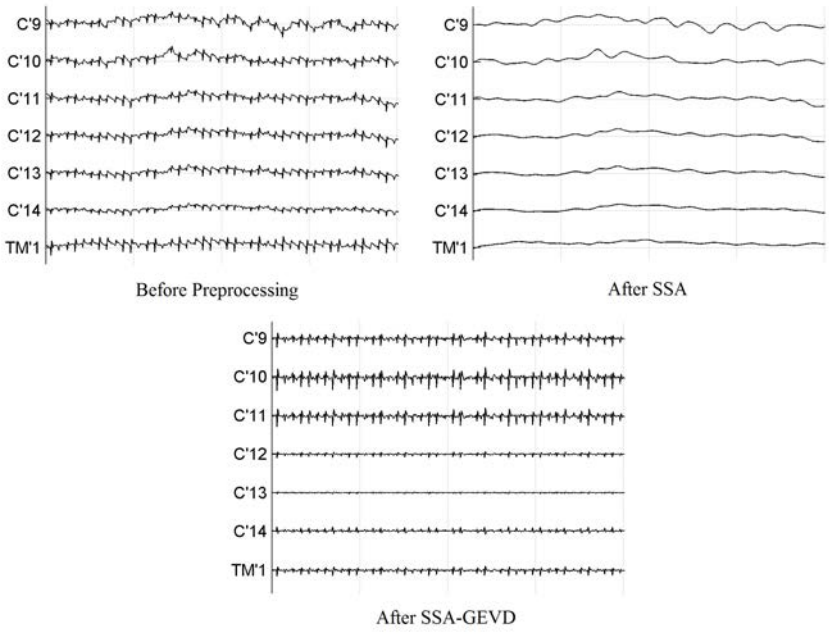

Figure 5.4: A Sample of SEEG signals before preprocessing (upper left) after SSA (upper right) and after SSA-GEVD (lower)

Table 5.2: The number of considered stimulations for each drug-resistant epileptic patients.

Patient	Deep	Intermediate	Lateral
Patient(1)	6	3	3
Patient(2)	13	4	0
Patient(3)	4	4	4

5.3 Optimizing the Conductivities in the Forward FEM Head Model

The real potentials corresponding to the first row vector of E^{-T} in GEVD were compared to the potentials of the five-compartment FEM head models by the RDM function as shown in Fig.5.1. The Nelder-Mead simplex, which gave the best performance in simulation (as was found in Chapter 3), was considered to find the optimal conductivities. Conductivity estimation was carried out under constraints: the Nelder-Mead simplex was set to estimate conductivities in the range of [0.03,0.99] S/m for scalp, [0.0008,0.0240] S/m for skull, [0.18,5.73] for CSF, [0.03,0.33] S/m for GM and [0.01,0.42] S/m for WM. These ranges were considered to cover the values that are found in the literature for human head conductivities [15, 42, 97]. Estimating the conductivities of the head compartments was performed for the three patients considering:

- The potentials of the SEEG electrodes.
- The potentials of the SEEG and EEG electrodes.
- The potential of the EEG electrodes.

These different scenarios were performed in order to find out whether adding the scalp EEG electrodes enhances the estimation when they are added to the SEEG electrodes. Moreover, considering only the EEG electrodes give an idea of whether the conductivities of the deep compartments can be estimated by considering only the scalp measurements. Stimulations were divided into deep, intermediate and lateral according to their positions in the gray matter as shown in Fig.3.5. Table 5.2 shows the number of stimulations which were considered for each patient. The results of in-vivo conductivity estimation for the three patients is discussed in the following subsection.

Table 5.3: Resulted conductivities of Patient(1) given his SEEG signals

IES position	Resulted Conductivities					Resulted RDM
	Scalp	Skull	CSF	GM	WM	
Deep	0.99	0.0082	0.18	0.64	0.10	0.23
	0.22	0.0198	5.36	0.04	0.01	0.86
	0.99	0.0071	0.18	0.78	0.11	0.23
	0.99	0.0240	0.18	0.05	0.07	0.75
	0.99	0.0059	0.18	0.04	0.06	0.29
	0.99	0.0097	0.18	0.06	0.06	0.18
Intermediate	0.99	0.0050	0.18	0.13	0.37	0.17
	0.99	0.0100	0.18	0.04	0.08	0.22
	0.03	0.0008	0.20	0.06	0.42	0.50
Lateral	0.99	0.0141	0.18	0.04	0.02	0.44
	0.95	0.0240	0.23	0.05	0.01	0.40
	0.87	0.0208	0.27	0.05	0.01	0.49

5.3.1 SEEG-based in-vivo Conductivity Estimation

In-vivo conductivity estimation was performed for three drug-resistant epileptic patients in an isotropic and homogeneous five-compartment FEM head model for each patient given the SEEG signals which were acquired in simultaneous with IES. The IES stimulations were acquired by 107 SEEG contacts, 106 SEEG contacts, and 157 SEEG contacts for Patient(1), Patient(2) and Patient(3) respectively. These stimulations were divided according to their depth in the brain as deep, intermediate and lateral as shown in Fig.3.5.

Table 5.3 shows the results of in-vivo conductivity estimation for Patient(1) considering the acquired SEEG potentials. The table shows that the scalp value is equal to its upper bound value in most of the cases. This is expected since the SEEG signals are recorded under the scalp compartment, then it is not expected to have an accurate estimation for this compartment. However, as the stimulation goes more lateral, as shown in the last two rows, the scalp conductivity started to have lower values than the upper boundary. When considering the RDM which is the main criteria for stopping the optimization, it can be noted that the lower RDM (0.17) happened when the conductivity of the gray matter is equal to 0.13 S/m which is the nearest value to the common gray matter conductivity (0.33 S/m). Having the greatest effect on the RDM by the gray matter conductivity is expected

Table 5.4: The means (S/m) and the relative standard deviations ($RSD\% = \frac{SD \times 100}{mean}$) of the resulted conductivities over all the selected stimulations of Patient(1) considering the SEEG potentials.

Position		Resulted Conductivities				
		Scalp	Skull	CSF	GM	WM
Deep	Mean	0.86	0.0125	1.04	0.27	0.07
	RSD%	36.6	60.6	202.9	128.8	49.6
Intermediate	Mean	0.67	0.0053	0.19	0.08	0.29
	RSD%	82.3	87.6	7.3	68.3	62.6
Lateral	Mean	0.94	0.0196	0.23	0.05	0.02
	RSD%	6.6	25.8	20.5	15.6	13.9

Table 5.5: The means (S/m) and the relative standard deviations ($RSD\% = \frac{SD \times 100}{mean}$) of the resulted conductivities over all the selected stimulations of Patient(2) considering the SEEG potentials.

Position		Resulted Conductivities				
		Scalp	Skull	CSF	GM	WM
Deep	Mean	0.40	0.0134	1.01	0.23	0.25
	RSD%	95.8	64.3	163.5	75.7	63.1
Intermediate	Mean	0.83	0.0197	0.18	0.50	0.32
	RSD%	39.1	21.5	0.0	92.8	31.2

since the stimulation and most of the other SEEG contacts are situated in the gray matter. Table 5.3 gives us information about the values which have high resulted RDM, and which values are equal to the boundary of the optimization algorithm. However, in order to get an overall view of the resulted conductivities given the different stimulation positions and for the different patients, the mean and the standard deviation over each deepness were determined and compared with the other deepness and with the results of the sensitivity analysis. While we kept the detailed results for all the subjects in the appendix.

Table 5.4 shows the mean and the standeard deviation results of in-vivo conductivity estimation for Patient(1) considering the acquired SEEG potentials. It can be noted that the estimated scalp and skull conductivities are in the range of the values which are found in the literature ([0.33-1.0] S/m for scalp and [0.0042-0.05] for skull [42, 136]). Moreover, the variances

Table 5.6: The means (S/m) and the relative standard deviations ($RSD\% = \frac{SD \times 100}{mean}$) of the resulted conductivities over all the selected stimulations of Patient(3) considering the SEEG potentials.

Position		Resulted Conductivities				
		Scalp	Skull	CSF	GM	WM
Deep	Mean	0.71	0.0190	0.32	0.12	0.08
	RSD%	45.7	44.7	51.0	45.9	56.2
Intermediate	Mean	0.20	0.0190	0.63	0.18	0.20
	RSD%	66.3	40.4	90.7	63.4	74.5
Lateral	Mean	0.59	0.0155	0.92	0.05	0.13
	RSD%	80.4	63.4	160.9	72.4	153.3

of the estimated scalp and skull conductivities decrease as the stimulation goes more lateral. The decrease in variances of the estimated scalp and skull is expected since the sensitivity analysis in Fig.4.6 showed that the sensitivity of the RDM to the scalp and the skull conductivities increases when considering the lateral stimulation. In agreement with the sensitivity analysis shown in Fig.4.6, the variance of the estimated CSF has its lowest value when considering the intermediate stimulation. However, the estimated CSF conductivity when considering the intermediate stimulation is not similar to the common values which are found in the literature (around 1.79 S/m [88]). Even though considering the deep stimulation gives the highest variance of the estimated CSF, the estimated CSF when considering the deep stimulation is similar to the CSF conductivity value in the literature ([0.33-3] S/m [42, 136]). The GM and the WM have their lowest variance when considering the lateral stimulation which agrees with the sensitivity analysis results, since the RDM has a high sensitivity to the GM and the WM when considering the lateral stimulation (as shown in Fig.4.6 for lateral2 stimulation). However, the resulted GM and WM conductivities when considering the lateral stimulation are far from the common values which are found in the literature ([0.33-1] S/m for GM and [0.14-0.48] for WM [42, 136]). The nearest estimated GM value to the common GM conductivity (0.33 S/m [87]) was obtained when considering the deep stimulation, although the estimated GM conductivity has a high variance when considering the deep stimulation.

Table 5.5 shows the results of in-vivo conductivity estimation for Patient(2) considering the acquired SEEG potentials. Even though the

sensitivity analysis results (shown in Fig.4.33) did not show a remarkable increase in the sensitivity of the RDM to the scalp and the skull conductivities between the deep and the intermediate stimulation, the resulted variances of the scalp and the skull conductivities are lower when considering the intermediate stimulation than when considering the deep stimulation. However, the lower standard deviations of the estimated scalp and the skull conductivities is expected when the stimulation becomes more closer the scalp and the skull compartments. Moreover, the estimated scalp and skull conductivities when considering both the deep and the intermediate stimulation are in the range of common values in the literature ([0.33-1.0] S/m for scalp and [0.0042-0.05] for skull [42, 136]). Even though the variance of the estimated CSF conductivity is higher when considering the deep stimulation (in contrary to the sensitivity results shown in Fig.4.33), the estimated CSF value when considering the deep stimulation is similar to the common CSF conductivity value ([0.33-3] S/m [42, 136]). In the case of intermediate stimulation, the optimization return always the boundary of search for the CSF conductivity (0.18 S/m), due to this the variance of the estimated CSF conductivity is 0. The estimated GM and WM conductivities in both deep and intermediate stimulation are in the range of the common conductivities in the literature ([0.33-1] S/m for GM and [0.14-0.48] S/m for WM [42, 136]).

Table 5.6 shows the results of in-vivo conductivity estimation for Patient(3) considering the acquired SEEG potentials. It can be noted that the estimated scalp and skull conductivities are in the range of the values which are found in the literature ([0.33-1.0] S/m for scalp and [0.0042-0.05] for skull [42, 136]). However, in contrary to the results of Patient(1) (shown in Table 5.4) the variances of the estimated conductivity have their highest values when considering the lateral stimulation. In addition, the variance of the estimated CSF conductivity has its lowest value when considering the deep stimulation. Yet, all the estimated CSF conductivities are in the range of the common conductivity values which are found in the literature ([0.33-3] S/m [42, 136]). In contrast to the results of Patient(1) (shown in Table 5.4) the variances of the estimated GM and WM conductivities have their highest values when considering the lateral stimulation. The estimated GM conductivity for Patient(3) is not in the range of common GM conductivity values ([0.33-1] S/m [42, 136]). However, the estimated WM conductivities are in the range of the common WM conductivity values ([0.14-0.48] S/m).

Table 5.7: The means (S/m) and the relative standard deviations ($RSD\% = \frac{SD \times 100}{mean}$) of the resulted conductivities over all the selected stimulations of Patient(1) considering the EEG potentials.

Position		Resulted Conductivities				
		Scalp	Skull	CSF	GM	WM
Deep	Mean	0.54	0.0047	1.88	0.47	0.11
	RSD%	46.4	200.0	93.7	76.6	143.7
Intermediate	Mean	0.43	0.0009	2.70	0.77	0.25
	RSD%	106.3	11.2	37.0	16.2	77.0
Lateral	Mean	0.88	0.0037	3.77	0.15	0.04
	RSD%	20.7	135.8	73.6	53.0	107.1

Table 5.8: The means (S/m) and the relative standard deviations ($RSD\% = \frac{SD \times 100}{mean}$) of the resulted conductivities over all the selected deep stimulations of Patient(2) considering the EEG potentials.

Position		Resulted Conductivities				
		Scalp	Skull	CSF	GM	WM
Deep	Mean	0.63	0.0046	1.97	0.37	0.17
	RSD%	46.3	135.7	81.8	95.7	89.8
Intermediate	Mean	0.73	0.0093	0.94	0.39	0.04
	RSD%	33.3	37.3	140.8	105.8	46.7

5.3.2 EEG-based in-vivo Conductivity Estimation

In order to find out if considering the EEG signals give different results than considering the SEEG signals, in-vivo conductivity estimation was performed in isotropic and homogeneous five-compartment FEM head models of the three drug-resistant epileptic patients given their EEG signals which were acquired in simultaneous with IES. The IES were acquired by 19 EEG electrodes, 20 EEG electrodes and 24 EEG electrodes for Patient(1), Patient(2) and Patient(3) respectively. For each patient, the same stimulations which were considered with SEEG recordings were considered with EEG recordings.

Table 5.7 shows the results of in-vivo conductivity estimation for Patient(1) considering the EEG potentials. It can be noted that the estimated scalp conductivities are in the range of the values which are found in the literature ([0.33-1.0] S/m [42, 136]). Moreover, the variances

Table 5.9: The means (S/m) and the relative standard deviations ($RSD\% = \frac{SD \times 100}{mean}$) of the resulted conductivities over all the selected stimulations of Patient(3) considering the EEG potentials.

Position		Resulted Conductivities				
		Scalp	Skull	CSF	GM	WM
Deep	Mean	0.82	0.0017	2.79	0.47	0.27
	RSD%	23.5	81.7	75.8	84.6	72.0
Intermediate	Mean	0.87	0.0022	1.42	0.54	0.10
	RSD%	13.8	67.9	63.6	70.1	144.0
Lateral	Mean	0.99	0.0008	1.91	0.51	0.30
	RSD%	0.0	7.4	128.1	107.9	64.1

of the estimated scalp conductivities decrease as the stimulation goes more lateral. Having smaller variances for the estimated scalp conductivities agrees with the results of the sensitivity analysis which showed that the sensitivity of the RDM to the scalp conductivity in the case of EEG electrodes is largest when considering the lateral stimulation (as shown in Fig.4.2 in the case of lateral1). The estimated skull conductivities in Table 5.7 when considering the EEG recordings are in general smaller than the estimated skull conductivities when considering the SEEG recordings shown in Table 5.4. Having smaller estimated skull conductivities when considering the EEG channels can be also noted in the results of Patient(2) and Patient(3) (when comparing Table 5.8 to Table 5.5 and Table 5.9 to Table 5.6). Getting smaller estimated skull conductivities when considering the EEG recordings is expected since the signals pass by the highly resistive skull compartment before being recorded by the EEG electrodes, while the SEEG recordings do not pass by the skull compartment. Even though the estimated skull conductivity has its lower variance in Table 5.7 when considering the intermediate stimulation, its value is not in the range of the estimated conductivities in the literature ([0.0042-0.05] S/m). However, the estimated skull conductivities in the both the deep stimulation and the lateral stimulation are in the range of the estimated skull conductivities in the literature, and the variance of estimated skull conductivity is smaller when considering the lateral stimulation which agrees the results of the sensitivity analysis (shown in Fig.4.2).

The estimated CSF conductivities for Patient(1) when considering the EEG recordings have the smallest variance when considering the intermedi-

ate stimulation, these results are in accordance with the sensitivity analysis results which showed that the sensitivity of the RDM to the CSF is higher when considering the intermediate stimulation (as shown in Fig.4.2). In general, the values of the estimated CSF conductivities when considering the EEG recordings are in the range of the CSF conductivity which are found in the literature ([0.33-3] S/m [42, 136]), and they are larger than the estimated CSF conductivities when considering the SEEG recordings. Since the stimulations were performed in the GM compartment, getting accurate values of the CSF when considering the EEG electrodes is expected since in this case the CSF compartment occurs between the stimulation and the recordings. The GM has its lowest variance when considering the intermediate stimulation which agrees the sensitivity analysis results, since the RDM has a high sensitivity to the GM and when considering the intermediate stimulation (as shown in Fig.4.6). However, although the RDM has a higher sensitivity to the WM in the lateral stimulation than in the intermediate stimulation, the estimated WM conductivity in lateral stimulation has a high variance and does not fit in the range of the estimated conductivities of the literature [0.14-0.48] S/m.

Table 5.8 shows the results of in-vivo conductivity estimation for Patient(2) considering the acquired EEG potentials. It can be noted that the estimated scalp and skull conductivities are in the range of the values which are found in the literature ([0.33-1.0] S/m for scalp and [0.0042-0.05] for skull [42, 136]). Even though the sensitivity of the RDM does not change remarkably between the deep and the intermediate stimulation, the variance of the estimated scalp and skull conductivities decreases when considering the lateral stimulation. The estimated CSF and GM conductivities are in the range of the conductivity which are found in the literature ([0.33-3] S/m for CSF and [0.33-1] S/m for GM). In addition, in agreement with the sensitivity results shown in Fig.4.29, the variances of the estimated CSF and GM conductivities are smaller when considering the deep stimulation. In spite of the fact that the estimated WM conductivity has smaller variance when considering the intermediate stimulation, its value when considering the intermediate stimulation does not fit in the range of the estimated conductivities which are found in the literature (0.14-0.48 S/m [42, 136]).

Table 5.9 shows the results of in-vivo conductivity estimation for Patient(3) considering the acquired EEG potentials. Even though the estimated scalp conductivity has its smallest variance when considering the lateral stimulation, its estimated value is equal to the boundary of the optimization. However, the estimated scalp conductivities in the case of deep

and intermediate stimulations have small variance and fit in the range of the estimated conductivities which are found in the literature. Similarly, the estimated skull conductivity in the case of lateral stimulation is equal to the boundary of the optimization, so this value cannot be considered. However, in contrast to the scalp estimated values, the estimated skull conductivities in the case of deep and intermediate stimulations do not fit in the range of the estimated conductivities which are found in the literature. Nevertheless these skull conductivity values are small compared to the estimated skull conductivities when considering the SEEG recordings (shown in Table 5.6). In agreement with the sensitivity analysis shown in Fig.4.2, the estimated CSF and GM conductivities have the lowest variance when considering the intermediate stimulation. In addition, all the estimated CSF and GM conductivities fit in the range of the estimated conductivities which are found in the literature ([0.33-3] S/m for CSF and [0.33-1] S/m for GM). Similarly, in accordance with the sensitivity analysis shown in Fig.4.2 the estimated WM conductivity has the lowest variance when considering the lateral stimulation. Moreover, its values, in general, fit in the range of the estimated values which are found in the literature.

5.3.3 SEEG+EEG-based in-vivo Conductivity Estimation

Since the purpose of this work is to verify whether considering the SEEG recording do enhance the conductivity estimation, in-vivo conductivity estimation in isotropic and homogeneous five-compartment FEM head models was performed for three drug-resistant epileptic patients given their SEEG and EEG signals which were acquired in simultaneous with IES. The IES stimulations were acquired by 107 SEEG/19 EEG, 106 SEEG/20 EEG, and 157 SEEG/24 EEG sensors for Patient(1), Patient(2) and Patient(3) respectively.

Table 5.10 shows the results of in-vivo conductivity estimation for Patient(1) considering the acquired SEEG+EEG potentials. It can be noted that the estimated scalp and skull conductivities are, in general, in the range of the values which are found in the literature ([0.33-1.0] S/m for scalp and [0.0042-0.05] for skull [42, 136]). Moreover, the variances of the estimated scalp and skull conductivities decrease as the stimulation goes more lateral. The decrease in variances of the estimated scalp and skull is expected since the sensitivity analysis in Fig.4.6 showed that the sensitivity of the RDM to

Table 5.10: The means (S/m) and the relative standard deviations ($RSD\% = \frac{SD \times 100}{mean}$) of the resulted conductivities over all the selected stimulations of Patient(1) considering the SEEG and the EEG potentials.

Position		Resulted Conductivities				
		Scalp	Skull	CSF	GM	WM
Deep	Mean	0.60	0.0152	0.22	0.30	0.14
	RSD%	56.8	58.9	32.8	125.9	95.6
Intermediate	Mean	0.31	0.0084	0.24	0.14	0.40
	RSD%	77.9	78.5	30.5	52.7	6.3
Lateral	Mean	0.95	0.0209	0.24	0.05	0.02
	RSD%	7.4	26.0	27.0	18.0	14.2

Table 5.11: The means (S/m) and the relative standard deviations ($RSD\% = \frac{SD \times 100}{mean}$) of the resulted conductivities over all the selected stimulations of Patient(2) considering the SEEG and the EEG potentials.

Position		Resulted Conductivities				
		Scalp	Skull	CSF	GM	WM
Deep	Mean	0.53	0.0096	0.73	0.23	0.28
	RSD%	75.7	71.3	178.4	73.8	55.0
Intermediate	Mean	0.87	0.0187	0.18	0.47	0.30
	RSD%	27.6	21.7	0.0	91.4	33.9

Table 5.12: The means (S/m) and the relative standard deviations ($RSD\% = \frac{SD \times 100}{mean}$) of the resulted conductivities over all the selected stimulations of Patient(3) considering the SEEG and the EEG potentials.

Position		Resulted Conductivities				
		Scalp	Skull	CSF	GM	WM
Deep	Mean	0.38	0.0082	1.12	0.32	0.24
	RSD%	119.7	123.4	86.3	87.0	74.9
Intermediate	Mean	0.21	0.0183	0.64	0.19	0.20
	RSD%	72.6	42.3	96.0	68.5	81.8
Lateral	Mean	0.81	0.0127	0.94	0.29	0.08
	RSD%	19.4	83.2	133.2	158.3	166.4

the scalp and the skull conductivities increases when considering the lateral stimulation. The estimated CSF conductivities do not fit in the range of the estimated conductivities which are found in the literature, and they are similar to the values obtained when considering the SEEG electrodes as shown in Table 5.4 due to the large number of the SEEG electrodes compared to the EEG electrodes. Even though the variance of the estimated GM conductivity becomes smaller as the stimulation goes more lateral, the estimated GM conductivities when considering the the lateral and the intermediate stimulations are not similar to the common conductivity values found in the literature. As shown in Fig.4.7 the sensitivity of the RDM to the WM is larger when considering the intermediate stimulation than when considering the deep stimulation, in agreement to that result, it can be noted that the variance of the estimated WM conductivity is smaller when considering the intermediate stimulation. However, when considering the lateral stimulation, the estimated WM conductivity value does not fit in the range of the conductivities which are found in the literature even though its variance is small.

Table 5.11 shows the results of in-vivo conductivity estimation for Patient(2) considering the acquired SEEG+EEG potentials. Even though the sensitivity analysis results (shown in Fig.4.34) did not show a remarkable increase in the sensitivity of the RDM to the scalp and the skull conductivities between the deep and the intermediate stimulation, the resulted variances of the scalp and the skull conductivities are lower when considering the intermediate stimulation than when considering the deep stimulation. However, the lower variance of the estimated scalp and the skull conductivities is expected when the stimulation becomes more closer the scalp and the skull compartments. Moreover, the estimated scalp and skull conductivities when considering both the deep and the intermediate stimulation are in the range of common values in the literature ([0.33-1.0] S/m for scalp and [0.0042-0.05] for skull [42, 136]). The estimated CSF conductivity has a zero variance when considering the intermediate stimulation, yet, the estimated values are equal to the boundary of the optimization, therefore this mean should not be considered. The estimated GM and WM conductivities are, in general, in the range of the common conductivities in the literature ([0.33-1] S/m for GM and [0.14-0.48] S/m for WM [42, 136]). Nevertheless, the estimated WM conductivity has a smaller variance when considering the intermediate stimulation although there is no remarkable difference between the sensitivity results in the deep and intermediate case as shown in Fig.4.34.

Table 5.12 shows the results of in-vivo conductivity estimation for Patient(3) considering the acquired SEEG+EEG potentials. It can be noted

that the estimated scalp and skull conductivities are, in general, in the range of the values which are found in the literature ([0.33-1.0] S/m for scalp and [0.0042-0.05] for skull [42]). In accordance with the sensitivity results shown in Fig.4.7, the variance of the estimated scalp conductivity has its smallest value when considering the lateral stimulation (in the sensitivity analysis the RDM is sensitivity to the scalp conductivity in lateral1 stimulation). In addition, the variance of the estimated skull conductivity has its lowest value when considering the intermediate stimulation which agrees the results of the sensitivity analysis shown in Fig.4.7, since the RDM is sensitive to the skull conductivity in the case of intermediate stimulation. The estimated GM conductivity has its smaller variance in the case of intermediate stimulation, but its value is not close to the conductivity values which are found in the literature. In addition, in contrast to the sensitivity analysis, which are shown in Fig.4.7, the variance of the estimated GM conductivity is smaller when considering the deep stimulation. For the WM conductivity, in contrary to the sensitivity analysis, the variance of the estimated WM conductivity has its largest value when considering the lateral stimulation. Yet, the estimated WM conductivity fit in the range of the estimated conductivities which are found in the literature when considering the stimulations which are nearer to the WM (deep and intermediate stimulations).

5.4 Conductivity Estimation Given the SEEG Measurements Within 50 mm from IES

From the previous results, it was found that in order to have a robust estimation of the compartment's conductivity, the stimulation should be close to that compartment. This can be explained by the fact that the propagated stimulation potentials are inversely proportional to the square of distance, so that the spatial energy decay is relatively fast and therefore the measurements which are away from the stimulation are not significant in the estimation process. In addition, previous results had a large variance which may be due to the large number of measurements that are spread over all the head of the patient. Hence, to find out whether reducing the number of measurements reduces the variance of the resulted conductivities, or enhances in-vivo conductivity estimation for some compartments; the SEEG contacts which are within 50 mm distance from the stimulation were considered for performing in-vivo conductivity estimation of Patient(1). The 50 mm distance was chosen in order to have a sufficient number of

measurements for performing in-vivo conductivity estimation.

Table 5.13 shows the results of in-vivo conductivity estimation for Patient(1) considering the acquired SEEG potentials within 50 mm of the stimulation. It can be noted that the estimated scalp and skull conductivities are, in general, in the range of the values which are found in the literature ([0.33-1.0] S/m for scalp and [0.0042-0.05] for skull [42, 136]). Although the estimated scalp conductivity in the case of deep stimulation has a zero variance, it cannot be considered since the estimated value is equal to the boundary of the optimization. However, the variances of the estimated scalp and the skull conductivities decrease as the stimulation goes more lateral as found in Table 5.4. Similarly, the estimated CSF conductivity in the case of deep stimulation is equal to the boundary of the optimization, so this value cannot be considered even though its variance is equal to zero. In general, the values of the estimated CSF are smaller than the common conductivity value (1.79 S/m [88]), this can be explained by the fact that the stimulation in addition to the measuring contacts are placed beneath the CSF compartment, so its conductivity value cannot be well-estimated. In spite of having a lower variance of the GM and WM when considering the lateral stimulation (in agreement with the results found in Table 5.4), the estimated values when considering the lateral stimulation are out of the range of the conductivity values which are found in the literature ([0.33-1] S/m for GM and [0.14-0.48] S/m for WM [42, 136]). However, the estimated GM and WM conductivities when considering the deep stimulation fit in the range of the values in the literature. This indicates the importance of having the stimulation near the compartment in order to estimate its conductivity. In general, the results found when considering the SEEG measurements within the 50 mm distance are similar to the results found when considering all the SEEG measurements. This similarity had been found in the previous chapter when the sensitivity pattern given all the measurements was compared with the sensitivity pattern when considering the measurements which are within 50 mm of the stimulation. However, there are changes in the values of standard deviations for some estimated conductivities (Skull, GM and WM) in the vicinity of the stimulation: they are clearly smaller.

5.5 Head Conductivity Frequency Response

As was shown in Chapter 2, Poisson's equation, Eq.2.3, is considered to solve the forward problem for all head geometries. However to solve the Poisson's equation, the conductivity values should be first estimated. In the previous

Table 5.13: The means (S/m) and the relative standard deviations ($RSD\% = \frac{SD \times 100}{mean}$) of the resulted conductivities over all the selected stimulations of Patient(1) considering the SEEG potentials within 50 mm from the stimulation.

Position		Resulted Conductivities				
		Scalp	Skull	CSF	GM	WM
Deep	Mean	0.99	0.0093	0.18	0.57	0.13
	RSD%	0.0	83.6	0.0	73.4	29.7
Intermediate	Mean	0.88	0.0082	0.22	0.10	0.16
	RSD%	22.1	23.9	34.0	31.7	33.3
Lateral	Mean	0.93	0.0197	0.26	0.06	0.02
	RSD%	11.2	23.1	45.6	23.3	18.9

section, we provide the resulted conductivity values that were obtained for three epileptic patients assuming that the head conductivity does not depend on the frequency of the stimulation. However, if the conductivity depends on the stimulation frequency, then the Poisson's equation would be written in the form:

$$\nabla \cdot \boldsymbol{J}^p = \nabla \cdot (\sigma(f) \nabla V) \tag{5.9}$$

Where f is the frequency of the stimulating current. In the literature, some publications have found that the conductivity values were not affected by changing of the frequency [88], while others have found that the conductivity values depend on the frequency of the stimulating current [95]. In this study, to examine the effect of changing the stimulation frequency on the conductivity; conductivity estimation was performed for Patient(1) considering the fundamental frequency of the IES (55 Hz) in addition to its two harmonics (110 Hz and 165 Hz) as shown in Fig.5.5. Here instead of considering the SSA to separate the stimulation signals from the noise; a narrow band band-pass filter was applied to get the desired frequency component of the stimulation signal.

As shown in Fig.5.6, for performing in-vivo conductivity estimation for Patient(1), a head model with initial conductivities was built and its simulated potentials were compared with the real potentials acquired from the patient. The initial conductivities of the head model were chosen as: 0.33 S/m for scalp, 0.008 S/m for skull, 1.79 S/m for CSF, 0.33 S/m for GM and 0.14 S/m for WM. The real potentials acquired from the patient

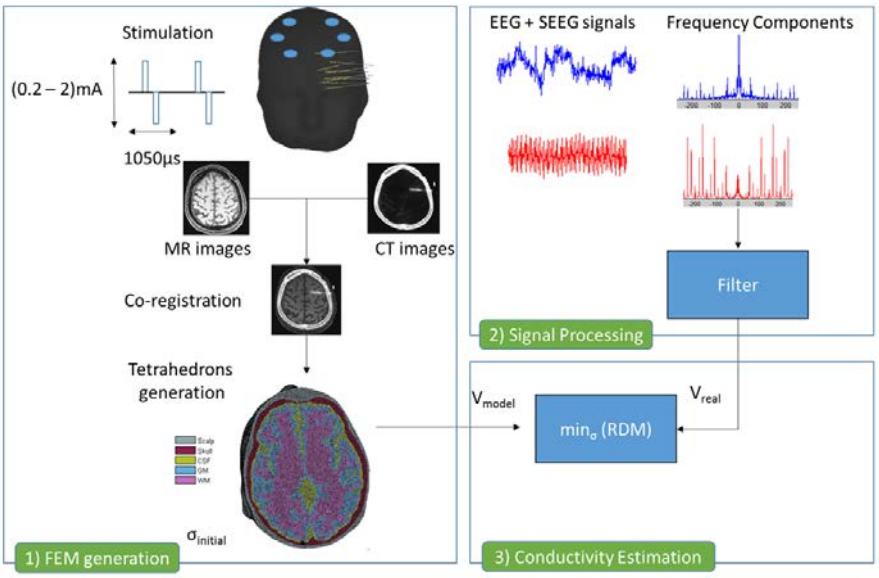

Figure 5.5: A scheme showing the procedure for estimating the conductivities in Patient(1) by considering the fundamental frequency (55 Hz) and the first two harmonics (110 and 165 Hz).

were represented by the amplitude of the target frequency component. The Nelder-Mead simplex algorithm was considered to estimate the conductivity values by minimizing the RDM between the real potentials and the model's potentials. The Nelder-Mead simplex algorithm was set to search in the positive values less than or equal to: 1 S/m for the scalp, 0.1 S/m for the skull, 3 S/m for the CSF, 1 S/m for the GM and 1 S/m for the WM. For each frequency component, conductivity estimation was performed first considering the SEEG potentials and then considering both the SEEG and EEG potentials. Fig.5.5, Table 5.14 and Table 5.15 show the resulted mean and the standard deviation for each frequency component while the detailed results are listed in the tables from Table A.11 to Table A.16.

From the results, it can be noted that, in general, the mean of the estimated conductivities changes with changing the stimulation frequency. The pattern of the scalp, the GM and the WM compartments did not change after adding the EEG potentials to the SEEG. As shown in Fig.5.6, the scalp conductivity increased with increasing the frequency, this support the conclusion of Dabek et al. about the increase in the scalp conductivity with frequency [95]. The increase pattern is also noted in the GM conductivity. However, the WM conductivity decreases with increasing the frequency while

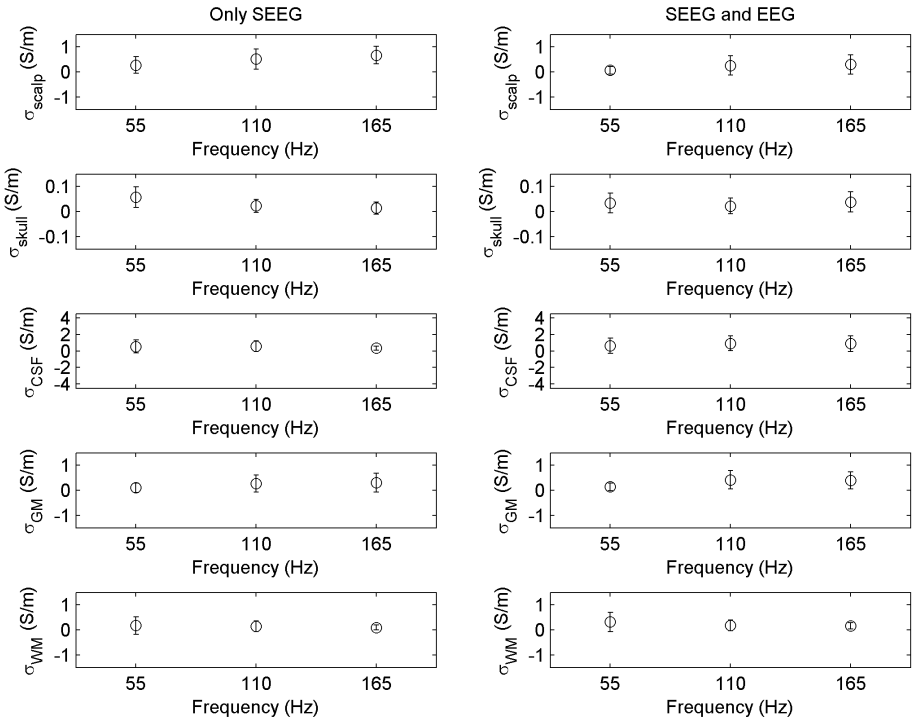

Figure 5.6: Resulted conductivities for Patient(1) given his SEEG and EEG data.

Table 5.14: The means ± the standard deviations of the resulted conductivities over all the selected stimulations of Patient(1) given the SEEG potentials and considering the fundamental frequency and the first two harmonics.

	Resulted Conductivities				
(Hz)	Scalp	Skull	CSF	GM	WM
55	0.27 ± 0.33	0.0572 ± 0.0409	0.54 ± 0.80	0.11 ± 0.19	0.17 ± 0.35
110	0.51 ± 0.40	0.0225 ± 0.0263	0.55 ± 0.65	0.27 ± 0.34	0.14 ± 0.21
165	0.67 ± 0.35	0.0136 ± 0.0245	0.34 ± 0.24	0.30 ± 0.37	0.10 ± 0.09

Table 5.15: The means ± the standard deviations of the resulted conductivities over all the selected stimulations of Patient(1) given the SEEG and the EEG potentials and considering the fundamental frequency and the first two harmonics.

	Resulted Conductivities				
(Hz)	Scalp	Skull	CSF	GM	WM
55	0.06 ± 0.15	0.0343 ± 0.0397	0.63 ± 0.91	0.14 ± 0.15	0.31 ± 0.39
110	0.26 ± 0.38	0.0218 ± 0.0314	0.92 ± 0.90	0.42 ± 0.37	0.18 ± 0.27
165	0.30 ± 0.39	0.0385 ± 0.0405	0.89 ± 0.95	0.39 ± 0.34	0.16 ± 0.13

the patterns of the skull and the CSF are not uniformly changing. These results must be carefully interpreted because the standard deviations are large with respect to the measurements. Even though there is a change in the estimated conductivity values given the different frequency components of the stimulation, this change may be due to the capacitive effect between the stimulation electrode and the tissue of the head [5].

5.6 Localization of the IES with the Estimated Conductivities

This part is included in this manuscript as an example of application. The estimation of head conductivities has a definite interest in solving the inverse problem, as has been specified in the first chapter, for performing source localization. Since the main objective of this thesis is to provide conductivity values based on different conditions and parameters for improving source localization, the robustness of these estimates can be examined by performing source localization of the IES. The location of the stimulation was estimated in the five-compartment FEM head model given the estimated conductivities and the reference conductivities in the literature in order to examine if the estimated conductivity outperform the reference conductivity. For this purpose, the stimulation positions which gave RDM less than or equal 0.25 in Patient(1) were considered. The estimated conductivities with the resulted RDM of these stimulation positions are shown in Table 5.16.

In order to compare the estimated conductivities with the common conductivities for source localization, the eLORETA (exact low resolution electromagnetic tomography) method was considered. The eLORETA has at-

Table 5.16: The estimated conductivities along with their RDM which were considered for performing source localization in Patient(1).

Index	Signals	IES position	Resulted Conductivities					Resulted
			Scalp	Skull	CSF	GM	WM	RDM
1	SEEG	Deep	0.99	0.0082	0.18	0.64	0.10	0.23
2			0.99	0.0071	0.18	0.78	0.11	0.23
3			0.99	0.0097	0.18	0.06	0.06	0.18
4	SEEG	Intermediate	0.99	0.0050	0.18	0.13	0.37	0.17
5			0.99	0.0100	0.18	0.04	0.08	0.22
6	SEEG-EEG	Deep	0.67	0.0041	0.36	0.77	0.12	0.25

tained zero localization errors in ideal noiseless conditions [142]. In the forward head model, the generated potentials are determined by the following equation [142]:

$$J_i = (A_i^T C A_i)^{-1/2} A_i^T C V \tag{5.10}$$

Where J_i is the current density of each source $i \in 3N$, V is a $(M \times 1)$ column vector of the recorded potentials and A_i is the i^{th} column of the $(M \times 3N)$ leadfield matrix. The lead field matrix contains the generated potentials at the recording positions from each source. At each position, three different sources can be generated by assigning three different orientations. Therefore, the size of the leadfield matrix would be $M \times 3N$ where N is the number of sources and M is the number of the measurements. The vector C in Eq.5.10 is calculated by the following equation:

$$C = (AW^{-1}A^T + \alpha H)^+ \tag{5.11}$$

Where W is a diagonal matrix of $w_{ii} = 1$, α is a constant greater than zero, and $(\cdot)^+$ represent a psedu-inverse operation and H an $(M \times M)$ matrix calculated by the following equation:

$$H = I - \frac{\mathbf{1}\mathbf{1}^{\mathbf{T}}}{\mathbf{1}^{\mathbf{T}}\mathbf{1}} \tag{5.12}$$

Where I is a $M \times M$ identity matrix and $\mathbf{1}$ is a $M \times 1$ vector of one elements. Since the number of elements in the FEM head model is large, it is hard to generate a leadfield matrix considering all the elements in the cortex. Due to this, the distance separating two arbitrary source positions were chosen as 10 mm. By doing so, the number of arbitrary source positions

Table 5.17: The resulted distances in mm between real source positions and the source positions with the greatest amplitude given the estimated conductivities and the reference conductivities. The index column indicates to which stimulations in Table 5.16 these results correspond.

Index	Estimated Conductivities	Reference Conductivities
1	23.24	87.98
2	12.02	12.02
3	8.16	70.55
4	5.78	75.86
5	25.54	78.60
6	11.33	15.41

was 1106 in the GM of the head model as shown in Fig.5.7. From the beginning of the columns of the matrix A, each three columns correspond to three orthogonal orientation of one source position, due to this the number of columns are 3318.

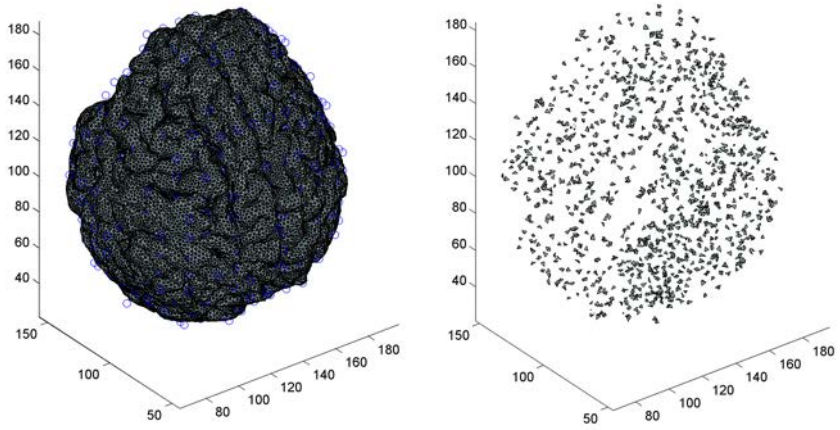

Figure 5.7: Left: The blue circles show the positions of the arbitrary sources in the head model of Patinet(1). Right: The tetrahedron elements which contains the arbitrary sources in the head model of Patient(1).

In this work, for each source position shown in Table 5.16, the leadfield matrix was calculated twice: given the estimated conductivities, and given the common conductivities $[0.33, 0.008, 1.79, 0.33, 0.14]$ S/m. Normally, the source which corresponds to the largest current density (i.e. $max(J)$) will

have the nearest distance to the stimulation position. Therefore the position of the source which has the maximum current density was compared to the real position of the IES. Table 5.17 shows the distance in millimeters between the determined source position by eLORETA and the real source position given the estimated conductivities and the common conductivities. The results in Table 5.17 shows that the performance of the estimated conductivities is superior to the common conductivities for localizing the IES. In addition, the small localization errors shown in Table 5.17 given the estimated conductivity indicates the accuracy of the eLORETA algorithm in source localization. Moreover, the large localization errors resulted when considering the common conductivities shows the importance of estimating in-vivo conductivities before performing source localization.

5.7 Discussion

This chapter showed the results that were obtained from in-vivo conductivity estimation of three drug-resistant epileptic patients. Most of the estimated conductivities were in the range or close to the conductivity values which are found in the literature [42, 136]. Although the ranges of the conductivities which is found in the literature are very wide for comparing the results, when an estimated conductivity lies in that range, it indicates that the method which was considered for in-vivo conductivity estimation is reasonable.

As was found in many studies [92, 96, 105], we found that the mean of the estimated conductivity values where different for different patients. In addition, it was found here that the estimated mean conductivities are different for the same patient when considering different stimulation positions and different measurements. Moreover, the variances which were determined given the same stimulation level (deep, intermediate and lateral) were large. The large variance is due to the difference of the anatomical position between two IES of one deepness since the distance between two deep (intermediate or lateral) IES is at least 2 mm. Moreover there are datasets for which estimates are not feasible; for which the RDM is greater than 1. This means that the correlation between data and model is less than or equal to 0.5. We believe that it is preferable to reject these solutions. Such high RDM could be due to different reasons like: the data are still disturbed despite the preprocessing and denoising, the segmentation of the structures in the MRI is not optimal, the location of the IES and the defined anatomical structures may not be optimal for the tools which are implemented.

Even though this study could not give precise values of conductivities to be considered for future work, there are general conclusions and guidelines which can be drawn from the obtained results. In general, and for all measurements (SEEG, EEG and SEEG+EEG), the variances of the estimated scalp and skull conductivites were decreasing for more lateral stimulations. This decrease in the variance agrees with the results obtained from the sensitivity analysis. Since the RDM is sensitive to the scalp and skull conductivities given the lateral stimulation, a minimum conductivity value is found, so the optimization can stuck most of the time with this minimum value due to which the variance between the estimated conductivities would be small. In addition, since lateral stimulation is nearer to the scalp and the skull compartment, having a small variance of the estimated scalp and the skull when considering the lateral stimulation is expected. However, the sensitivity analysis results does not always agree with the obtained variances, as for the GM and WM which have high variances when considering the deep stimulation even though the RDM is not sensitive to the GM and WM when considering the deep stimulation. Yet, the estimated GM and WM conductivities when considering the deep stimulation were closer to the conductivity values which are found in the literature since the deep stimulation is closer to the GM and the WM compartments.

In general the estimated skull conductivity was larger when considering the SEEG measurements than when considering the EEG measurements. Having a lower skull conductivity when considering the EEG scalp electrodes makes sense, since the current passes by this high-resistive compartment before reaching the scalp EEG electrodes. From this, the lower brain-to-skull conductivity ratio of 25 (over five subjects) which was obtained by Lai et al. when considering the subdural measurements [105] compared to the ratio of 44 (over two subjects) which was obtained by Acar et al. when considering scalp EEG measurements [92] can be explained by the lower skull conductivity which is obtained when considering the scalp EEG measurements. In addition, the estimated CSF conductivities were closer to the range found in the literature when considering the EEG measurements, this is because in the case of the SEEG, both the IES and the measurements are located beneath the CSF compartment. However, when considering the EEG measurements, the CSF compartment is located between the stimulation and the measurements.

Similar to the results which were obtained in Chapter 4, there was no remarkable difference after reducing the number of measurements around

the stimulating electrode. In addition, the results obtain when considering the SEEG+EEG measurements were similar to the results obtained when considering the SEEG measurements, because the number of the SEEG measurements is larger than the number of the EEG measurements. Moreover, when in-vivo conductivity estimation was performed considering the different frequency components, the estimated means were different for different frequency components. When considering SEEG or both SEEG+EEG, the conductivity of the scalp and the GM were increasing as the frequency increases but the conductivity of the WM was decreasing as the frequency increases. The increase in the scalp conductivity with the increase in stimulation frequency support the finding of Dabek et al. [95]. However, as it is emphasized earlier, it is necessary to remain very careful since the variances are large and the variations of the estimates are not very significant. Moreover, these changes in the estimated conductivities may be due to the capacitive effects that are generated between the stimulation electrode and the tissues of the head [5].

5.8 Summary

Source localization is performed by solving the inverse problem in the forward head model. Hence, in order to do an accurate source localization the geometry and the conductivity values of the forward head model should be accurate. Currently, the geometry of the head model can be very similar to the real geometries of the human head thanks to the MRI and the CT scans. However, still the literature is full of different conductivity values estimated on different subjects and using different methods. The materials which are considered in this study for localizing the epiliptogenic zones in the head of epileptic patients (SEEG/EEG + IES) are unprecedented techniques, in the field of in-vivo conductivity estimation, to the best of our knowledge.

In-vivo conductivity estimation by optimizing the forward head model is performed by comparing the real potentials (SEEG/EEG) with the model potentials, then changing the conductivity assigned in the head model until the error between the model potentials and the real potentials reaches its minimum value. In this study, the head model was assumed to be isotropic and homogeneous and contains five compartments (scalp, skull, CSF, GM and WM). In-vivo conductivity estimation was performed for three different drug-resistant epileptic patients where the IES were classified

into three classes according to their deepness: deep, intermediate and lateral. In general, the estimated conductivities in this study were in the range of the conductivities which are found in the literature. This indicates that our method is reasonable. However, the resulted standard deviations were large in general. The large standard deviation could be due to the difference in distance between one stimulation and another; even though the stimulations were divided according to their deepness, still the distance between one deep stimulation and another deep stimulation is at least 2 mm. The high variance in addition to the difference between the resulted conductivities given different stimulation and different measurements give an important remark for future studies. Away from the high variance and the difference based on measurements and patients, there are general important general points which can be concluded from this study: 1) The skull conductivity is lower when considering the scalp EEG measurements than when considering the SEEG measurement. 2) The standard deviation of the estimated conductivity is lower when the stimulation is nearer to that compartment. In a similar manner with the sensitivity analysis, neglecting the measurements of the farthest electrodes did not change the result of conductivity estimation notably.

The Poisson equation, on which in-vivo conductivity estimation is based depends on the quasi-static condition which means that the frequency does not affect the conductivity of the tissues. However, there are some studies which have shown that the estimated conductivities change when changing the current frequency. In order to verify whether the conductivities are frequency-dependent or not, in-vivo conductivity estimation was performed given the fundamental frequency of the stimulation and its first two harmonics. The results of this study shows that there is change in the mean estimated conductivity as the frequency change. However, this change is accompanied with high variance. In addition, when determining the effect of frequencies on different compartments one should keep in mind the capacitive effect resulted between the electrodes and the tissues.

Chapter 6

Conclusion and Perspectives

6.1 Summary and Conclusion

This thesis introduced in-vivo conductivity estimation by optimizing the forward head model given relatively new materials. These materials included the simultaneous SEEG and EEG recordings of intercerebral electrical stimulations. Apart from the introduction, four major topics were covered in this these. The first part presented the generation of a homogeneous and isotropic five-compartment (scalp, skull, CSF, gray matter and white matter) FEM head model from the CT and the MRI of an epileptic patient. We chose to refine the model into five anatomical compartments while other studies in source localization considered spherical model or less number of compartments. Obviously our model is very complex but in addition to conductivity estimation our purpose was to calculate the sensitivity of the model to certain configurations such as the position of the stimulation. The second part performed a comparison among common optimization algorithms in order to optimize the forward head model. The third part analyzed the sensitivity of the output potentials to the input conductivities given different conditions on the stimulation position, the measurement positions and the number of compartments in the head model. While the forth part provided some in-vivo conductivity results based on the conditions which were applied in the sensitivity analysis. These major topics were described in detail in the chapters from Chapter 2 to Chapter 5 of this thesis.

Chapter 2 introduces the Poisson equation from which the potentials in a volume conduction model are determined given the quasi-static condition. Then the Poisson equation was derived by the FEM method to calculate the potentials from a dipolar source in a realistic head model generated from

discretizing the head volume into tetrahedrons. In addition, the generation of the realistic geometries from MRI and CT of the epileptic patients was introduced. MRI and CT were segmented and registered in order to have a five-compartment head model along with the positions of the intracerebral electrodes.

In estimating in-vivo conductivities, the optimization algorithm plays a major role since estimating in-vivo conductivities is based on optimizing the forward head model. In order to choose a robust optimization algorithm, Chapter 3 presented a method for comparing three common optimization algorithms: the Nelder-Mead simplex algorithm, the genetic algorithm and the simulating annealing. The comparison was performed in simulation and given many different conditions on the stimulation position, the measurement positions and the existence of noise. Given all the different conditions, the Nelder-Mead simplex outperformed the genetic algorithm and the simulating annealing in both speed and convergence to the solution.

Apart from the optimization algorithm, for obtaining a robust conductivity estimation, the error function comparing the model potentials with the real potentials should be sensitive to the conductivity values, so that the optimization algorithm can find a minimum solution. If the error function is not sensitive, more than one result could be obtained as an optimal solution. In Chapter 4, a one-at-a-time sensitivity analysis was performed given different conditions on the stimulation positions, the measurement positions, the error function and the number of compartments. It was found in this chapter that the measurement positions and the stimulation position have a great effect on the pattern of the sensitivity. In addition, by changing the number of compartments, the sensitivity patterns changed indicating the dependency between the conductivity values assigned in the different compartments.

In Chapter 5, in-vivo conductivity estimation was performed for three drug-resistant epileptic patients given the conditions which were considered in Chapter 4. This chapter showed that in addition to the effect of inter-subject variability, and method variability, the stimulation position and the measurement positions lead to variability in the resulted conductivity values. Moreover, the resulted conductivity values given different frequencies were different showing that the resulted conductivity depends on the stimulation frequency, however, this cannot be a decisive conclusion since the capacitive effect between the electrodes and the tissue is uncontrolled. In general, the five-compartment head model which were considered in this study is very rich

compared to the spherical, and the BEM head models which were considered in the literature. Due to this, the position of stimulation has a great effect on such model and it is not enough to consider one stimulation position for estimating in-vivo conductivities.

6.2 Perspectives

This thesis presented new contribution on the effect of considering SEEG and/or EEG measurements and changing the position of the electrical stimulation on in-vivo conductivity estimation. Even though the work has covered many aspects, more possible extensions can be applied to this work in terms of:

- **Head Models**: The work considered a homogeneous and isotropic five-compartment FEM head model for estimating conductivities. The large number of elements in such model is expected to play a major role in making the resulted conductivities depends on stimulation position and measurement position. In order to examine this, simpler head models (like one-sphere, three-sphere and BEM head models) can be considered in future studies with similar materials in order to check the effect of stimulation position and the measurement positions. In simple models (three-compartment), the different compartments can be separated visually, so that the compartment that contains the stimulation can be determined more easily than in five-compartment head models where the the difference between the white matter and the gray matter is very hard to distinguish.

- **Stimulation position**: Due to medical reasons, stimulation were not performed more than one time in the same anatomical position. In addition the positions and the number of intracerebral electrodes were different for different patients according to their epilepsy. Due to this, it was hard to fix the position variable while performing real in-vivo conductivity estimation. It would be possible to check whether conductivity estimation from the same position lead to the same results if the IES were performed more than one time from the same anatomical position. In addition, considering two patients with the same positions and number of intracerebral electrodes will provide a valuable material for measuring the inter-subject variability more precisely.

- **Validation** No additional information was considered in this study to validate our estimated conductivity values. However, since the epileptic

patients are investigated by a surgery and some of them are operated by a resection surgery, small samples from their different compartments can be taken in future studies and measured in-vitro. These measured samples will form a reference values for in-vivo conductivity estimation so that the purpose would be to obtain the best conditions and parameters for obtaining such reference values.

- **Localization** The aim of this study was to provide the source localization research with accurate conductivity values for performing source localization. So, in order to examine the accuracy of estimated conductivities, source localization should be performed based on the estimated conductivities and the reference conductivities in order to find out if the estimated conductivities gives a better performance. However, such source localization study should consider the position variable since our estimated conductivities were position-dependent.

Bibliography

[1] Minkyu Ahn and Sung Chan Jun. Performance variation in motor imagery brain–computer interface: A brief review. *Journal of neuroscience methods*, 243:103–110, 2015.

[2] Christoph M Michel, Gregor Thut, Stephanie Morand, Asaid Khateb, Alan J Pegna, Rolando Grave de Peralta, Sara Gonzalez, Margitta Seeck, and Theodor Landis. Electric source imaging of human brain functions. *Brain Research Reviews*, 36(2):108–118, 2001.

[3] schoolofthinking.org. Explainer: the brain. http://schoolofthinking.org/2013/04/explainer-the-brain/.

[4] Enchantedlearning.com. The brain - brain cells. http://www.enchantedlearning.com/subjects/anatomy/brain/Neuron.shtml.

[5] Paul L Nunez and Ramesh Srinivasan. *Electric fields of the brain: the neurophysics of EEG*. Oxford University Press, USA, 2006.

[6] Carsten H Wolters, Lars Grasedyck, and Wolfgang Hackbusch. Efficient computation of lead field bases and influence matrix for the fem-based eeg and meg inverse problem. *Inverse problems*, 20(4):1099, 2004.

[7] Hiroshima University Hospital MEG Room. Contrast to eeg. http://meg.aalip.jp/vsEEG/vsEEGE.html.

[8] Prasanna Jayakar, Michael Duchowny, Trevor J Resnick, and Luis A Alvarez. Localization of seizure foci: pitfalls and caveats. *Journal of Clinical Neurophysiology*, 8(4):414–431, 1991.

[9] Chris Plummer, A Simon Harvey, and Mark Cook. Eeg source localization in focal epilepsy: where are we now? *Epilepsia*, 49(2):201–218, 2008.

[10] M Dyson, Francisco Sepulveda, and John Q Gan. Localisation of cognitive tasks used in eeg-based bcis. *Clinical Neurophysiology*, 121(9):1481–1493, 2010.

[11] B Neil Cuffin. Eccentric spheres models of the head. *IEEE transactions on biomedical engineering*, 38(9):871–878, 1991.

[12] Zeynep Akalin Acar and Scott Makeig. Effects of forward model errors on eeg source localization. *Brain topography*, 26(3):378–396, 2013.

[13] Gildas Marin, Christophe Guerin, Sylvain Baillet, Line Garnero, and Gérard Meunier. Influence of skull anisotropy for the forward and inverse problem in eeg: simulation studies using fem on realistic head models. *Human brain mapping*, 6(4):250–269, 1998.

[14] Roberta Grech, Tracey Cassar, Joseph Muscat, Kenneth P Camilleri, Simon G Fabri, Michalis Zervakis, Petros Xanthopoulos, Vangelis Sakkalis, and Bart Vanrumste. Review on solving the inverse problem in eeg source analysis. *Journal of neuroengineering and rehabilitation*, 5(1), 2008.

[15] LA Geddes and LE Baker. The specific resistance of biological materiala compendium of data for the biomedical engineer and physiologist. *Medical and biological engineering*, 5(3):271–293, 1967.

[16] George W Crile, Helen R Hosmer, and Amy F Rowland. The electrical conductivity of animal tissues under normal and pathological conditions. *American Journal of Physiology–Legacy Content*, 60(1):59–106, 1922.

[17] World Health Organization. Epilepsy. `http://www.who.int/mediacentre/factsheets/fs999/en/`. Accessed: 2016-06-17.

[18] Epilepsy Foundation. Epilepsy diagnosing epilepsy. `http://www.epilepsy.com`. Accessed: 2016-06-17.

[19] I Merlet and J Gotman. Dipole modeling of scalp electroencephalogram epileptic discharges: correlation with intracerebral fields. *Clinical neurophysiology*, 112(3):414–430, 2001.

[20] Martine Gavaret, Anne-Sophie Dubarry, Romain Carron, Fabrice Bartolomei, Agnès Trébuchon, and Christian-George Bénar. Simultaneous seeg-meg-eeg recordings overcome the seeg limited spatial sampling. *Epilepsy Research*, 128:68–72, 2016.

[21] Hans Berger. Über das elektrenkephalogramm des menschen. *European Archives of Psychiatry and Clinical Neuroscience*, 87(1):527–570, 1929.

[22] Fadi N Karameh and Munther A Dahleh. Automated classification of eeg signals in brain tumor diagnostics. In *American Control Conference, 2000. Proceedings of the 2000*, volume 6, pages 4169–4173. IEEE, 2000.

[23] Dhiya Al-Jumeily, Shamaila Iram, Abir Jaffar Hussain, Vialatte Francois-Benois, and Paul Fergus. Early detection method of alzheimers disease using eeg signals. In *Intelligent Computing in Bioinformatics*, pages 25–33. Springer, 2014.

[24] Verena Brodbeck, Laurent Spinelli, Agustina M Lascano, Claudio Pollo, Karl Schaller, Maria I Vargas, Michael Wissmeyer, Christoph M Michel, and Margitta Seeck. Electrical source imaging for presurgical focus localization in epilepsy patients with normal mri. *Epilepsia*, 51(4):583–591, 2010.

[25] Hamza Altakroury. Error detection and new stimulus mechanisms in brain-computer interfaces. Master's thesis, Sabanci University, 2013.

[26] Patricia S. Churchland and Terrence J. Sejnowski. Perspectives on cognitive neuroscience. *Science*, 242:741–745, 1988.

[27] Borís Burle, Laure Spieser, Clémence Roger, Laurence Casini, Thierry Hasbroucq, and Franck Vidal. Spatial and temporal resolutions of eeg: Is it really black and white? a scalp current density view. *International Journal of Psychophysiology*, 97(3):210–220, 2015.

[28] Rebeca Romo-Vázquez, Radu Ranta, Valérie Louis-Dorr, and Didier Maquin. Ocular artifacts removal in scalp eeg: combining ica and wavelett denoising. In *5th International Conference on Physics in Signal and Image Processing*, 2007.

[29] T-P Jung, Colin Humphries, T-W Lee, Scott Makeig, Martin J McKeown, Vicente Iragui, and Terrence J Sejnowski. Removing electroencephalographic artifacts: comparison between ica and pca. In *Neural Networks for Signal Processing VIII, 1998. Proceedings of the 1998 IEEE Signal Processing Society Workshop*, pages 63–72. IEEE, 1998.

[30] George H Klem, Hans Otto Lüders, HH Jasper, C Elger, et al. The ten-twenty electrode system of the international federation. *Electroencephalogr Clin Neurophysiol*, 52(3), 1999.

[31] Robert Oostenveld and Peter Praamstra. The five percent electrode system for high-resolution eeg and erp measurements. *Clinical neurophysiology*, 112(4):713–719, 2001.

[32] Dezhong Yao. A method to standardize a reference of scalp eeg recordings to a point at infinity. *Physiological measurement*, 22(4):693, 2001.

[33] Ricardo A Salido Ruiz, Radu Ranta, and Valerie Louis-Dorr. Eeg montage analysis in the blind source separation framework. *Biomedical Signal Processing and Control*, 6(1):77–84, 2011.

[34] Jaakko Malmivuo and Robert Plonsey. *Bioelectromagnetism: principles and applications of bioelectric and biomagnetic fields*. Oxford University Press, USA, 1995.

[35] G Alarcon, CD Binnie, RDC Elwes, and CE Polkey. Power spectrum and intracranial eeg patterns at seizure onset in partial epilepsy. *Electroencephalography and clinical neurophysiology*, 94(5):326–337, 1995.

[36] Sampsa Vanhatalo, Juha Voipio, and Kai Kaila. Full-band eeg (fbeeg): a new standard for clinical electroencephalography. *Clinical EEG and neuroscience*, 36(4):311–317, 2005.

[37] Ümit Aydin, Johannes Vorwerk, Matthias Dümpelmann, Philipp Küpper, Harald Kugel, Marcel Heers, Jörg Wellmer, Christoph Kellinghaus, Jens Haueisen, Stefan Rampp, et al. Combined eeg/meg can outperform single modality eeg or meg source reconstruction in presurgical epilepsy diagnosis. *PloS one*, 10(3):e0118753, 2015.

[38] Manfred Fuchs, Michael Wagner, Hans-Aloys Wischmann, Thomas Köhler, Annette Theißen, Ralf Drenckhahn, and Helmut Buchner. Improving source reconstructions by combining bioelectric and biomagnetic data. *Electroencephalography and clinical neurophysiology*, 107(2):93–111, 1998.

[39] Jürgen Mellinger, Gerwin Schalk, Christoph Braun, Hubert Preissl, Wolfgang Rosenstiel, Niels Birbaumer, and Andrea Kübler. An meg-based brain–computer interface (bci). *Neuroimage*, 36(3):581–593, 2007.

[40] Alberto Fernández, Roberto Hornero, Agustín Mayo, Jesús Poza, Pedro Gil-Gregorio, and Tomás Ortiz. Meg spectral profile in alzheimer's disease and mild cognitive impairment. *Clinical Neurophysiology*, 117(2):306–314, 2006.

[41] Richard Wennberg, Taufik Valiante, and Douglas Cheyne. Eeg and meg in mesial temporal lobe epilepsy: where do the spikes really come from? *Clinical neurophysiology*, 122(7):1295–1313, 2011.

[42] Robert Van Uitert, Chris Johnson, and Leonid Zhukov. Influence of head tissue conductivity in forward and inverse magnetoencephalographic simulations using realistic head models. *IEEE Transactions on Biomedical Engineering*, 51(12):2129–2137, 2004.

[43] David Gutiérrez, Arye Nehorai, and Carlos H Muravchik. Estimating brain conductivities and dipole source signals with eeg arrays. *IEEE transactions on biomedical engineering*, 51(12):2113–2122, 2004.

[44] Nobukazu Nakasatp, Michel F Levesque, Daniel S Barth, Christoph Baumgartner, Robert L Rogers, and William W Sutherling. Comparisons of meg, eeg, and ecog source localization in neocortical partial epilepsy in humans. *Electroencephalography and clinical neurophysiology*, 91(3):171–178, 1994.

[45] Vairis Caune, Radu Ranta, Steven Le Cam, Janis Hofmanis, Louis Maillard, Laurent Koessler, and Valérie Louis-Dorr. Evaluating dipolar source localization feasibility from intracerebral seeg recordings. *NeuroImage*, 98:118–133, 2014.

[46] Fabrice Wendling, Patrick Chauvel, Arnaud Biraben, and Fabrice Bartolomei. From intracerebral eeg signals to brain connectivity: identification of epileptogenic networks in partial epilepsy. *Frontiers in systems neuroscience*, 4:2010, 154.

[47] Janis Hofmanis. *Contribution au modele direct cérébral par stimulation électrique de profondeur et mesures SEEG: applicationa lépilepsie (Contribution to the cerebral forward model by depth electric stimulation and SEEG measurements: application in epilepsy).* PhD thesis, Université de Lorraine, 2013.

[48] Massimo Cossu, Francesco Cardinale, Laura Castana, Alberto Citterio, Stefano Francione, Laura Tassi, Alim L Benabid, and Giorgio Lo Russo. Stereoelectroencephalography in the presurgical evaluation of focal epilepsy: a retrospective analysis of 215 procedures. *Neurosurgery*, 57(4):706–718, 2005.

[49] Laurent Koessler, Christian Benar, Louis Maillard, Jean-Michel Badier, Jean Pierre Vignal, Fabrice Bartolomei, Patrick Chauvel, and Martine

Gavaret. Source localization of ictal epileptic activity investigated by high resolution eeg and validated by seeg. *Neuroimage*, 51(2):642–653, 2010.

[50] F Pothof, L Bonini, M Lanzilotto, A Livi, L Fogassi, GA Orban, O Paul, and P Ruther. Chronic neural probe for simultaneous recording of single-unit, multi-unit, and local field potential activity from multiple brain sites. *Journal of neural engineering*, 13(4):46006–46006, 2016.

[51] Katrina Elizabeth Wendel. *The influence of tissue conductivity and head geometry on EEG measurement sensitivity distributions*. PhD thesis, Tampere University of Technology, 2010.

[52] J Adam Wilson, Elizabeth A Felton, P Charles Garell, Gerwin Schalk, and Justin C Williams. Ecog factors underlying multimodal control of a brain-computer interface. *IEEE transactions on neural systems and rehabilitation engineering*, 14(2):246–250, 2006.

[53] Benjamin Lanfer, Christian Röer, Michael Scherg, Stefan Rampp, Christoph Kellinghaus, and Carsten Wolters. Influence of a silastic ecog grid on eeg/ecog based source analysis. *Brain topography*, 26(2):212–228, 2013.

[54] Matthias Dümpelmann, Jürgen Fell, Jörg Wellmer, Horst Urbach, and Christian E Elger. 3d source localization derived from subdural strip and grid electrodes: a simulation study. *Clinical Neurophysiology*, 120(6):1061–1069, 2009.

[55] Eugene Lin and Adam Alessio. What are the basic concepts of temporal, contrast, and spatial resolution in cardiac ct? *Journal of cardiovascular computed tomography*, 3(6):403–408, 2009.

[56] Maria Werner-Wasik, Ying Xiao, Edward Pequignot, Walter J Curran, and Walter Hauck. Assessment of lung cancer response after nonoperative therapy: tumor diameter, bidimensional product, and volume. a serial ct scan-based study. *International Journal of Radiation Oncology* Biology* Physics*, 51(1):56–61, 2001.

[57] Giuseppe Vallar and Daniela Perani. The anatomy of unilateral neglect after right-hemisphere stroke lesions. a clinical/ct-scan correlation study in man. *Neuropsychologia*, 24(5):609–622, 1986.

[58] D Orwig and Michael P Federle. Localized clotted blood as evidence of visceral trauma on ct: the sentinel clot sign. *American Journal of Roentgenology*, 153(4):747–749, 1989.

[59] Janis Hofmanis, Valérie Louis-Dorr, Olivier Caspary, and Louis Maillard. Automatic depth electrode localization in intracranial space. In *BIOSIGNALS*, pages 459–462, 2011.

[60] Abi Berger. How does it work?: Magnetic resonance imaging. *BMJ: British Medical Journal*, 324(7328):35, 2002.

[61] Raymond Damadian. Apparatus and method for detecting cancer in tissue. *Google Patents*, 1974.

[62] Juhani Dabek. *Method development for ultra-low-field magnetic resonance imaging and magnetoencephalography*. PhD thesis, Aalto University School of Science, 2014.

[63] Shang-Ling Jui, Shichen Zhang, Weilun Xiong, Fangxiaoqi Yu, Mingjian Fu, Dongmei Wang, Aboul Ella Hassanien, and Kai Xiao. Brain mri tumor segmentation with 3d intracranial structure deformation features. *IEEE Intelligent Systems*, 31(2):66–76, 2016.

[64] CK Kuhl. Mri of breast tumors. *European radiology*, 10(1):46–58, 2000.

[65] SJ Graham, L Chen, M Leitch, RD Peters, MJ Bronskill, FS Foster, RM Henkelman, and DB Plewes. Quantifying tissue damage due to focused ultrasound heating observed by mri. *Magnetic resonance in medicine*, 41(2):321–328, 1999.

[66] LP Clarke, RP Velthuizen, MA Camacho, JJ Heine, M Vaidyanathan, LO Hall, RW Thatcher, and ML Silbiger. Mri segmentation: methods and applications. *Magnetic resonance imaging*, 13(3):343–368, 1995.

[67] George Varvatsoulias. The physiological processes underpinning pet and fmri techniques with an emphasis on the temporal and spatial resolution of these methods. *Psychological Thought*, 6(2):173–195, 2013.

[68] Roberto Cabeza and Lars Nyberg. Imaging cognition: An empirical review of pet studies with normal subjects. *Cognitive Neuroscience, Journal of*, 9(1):1–26, 1997.

[69] Ryogo Minamimoto, Michio Senda, Seishi Jinnouchi, Takashi Terauchi, Tsuyoshi Yoshida, and Tomio Inoue. Detection of breast cancer in an

fdg-pet cancer screening program: results of a nationwide japanese survey. *Clinical breast cancer*, 15(2):e139–e146, 2015.

[70] Drugs.com. Positron emission tomography (pet scan). https://www.drugs.com/health-guide/positron-emission-tomography-pet-scan.html.

[71] Beatriz Calvo-Merino, Daniel E Glaser, Julie Grezes, Richard E Passingham, and Patrick Haggard. Action observation and acquired motor skills: an fmri study with expert dancers. *Cerebral cortex*, 15(8):1243–1249, 2005.

[72] Mayfield Clinic Brain and Spine. Brain mapping: functional mri and dti. http://www.mayfieldclinic.com/PE-fMRI_DTI.htm.

[73] Y Zou and Z Guo. A review of electrical impedance techniques for breast cancer detection. *Medical engineering & physics*, 25:79–90, 2003.

[74] DS Holder. Electrical impedance tomography (eit) of brain function. *Brain Topography*, 5(2):87–93, 1992.

[75] Mariano Fernández-Corazza, Leandro Beltrachini, Nicolás von Ellenrieder, and Carlos H Muravchik. Analysis of parametric estimation of head tissue conductivities using electrical impedance tomography. *Biomedical Signal Processing and Control*, 8(6):830–837, 2013.

[76] Ruth Williams. Alim-louis benabid: stimulation and serendipity. *The Lancet Neurology*, 9(12):1152, 2010.

[77] Morten L Kringelbach, Ned Jenkinson, Sarah LF Owen, and Tipu Z Aziz. Translational principles of deep brain stimulation. *Nature Reviews Neuroscience*, 8(8):623–635, 2007.

[78] Ralph E Hoffman, Nashaat N Boutros, Robert M Berman, Elizabeth Roessler, Aysenil Belger, John H Krystal, and Dennis S Charney. Transcranial magnetic stimulation of left temporoparietal cortex in three patients reporting hallucinated voices. *Biological psychiatry*, 46(1):130–132, 1999.

[79] Hans Martin Kolbinger, Gereon Höflich, Andreas Hufnagel, Hans-Jürgen Müller, and Siegfried Kasper. Transcranial magnetic stimulation (tms) in the treatment of major depressiona pilot study. *Human Psychopharmacology: Clinical and Experimental*, 10(4):305–310, 1995.

[80] Antonio Valentin, Ramamurthy Arunachalam, Arvin Mesquita-Rodrigues, Jorge J Garcia Seoane, Mark P Richardson, Kerry R Mills, and Gonzalo Alarcon. Late eeg responses triggered by transcranial magnetic stimulation (tms) in the evaluation of focal epilepsy. *Epilepsia*, 49(3):470–480, 2008.

[81] Psychology Today. Transcranial magnetic stimulation (tms) treats depression. https://www.psychologytoday.com/blog/reading-between-the-headlines/201401/transcranial-magnetic-stimulation-tms-treats-depression.

[82] Michael A Nitsche, Paulo S Boggio, Felipe Fregni, and Alvaro Pascual-Leone. Treatment of depression with transcranial direct current stimulation (tdcs): a review. *Experimental neurology*, 219(1):14–19, 2009.

[83] Abhishek Datta, Julie M Baker, Marom Bikson, and Julius Fridriksson. Individualized model predicts brain current flow during transcranial direct-current stimulation treatment in responsive stroke patient. *Brain stimulation*, 4(3):169–174, 2011.

[84] tDCS News. History of tdcs. http://www.tdcsnews.com/history-of-tdcs/.

[85] Saburo Homma, Toshimitsu Musha, Yoshio Nakajima, Yoshiwo Okamoto, Sigge Blom, Roland Flink, and Karl-Erik Hagbarth. Conductivity ratios of the scalp-skull-brain head model in estimating equivalent dipole sources in human brain. *Neuroscience research*, 22(1):51–55, 1995.

[86] Robert Pohlmeier, Helmut Buchner, Gunter Knoll, Adrian RienÄcker, Rainer Beckmann, and Jörg Pesch. The influence of skull-conductivity misspecification on inverse source localization in realistically shaped finite element head models. *Brain topography*, 9(3):157–162, 1997.

[87] Jens Haueisen, David S Tuch, C Ramon, PH Schimpf, VJ Wedeen, JS George, and JW Belliveau. The influence of brain tissue anisotropy on human eeg and meg. *Neuroimage*, 15(1):159–166, 2002.

[88] Stephen B Baumann, David R Wozny, Shawn K Kelly, and Frank M Meno. The electrical conductivity of human cerebrospinal fluid at body temperature. *Biomedical Engineering, IEEE Transactions on*, 44(3):220–223, 1997.

[89] Massoud Akhtari, HC Bryant, AN Mamelak, ER Flynn, L Heller, JJ Shih, M Mandelkem, A Matlachov, DM Ranken, ED Best, et al. Conductivities of three-layer live human skull. *Brain topography*, 14(3):151–167, 2002.

[90] Thom F Oostendorp, Jean Delbeke, and Dick F Stegeman. The conductivity of the human skull: results of in vivo and in vitro measurements. *IEEE transactions on biomedical engineering*, 47(11):1487–1492, 2000.

[91] Richard D Stoy, Kenneth R Foster, and Herman P Schwan. Dielectric properties of mammalian tissues from 0.1 to 100 mhz; a summary of recent data. *Physics in medicine and biology*, 27(4):501, 1982.

[92] Zeynep Akalin Acar, Can E Acar, and Scott Makeig. Simultaneous head tissue conductivity and eeg source location estimation. *NeuroImage*, 124:168–180, 2016.

[93] Seok Lew, Carsten H Wolters, Alfred Anwander, Scott Makeig, and Rob S MacLeod. Improved eeg source analysis using low-resolution conductivity estimation in a four-compartment finite element head model. *Human brain mapping*, 30(9):2862–2878, 2009.

[94] Sónia I Gonçalves, Jan C de Munck, Jeroen PA Verbunt, Fetsje Bijma, Rob M Heethaar, and F Lopes da Silva. In vivo measurement of the brain and skull resistivities using an eit-based method and realistic models for the head. *IEEE Transactions on Biomedical Engineering*, 50(6):754–767, 2003.

[95] Juhani Dabek, Konstantina Kalogianni, Edwin Rotgans, Frans CT van der Helm, Gert Kwakkel, Erwin EH van Wegen, Andreas Daffertshofer, and Jan C de Munck. Determination of head conductivity frequency response in vivo with optimized eit-eeg. *NeuroImage*, 2015.

[96] Yingchun Zhang, Wim Van Drongelen, and Bin He. Estimation of in vivo brain-to-skull conductivity ratio in humans. *Applied physics letters*, 89(22):223903, 2006.

[97] Laurent Koessler, Sophie Colnat-Coulbois, Thierry Cecchin, Janis Hofmanis, Jacek P Dmochowski, Anthony M Norcia, and Louis G Maillard. In-vivo measurements of human brain tissue conductivity using focal electrical current injection through intracerebral multicontact electrodes. *Human Brain Mapping*, 38(2):974–986, 2017.

[98] David S Tuch, Van J Wedeen, Anders M Dale, John S George, and John W Belliveau. Conductivity tensor mapping of the human brain using diffusion tensor mri. *Proceedings of the National Academy of Sciences*, 98(20):11697–11701, 2001.

[99] Richard Frackowiak and Henry Markram. The future of human cerebral cartography: a novel approach. *Phil. Trans. R. Soc. B*, 370(1668), 2015.

[100] EJ Speckmann, CE Elger, and A Gorji. Neurophysiologic basis of eeg and dc potentials. In *Electroencephalography: Basic Principles, Clinical Applications and Related Fields*. Lippincott Williams & Wilkins, 2005.

[101] Fernando Lopes da Silva. Origin of eeg and meg i: Cellular sources. In *EEG: origin and measurement*. Springer, 2009.

[102] Paul H Schimpf, Ceon Ramon, and Jens Haueisen. Dipole models for the eeg and meg. *IEEE Transactions on Biomedical Engineering*, 49(5):409–418, 2002.

[103] Athinoula A. Martinos Center for Biomedical Imaging. Inspection of freesurfer output. https://surfer.nmr.mgh.harvard.edu/fswiki/FsTutorial/OutputData_freeview.

[104] Hans Hallez, Bart Vanrumste, Roberta Grech, Joseph Muscat, Wim De Clercq, Anneleen Vergult, Yves D'Asseler, Kenneth P Camilleri, Simon G Fabri, Sabine Van Huffel, et al. Review on solving the forward problem in eeg source analysis. *Journal of neuroengineering and rehabilitation*, 4(1):1, 2007.

[105] Y Lai, W Van Drongelen, L Ding, KE Hecox, VL Towle, DM Frim, and B He. Estimation of in vivo human brain-to-skull conductivity ratio from simultaneous extra-and intra-cranial electrical potential recordings. *Clinical neurophysiology*, 116(2):456–465, 2005.

[106] M Fernández-Corazza, N Von-Ellenrieder, and CH Muravchik. Estimation of electrical conductivity of a layered spherical head model using electrical impedance tomography. *Journal of Physics: Conference Series*, 332(1):012022, 2011.

[107] Thomas C Ferree, K Jeffrey Eriksen, and Don M Tucker. Regional head tissue conductivity estimation for improved eeg analysis. *IEEE Transactions on Biomedical Engineering*, 47(12):1584–1592, 2000.

[108] Maureen Clerc, Alain Dervieux, O Faugeras, R Keriven, Jan Kybic, and Théo Papadopoulo. Comparison of bem and fem methods for the e/meg problem. In *Proceedings of BIOMAG Conference*, 2002.

[109] Geoffray Adde, Maureen Clerc, Olivier Faugeras, Renaud Keriven, Jan Kybic, and Théodore Papadopoulo. Symmetric bem formulation for the m/eeg forward problem. In *Information Processing in Medical Imaging*, pages 524–535. Springer, 2003.

[110] Ceon Ramon, P Schimpf, J Haueisen, M Holmes, and A Ishimaru. Role of soft bone, csf and gray matter in eeg simulations. *Brain topography*, 16(4):245–248, 2004.

[111] Johannes Vorwerk, Jae-Hyun Cho, Stefan Rampp, Hajo Hamer, Thomas R Knösche, and Carsten H Wolters. A guideline for head volume conductor modeling in eeg and meg. *NeuroImage*, 100:590–607, 2014.

[112] Christopher R Johnson. Computational and numerical methods for bioelectric field problems. *Critical Reviews in Biomedical Engineering*, 25(1), 1997.

[113] SCI Institute. Scirun: A scientific computing problem solving environment, scientific computing and imaging institute (sci). http://www.scirun.org, 2015.

[114] Moritz Dannhauer, Benjamin Lanfer, Carsten H Wolters, and Thomas R Knösche. Modeling of the human skull in eeg source analysis. *Human brain mapping*, 32(9):1383–1399, 2011.

[115] Bruce Fischl, David H Salat, André JW van der Kouwe, Nikos Makris, Florent Ségonne, Brian T Quinn, and Anders M Dale. Sequence-independent segmentation of magnetic resonance images. *Neuroimage*, 23:S69–S84, 2004.

[116] Sylvain Vallaghé and Maureen Clerc. A global sensitivity analysis of three-and four-layer eeg conductivity models. *IEEE Transactions on Biomedical Engineering*, 56(4):988–995, 2009.

[117] Victoria Montes-Restrepo, Pieter van Mierlo, Gregor Strobbe, Steven Staelens, Stefaan Vandenberghe, and Hans Hallez. Influence of skull modeling approaches on eeg source localization. *Brain topography*, 27(1):95–111, 2014.

[118] Geertjan Huiskamp, Maurice Vroeijenstijn, René van Dijk, George Wieneke, and Alexander C van Huffelen. The need for correct realistic geometry in the inverse eeg problem. *IEEE Transactions on Biomedical Engineering*, 46(11):1281–1287, 1999.

[119] Frederik Maes, Andre Collignon, Dirk Vandermeulen, Guy Marchal, and Paul Suetens. Multimodality image registration by maximization of mutual information. *Medical Imaging, IEEE Transactions on*, 16(2):187–198, 1997.

[120] Hang Si. Tetgen, a delaunay-based quality tetrahedral mesh generator. *ACM Transactions on Mathematical Software (TOMS)*, 41(2):11, 2015.

[121] CGAL. The computational geometry algorithms library. http://www.cgal.org/index.html.

[122] Iso2mesh. A 3d surface and volumetric mesh generator for matlab/octave. http://iso2mesh.sourceforge.net/cgi-bin/index.cgi.

[123] Niclas Andréasson, Anton Evgrafov, and Michael Patriksson. An introduction to optimization: Foundations and fundamental algorithms. Chalmers University of Technology Press, 2005.

[124] Edwin KP Chong and Stanislaw H Zak. *An introduction to optimization*, volume 76. John Wiley & Sons, 2013.

[125] Rania Hassan, Babak Cohanim, Olivier De Weck, and Gerhard Venter. A comparison of particle swarm optimization and the genetic algorithm. In *46th AIAA/ASME/ASCE/AHS/ASC Structures, Structural Dynamics and Materials Conference*, 2005.

[126] Rob A Rutenbar. Simulated annealing algorithms: an overview. *IEEE Circuits and Devices Magazine*, 5(1):19–26, 1989.

[127] Daniel S Weile and Eric Michielssen. Genetic algorithm optimization applied to electromagnetics: A review. *IEEE Transactions on Antennas and Propagation*, 45(3):343–353, 1997.

[128] John H Holland. *Adaptation in natural and artificial systems: an introductory analysis with applications to biology, control, and artificial intelligence.* U Michigan Press, 1975.

[129] MathWorks. Genetic algorithm options. http://fr.mathworks.com/help/gads/genetic-algorithm-options.html. Accessed: 2016-07-28.

[130] JE Dennis and Daniel J Woods. Optimization on microcomputers: The nelder-mead simplex algorithm. *New computing environments: microcomputers in large-scale computing*, pages 116–122, 1987.

[131] Roger Fletcher. *Practical methods of optimization*. John Wiley & Sons, 2013.

[132] S. Kirkpatrick, C. D. Gellat, and M. P. Vecchi. Optimization by simmulated annealing. *Science*, 220(4598):671–680, 1983.

[133] Jan WH Meijs, Onno W Weier, Maria J Peters, and ADRIAAN Van Oosterom. On the numerical accuracy of the boundary element method (eeg application). *IEEE Transactions on Biomedical Engineering*, 36(10):1038–1049, 1989.

[134] S Goncalves, JC De Munck, RM Heethaar, FH Lopes Da Silva, and BW Van Dijk. The application of electrical impedance tomography to reduce systematic errors in the eeg inverse problem-a simulation study. *Physiological measurement*, 21(3):379, 2000.

[135] Ant Neuro. Eeg cap and accessories. http://www.ant-neuro.com/products/waveguard/electrode-layouts.

[136] Jens Haueisen, Ceon Ramon, Michael Eiselt, Hartmut Brauer, and Hannes Nowak. Influence of tissue resistivities on neuromagnetic fields and electric potentials studied with a finite element model of the head. *IEEE Transactions on Biomedical Engineering*, 44(8):727–735, 1997.

[137] Vairis Caune. *Brain source localization using SEEG intra-cerebral electrodes*. PhD thesis, Université de Lorraine, 2017.

[138] G Lantz, R Grave De Peralta, L Spinelli, M Seeck, and CM Michel. Epileptic source localization with high density eeg: how many electrodes are needed? *Clinical neurophysiology*, 114(1):63–69, 2003.

[139] Janis Hofmanis, Olivier Caspary, Valerie Louis-Dorr, Radu Ranta, and Louis Maillard. Denoising depth eeg signals during dbs using filtering and subspace decomposition. *Biomedical Engineering, IEEE Transactions on*, 60(10):2686–2695, 2013.

[140] Reza Sameni, Christian Jutten, and Mohammad B Shamsollahi. Multichannel electrocardiogram decomposition using periodic component analysis. *IEEE Transactions on Biomedical Engineering*, 55(8):1935–1940, 2008.

[141] Ladan Amini, Reza Sameni, Christian Jutten, Gholam-Ali Hossein-Zadeh, and Hamid Soltanian-Zadeh. Mr artifact reduction in the simultaneous acquisition of eeg and fmri of epileptic patients. In *Signal Processing Conference, 2008 16th European*, number 1–5, 2008.

[142] Roberto D Pascual-Marqui, Dietrich Lehmann, Martha Koukkou, Kieko Kochi, Peter Anderer, Bernd Saletu, Hideaki Tanaka, Koichi Hirata, E Roy John, Leslie Prichep, et al. Assessing interactions in the brain with exact low-resolution electromagnetic tomography. *Philosophical Transactions of the Royal Society of London A: Mathematical, Physical and Engineering Sciences*, 369(1952):3768–3784, 2011.

Appendices

Appendix A

In-vivo Conductivity Estimation Results

Table A.1: Resulted conductivities of Patient(1) given his SEEG signals

IES position	Resulted Conductivities					Resulted RDM
	Scalp	Skull	CSF	GM	WM	
Deep	0.99	0.0082	0.18	0.64	0.10	0.23
	0.22	0.0198	5.36	0.04	0.01	0.86
	0.99	0.0071	0.18	0.78	0.11	0.23
	0.99	0.0240	0.18	0.05	0.07	0.75
	0.99	0.0059	0.18	0.04	0.06	0.29
	0.99	0.0097	0.18	0.06	0.06	0.18
Intermediate	0.99	0.0050	0.18	0.13	0.37	0.17
	0.99	0.0100	0.18	0.04	0.08	0.22
	0.03	0.0008	0.20	0.06	0.42	0.50
Lateral	0.99	0.0141	0.18	0.04	0.02	0.44
	0.95	0.0240	0.23	0.05	0.01	0.40
	0.87	0.0208	0.27	0.05	0.01	0.49

Table A.2: Resulted conductivities of Patient(1) given his EEG potentials

IES position	Resulted Conductivities					Resulted RDM
	Scalp	Skull	CSF	GM	WM	
Deep	0.38	0.0240	1.81	0.40	0.01	0.47
	0.38	0.0008	5.18	0.26	0.42	0.88
	0.96	0.0008	0.33	0.08	0.04	0.56
	0.27	0.0009	2.25	0.90	0.01	0.77
	0.61	0.0009	1.01	0.24	0.15	0.68
	0.63	0.0010	0.73	0.90	0.03	0.67
Intermediate	0.95	0.0010	1.86	0.66	0.04	0.77
	0.17	0.0008	3.80	0.76	0.29	0.80
	0.16	0.0008	2.43	0.90	0.42	0.34
Lateral	0.67	0.0095	0.57	0.20	0.08	0.29
	0.99	0.0008	5.37	0.06	0.01	0.79
	0.99	0.0008	5.37	0.19	0.01	1.02

Table A.3: Resulted conductivities of Patient(1) given his SEEG and EEG signals

IES position	Resulted Conductivities					Resulted RDM
	Scalp	Skull	CSF	GM	WM	
Deep	0.67	0.0041	0.36	0.77	0.12	0.25
	0.03	0.0240	0.18	0.05	0.42	1.14
	0.75	0.0098	0.18	0.78	0.10	0.26
	0.38	0.0240	0.18	0.03	0.06	0.92
	0.99	0.0078	0.18	0.05	0.07	0.35
	0.76	0.0215	0.22	0.09	0.09	0.40
Intermediate	0.47	0.0118	0.32	0.17	0.37	0.42
	0.41	0.0126	0.19	0.20	0.40	0.49
	0.03	0.0008	0.20	0.06	0.42	0.51
Lateral	0.99	0.0146	0.18	0.04	0.02	0.44
	0.87	0.0240	0.23	0.05	0.01	0.41
	0.99	0.0240	0.31	0.06	0.01	0.50

Table A.4: Resulted conductivities of Patient(2) given his SEEG signals

IES position	Resulted Conductivities					Resulted RDM
	Scalp	Skull	CSF	GM	WM	
Deep	0.46	0.0008	5.37	0.03	0.10	0.60
	0.99	0.0116	0.30	0.16	0.01	0.60
	0.03	0.0178	0.57	0.44	0.42	0.36
	0.99	0.0130	0.18	0.07	0.42	0.20
	0.99	0.0155	0.18	0.07	0.42	0.23
	0.37	0.0240	0.18	0.16	0.12	0.53
	0.60	0.0240	0.18	0.45	0.14	0.45
	0.12	0.0112	0.65	0.35	0.27	0.26
	0.28	0.0211	0.73	0.22	0.23	0.39
	0.03	0.0230	0.33	0.09	0.23	0.20
	0.08	0.0008	3.94	0.18	0.04	0.32
	0.18	0.0105	0.18	0.14	0.42	0.16
	0.03	0.0008	0.37	0.57	0.42	0.32
Intermediate	0.99	0.0217	0.18	0.12	0.42	0.22
	0.99	0.0189	0.18	0.95	0.34	0.20
	0.99	0.0141	0.18	0.08	0.18	0.12
	0.34	0.0240	0.18	0.84	0.32	0.76

Table A.5: Resulted conductivities of Patient(2) given his EEG potentials

IES position	Resulted Conductivities					Resulted RDM
	Scalp	Skull	CSF	GM	WM	
Deep	0.40	0.0076	1.72	0.43	0.14	0.81
	0.57	0.0240	1.10	0.03	0.42	0.73
	0.89	0.0034	3.44	0.99	0.01	0.53
	0.93	0.0024	4.45	0.12	0.42	0.69
	0.47	0.0011	2.10	0.05	0.32	0.67
	0.99	0.0041	0.18	0.03	0.06	0.80
	0.99	0.0040	0.18	0.07	0.01	0.71
	0.53	0.0008	5.34	0.43	0.15	0.71
	0.40	0.0008	0.28	0.74	0.20	0.77
	0.99	0.0056	1.75	0.04	0.01	0.65
	0.11	0.0010	2.51	0.97	0.01	0.74
	0.42	0.0023	1.56	0.35	0.26	0.63
	0.52	0.0022	1.00	0.60	0.13	0.79
Intermediate	0.83	0.0132	0.26	0.31	0.04	0.71
	0.77	0.0112	2.93	0.18	0.05	0.77
	0.38	0.0072	0.18	0.99	0.01	0.78
	0.95	0.0057	0.41	0.07	0.04	0.70

Table A.6: Resulted conductivities of Patient(2) given his SEEG and EEG signals

IES position	Resulted Conductivities					Resulted RDM
	Scalp	Skull	CSF	GM	WM	
Deep	0.99	0.0053	0.18	0.05	0.42	0.57
	0.99	0.0124	0.32	0.17	0.01	0.61
	0.03	0.0025	0.50	0.37	0.42	0.36
	0.99	0.0118	0.18	0.07	0.42	0.24
	0.99	0.0137	0.18	0.07	0.42	0.27
	0.76	0.0105	0.40	0.12	0.11	0.55
	0.82	0.0240	0.18	0.51	0.15	0.46
	0.15	0.0091	0.67	0.35	0.28	0.27
	0.31	0.0182	0.75	0.22	0.23	0.40
	0.35	0.0118	0.51	0.16	0.31	0.21
	0.11	0.0008	4.99	0.24	0.05	0.34
	0.24	0.0045	0.21	0.13	0.41	0.18
	0.10	0.0008	0.38	0.59	0.42	0.32
Intermediate	0.99	0.0196	0.18	0.13	0.42	0.26
	0.99	0.0166	0.18	0.97	0.34	0.23
	0.99	0.0146	0.18	0.09	0.21	0.20
	0.51	0.0240	0.18	0.70	0.23	0.78

Table A.7: Resulted conductivities of Patient(3) given his SEEG signals

IES position	Resulted Conductivities					Resulted RDM
	Scalp	Skull	CSF	GM	WM	
Deep	0.37	0.0218	0.45	0.20	0.14	0.33
	0.50	0.0239	0.47	0.11	0.09	0.33
	0.99	0.0240	0.18	0.10	0.04	0.55
	0.99	0.0063	0.18	0.07	0.05	0.56
Intermediate	0.03	0.0078	1.37	0.31	0.40	0.47
	0.36	0.0203	0.79	0.18	0.15	0.24
	0.19	0.0240	0.18	0.20	0.20	0.61
	0.23	0.0240	0.18	0.03	0.05	0.43
Lateral	0.03	0.0240	0.18	0.03	0.01	0.50
	0.99	0.0067	3.13	0.03	0.06	0.45
	0.36	0.0073	0.18	0.11	0.42	0.49
	0.99	0.0240	0.18	0.03	0.01	0.89

Table A.8: Resulted conductivities of Patient(3) given his EEG signals

IES position	Resulted Conductivities					Resulted RDM
	Scalp	Skull	CSF	GM	WM	
Deep	0.62	0.0008	2.82	0.51	0.42	0.70
	0.98	0.0037	0.20	0.04	0.01	0.64
	0.69	0.0014	2.76	0.34	0.22	0.67
	0.99	0.0008	5.37	0.99	0.42	0.58
Intermediate	0.71	0.0011	2.44	0.54	0.05	0.75
	0.86	0.0008	1.41	0.64	0.31	0.74
	0.99	0.0028	1.58	0.03	0.01	0.48
	0.93	0.0039	0.24	0.94	0.02	0.47
Lateral	0.99	0.0008	0.18	0.03	0.36	1.03
	0.99	0.0008	5.37	0.99	0.42	0.37
	0.99	0.0008	1.90	0.99	0.42	0.39
	0.99	0.0009	0.18	0.03	0.01	0.74

Table A.9: Resulted conductivities of Patient(3) given his SEEG and EEG signals

IES position	Resulted Conductivities					Resulted RDM
	Scalp	Skull	CSF	GM	WM	
Deep	0.03	0.0023	1.54	0.52	0.38	0.70
	0.46	0.0232	0.49	0.11	0.09	0.36
	0.03	0.0036	2.29	0.60	0.42	1.17
	0.99	0.0035	0.18	0.05	0.08	0.64
Intermediate	0.03	0.0076	1.47	0.34	0.42	0.48
	0.41	0.0177	0.72	0.17	0.13	0.28
	0.18	0.0240	0.18	0.20	0.19	0.62
	0.23	0.0240	0.18	0.03	0.05	0.44
Lateral	0.88	0.0240	0.18	0.03	0.01	0.97
	0.71	0.0060	0.61	0.97	0.01	0.47
	0.65	0.0017	2.80	0.12	0.29	0.61
	0.99	0.0192	0.18	0.03	0.01	1.05

Table A.10: Resulted conductivities of Patient(3) given his SEEG signals within 50 mm from stimulation

IES position	Resulted Conductivities					Resulted RDM
	Scalp	Skull	CSF	GM	WM	
Deep	0.99	0.0010	0.18	0.99	0.12	0.15
	0.99	0.0060	0.18	0.75	0.14	0.24
	0.99	0.0072	0.18	0.99	0.18	0.19
	0.99	0.0240	0.18	0.05	0.09	0.63
	0.99	0.0086	0.18	0.58	0.15	0.19
	0.99	0.0089	0.18	0.09	0.08	0.14
Intermediate	0.65	0.0066	0.31	0.11	0.15	0.13
	0.99	0.0103	0.18	0.06	0.11	0.19
	0.99	0.0076	0.18	0.12	0.21	0.22
Lateral	0.99	0.0146	0.18	0.04	0.02	0.39
	0.81	0.0233	0.21	0.06	0.01	0.33
	0.99	0.0212	0.40	0.07	0.01	0.57

Table A.11: Resulted conductivities of Patient(1) by the frequency component 55 Hz given his SEEG signals

IES position	Resulted Conductivities					Resulted RDM
	Scalp	Skull	CSF	GM	WM	
Deep	0.12	0.0170	1.84	0.00	0.00	0.53
	0.01	0.0782	0.19	0.00	0.00	0.65
	0.31	0.0713	2.46	0.00	0.00	0.57
	0.00	0.0952	0.17	0.00	0.00	0.63
	0.60	0.0995	0.06	0.66	0.11	0.37
	0.30	0.0986	0.04	0.07	0.89	0.47
Intermediate	0.02	0.0398	0.01	0.01	0.01	0.35
	0.17	0.0993	0.05	0.22	0.05	0.38
	0.00	0.0000	0.79	0.16	0.96	0.32
Lateral	0.94	0.0002	0.36	0.07	0.03	0.24
	0.80	0.0103	0.51	0.06	0.02	0.29
	0.00	0.0772	0.02	0.01	0.00	0.39

Table A.12: Resulted conductivities of Patient(1) by the frequency component 110 Hz given his SEEG signals

IES position	Resulted Conductivities					Resulted RDM
	Scalp	Skull	CSF	GM	WM	
Deep	0.00	0.0000	0.82	0.91	0.21	0.31
	0.03	0.0863	0.24	0.17	0.04	0.47
	0.00	0.0000	0.54	0.99	0.16	0.36
	0.57	0.0545	2.38	0.00	0.00	0.67
	0.98	0.0000	0.00	0.00	0.00	0.26
	0.63	0.0334	0.15	0.28	0.18	0.18
Intermediate	0.53	0.0183	0.51	0.17	0.19	0.18
	0.94	0.0326	0.37	0.13	0.13	0.22
	0.75	0.0030	0.96	0.37	0.75	0.25
Lateral	0.98	0.0037	0.21	0.07	0.03	0.18
	0.76	0.0222	0.42	0.09	0.02	0.28
	0.00	0.0156	0.00	0.00	0.00	0.47

Table A.13: Resulted conductivities of Patient(1) by the frequency component 165 Hz given his SEEG signals

IES position	Resulted Conductivities					Resulted RDM
	Scalp	Skull	CSF	GM	WM	
Deep	0.54	0.0000	0.44	0.88	0.13	0.25
	0.00	0.0000	0.74	0.96	0.18	0.38
	0.47	0.0000	0.49	0.89	0.15	0.29
	0.71	0.0117	0.64	0.00	0.00	0.57
	0.93	0.0001	0.08	0.07	0.03	0.24
	0.90	0.0018	0.07	0.04	0.03	0.14
Intermediate	0.88	0.0087	0.43	0.14	0.18	0.14
	0.86	0.0122	0.20	0.06	0.09	0.19
	0.87	0.0039	0.45	0.21	0.30	0.23
Lateral	0.96	0.0817	0.09	0.22	0.06	0.20
	0.90	0.0421	0.47	0.13	0.03	0.32
	0.00	0.0008	0.00	0.00	0.00	0.51

Table A.14: Resulted conductivities of Patient(1) by the frequency component 55 Hz given his SEEG and EEG signals

IES position	Resulted Conductivities					Resulted RDM
	Scalp	Skull	CSF	GM	WM	
Deep	0.00	0.0000	1.30	0.32	0.61	1.00
	0.00	0.0178	0.04	0.04	0.99	1.06
	0.00	0.0045	0.01	0.01	0.21	1.02
	0.00	0.0000	1.72	0.14	0.84	0.98
	0.05	0.0964	0.09	0.27	0.03	0.87
	0.07	0.0997	0.04	0.04	0.00	0.94
Intermediate	0.01	0.0164	0.01	0.00	0.00	0.85
	0.09	0.0674	0.03	0.11	0.03	0.89
	0.00	0.0001	0.68	0.14	0.83	0.64
Lateral	0.00	0.0000	2.87	0.48	0.21	0.55
	0.54	0.0308	0.76	0.10	0.03	0.50
	0.00	0.0782	0.02	0.01	0.00	0.42

Table A.15: Resulted conductivities of Patient(1) by the frequency component 110 Hz given his SEEG and EEG signals

IES position	Resulted Conductivities					Resulted RDM
	Scalp	Skull	CSF	GM	WM	
Deep	0.00	0.0000	1.47	0.99	0.27	0.33
	0.00	0.0000	1.58	0.68	0.14	0.48
	0.02	0.0002	0.29	0.99	0.13	0.38
	0.00	0.0000	2.19	0.14	0.23	1.04
	0.00	0.0369	0.03	0.06	0.01	0.75
	0.23	0.0992	0.26	0.89	0.12	0.78
Intermediate	0.00	0.0000	2.78	0.21	0.18	0.69
	0.40	0.0466	0.22	0.30	0.20	0.67
	0.49	0.0057	0.98	0.38	0.80	0.25
Lateral	0.99	0.0195	0.52	0.21	0.09	0.19
	0.98	0.0528	0.73	0.16	0.04	0.43
	0.00	0.0011	0.00	0.00	0.00	0.55

Table A.16: Resulted conductivities of Patient(1) by the frequency component 165 Hz given his SEEG and EEG signals

IES position	Resulted Conductivities					Resulted RDM
	Scalp	Skull	CSF	GM	WM	
Deep	0.03	0.0003	0.30	0.88	0.11	0.27
	0.00	0.0000	1.59	0.93	0.17	0.40
	0.00	0.0000	0.83	0.99	0.16	0.31
	0.00	0.0000	3.00	0.24	0.26	1.00
	0.00	0.0898	0.27	0.36	0.08	0.64
	0.36	0.0716	0.71	0.07	0.06	0.65
Intermediate	0.17	0.0144	2.39	0.26	0.26	0.58
	0.42	0.0249	0.22	0.21	0.24	0.58
	0.73	0.0106	0.65	0.32	0.47	0.24
Lateral	0.99	0.0970	0.10	0.24	0.07	0.21
	0.94	0.0609	0.55	0.16	0.04	0.43
	0.00	0.0930	0.02	0.01	0.00	0.62

In-vivo Human Head Conductivity Estimation by SEEG and EEG Recorded in Simultaneous with Intracerebral Electrical Stimulation

Abstract: EEG source localization is becoming an important tool for treating epileptic patients by localizing the epileptogenic zones before performing a resection surgery. Given a forward head model, EEG source localization is performed by solving the inverse problem. The forward head model is a biophysical model which describes the electrical distribution in the human head. When considering the propagation as the only way for the current distribution to move in the head, the focus is directed primarily on two parameters for having an accurate forward head model. These parameters are: the geometry of the head model and the conductivity value of each compartment of the head model. Due to the recent advances in computers and imaging techniques (like MRI and CT), it is possible to generate human head models that represent with a high accuracy the geometry of the real head. However, there is still an argument about the conductivity values and the method by which it should be estimated. In literature, the common values for conductivities come mostly from in-vitro experiments. In this work we are performing in-vivo conductivity estimation by considering the data of three epileptic patients. This data consists of MR images and CT scans for building a five-compartment FEM head model for each patient along with SEEG and EEG recordings that were acquired in simultaneous with intracerebral electrical stimulation (IES). The originality of this work lies in evaluating the performance of in-vivo conductivity estimation by EEG and/or SEEG measurements in function of different spatial parameters and locations of the IES. The following work consists of three major parts: the first part aims to determine the most robust optimization algorithm among common algorithms for optimizing the forward head model. The objective of the second part is to analyze the sensitivity of the conductivity values given different conditions on stimulation position, measurement positions and number of compartments. While in the final part, the conductivities of an isotropic and homogeneous five-compartment FEM head model were estimated with previously selected parameters for three drug-resistant epileptic patients. Finally the effect of changing the stimulation frequency on the estimated conductivities was determined.

Key words: Conductivity estimation, Forward problem, Intracerebral electrical stimulation, Propagation model, SEEG/EEG.

Estimation de conductivités cérébrales in vivo chez l'homme à partir de la stimulation électrique et de mesures EEG intracérébrales et de scalp

Résumé: La localisation de source d'EEG devient un outil important pour traiter les patients atteints d'épilepsie en localisant les zones épileptogènes avant d'effectuer une chirurgie de résection. Compte tenu d'un modèle de tête direct, la localisation de la source EEG est réalisée en résolvant le problème inverse. Le modèle de tête direct est un modèle biophysique de tête plus ou moins complexe qui décrit la distribution électrique. En considérant la propagation électrique expliquant la distribution de potentiels, outre la numérisation, le modèlenécessite le réglage deux paramètres lesquels sont la géométrie du modèle de tête et la valeur des conductivités de chaque compartiment du modèle de tête. En raison des progrès computationnel et des techniques d'imagerie (comme l'IRM et la CT), il est possible de générer des modèles de tête humaine qui représentent avec une grande précision la géométrie de la tête réelle. Cependant, il existe une incertitude sur les valeurs de conductivité de chaque compartiment et la méthode avec laquelle ils devraient être estimés. Dans la littérature, les valeurs communes pour les conductivités proviennent principalement des expériences in-vitro. Dans ce travail, nous effectuons une estimation de la conductivité in-vivo à partir de données EEG/SEEG/Stimulation électrique de trois patients épileptiques. Ces données sont constituées des images IRM et des CT SCAN pour la construction d'un modèle de tête FEM à cinq compartiments pour chaque patient, ainsi que les enregistrements SEEG et EEG qui ont été acquis en même temps que la stimulation électrique intracérébrale (IES). L'originalité de ce travail réside dans l'évaluation de la performance de l'estimation des conductivités in-vivo par des mesures EEG et / ou SEEG en fonction de différents paramètres spatiaux et de la localisation des IES. Le travail se compose de trois parties principales: la première partie vise déterminer la méthode d'optimisation sous contraintes la plus robuste parmi les algorithmes courants pour optimiser les paramètres du modèle direct de tête. L'objectif de la deuxième partie est d'analyser la sensibilité des valeurs de conductivité à différentes conditions sur la position de stimulation, le conditionnement du problème avec les positions de mesure et leur nombre et le nombre de compartiments. Alors que dans la partie finale, les conductivités d'un modèle de tête FEM isotrope et homogène à cinq compartiments ont été estimées avec des paramètres précédemment déterminés pour les trois patients. Enfin, l'effet de la fréquence de stimulation sur les conductivités estimées est analysé.

Mots clés: Estimation de conductivité, électrique intracérébrale stimulation, Modèle de propagation, Problème direct, SEEG/EEG.